Spectral Analysis in High Frequency Radar Oceanography

Andrew Middleditch

Department of Applied Mathematics
School of Mathematics and Statistics
The University of Sheffield

Thesis submitted for the degree of
Doctor of Philosophy, July 2006

Abstract

High Frequency radar systems provide a unique opportunity to measure evolving littoral oceanic dynamics at high temporal and spatial resolution. Backscattered electromagnetic signals from ocean waves are modulated by Bragg resonant scattering. A perturbation analysis yields an expression for the spectral content of radar signals which can be exploited to provide estimates of oceanographic parameters: the radial component of surface current can be extracted from the frequency locations of the first order peaks; the ocean wave directional spectrum is related to the second order continuum via a non-linear integral equation. The periodogram, based on a Fourier decomposition of radar data, is the standard method used to derive frequency spectra. Limitations in this approach, caused by inhomogeneities in the underlying ocean field, are investigated.

An instantaneous frequency technique is proposed in this thesis which mitigates the spectral distortion by demodulating the backscattered radar signals – a filtering procedure is developed which measures the temporally varying Bragg components. Alternative spectral techniques are analysed in order to validate the filter: an autoregressive parametric modelling approach and an eigendecomposition method. The filter is evaluated, using radar and in situ data, which establishes its potential for ocean remote sensing. Significant improvements in the quantity and accuracy of wave measurements are demonstrated. Properties and constraints of the filter are derived using simulated data. Finally, the generic structure of the extracted instantaneous frequency signals is investigated and related to oceanographic processes.

Acknowledgements

I would like to thank my supervisor, Lucy Wyatt, for her excellent guidance and patience. I am also grateful to a number of people who have contributed, directly or indirectly, to this work: Maureen Maltby, Lynda Harrison, Mari Bullock and Richard Balthazor from the Department of Applied Mathematics; Oli Johnson, Paul Harrington and Mark Bown for their assistance during the writing of this thesis; David Sharpe for his help during my years as an undergraduate student; Rose Player from the Proudman Oceanographic Laboratory; and the Natural Environment Research Council for funding my Ph.D.

A special mention must go to Jim Green – I have taken advantage of his immense mathematical and computing knowledge on countless occasions. However, I have yet to challenge him with a Linux question that he could not instantly answer.

Finally, I would like to thank my parents who have always supported and encouraged me in everything I have ever done. In addition, the proof reading of this thesis by my Dad was invaluable.

Hofstadter's Law: it always takes longer than you expect, even when you take into account Hofstadter's Law.

Douglas Hofstadter
(*Gödel, Escher, Bach*)

Contents

List of Figures

1 Introduction

> The basic law of the seaway is
> the apparent lack of any law.
>
> *(Rayleigh)*

The development of a universal mathematical foundation of oceanic hydrodynamics has proved an enigma for scientists. The complex topography and bathymetry inherent in coastal regions adds to the challenge of understanding littoral processes. Numerous methods to quantify this stochastic field have evolved although most conventional instruments, such as current meters and wave buoys, are limited to single point measurements.

High Frequency (HF) radar is an established technique that can provide a synoptic view of oceanic conditions at high temporal and spatial resolution. Transmitted electromagnetic waves interact with the ocean's surface and are modulated by Bragg resonant scattering. The Bragg mechanism, which is analogous to the diffraction of X-rays in crystals, causes a phase coherent addition in the signal from ocean wave trains with exactly half the radar wavelength. Barrick derived a mathematical relationship between these backscattered signals and ocean waves by modelling the sea surface as a linear superposition of infinite sinusoidal functions. A perturbation analysis yielded an expression for the spectral content of the radar signal: the dominant first order components contain information on surface currents; a non-linear integral equation relates the second order continuum to the ocean wave directional spectrum.

Oceanographic parameters are generated by transforming the backscattered radar signals into Doppler spectra. A software package has been developed at the University of Sheffield which extracts wave, current and wind information from these spectra. Multiple spatially separated radar sites are used to resolve directional ambiguities. Figure 1.1 shows current vectors generated from a deployment at Fedje in Norway. Figure 1.2 shows the spatial distribution of significant waveheight and mean wave direction from an experiment at Gijon in Spain. The maps illustrate the extensive coverage region achievable with HF radar. The data are interpolated onto a Cartesian grid which enables the evolving oceanic dynamics to be studied.

The standard technique used to form Doppler spectra is the periodogram which is based on a Fourier decomposition of the backscattered data into periodic trigonometric functions. The accuracy of the generated oceanic parameters is dependent on the precision of these spectral estimates. Temporal and spatial inhomogeneities within the radar measurement period have been identified as limiting factors in HF radar technology; compound first order structure creates distortion in Doppler spectra which constrains the quantity and quality of oceanographic measurements. Modern spectral analysis techniques have the potential to mitigate this problem – the work in this thesis is concerned with the development and evaluation of an alternative spectral method to the periodogram.

Instantaneous frequency has been conjectured as a mechanism for measuring the time varying characteristics of radar signals. Preliminary investigations have established the feasibility of a filtering approach to demodulate the backscattered data. This idea is validated and refined for use in HF radar oceanography. A significant improvement in the availability and accuracy of wave measurements is demonstrated. The structure of the

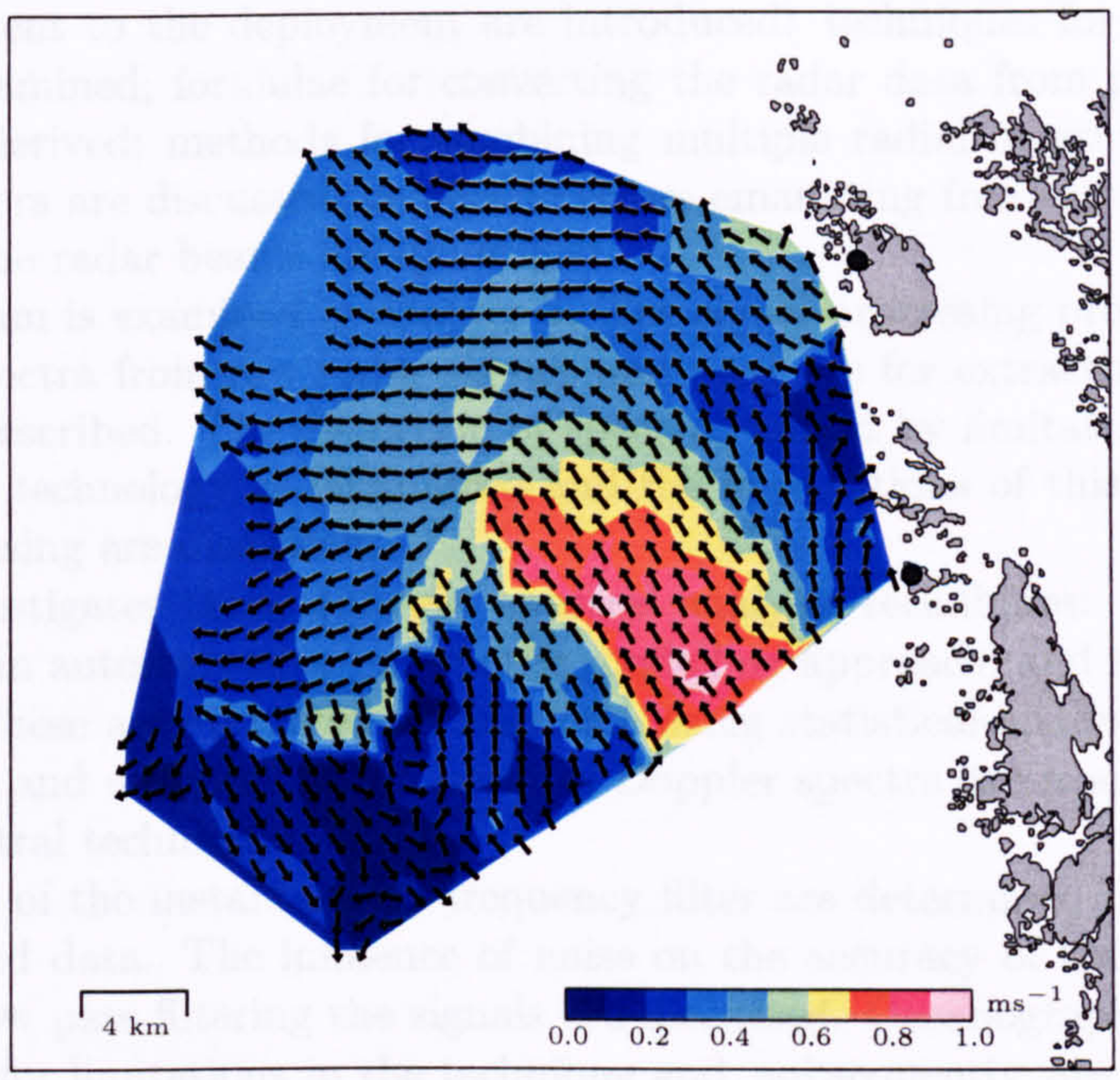

Figure 1.1: Map showing ocean current vectors derived from an HF radar system. Data taken from the Fedje deployment in Norway at 21:00, 16/03/2000.

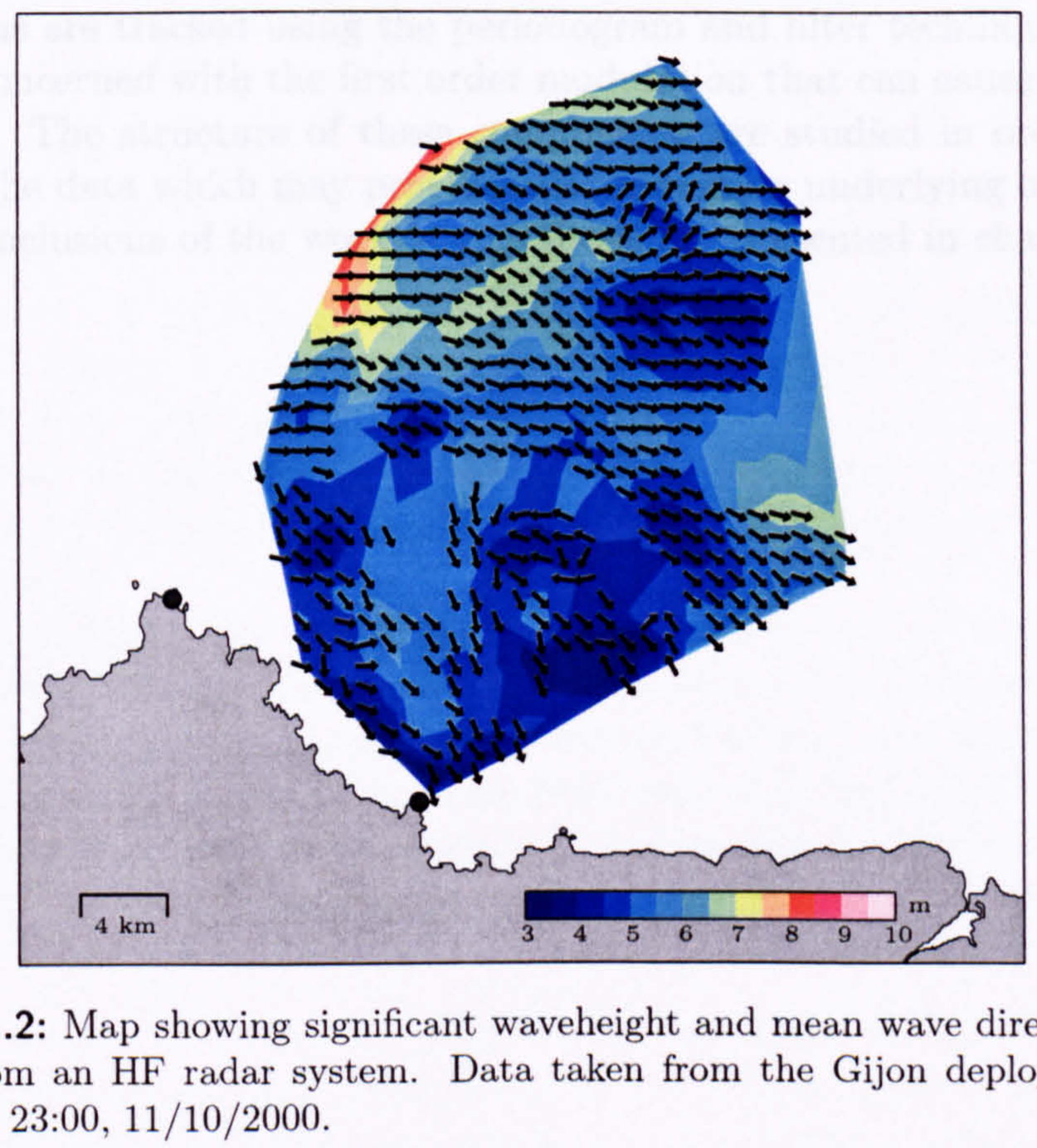

Figure 1.2: Map showing significant waveheight and mean wave direction derived from an HF radar system. Data taken from the Gijon deployment in Spain at 23:00, 11/10/2000.

first order modulation is examined and related to underlying oceanographic processes.

Chapter 2 presents an overview of HF radar systems. The configuration of the Holderness experiment, which provided the data used in this thesis, is described. Concepts and definitions pertinent to the deployment are introduced: techniques for resolving spatial resolution are examined; formulae for converting the radar data from polar to spherical coordinates are derived; methods for combining multiple radial measurements into two dimensional vectors are discussed; geometric errors emanating from extreme intersection angles between the radar beams are quantified.

The periodogram is examined in chapter 3. The signal processing procedure for generating Doppler spectra from raw radar signals and methods for extracting oceanographic parameters are described. The distortion of spectra, caused by limitations in the resolution of HF radar technology, is introduced and the implications of this phenomenon for ocean remote sensing are discussed.

Chapter 4 investigates three different spectral analysis techniques: an instantaneous frequency filter; an autoregressive parametric modelling approach; and an eigendecomposition method. These are evaluated in chapter 5 using statistical analysis. Data from an S4 current meter and an invariant property of Doppler spectra are examined in order to validate the spectral techniques.

The properties of the instantaneous frequency filter are determined in chapter 6 using real and simulated data. The influence of noise on the accuracy of the method and the implications of low pass filtering the signals are discussed. Oceanographic conditions are modelled to test for limitations in the technique and, subsequently, are used to ascertain the optimum filter bandwidth parameters.

Ocean wave measurements are investigated in chapter 7 and compared with data from a directional waverider. The development of the wave spectra during periods of dynamic oceanic conditions are tracked using the periodogram and filter techniques.

Chapter 8 is concerned with the first order modulation that can cause distortion in the Doppler spectra. The structure of these components are studied in order to determine any patterns in the data which may provide information on underlying oceanic processes.

The overall conclusions of the work in this thesis are presented in chapter 9.

2 High Frequency Radar

High Frequency (HF) radar is a remote sensing tool with the capability to measure oceanographic parameters. The spectral content of scattered radio waves from the ocean's surface can be analysed to derive current, wave and wind information. This chapter examines HF radar technology:

- A synopsis of HF radar systems is given.
- Contrasting spatial resolution techniques are described.
- Radar data from the SCAWVEX Holderness deployment are introduced.
- The conversion of spatial data from polar to spherical coordinates is derived.
- Geometric properties of dual radar systems are investigated.

2.1 Historical Review

Radar systems were originally developed in order to identify and track targets, such as ships and aircraft, for military applications [30]. During World War II, radar operating in the HF band of the electromagnetic spectrum was used to create ocean maps identifying the positions of enemy ships. Backscattered signals from the ocean surface were first reported during this period but were characterized as clutter since they often hindered the detection of military targets.

This phenomenon was subsequently studied by scientists and, in 1955, Crombie [10] established a relationship between scattering radio waves in the HF spectral band and ocean surface waves. A 13 MHz, vertically polarized radar that measured the Doppler shifts of reflected signals from the ocean surface was deployed in New Zealand. The recorded Doppler shifts were predominantly concentrated around two distinct frequencies which corresponded to the velocities of ocean wave trains with exactly half the radar wavelength travelling towards and away from the radar. This process is known as Bragg resonant scattering.

In 1972, development of this idea by Barrick [2] led to the formation of a quantitative relationship between backscattered signals from the sea surface and the ocean wave spectrum. In recent years, this technology has been used extensively throughout the world to measure oceanographic parameters. The development of sophisticated signal processing methods means that HF radar provides a unique opportunity to measure oceanic conditions at high resolution over a large spatial area.

2.2 HF Radar Systems

HF radar systems can be divided into two categories: skywave and groundwave radars – depending upon the propagation path of the transmitted signal [30]. Skywave radars transmit radio waves which are refracted by the ionosphere before reaching their target. The maximum achievable range is of the order of thousands of kilometres but the backscattered signal suffers from ionospheric contamination and can be difficult to interpret. The work in this thesis concentrates on groundwave propagation; electromagnetic waves travel along the curvature of the earth, beyond the horizon, achieving maximum ranges of the order of hundreds of kilometres.

HF radars span the 3-30 MHz band of the electromagnetic spectrum, generating decametric wavelengths. The frequency, f, and wavelength, λ, of a radar signal are related by the equation

$$\lambda = c/f, \tag{2.1}$$

where c represents the speed of light. Radars transmit radio waves which are reflected by ocean waves and any other surface with which they interact. Some of this energy is reflected back towards the radar where the receiver calculates its phase and amplitude components. The backscattered signal is modulated by the dynamics of the ocean waves. The frequency shift of a signal caused by the motion of a target is called the Doppler shift effect. This offset, Δf, is related to the velocity of the target by

$$\Delta f = 2v_r/\lambda, \tag{2.2}$$

where v_r is the component of the target velocity acting towards the radar. Measurements of oceanographic parameters in a radial direction from the radar can be derived from the Doppler shifted signal. The signal processing techniques required to generate oceanic parameters from the radar signal are described in the following chapters.

The first commercial system to utilise the ocean sensing potential of HF radar was the CODAR: an acronym for Coastal Ocean Dynamics Applications Radar. CODAR was introduced by Barrick in the USA and was originally designed for mapping surface current fields [4]. Refinement of the CODAR design in the 1990's led to the evolution of the SeaSonde radar. The omnidirectional capability of the antennae configuration maximises the ocean coverage region.

The Ocean Surface Current Radar (OSCR) was introduced by the SERC Rutherford/Appleton laboratory and Marex/Marconi in the UK and can operate in either the HF or the VHF frequency band. The system uses phased array technology to steer the radar beam to a specific direction. The University of Hamburg subsequently developed the Wellen Radar (WERA) which was designed to provide a larger working range and more flexible range resolution than the OSCR system [19].

Other groundwave systems have been demonstrated throughout the world: the LSEET radar was developed by the University of Toulon and operates in the VHF band of the electromagnetic spectrum; the SeaWatcher is a Japanese radar marketed by Kokusai Kogyo which operates at a frequency of 42 MHz; the American HiFAR radar system is a joint development between Metratek, the University of Michigan and the University of Miami, which can utilise multiple operating frequencies to measure vertical current shear; the Pisces radar was developed by Neptune Radar Ltd from a University of Birmingham prototype and operates at a lower radio frequency to provide long range wave and current measurements.

2.3 Spatial Resolution

The main distinguishing properties of HF radar systems concern the technology that is used to isolate the target patch of the ocean. All systems operate by the same scattering principle but there are distinct differences in methods for resolving spatial position from the backscattered signal. These can be divided into techniques for determining the range and direction relative to the radar site.

2.3.1 Range Resolution

Range can be calculated in the time domain using Continuous Wave (CW) pulses. The time delay, t, between transmitting the pulse and receiving the echo determines the range of the target

$$r = ct/2. \tag{2.3}$$

The advantage of this technique is the relatively simple design. However, range resolution is dependent on the length of the transmitted pulse. To obtain high resolution the pulse length must be short (in order to increase the signal bandwidth) but this consequently causes a decrease in the average transmitted power. The resultant attenuation of signal-to-noise ratio in the received signal limits the achievable range [45]. CW signal processing is used in the OSCR system.

An alternative approach involves calculating range in the frequency domain using Frequency Modulated Continuous Wave (FMCW) chirps [18]. The transmitted signal is defined as

$$x(t) = \sin\left[2\pi\left(f_0 + \frac{bt}{2T}\right)t\right], \tag{2.4}$$

where T is the chirp length and b represents the bandwidth. The frequency representation of $x(t)$ increases linearly during transmission.

$$f(t) = f_0 + \frac{bt}{T} \tag{2.5}$$

The received signal is a superposition of scattered electromagnetic waves from a myriad of different locations on the ocean's surface.

$$y(t) = \int \alpha(\tau)\sin\left[2\pi\left(f_0 + \frac{b(t-\tau)}{2T}\right)(t-\tau) + \phi(\tau)\right]\mathrm{d}\tau \tag{2.6}$$

τ represents the elapsed time from data transmission to receiving the reflected signal and provides a measure of the range of the target waves. $\alpha(\tau)$ and $\phi(\tau)$ represent the amplitude and phase of the signal at time τ respectively: stationarity is assumed during the chirp period. Range is determined using Fourier analysis by calculating the frequency shift between the transmitted signal and received echo [19].

FMCW techniques were developed by the University of Hamburg for use in the WERA system. The range resolution is related to the bandwidth of the transmitted chirp. The transmitter and receiver design must enable extreme dynamic range and linearity in order to distinguish between high energy signals from near ranges and low energy signals from far ranges. Frequency Modulated Interrupted Continuous Wave (FMICW) chirps can be used to avoid signal interference and enable the transmit and receive antenna to be located together. FMICW processing is used in the Pisces and SeaSonde systems.

2.3.2 Azimuthal Resolution

The angular distribution of backscattered electromagnetic signals can be determined using Direction Finding (DF) techniques. The DF algorithm is based on the assumption that signals representing distinct radial speeds arrive from different directions at the receive antenna array. Analysis in the frequency domain determines complex Fourier coefficients from the time series at each antenna: these are attributed to different radial speeds. Azimuth is computed by measuring the phase differences between the echoes arriving at each antenna. These differences are then fitted to a theoretical function of angle [18].

The method can be easily implemented in coastal areas as a small antenna array is used. The original CODAR system used the DF algorithm with a square four-element antenna configuration [27]. The SeaSonde employs an eigendecomposition method to resolve the angle of the incoming signal: a MUSIC algorithm is applied to the complex voltages measured at three co-located directional receive antennae [3]. To avoid directional ambiguities, the spacing between the antenna elements must not exceed half the radar wavelength. The main disadvantage of direction finding is that sea state information cannot be extracted easily because the second order portion of the spectrum is obscured by the first order signals from other directions. The DF technique assumes a unique correspondence between radial speed and direction but empirical evidence suggests this may be invalid in very inhomogeneous ocean current fields [19].

Beamforming (BF) techniques utilise a linear array of identical receiving elements to determine direction in the time domain [45]. A beam to a specific direction is generated from the summation of weighted and phase shifted signals from each antenna. The weighting function suppresses side lobes and the phase shift steers the beam to the required direction. The optimum configuration consists of a linear array aligned perpendicular to the principal receive direction with adjacent elements separated by half the radar wavelength. The width of the generated beam is related to the length of the receive array; the spatial requirements are significantly higher for phased array systems than for compact direction finding antennas. The angular resolution of a linear receive array of length l metres is approximately λ/l radians [19].

The OSCR and PISCES radars employ beamforming techniques whilst the WERA system can be configured to use either beamforming or direction finding methods. The advantage of beamforming is that the beams are steered to a specific direction which enables wave information to be extracted from the second order continuum in the Doppler spectra.

2.4 HF Radar Data

2.4.1 SCAWVEX Holderness

The HF radar data investigated in this thesis are taken from the SCAWVEX (Surface Current And Wave Variability EXperiment) deployment at Holderness in the winter of 1995/96. This data set was used, in preference to more recent experiments, since prolonged time periods of raw data were available for analysis. Figure 2.1 illustrates the radar configuration and the local topography in the Holderness region. The project was run in collaboration with the University of Sheffield and the Proudman Oceanographic Laboratory. The primary objective of SCAWVEX was to measure the spatial and temporal variability of oceanographic parameters in coastal regions.

The Holderness area is characterised by severe erosion and the location was chosen to monitor the contributing factors to sediment transport in the region; the littoral hy-

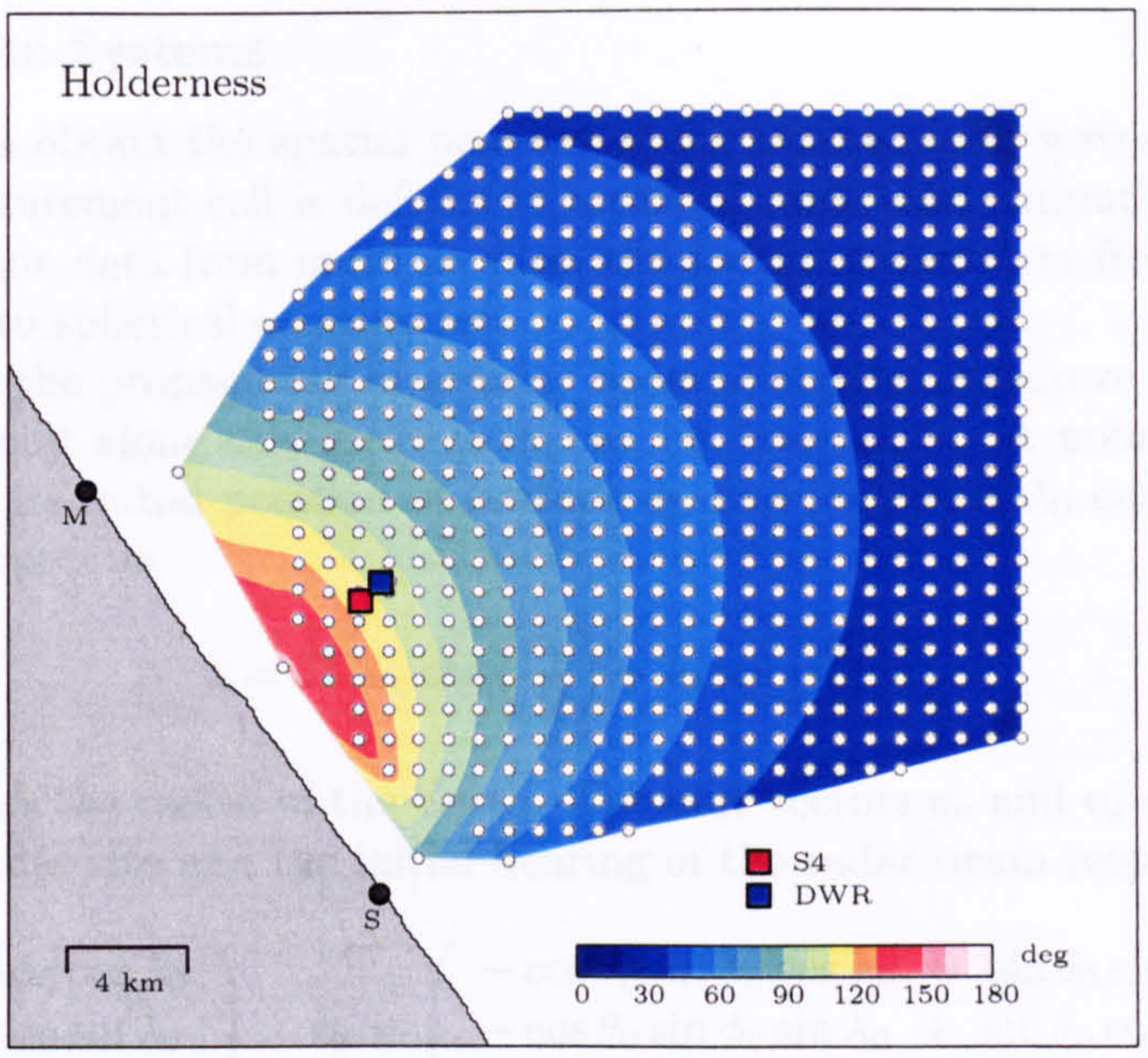

Figure 2.1: The spatial configuration of the Holderness deployment showing the intersection angles between the radar beams. The master and slave OSCR sites are represented by M and S respectively. The locations of a current meter (S4) and a directional waverider (DWR) are shown.

drodynamics are dominated by a strong tidal current regime. An OSCR (Ocean Surface Current Radar) system was deployed on the north-east coastline of the UK. Over a period of one month, between December 1995 and January 1996, a total of 433 hours of data were recorded with range extending to approximately 40 km offshore. The backscattered data were interpolated onto a Cartesian measurement grid with 1.2 km spatial resolution. At each of the 565 grid points, radar data were processed into radial and vector oceanographic parameters using the techniques described in the following chapters.

The OSCR system comprised of two radars, termed master and slave, positioned approximately 15 km apart on the coastline. The angles between the intersecting beams at each grid cell are shown in figure 2.1. Each radar site consisted of a Yagi transmit antenna, a 16 element linear receive array and a PDP11 DEC processor. Spatial resolution was achieved in the time domain using the techniques described in section 2.3: range gating was performed using continuous wave pulses; angular resolution was obtained using beamforming techniques. The radars operated at a frequency of 25.4 MHz which corresponds to a transmission radio wavelength of 11.8031 m. Each unit made independent measurements sequentially in order to avoid signal interference. Measurements of five minutes duration were made alternately every twenty minutes to produce the raw backscattered data. The remaining ten minutes of the twenty minute measurement cycle were used for processing the received signal. The raw backscattered signal generated from the radar sites during each measurement period consisted of 896 samples separated by a sampling interval of 0.3289 seconds.

Data from a current meter (S4) and a directional waverider (DWR) are used in later chapters to validate the radar measurements. The locations of these in situ instruments are shown in figure 2.1.

2.4.2 Coordinate Systems

HF radar systems obtain the spatial position of the target ocean waves in polar coordinates. Each measurement cell is defined in terms of range and azimuth from the radar. In order to combine data from multiple sites, the spatial parameters from each radar are first converted into spherical coordinates.

By considering the propagation of a radar beam along the curvature of the Earth, the position $\mathbf{x}$ of a point along this great circle can be determined. A point at range r_i and direction θ_i from its initial position of latitude ϕ_0 and longitude λ_0 can be expressed in Cartesian coordinates as

$$\mathbf{x} = R\left[\mathbf{e_c}\cos\left(\frac{r_i}{R}\right) + \mathbf{e_s}\sin\left(\frac{r_i}{R}\right)\right], \tag{2.7}$$

where R represents the radius of the Earth. The unit vectors $\mathbf{e_c}$ and $\mathbf{e_s}$ correspond to the position of the radar site and the initial bearing of the radar beam respectively.

$$\mathbf{e_c} = \begin{pmatrix} \cos\phi_0\cos\lambda_0 \\ \cos\phi_0\sin\lambda_0 \\ \sin\phi_0 \end{pmatrix}, \quad \mathbf{e_s} = \begin{pmatrix} -\cos\theta_0\sin\phi_0\cos\lambda_0 - \sin\theta_0\sin\lambda_0 \\ -\cos\theta_0\sin\phi_0\sin\lambda_0 + \sin\theta_0\cos\lambda_0 \\ \cos\theta_0\cos\phi_0 \end{pmatrix} \tag{2.8}$$

The latitude ϕ_x and longitude λ_x of this new position can be determined by writing $\mathbf{x}$ in spherical coordinates.

$$\mathbf{x} = \begin{pmatrix} \cos\phi_x\cos\lambda_x \\ \cos\phi_x\sin\lambda_x \\ \sin\phi_x \end{pmatrix} \tag{2.9}$$

As the radar beam moves along the curvature of the Earth's surface, the bearing (relative to north) at each range gate along this beam changes. The local direction $\mathbf{y}$ is calculated by differentiating equation 2.7.

$$\mathbf{y} = \mathbf{e_s}\cos\left(\frac{r_i}{R}\right) - \mathbf{e_c}\sin\left(\frac{r_i}{R}\right) \tag{2.10}$$

The local bearing ϵ_i is then determined using scalar products

$$\cos\epsilon_i = \mathbf{e_n}.\mathbf{y}, \quad \sin\epsilon_i = \mathbf{e_p}.\mathbf{y}, \tag{2.11}$$

where $\mathbf{e_n}$ and $\mathbf{e_p}$ are the local northward and eastward unit vectors respectively.

$$\mathbf{e_n} = \begin{pmatrix} -\sin\phi_x\cos\lambda_x \\ -\sin\phi_x\sin\lambda_x \\ \cos\phi_x \end{pmatrix}, \quad \mathbf{e_p} = \begin{pmatrix} -\sin\lambda_x \\ \cos\lambda_x \\ 0 \end{pmatrix} \tag{2.12}$$

2.4.3 Geometric Configuration

HF radars measure ocean surface currents in a radial direction. The corresponding two-dimensional spatial structure can be derived by combining radials emanating from multiple radar sites to form vectors. Each radial component R_i has an associated magnitude r_i and direction θ_i where the direction is measured clockwise from north. The radials contains information about the underlying vector and can be expressed in terms of the east and north components Λ_e, Λ_n of this vector.

$$r_i = \Lambda_e \sin\theta_i + \Lambda_n \cos\theta_i \tag{2.13}$$

For N radial measurements the system of equations to be solved can be written in matrix form.

$$\begin{pmatrix} \sin\theta_1 & \cos\theta_1 \\ \vdots & \vdots \\ \sin\theta_N & \cos\theta_N \end{pmatrix} \begin{pmatrix} \Lambda_e \\ \Lambda_n \end{pmatrix} = \begin{pmatrix} r_1 \\ \vdots \\ r_N \end{pmatrix} \tag{2.14}$$

For $N > 2$, the system is an over-determined linear least squares problem which can be solved by Singular Value Decomposition (SVD). A modified form of this equation is used

$$\begin{pmatrix} \frac{\sin\theta_1}{\epsilon_1} & \frac{\sin\theta_1}{\epsilon_1} \\ \vdots & \vdots \\ \frac{\sin\theta_N}{\epsilon_N} & \frac{\cos\theta_N}{\epsilon_N} \end{pmatrix} \begin{pmatrix} \Lambda_e \\ \Lambda_n \end{pmatrix} = \begin{pmatrix} \frac{r_1}{\epsilon_1} \\ \vdots \\ \frac{r_N}{\epsilon_N} \end{pmatrix}, \tag{2.15}$$

where ϵ_i is the error term associated with the radial component r_i. The system is in the form $\mathbf{Ax} = \mathbf{b}$ where A is the Design Matrix of the problem [40]. Using SVD, the matrix A can be expressed as the product of three constituent matrices.

$$\mathrm{A} = \mathrm{UWV}^{\mathrm{T}} \tag{2.16}$$

U is an $N \times 2$ column-orthogonal matrix, V is a 2×2 orthogonal matrix and W is a 2×2 diagonal matrix. The function ς^2 is minimised.

$$\varsigma^2 = |\mathbf{Ax} - \mathbf{b}|^2 \tag{2.17}$$

The solution to this problem is

$$\mathbf{x} = \mathrm{V}\left[\mathrm{diag}\left(\frac{1}{\omega_j}\right)\right]\left(\mathrm{U}^{\mathrm{T}}\mathbf{b}\right). \tag{2.18}$$

If $N = 2$, equation 2.14 can be solved directly to provide the orthogonal components of the vector. The OSCR system deployed in the Holderness experiment used two spatially separated radars to measure the same patch of ocean from different directions; radial data from the master and slave sites were combined to generate vectors.

$$\Lambda_e = \frac{r_2\cos\theta_1 - r_1\cos\theta_2}{\sin(\theta_2 - \theta_1)} \tag{2.19}$$

$$\Lambda_n = \frac{r_2\sin\theta_1 - r_1\sin\theta_2}{\sin(\theta_1 - \theta_2)} \tag{2.20}$$

The accuracy of each resolved two-dimensional vector is dependent on the measurement errors in each radial and the intersection angle between the overlapping radar beams. The precision of each radial component can be attributed to numerous factors: the intrinsic

resolution of the radar; atmospheric and system noise; limitations in the spectral analysis processing; and calibration errors in the radar system [16]. The sources of radial error pertinent to the Holderness experiment are examined in later chapters.

The Geometric Dilution of Precision (GDOP) is an established technique used to describe the geometrical constraints of HF radar systems. The GDOP technique was developed from Global Positioning System (GPS) technology and provides an indicator of the geometric errors in terms of the intersection angle between the radar beams [8]. The vector components parallel, Λ_p, and normal, Λ_l, to the intersecting radials are

$$\Lambda_p = \frac{r_1 + r_2}{2\cos\theta}, \qquad \Lambda_l = \frac{r_1 - r_2}{2\sin\theta}, \tag{2.21}$$

where $2\theta = \theta_2 - \theta_1$ is the angle between the radar beams. These can be rotated to provide alternative expressions for the vector components given in equations 2.19 and 2.20

$$\Lambda_e = \Lambda_p \sin\alpha - \Lambda_l \cos\alpha, \tag{2.22}$$

$$\Lambda_n = \Lambda_p \cos\alpha + \Lambda_l \sin\alpha, \tag{2.23}$$

where $\alpha = (\theta_1 + \theta_2)/2$ represents the bisecting angle of the two radials. Substitution yields

$$\Lambda_e = \left(\frac{\sin\alpha}{2\cos\theta} - \frac{\cos\alpha}{2\sin\theta}\right) r_1 + \left(\frac{\sin\alpha}{2\cos\theta} + \frac{\cos\alpha}{2\sin\theta}\right) r_2, \tag{2.24}$$

$$\Lambda_n = \left(\frac{\cos\alpha}{2\cos\theta} + \frac{\sin\alpha}{2\sin\theta}\right) r_1 + \left(\frac{\cos\alpha}{2\cos\theta} - \frac{\sin\alpha}{2\sin\theta}\right) r_2. \tag{2.25}$$

Under the assumption that the radial errors emanating from the master and slave sites are identical ($\varepsilon_1 = \varepsilon_2 = \varepsilon$), the errors in the east and north orthogonal components can be written as

$$\varepsilon_e = \left\{2\left(\frac{\sin^2\alpha\sin^2\theta + \cos^2\alpha\cos^2\theta}{\sin^2(2\theta)}\right)\right\}^{\frac{1}{2}} \varepsilon, \tag{2.26}$$

$$\varepsilon_n = \left\{2\left(\frac{\cos^2\alpha\sin^2\theta + \sin^2\alpha\cos^2\theta}{\sin^2(2\theta)}\right)\right\}^{\frac{1}{2}} \varepsilon. \tag{2.27}$$

The ratios

$$\mathrm{GDOP_e} = \varepsilon_e/\varepsilon, \qquad \mathrm{GDOP_n} = \varepsilon_n/\varepsilon, \tag{2.28}$$

are the east and north GDOP values respectively and represent the multipliers of the radial errors associated with the geometric configuration.

Figure 2.2 shows the GDOP values in the Holderness region. As the angle between the radar beams becomes extreme, the vector errors are amplified since the denominator in equations 2.26 and 2.27 approaches zero. In general, vectors are only resolved from radial components when the intersection angle lies in the range $20 \leq \alpha \leq 160$ [16].

Near the coastline between the two radar sites, the radials are measuring the underlying vector in the same direction which causes errors perpendicular to the baseline. At the north and east boundaries of the grid, the intersection angles between the radar beams are acute. The errors in the $\mathrm{GDOP_e}$ and $\mathrm{GDOP_n}$ components increase towards the northern and eastern edges respectively. These regions may also be corrupted by noise since the backscattered signal strength attenuates with range.

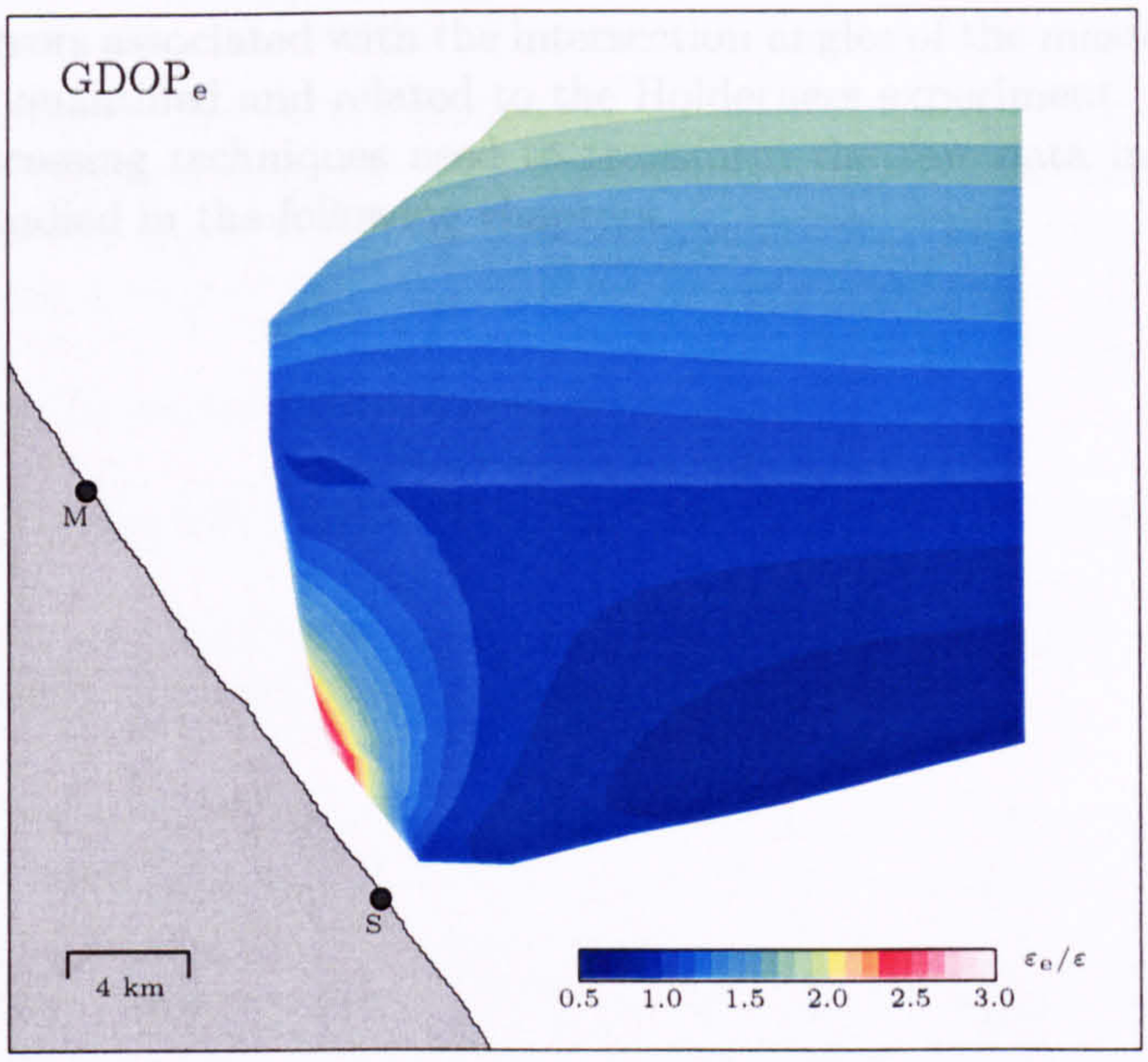

Figure 2.2: GDOP values in the Holderness region.

2.5 Summary

A general overview of HF radar has been provided in this chapter. The spatial configuration of the Holderness deployment and the format of the OSCR data were described. Formulae for converting data between polar and spherical coordinate systems have been derived. Methods to determine two dimensional vectors from radial measurements were examined. The errors associated with the intersection angles of the master and slave radar beams have been quantified and related to the Holderness experiment.

The signal processing techniques used to transform the raw data into oceanographic parameters are studied in the following chapters.

3 Doppler Spectra

Radar backscatter from the ocean surface is interpreted by transforming the received signals into frequency spectra, called Doppler spectra. The study of the frequency domain content of a time series signal is known as spectral analysis. This chapter investigates the structure of Doppler spectra:

- The periodogram signal processing is examined.
- Techniques for extracting oceanographic parameters are introduced.
- The distortion of spectra caused by the inherent temporal and spatial resolution constraints of HF radar technology is described.

3.1 Periodogram

3.1.1 Historical Review

The origins of modern spectral estimation began with the scientist Isaac Newton in the 17th century [35]. He observed the diffraction of light, into a band of different colours, when passed through a glass prism. Newton discovered that white light contains all wavelengths and introduced the word spectrum to represent this phenomenon. In the following centuries, work by mathematicians Daniel Bernoulli [5] and Joseph Fourier [14] extended this theory to the solution of wave equations. In 1822, Fourier deduced that any arbitrary periodic function can be represented by an infinite sum of harmonic terms. The Fourier series of a function $x(t)$ is defined as

$$x(t) = \frac{a_0}{2} + \sum_{n=1}^{\infty} \{a_n \cos(nt) + b_n \sin(nt)\}, \tag{3.1}$$

where

$$\begin{aligned} a_0 &= \frac{1}{\pi}\int_{-\pi}^{\pi} x(t)\,\mathrm{d}t, \\ a_n &= \frac{1}{\pi}\int_{-\pi}^{\pi} x(t)\cos(nt)\,\mathrm{d}t, \\ b_n &= \frac{1}{\pi}\int_{-\pi}^{\pi} x(t)\sin(nt)\,\mathrm{d}t. \end{aligned} \tag{3.2}$$

In the 19th century, calculating machines were built to determine Fourier coefficients for practical applications such as tidal prediction. A generalised form of the complex Fourier series as $n \longrightarrow \infty$ was subsequently introduced – this was called the Fourier Transform. In 1898, Schuster [41] suggested plotting the squared envelope of the Fourier transform coefficients over a range of frequencies. This method, known as the periodogram, forms the basis of the spectral estimation technique used in HF radar oceanography.

3.1.2 HF Radar Signal Processing

The periodogram was used during the Holderness deployment to transform raw radar data into Doppler spectra. Each OSCR unit measured ocean backscatter at 565 cells on a regular grid. The signal at each of these grid cells, $x(nT)$, consists of N (896) complex data points separated by a sampling interval of T (0.3289) seconds.

The raw data are partitioned into four overlapping segments, each containing M (512) samples. The objective of this procedure is to increase the number of data sets which, when averaged, will reduce the variance in the generated Doppler spectrum. Consecutive segments exhibit a 75% overlap which corresponds to a shift of ϕ (128) data samples. Each segment ($0 \leq k < 4$) is processed separately into a spectrum and then averaged to produce the final periodogram.

$$x^{(k)}(nT) = x((n + \phi k)T) \qquad (0 \leq n < M) \tag{3.3}$$

Processing a truncated and discretely sampled time signal can cause spectral leakage in the frequency domain. Data windows are used to control the effect of sidelobes in spectral estimation [35]. A multiplicative weighting function, $w(nT)$, is applied to each segmented time signal.

$$y^{(k)}(nT) = w(nT)\, x^{(k)}(nT) \qquad (0 \leq n < M) \tag{3.4}$$

Window functions can be categorised according to their effect on the frequency response of a signal: the half-power bandwidth statistic measures the mainlobe width which determines the frequency resolution; the peak sidelobe level and sidelobe decay rate provide an indication of the sidelobe response of the window. A Blackman-Harris function was chosen in the OSCR signal processing since its power spectrum exhibits low sidelobe levels (92 dB) below the main peak [20]. This mitigates the influence of leakage on the second order spectral components which is critical for ocean wave measurements. The window is defined as

$$w(nT) = \alpha_0 - \alpha_1 \cos\left(\frac{2\pi nT}{M}\right) + \alpha_2 \cos\left(\frac{4\pi nT}{M}\right) - \alpha_3 \cos\left(\frac{6\pi nT}{M}\right), \tag{3.5}$$

where

$$(\alpha_0, \alpha_1, \alpha_2, \alpha_3) = (0.35875, 0.48829, 0.14128, 0.01168). \tag{3.6}$$

Fourier Transforms are the mathematical foundation for relating a time signal to its frequency domain representation. A Discrete Fourier Transform (DFT) is applied to each windowed segment.

$$Y^{(k)}\left(\frac{2\pi m}{MT}\right) = \sum_{n=0}^{M-1} y^{(k)}(nT) \exp\left\{\frac{-2\pi imn}{M}\right\} \qquad (0 \leq m < M) \tag{3.7}$$

A Fast Fourier Transform (FFT) algorithm is used to speed up this procedure since the number of data samples, M, is a power of two [40]. The final periodogram, representing the distribution of power as a function of frequency, is formed from the averaged magnitude of the four spectral segments.

$$P\left(\frac{2\pi m}{MT}\right) = 10 \log_{10}\left[\frac{1}{4}\sum_{k=0}^{3}\left|Y^{(k)}\left(\frac{2\pi m}{MT}\right)\right|^2\right] \qquad (0 \leq m < M) \tag{3.8}$$

In order to make comparisons between different data sets, the spectra are normalised, with respect to the largest power value, so that the dominant peak occurs at 0 dB. Figure 3.1 shows a periodogram, known as a Doppler spectrum, generated from Holderness data. Measurements of oceanographic parameters can be derived from the first and second order components in this spectrum.

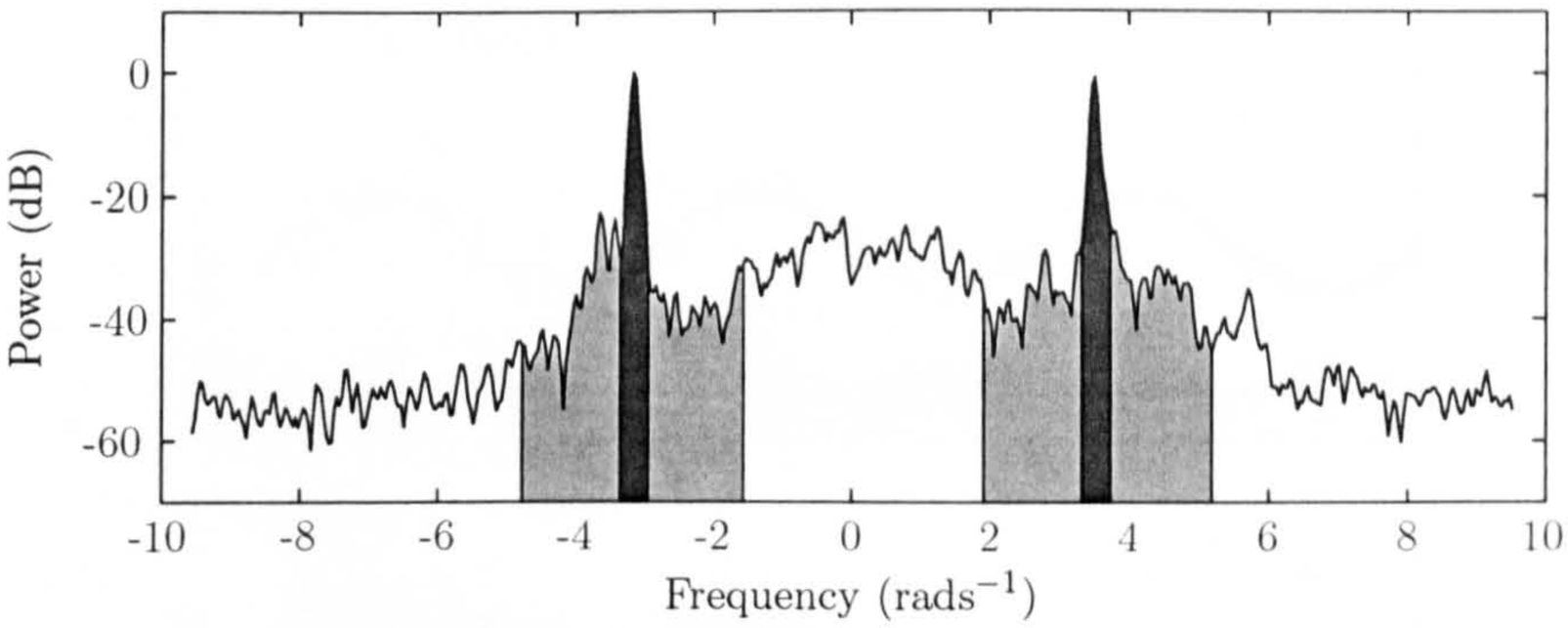

Figure 3.1: Doppler spectrum showing the first order (dark) and second order (light) components. Data taken from master site at 20:00, 08/12/95, cell 562.

3.2 First Order Spectra

Each Doppler spectrum represents a temporal and spatial average. The coherent integration time of each OSCR unit is approximately five minutes; the spatial resolution represents a region of about one square kilometre on the ocean surface.

Doppler spectra formed from ocean backscatter are characterised by two dominant first order lines. Figure 3.1 illustrates these components, known as Bragg peaks, which are positioned roughly symmetrically around zero frequency. Radial components of ocean surface currents are derived by identifying the frequency locations of the Bragg peaks in Doppler spectra. This section examines the cause of the first order structure and discusses current measurement techniques.

3.2.1 Scattering Theory

HF radar signals reflected by the ocean's surface are influenced by Bragg resonant scattering. In 1955, Crombie [10] discovered that backscatter from the sea's surface was dominated by ocean wave trains, with exactly half the radar wavelength, propagating in a radial direction relative to the radar.

$$\lambda_{\mathrm{b}} = \frac{\lambda_{\mathrm{r}}}{2} \tag{3.9}$$

Transmitted electromagnetic signals from the radar reflect off all waves on the sea's surface but ocean waves that satisfy the Bragg relation cause a phase coherent addition in the backscattered signal. Figure 3.2 illustrates the Bragg scattering mechanism for ocean waves which is analogous to the diffraction of X-rays in crystals.

Barrick derived mathematically the interaction of HF radar with ocean waves [1],[33]. The ocean surface was modelled as a linear superposition of infinite waves. A perturbation analysis yielded an expression for the first order radar spectral cross section as a function of Doppler frequency shift ω and bearing angle ϕ.

$$\sigma_1(\omega, \phi) = 2^6 \pi k_0^4 \sum_{m=\pm 1} S(-2m\mathbf{k}_0)\delta(\omega - m\omega_{\mathrm{b}}) \tag{3.10}$$

$\mathbf{k}_0$ is the wave vector of the incident radar signal (with wavenumber k_0), S is the ocean wavenumber spectrum, ω_{b} is the Bragg frequency and m denotes the sign of the Doppler shift. σ_1 is expressed as a linear combination of dirac delta functions, δ, which imposes the Bragg resonance condition. The observed first order structure in Doppler spectra does not conform exactly to the theory. The Bragg peaks are broadened by non-linear interactions, current turbulence and system effects [33].

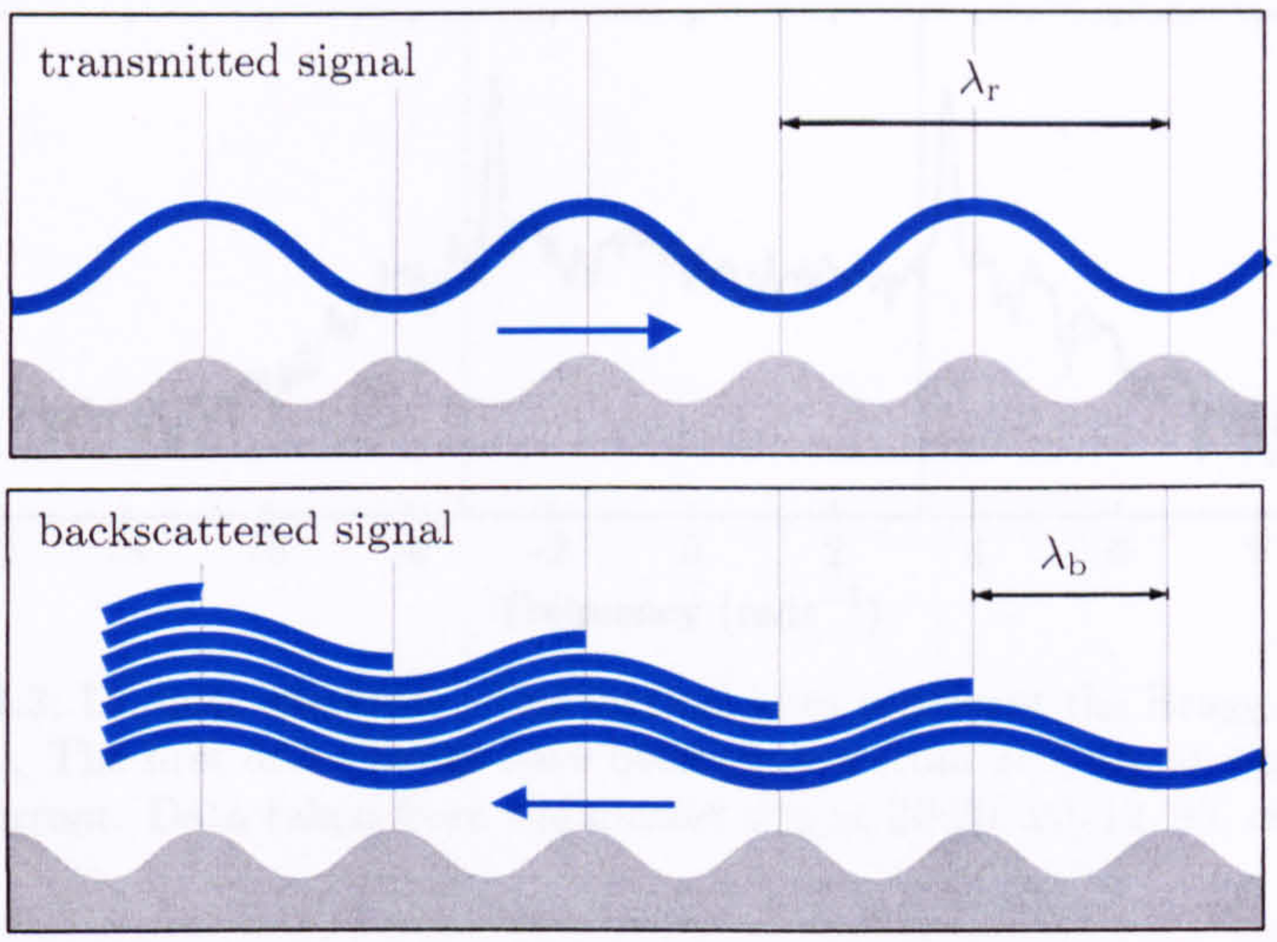

Figure 3.2: The Bragg scattering mechanism. Ocean waves, with exactly half the radar wavelength, create coherent addition in the reflected radar signal.

3.2.2 Current Measurements

HF radars measure surface current velocity components parallel to the direction of the radar beam. Radial components can be derived from the frequency locations of the first order Bragg peaks in Doppler spectra. These large peaks represent ocean wave trains, with wavelength λ_b, travelling directly towards and away from the radar. The phase velocity c_b of these Bragg waves is known from the gravity wave dispersion relationship

$$c_b = \pm\sqrt{\frac{g}{k_b}\tanh k_b h}, \tag{3.11}$$

where g is the acceleration due to gravity, h represents the water depth and k_b is the Bragg wave number.

$$k_b = \frac{2\pi}{\lambda_b} \tag{3.12}$$

A moving target modulates the frequency of the backscattered electromagnetic signal due to the Doppler shift effect. In the absence of an underlying surface current, the Bragg wave trains cause the power in the frequency domain to be shifted by $\pm\omega_b$ rads^{-1}.

$$\omega_b = \sqrt{g k_b \tanh k_b h} \tag{3.13}$$

The frequencies $+\omega_b$ and $-\omega_b$ represent the incoming and outgoing Bragg wave trains respectively. Figure 3.3 shows a Doppler spectrum from the Holderness deployment. The vertical lines, representing the Bragg frequencies, are at the exact theoretical location of the first order peaks if no surface current was present.

An underlying surface current with radial component u ms^{-1} towards the radar, causes an additional Doppler Shift, Δf rads^{-1}, in the spectrum.

$$\Delta f = \frac{2\pi u}{\lambda_b} \tag{3.14}$$

The accuracy of the radial components is dependent on the precision of identifying the current shift Δf. The simplest approach involves taking a point measurement from the maximum power values in the vicinity of the Bragg frequencies $\pm\omega_b$. This method is

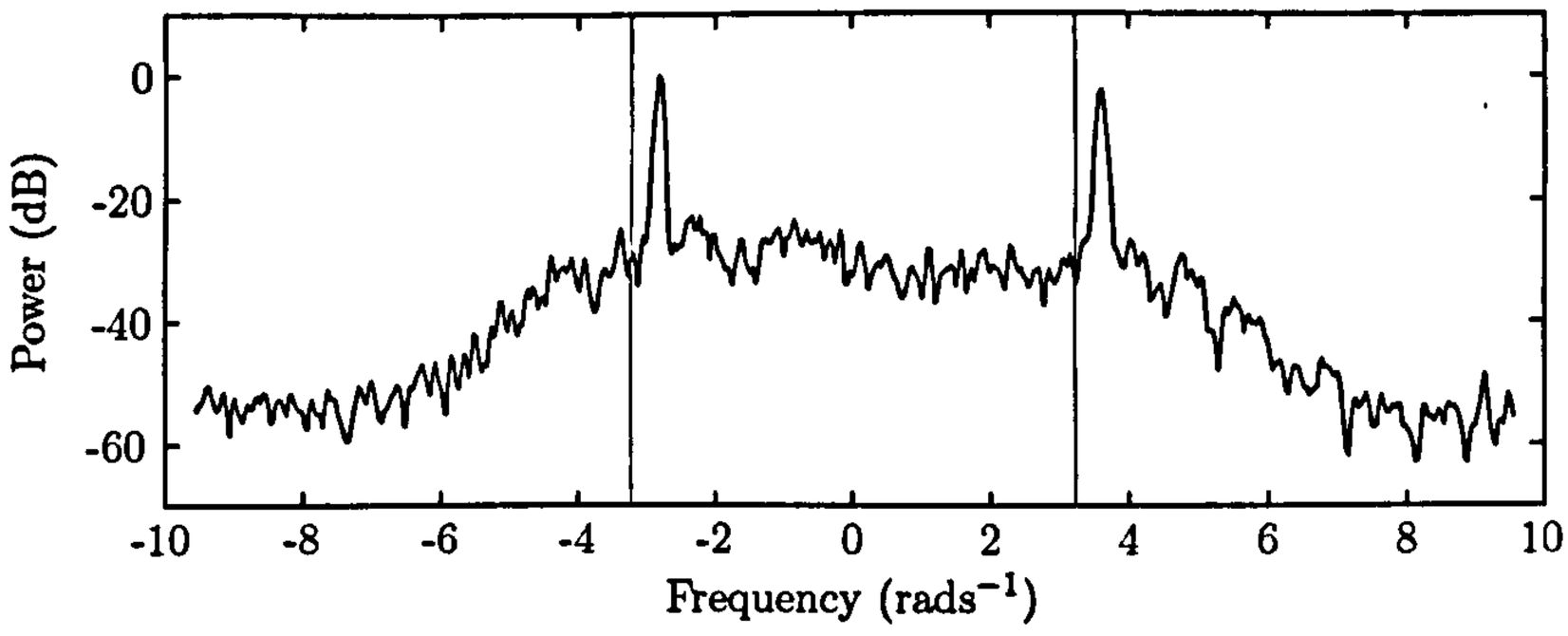

Figure 3.3: Doppler spectrum. The vertical lines represent the Bragg frequencies $\pm\omega_b$. The first order peaks have been shifted from $\pm\omega_b$ by an underlying ocean current. Data taken from the master site at 20:20, 20/12/95, cell 20.

limited by the discrete form of the data; truncation of the radar signal constrains the Doppler spectrum frequency range to $2\pi/T$ rads^{-1}. The frequency resolution of an N point discrete time signal is

$$\omega_{\text{res}} = \frac{2\pi}{NT}. \tag{3.15}$$

The radar system in the Holderness deployment operated at a frequency of 25.4 MHz, isolating Bragg ocean wave trains with $\lambda_b = 5.9016\,\text{m}$. The resolution of each OSCR unit corresponds to a current speed of approximately 0.02 ms^{-1}. Alternative methods to resolve the Bragg peaks include centroid and quadratic calculations. These approaches can reduce the intrinsic errors associated with the discrete data. The radial component of surface current is obtained from the observed frequency shift.

$$u = \frac{\Delta f \lambda_b}{2\pi} \tag{3.16}$$

Figure 3.4 shows Holderness maps which illustrate the radial current magnitudes generated from OSCR data on the 22nd December 1995. The radials have been formed using a centroid calculation on each Bragg peak. The gaps in radial coverage can be attributed to the quality criteria which are imposed on the Doppler spectra. Corruption of the spectra can be caused by numerous factors: atmospheric and system noise; ships; radio interference; oceanographic effects; a low signal-to-noise ratio in the backscattered signal.

The spatial structure of ocean currents can be resolved by combining radial data from multiple radar sites. In the Holderness deployment, current vectors were determined from master and slave radials using the formulae derived in section 2.4. Figure 3.5 shows current vectors produced from the radial components in figure 3.4. The map illustrates a time period midway through the tidal cycle, when the current field is uniform and propagating in a north-westerly direction, parallel to the coastline.

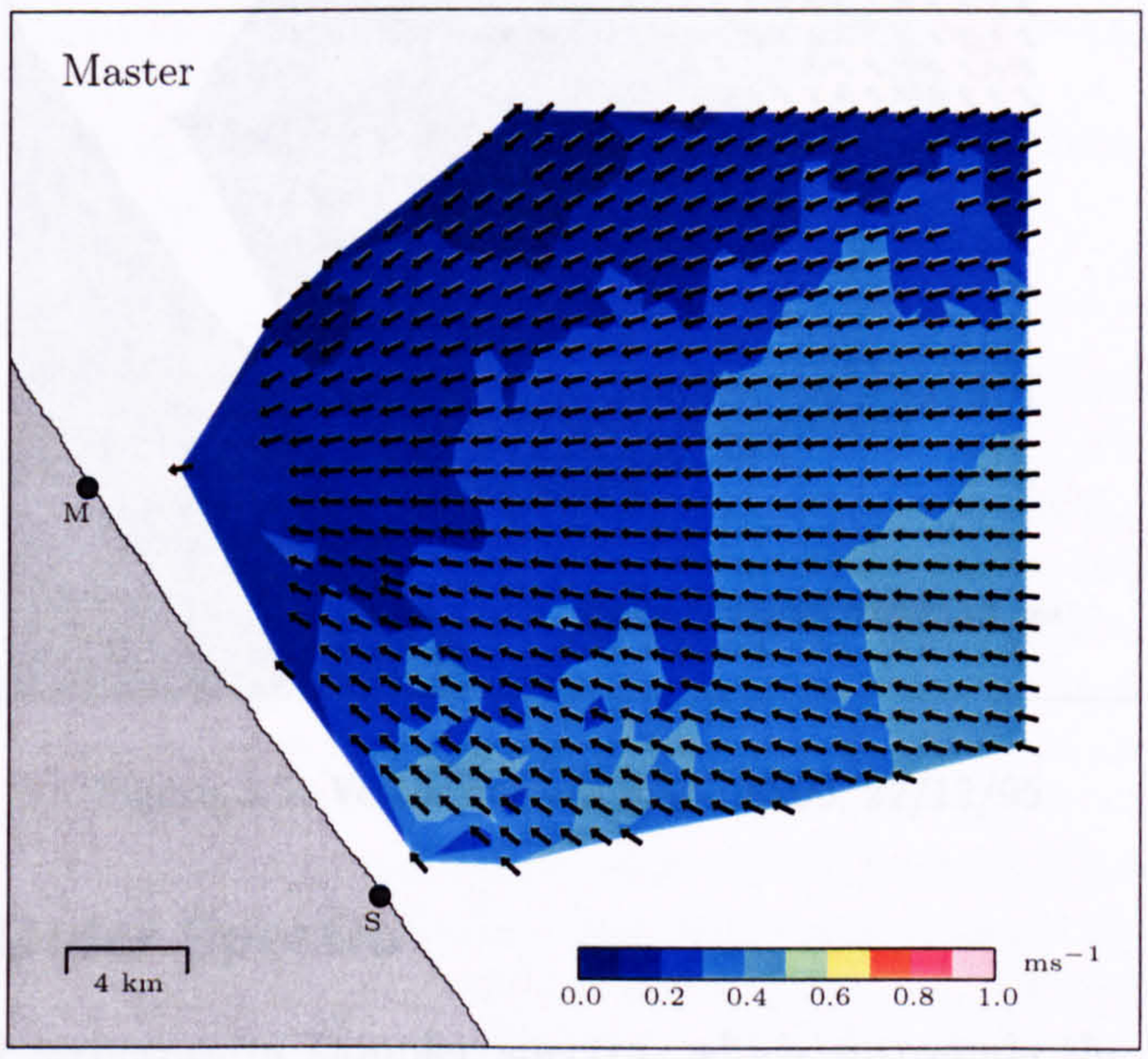

Figure 3.4: Radial current maps. 23:00, 22/12/95.

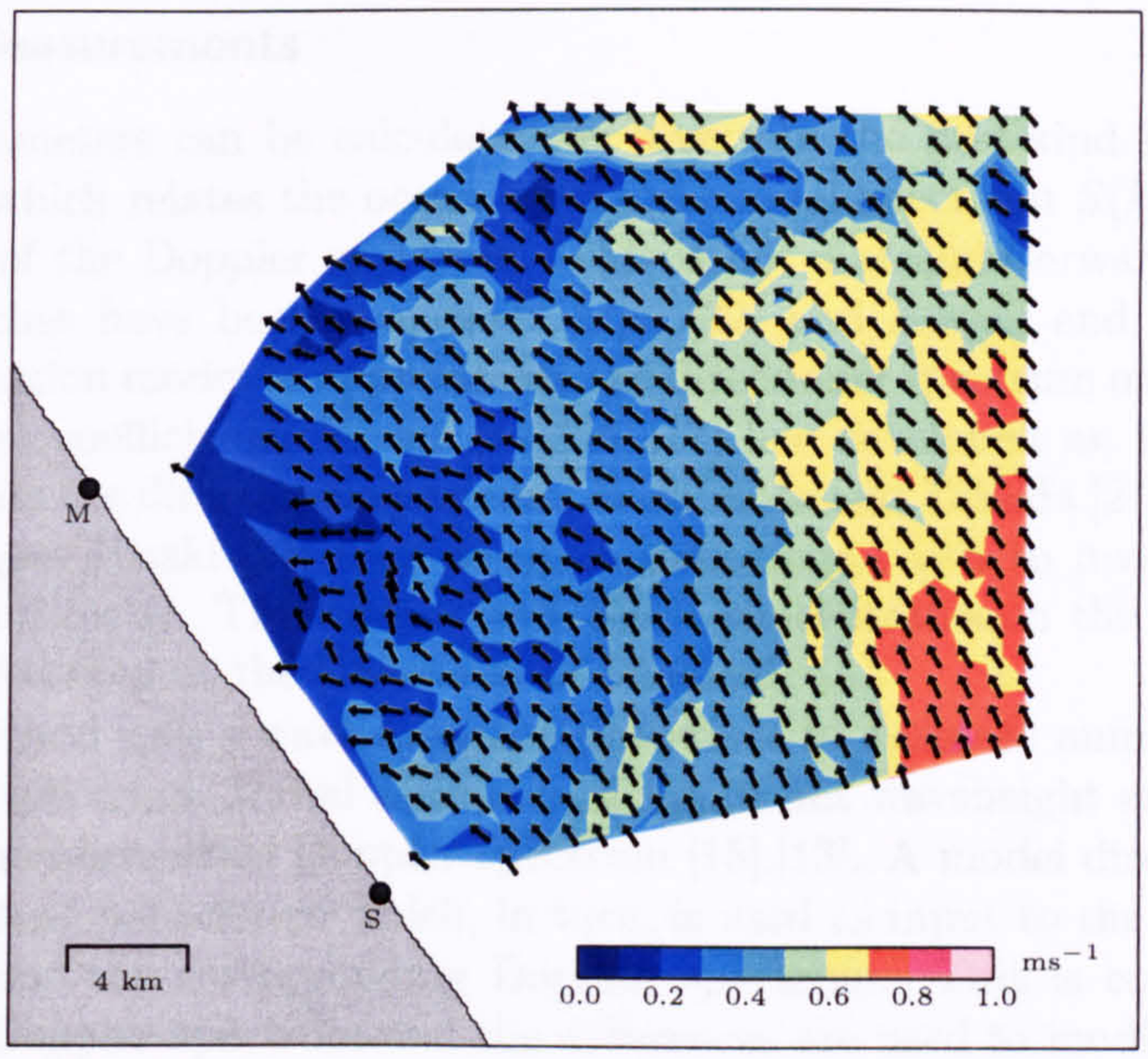

Figure 3.5: Vector current map. 23:00, 22/12/95.

3.3 Second Order Spectra

The second order structure in Doppler spectra, which surrounds the first order Bragg peaks, is illustrated in figure 3.1. The ocean wave directional spectrum is related to these second order continuous sidebands by means of a non-linear integral equation. A wave inversion procedure has been developed at the University of Sheffield which enables wave parameters to be extracted [52]. This section examines the second order spectra and discusses wave measurement techniques.

3.3.1 Scattering Theory

The second order continuum that characterises Doppler Spectra is also a Bragg resonance phenomenon. This continuous function of frequency is generated by two principal mechanisms:

1. Double electromagnetic scattering processes.
2. Non-linear ocean wave trains with wavelength λ_b that do not satisfy the linear dispersion relation. They propagate with different speeds to the Bragg linear ocean waves and, consequently, produce different Doppler shifts.

Barrick [2] analysed the interaction between transmitted radio waves and ocean waves to second order using electromagnetic and hydrodynamics theory. He deduced that the normalised second order sidebands in a Doppler spectrum, σ_2, can be described by

$$\sigma_2(\eta) = \int_{\theta_1}^{\theta_2} K(\eta,\theta) S(k',\theta') S(k,\theta)\ \mathrm{d}\theta, \tag{3.17}$$

where η is the normalised Doppler frequency, S is the ocean wave directional spectrum, k and k' are the ocean wavenumbers of the interacting waves and K is a coupling function containing the scattering physics and non-linear hydrodynamics.

3.3.2 Wave Measurements

Ocean wave parameters can be calculated by inverting the first-kind Fredholm integral equation (3.17) which relates the ocean wave directional spectrum $S(k, \theta)$ to the second order sidebands of the Doppler spectrum. This is not a straightforward task and many different approaches have been proposed: Lipa [32] and Howell and Walsh [26] use a Fourier decomposition model to approximate the directional spectrum using five frequency dependent Fourier coefficients; Wyatt [54],[56],[17] has developed an iterative inversion method to estimate the directional spectrum; Hashimoto and Tokuda [21] apply a bayesian inversion technique; Hisaki [25] uses an optimisation approach to invert the non-linear integral equation directly. The work in this thesis concentrates on the Wyatt procedure that has been developed at the University of Sheffield.

The Wyatt method uses a wave inversion procedure to estimate numerically the ocean wave directional spectrum. Initial estimates of significant waveheight and wind direction are made from the normalised Doppler spectrum [15],[13]. A model directional spectrum is derived from these parameters which, in turn, is used as input to the integral equation (3.17) to determine the corresponding Doppler spectrum. This is compared with the radar measured Doppler spectrum and the differences are used to modify the directional spectrum at each wave number and direction. The iterative procedure is repeated until the differences become sufficiently small.

The inversion technique places an upper limit on the wave frequencies that can be measured. The method fails to calculate the ocean wave directional spectrum at all frequencies since higher frequency waves are not adjusted in the procedure [54]. This upper limit, which is dependent on the radio frequency and the intersection angles between the two radar beams, was approximately 0.38 Hz in the Holderness experiment.

Estimates of various wave parameters can be extracted from the directional frequency spectra, which are generated from the inversion procedure. Ocean wave measurements are described in more detail in chapter 7.

3.4 Spectral Distortion

The potential of HF radar as an oceanographic tool has been demonstrated in numerous diverse experiments throughout the world. Comparisons with established in situ instruments, such as current meters and waveriders, have shown strong correlation [12],[16], [55],[57]. However, distortion in Doppler spectra has been identified as a limiting factor in HF radar technology [53],[58]. Compound first order structure constrains the quality and quantity of generated ocean measurements. The causes of spectral distortion in the Holderness data are investigated in this section.

3.4.1 Doppler3 Spectra

During the Holderness deployment, Doppler spectra, with a temporal resolution of approximately five minutes, were generated using the periodogram method. The OSCR system was originally designed to map ocean currents. The periodogram provides sufficient SNR levels for this purpose since current measurements only depend on the frequency locations of the first order peaks. Wave measurements, which utilise the second order components, require amplitude and frequency stability.

The random nature of the ocean surface can produce large fluctuations in the backscattered radar signal. These are more prevalent in the weaker second order spectral components. The objective of the averaging procedure is to decrease the spectral variance to

produce stable estimates, since the accuracy of the generated wave parameters is dependent on the precision of the second order sidebands.

The reduction in the variance of the periodogram due to the segmentation and windowing processes can be quantified. With no overlapping, the fractional variance decrease is $1/K$ when averaging K independent segments. Harris [20] showed that the reduction in spectral variance for the case of 75% window overlapping is given by

$$\sigma^2 = \frac{1}{K}\left[1 + 2c^2(0.75) + 2c^2(0.5)\right] - \frac{2}{K^2}\left[c^2(0.75) + 2c^2(0.5)\right], \tag{3.18}$$

where $c(r)$ represents the correlation coefficient between consecutive segments as a function of the fractional overlap r.

$$c(r) = \frac{\sum_{n=0}^{M-1} W(n)W(n + (1-r)M)}{\sum_{n=0}^{M-1} W^2(n)} \tag{3.19}$$

W is the Fourier Transform of the window function. The correlation statistics for the Blackman-Harris window are $c^2(0.75) = 0.46$ and $c^2(0.5) = 0.038$. The variance of the periodogram is related to the variance of each individual data segment by a factor $\sigma^2 = 0.33$.

Vizinho [49] investigated the statistical properties of radar data from the Holderness deployment. The averaging process in the periodogram was limited by the operational constraints of the OSCR system. In order to reduce the variance further, three consecutive Doppler spectra were averaged together – these will be denoted Doppler3 spectra for the remainder of this thesis. The additional averaging reduces the variance factor to $\sigma^2 = 0.11$. A comparison of data generated from the OSCR and Pisces radar systems showed that this provides spectra of sufficient quality to be applied to the wave inversion technique [49]. However, the temporal resolution is constrained to approximately 45 minutes.

In order to apply the Wyatt inversion procedure, the Doppler3 spectra must pass criteria which ensure the data are of sufficient quality to provide accurate oceanic measurements. The quality criteria used to determine whether the spectra could be inverted in the Holderness experiment were [31]:

1. The spectrum must contain a peak.
2. The dominant peak must lie within $\pm f_r/75$ rads^{-1} of the Bragg frequency.
3. The local minima must lie on the correct side of the spectrum.
4. The second order region must contain a non-zero number of frequency values.
5. The SNR of each Bragg peak must exceed 10 dB.
6. The SNR of the largest second order peak must exceed 15 dB.
7. The second order peaks must be at least 3 dB below the first order peaks.

Figure 3.6 shows a Doppler3 spectrum produced from Holderness data on the 6th January 1996. The Wyatt inversion technique cannot be performed on this spectrum since both Bragg peaks are split and the nulls which separate the first and second order structure are indistinct. In the Holderness deployment, up to 80% of radar data were unusable for wave measurements. Figure 3.7 shows the number of grid cells which failed the quality criteria during a 72 hour period between the 20th and 23rd December 1995. Examination of spectra from the master and slave OSCR sites revealed that, during periods of sufficient SNR, splitting of the Bragg peaks was the predominant cause of data failure.

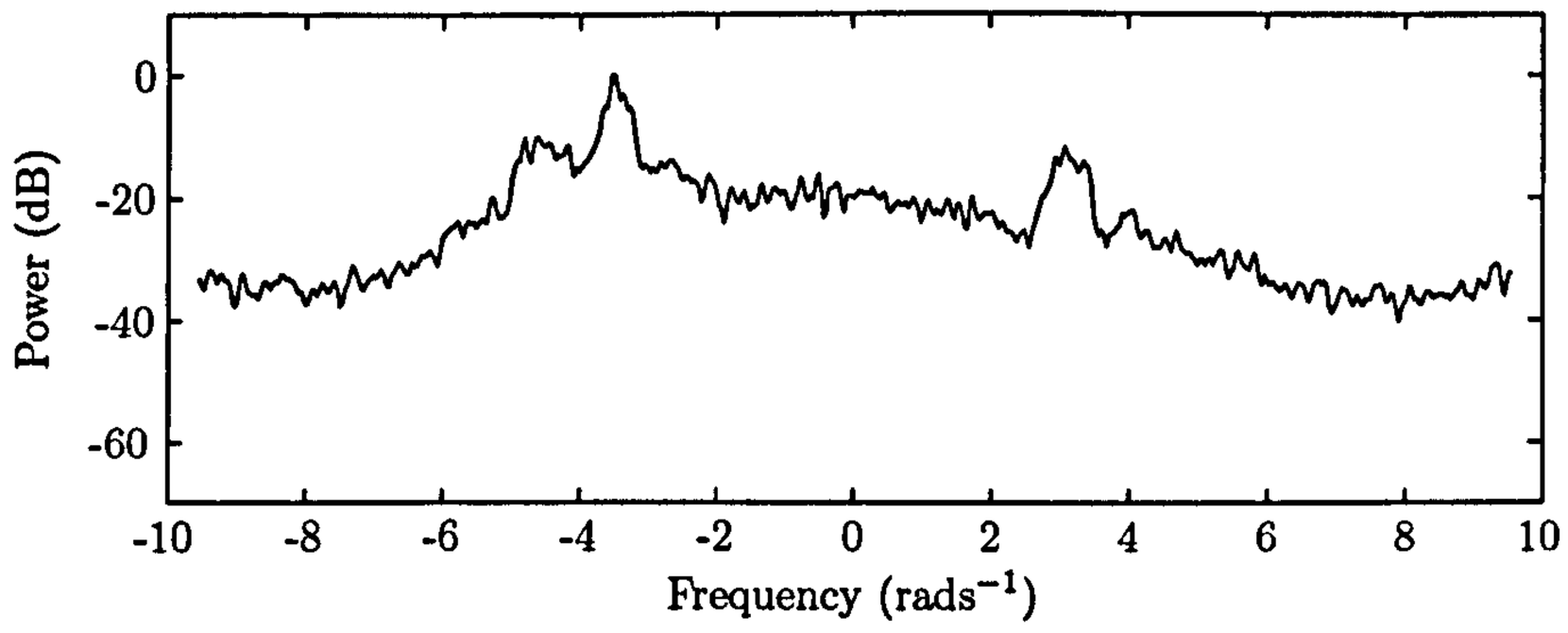

Figure 3.6: Doppler3 spectrum. The first order Bragg peaks exhibit compound structure. Data taken from the slave site at 18:05, 06/01/96, cell 19.

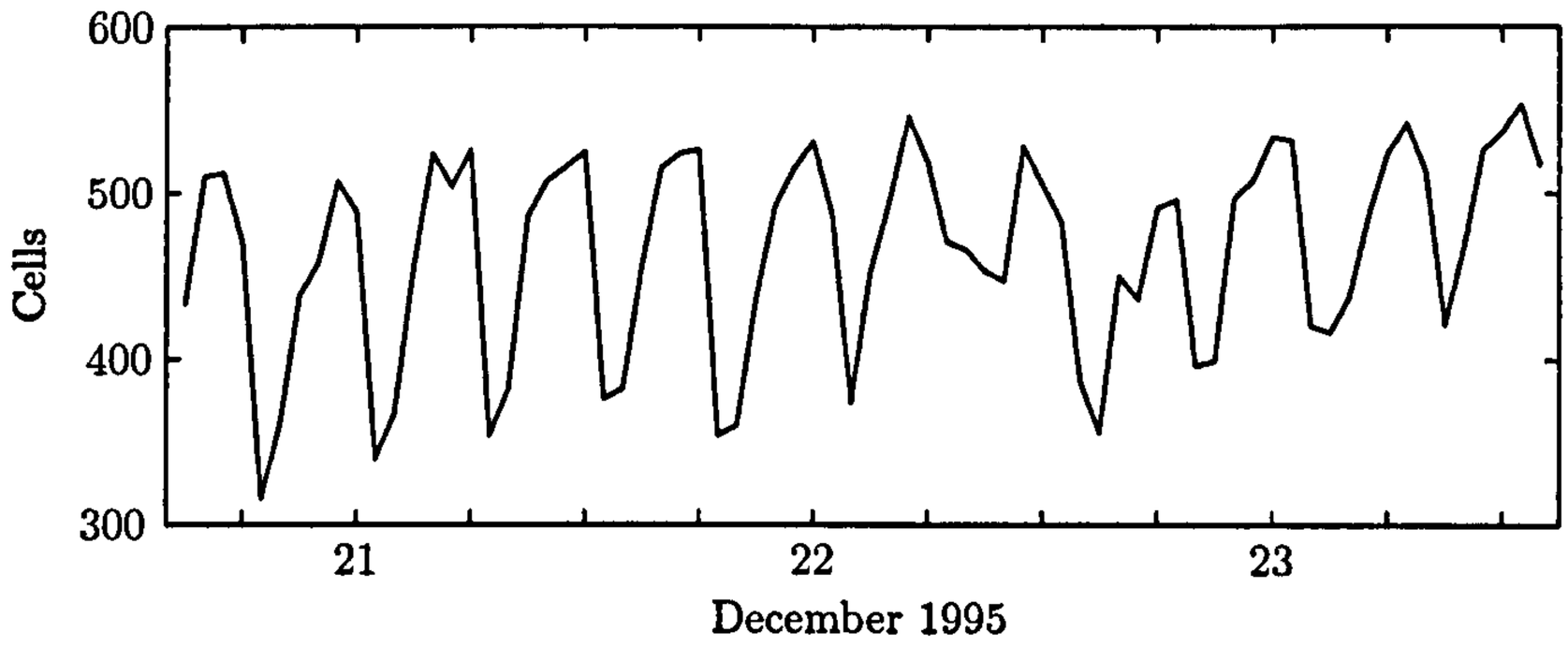

Figure 3.7: Time series showing the number of cells which failed the spectral quality criteria. Data taken between 15:00, 20/12/95 and 14:00, 23/12/95.

Previous investigations [53] indicate that current variability within the measurement region may cause complex first order structure and, subsequently, limit the number of wave inversions. Stable Doppler3 spectra require homogeneity within the temporal and spatial scales of the OSCR system.

3.4.2 Current Variability

The periodogram technique assumes stationarity within the OSCR measurement period. The time series in figure 3.7 exhibits a tidal distribution and the pattern of deteriorating data quality correlates with direction changes in the underlying current field. It is thought that temporal variability during the data collection period causes multiple Doppler shifts in the backscattered radar signal which, subsequently, broadens the first order peaks. Doppler3 spectra are more susceptible to this distortion since they are averaged over longer time periods [31].

Figure 3.8 illustrates the average current field at 00:00 on the 23rd December 1995. The ocean dynamics in the Holderness region are dominated by a tidal pattern: the current propagates parallel to the coastline, alternating in direction at approximately six hourly intervals. The map represents a time period at the turn of the tide, which corresponds to a low data quality point in figure 3.7.

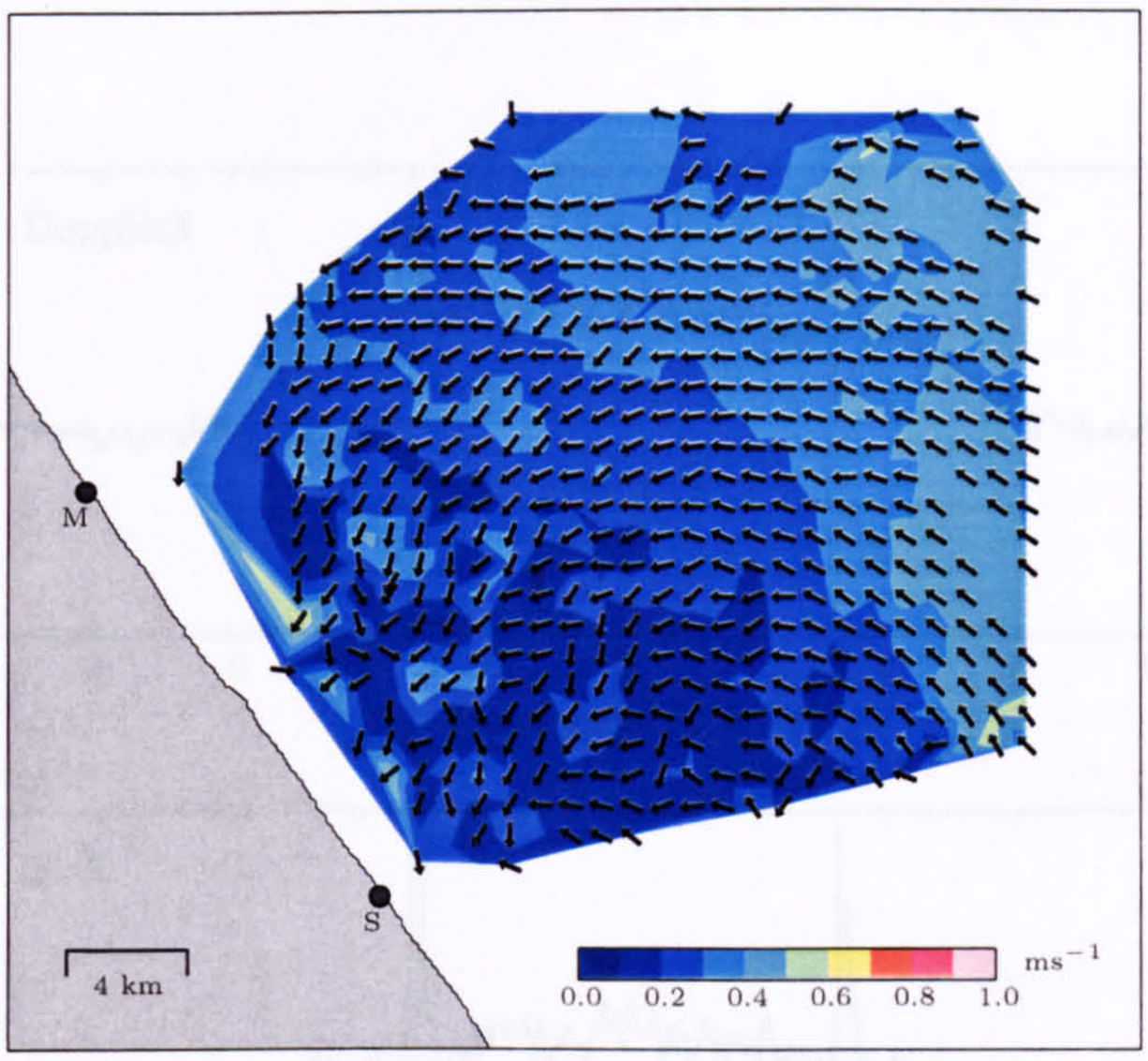

Figure 3.8: Vector current map. Average current field during Doppler3 data collection period. Data taken at 00:00, 23/12/95.

The temporal current variability in the data can be observed in figure 3.9. The Bragg peaks in consecutive Doppler spectra are located at differing frequencies due to the varying underlying current field. The averaged Doppler3 spectrum exhibits complex first order structure which prevents an inversion. The driving mechanism of this structure can also be observed using simulated data of the form

$$x(nT) = \alpha \exp\{-i(\omega_b + \tau)nT\} + \alpha \exp\{i(\omega_b + \tau)nT\} + \eta(nT), \qquad (3.20)$$

where α is the signal amplitude, τ is a constant frequency shift term and $\eta(nT)$ is a complex valued white noise term. When $\tau = 0$, the signal $x(nT)$ simulates an underlying surface current which is either zero or travelling perpendicular to the radar beam. The corresponding frequency spectrum is characterised by two dominant first order peaks located at the Bragg frequencies $\pm\omega_b$.

The Doppler spectra shown in figure 3.10 illustrate temporal variability within the 45 minute measurement period. The variable τ increments from 0.2 to 0.6 rads^{-1} during the three OSCR measurement periods which represents a discrete time variation in the surface current field. The peaks in each Doppler spectrum occur at distinct frequencies which are dependent on their respective current shifts. The averaged Doppler3 spectrum, which is generated from these constituent spectra, exhibits compound first order structure due to the temporal variability of the current components. This modelled case illustrates the problems that can occur in radar wave measurements due to the large time scales required for data collection using the periodogram method.

HF radar systems can be used to calculate ocean parameters at multiple grid cells over an extensive region. The spatial resolution of the backscattered signal at each measurement cell is dependent on the range and azimuthal resolution of the radar. During the Holderness deployment the OSCR units received backscattered signals from a cell footprint of approximately 1 km^2. The periodogram spectral technique assumes spatial homogeneity within each cell.

Heron [23] investigated the broadening of the first order peaks due to a non uniform current velocity distribution. Multiple current meter observations located within an HF

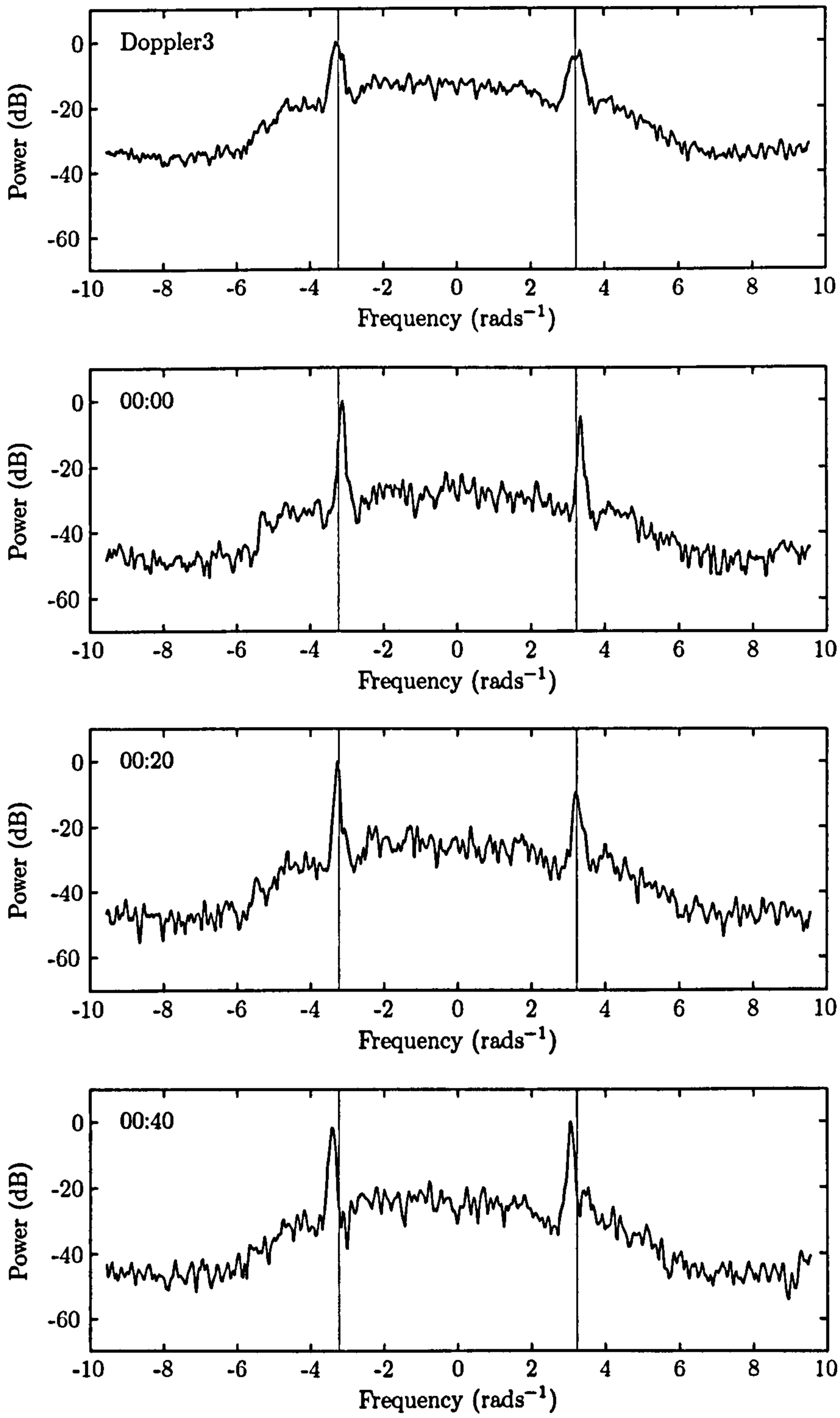

Figure 3.9: Averaged Doppler3 spectrum and constituent Doppler spectra. The vertical lines represent the Bragg frequencies $\pm\omega_b$. Data taken from the master site at 00:00, 23/12/95, cell 51.

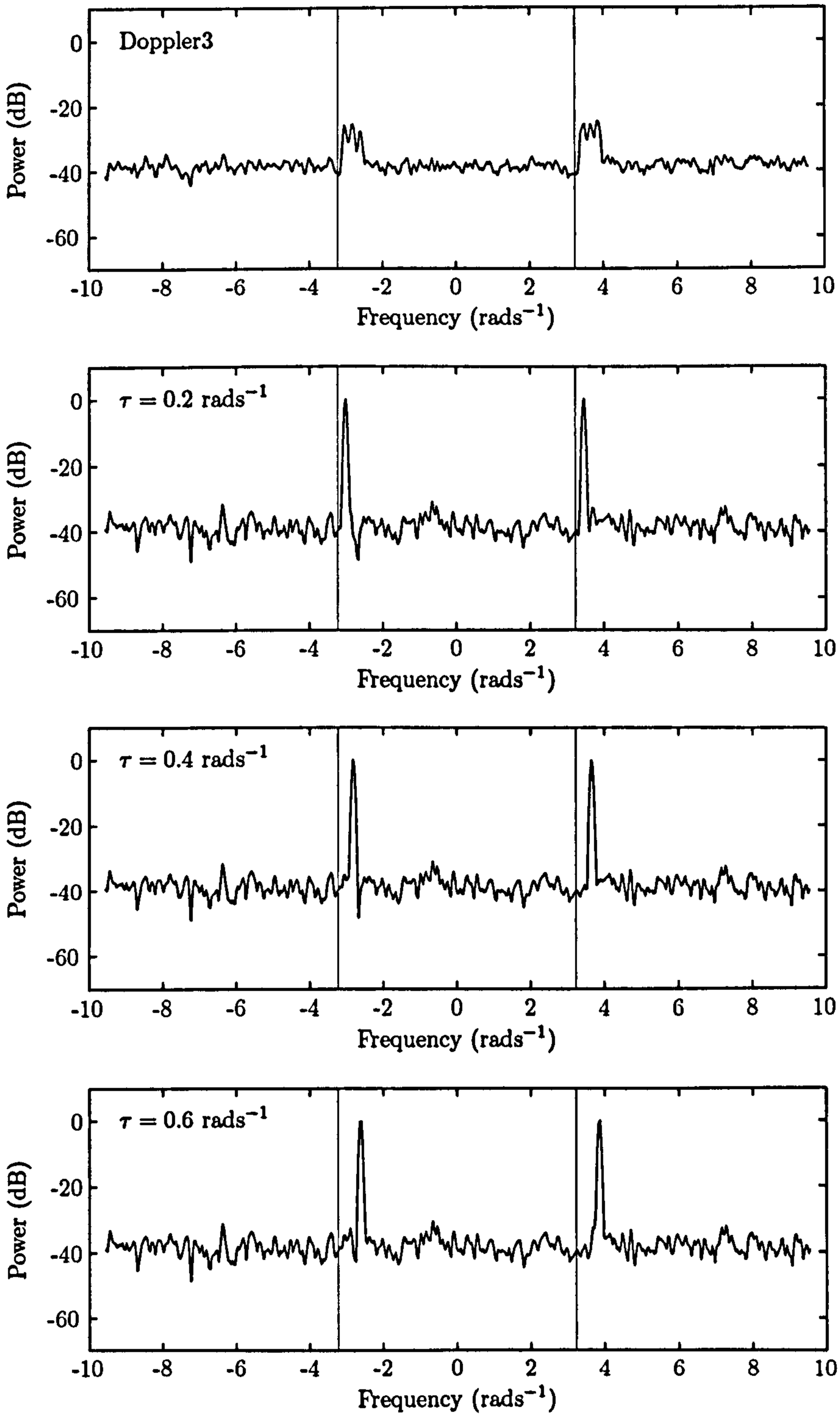

Figure 3.10: Averaged Doppler3 spectrum and constituent Doppler spectra. The vertical lines represent the Bragg frequencies $\pm\omega_b$. Data generated from modelled signal with $0.2 \leq \tau \leq 0.6$ rads^{-1}. SNR = 40 dB.

radar cell were used to synthesize the first order Bragg peaks under the assumption that the line broadening was due solely to the spatial distribution of velocities. The target cell, located inshore of the Great Barrier Reef, was characterised by turbulent processes produced by tidal currents. His work illustrated that uneven currents may contribute to the splitting of the first order Bragg peaks.

The spatial resolution of each ocean measurement cell is determined from the configuration of the HF radar system and cannot be altered through different spectral analysis methods. Improvements in range and azimuthal resolution algorithms for HF radar will limit the extent of variability within a measurement cell.

3.5 Summary

The periodogram method that is used to generate Doppler spectra from backscattered radar signals was studied in this chapter. Techniques for extracting oceanographic parameters from the first and second order spectral components were discussed. Examples of the spatial structure of current fields which are achievable with HF radar were illustrated.

The cause of distortion in Doppler spectra was investigated and attributed to temporal and spatial inhomogeneity in surface current fields. The aim of this thesis is to investigate whether alternative spectral estimation techniques can mitigate these problems. The following work will concentrate on a method which attempts to reduce the limitations due to current variability within the radar measurement period.

4 Spectral Analysis Techniques

Distortion in the Holderness Doppler spectra, caused by temporal and spatial inhomogeneities, has been identified as a limiting factor for the measurement of oceanographic parameters. Alternative spectral estimation techniques for the analysis of HF radar data have been proposed and three of these methods are studied in this chapter:

- Instantaneous Frequency
- Autoregressive
- MUSIC

Instantaneous Frequency has been conjectured as a mechanism for measuring the time varying structure of backscattered radar signals [37]; the development of a filter to extract the first order modulation provides the motivation behind the work in this thesis. Autoregressive [36] and MUSIC [42] algorithms are established techniques in HF radar oceanography and are used in chapter 5 to validate the filtering approach.

4.1 Instantaneous Frequency Method

4.1.1 Historical Review

Instantaneous Frequency (IF) is a mathematical concept for characterising a signal with a time varying spectral content. The term frequency is synonymous with the Fourier definition but, in 1937, Carson and Fry [7] generalised this notion to include the variation of frequency as a function of time. IF has subsequently been studied as a spectral analysis method with applications in communications, radar and sonar [6],[34],[44]. IF is defined for monocomponent signals which contain a narrow band of frequencies. Backscattered electromagnetic signals from the ocean's surface are dominated by two distinct spectral components, concentrated around the Bragg frequencies $\pm\omega_b$, which indicates that IF is an appropriate technique.

A filtering method is described based on work in France by Parent and Bourdillon [37]. The original concept was designed to remove the turbulence which appeared in reflected signals from skywave radar systems. An IF technique was used to correct contaminated Doppler spectra for ionospheric frequency modulation. Traylen and Wyatt [46] subsequently introduced a method to measure the temporal variability of Bragg frequency components using groundwave radar. The filter is developed and validated in this thesis in order to determine the optimum approach for HF radar oceanography. Properties of the filter are studied and a dynamic approach to isolate the Bragg peaks is proposed. The extracted first order structure is examined and related to underlying oceanographic processes.

4.1.2 Instantaneous Frequency

Instantaneous frequency is defined as the time derivative of the phase component of a signal. This corresponds to the frequency of a sine wave which locally fits the signal under analysis [6]. A time signal $y(t)$ can be expressed in polar form as

$$y(t) = a(t)\, e^{i\sigma(t)}, \tag{4.1}$$

where $a(t)$ and $\sigma(t)$ represent the amplitude and phase respectively. The instantaneous frequency function, $z(t)$, is given by

$$z(t) = \sigma'(t). \tag{4.2}$$

The conventional way of defining frequency is in terms of a signal's Fourier frequency, ω, which is derived using a Fourier Transform. The following Fourier Transform pair converts a signal between its time and frequency domain representation.

$$Y(\omega) = \int_{-\infty}^{\infty} y(t)\, e^{-i\omega t}\, \mathrm{d}t \tag{4.3}$$

$$y(t) = \frac{1}{2\pi} \int_{-\infty}^{\infty} Y(\omega)\, e^{i\omega t}\, \mathrm{d}\omega \tag{4.4}$$

Instantaneous frequency is a function of time and represents an alternative concept to the standard Fourier definition. However, the means of the two distributions can be related [44]. Differentiating (4.4) gives

$$y'(t) = \frac{i}{2\pi} \int_{-\infty}^{\infty} \omega Y(\omega)\, e^{i\omega t}\, \mathrm{d}\omega, \tag{4.5}$$

which is in the form of a Fourier transform

$$\omega Y(\omega) = -i \int_{-\infty}^{\infty} y'(t)\, e^{-i\omega t}\, \mathrm{d}t. \tag{4.6}$$

The complex conjugate of (4.3) can be expressed as

$$Y^*(\omega) = \int_{-\infty}^{\infty} y^*(t)\, e^{i\omega t}\, \mathrm{d}t. \tag{4.7}$$

The mean Fourier frequency of a signal is defined as

$$\overline{\omega} = \frac{\int_{-\infty}^{\infty} \omega |Y(\omega)|^2\, \mathrm{d}\omega}{\int_{-\infty}^{\infty} |Y(\omega)|^2\, \mathrm{d}\omega} \tag{4.8}$$

$$= \frac{\int_{-\infty}^{\infty} \omega Y(\omega) Y^*(\omega)\, \mathrm{d}\omega}{\int_{-\infty}^{\infty} Y(\omega) Y^*(\omega)\, \mathrm{d}\omega}. \tag{4.9}$$

By analogy, $\overline{\omega}$ is located at the centroid of $|Y(\omega)|^2$, where the Fourier transform is considered as a mass distribution along the ω axis. Substituting (4.3), (4.6) and (4.7) into (4.9) provides

$$\overline{\omega} = \frac{-i \int_{-\infty}^{\infty} y'(t) y^*(t)\, \mathrm{d}t}{\int_{-\infty}^{\infty} y(t) y^*(t)\, \mathrm{d}t}. \tag{4.10}$$

Substituting $y(t) = a(t)e^{i\sigma(t)}$ gives

$$\overline{\omega} = \frac{\int_{-\infty}^{\infty} \sigma'(t)(a(t))^2 - ia'(t)a(t)\ \mathrm{d}t}{\int_{-\infty}^{\infty}(a(t))^2\ \mathrm{d}t} \tag{4.11}$$

$$= \frac{\int_{-\infty}^{\infty} \sigma'(t)(a(t))^2\ \mathrm{d}t}{\int_{-\infty}^{\infty}(a(t))^2\ \mathrm{d}t} \tag{4.12}$$

$$= \frac{\int_{-\infty}^{\infty} z(t)(a(t))^2\ \mathrm{d}t}{\int_{-\infty}^{\infty}(a(t))^2\ \mathrm{d}t}. \tag{4.13}$$

This provides the result that the mean Fourier frequency is equal to the weighted mean of instantaneous frequency.

4.1.3 HF Radar Signal Processing

An IF method for measuring oceanographic parameters with HF radar is introduced in this section. A filtering technique is described which isolates the Bragg peaks in a Doppler spectrum and provides an estimate of the first order frequency modulation. The method can be divided into four stages:

- Isolate the first order spectral components.
- Transform the band limited signal into the time domain.
- Calculate the first order frequency variability as a function of time.
- Filter the raw radar signal to remove the measured modulation.

Bragg Peak Identification

The OSCR output signal, $x(nT)$, consists of N discrete data points with a sampling interval of T seconds. This raw signal is transformed into the frequency domain using a Discrete Fourier Transform (DFT).

$$X\left(\frac{2\pi m}{NT}\right) = \sum_{n=0}^{N-1} x(nT)\ \exp\left\{\frac{-2\pi imn}{N}\right\} \qquad (0 \leq m < N) \tag{4.14}$$

Figure 4.1 shows a power spectrum from the Holderness deployment which is characterised by two dominant Bragg peaks. The frequency positions of the positive and negative peaks are estimated from the maximum values in the spectrum.

$$\beta^{+} = \max_{m=[0,\frac{N}{2})} \left|X\left(\frac{2\pi m}{NT}\right)\right|^2 \tag{4.15}$$

$$\beta^{-} = \max_{m=[\frac{N}{2},N)} \left|X\left(\frac{2\pi m}{NT}\right)\right|^2 \tag{4.16}$$

The two Bragg peaks are extracted in the frequency domain using a bandpass filter (width of 2θ samples) centred on $\beta^{\pm}$.

$$Y^{\pm}\left(\frac{2\pi m}{NT}\right) = \begin{cases} X\left(\frac{2\pi m}{NT}\right) & \text{if } \beta^{\pm} - \theta \leq m < \beta^{\pm} + \theta \\ 0 & \text{otherwise} \end{cases} \tag{4.17}$$

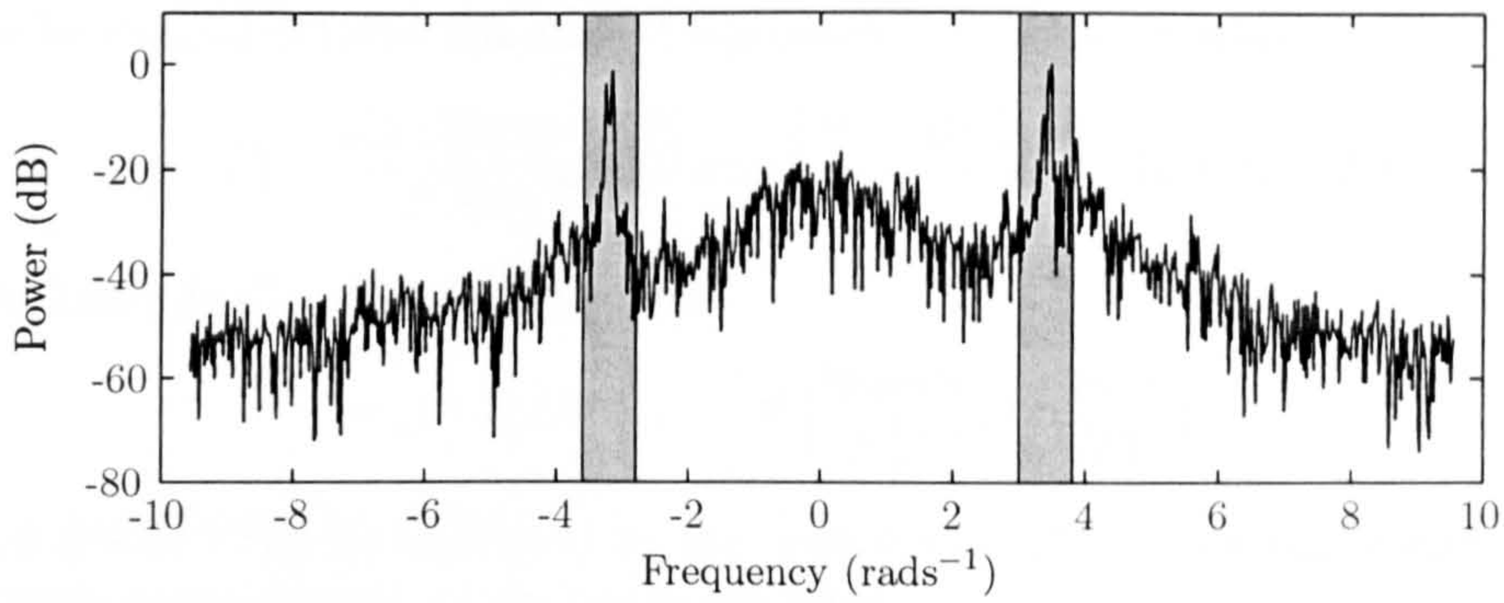

Figure 4.1: Power spectrum. The shaded regions illustrate the bandpass filter width. Data taken from the master site at 20:00, 08/12/95, cell 562.

The shaded regions in figure 4.1 illustrate the extent of the bandpass filter. The objective is to remove the first order spectral components which may contain information on the current modulation. The bandwidth parameter θ is important since it determines the input to the filtering procedure. An insufficient value of θ will exclude some of the first order modulation but unwanted second order structure will be included if θ is too large.

Time Domain Transformation

The extracted first order signals are converted into the time domain using an inverse DFT. The time signals of the positive and negative Bragg peaks are represented by $y^{\pm}(nT)$.

$$y^{\pm}(nT) = \frac{1}{N} \sum_{m=\beta^{\pm}-\theta}^{\beta^{\pm}+\theta} X\left(\frac{2\pi m}{NT}\right) \exp\left\{\frac{2\pi imn}{N}\right\} \qquad (0 \leq n < N) \qquad (4.18)$$

This result can also be expressed in terms of two time signals using the convolution property of the Fourier transform. The band limited signals can be written in the form

$$y^{\pm}(nT) = \frac{1}{N} \sum_{m=0}^{N-1} X\left(\frac{2\pi m}{NT}\right) P_{\theta}\left(\frac{2\pi(m-\beta^{\pm})}{NT}\right) \exp\left\{\frac{2\pi imn}{N}\right\}, \qquad (4.19)$$

where P is a rectangular window function defined by

$$P_{\theta}\left(\frac{2\pi(m-\beta^{\pm})}{NT}\right) = \begin{cases} 1 & |m-\beta^{\pm}| \leq \theta \\ 0 & |m-\beta^{\pm}| > \theta. \end{cases} \qquad (4.20)$$

The inverse Fourier transform of P is given by

$$p(nT) = \frac{1}{N} \sum_{m=0}^{N-1} P_{\theta}\left(\frac{2\pi(m-\beta^{\pm})}{NT}\right) \exp\left\{\frac{2\pi imn}{N}\right\} \qquad (0 \leq n < N) \qquad (4.21)$$

$$= \frac{1}{N} \sum_{m=\beta^{\pm}-\theta}^{\beta^{\pm}+\theta} \exp\left\{\frac{2\pi imn}{N}\right\} \qquad (0 \leq n < N). \qquad (4.22)$$

The substitution $k = m - \beta^{\pm} + \theta$ simplifies the summation limits.

$$p(nT) = \frac{1}{N} \sum_{k=0}^{2\theta} \exp\left\{\frac{2\pi in(k+\beta^{\pm}-\theta)}{N}\right\} \qquad (0 \leq n < N) \qquad (4.23)$$

$$= \frac{1}{N} \exp\left\{\frac{2\pi in(\beta^{\pm}-\theta)}{N}\right\} \sum_{k=0}^{2\theta} \exp\left\{\frac{2\pi ink}{N}\right\} \qquad (0 \leq n < N) \qquad (4.24)$$

This can be expanded using the sum of a geometric series to provide

$$\mathrm{p}(nT) = \frac{\sin\left(\frac{\pi n}{N}(2\theta+1)\right)}{N\sin\left(\frac{\pi n}{N}\right)} \exp\left\{\frac{2\pi i n\beta^{\pm}}{N}\right\} \qquad (1 \leq n < N). \tag{4.25}$$

Using the Discrete Convolution Theorem

$$f(nT) * g(nT) \longleftrightarrow F\left(\frac{2\pi m}{NT}\right) G\left(\frac{2\pi m}{NT}\right), \tag{4.26}$$

the signal $y^{\pm}(nT)$ can be expressed as the convolution of the raw radar signal with the time domain representation of the bandpass filter.

$$y^{\pm}(nT) = \frac{\sin\left(\frac{\pi n}{N}(2\theta+1)\right)}{N\sin\left(\frac{\pi n}{N}\right)} \exp\left\{\frac{2\pi i n\beta^{\pm}}{N}\right\} * x(nT) \qquad (1 \leq n < N) \tag{4.27}$$

First Order Modulation

IF signals provide a measure of the first order frequency distribution as a function of time. The signals $y^{\pm}(nT)$ can be expressed as

$$y^{\pm}(nT) = a^{\pm}(nT)\exp\left\{i\sigma^{\pm}(nT)\right\} \qquad (0 \leq n < N). \tag{4.28}$$

$a^{\pm}(nT)$ and $\sigma^{\pm}(nT)$ are the amplitude and phase components respectively. The phase signals are determined by

$$\sigma^{\pm}(nT) = \tan^{-1}\left[\frac{y_{\mathrm{I}}^{\pm}(nT)}{y_{\mathrm{R}}^{\pm}(nT)}\right] \qquad (0 \leq n < N), \tag{4.29}$$

where $y_{\mathrm{R}}^{\pm}(nT)$ and $y_{\mathrm{I}}^{\pm}(nT)$ represent the real and imaginary components of $y^{\pm}(nT)$. The IF function is then determined using a backwards difference formula: Sun [44] showed that this approach provides the best approximation of the continuous IF.

$$z^{\pm}(nT) = \frac{\sigma^{\pm}(nT) - \sigma^{\pm}((n-1)T)}{T} \qquad (1 \leq n < N) \tag{4.30}$$

The average first order frequencies can be calculated from the IF signals.

$$\Lambda^{\pm} = \frac{\sum_{n=0}^{N-1} |y^{\pm}(nT)|^2 z^{\pm}(nT)}{\sum_{n=0}^{N-1} |y^{\pm}(nT)|^2} \tag{4.31}$$

The amplitudes of the band limited time signals are used as weighting functions to reduce the effect of noise: the significance of this is illustrated in chapter 6. Figure 4.2 shows IF signals from the Holderness deployment. The horizontal line in each graph represents the calculated peak frequency estimates.

The first order structure needs to be isolated carefully from the raw radar signal. The initial estimates of the Bragg peak frequencies, $\beta^{\pm}$, are used to determine the locations of the bandpass filters. These values are calculated from the maxima in a power spectrum and are consequently constrained by the frequency resolution of the Fourier transform process. In order to increase the likelihood of extracting the first order structure from the radar signal, the filtering procedure is repeated using bandpass filters centred on $\Lambda^{\pm}$. A smaller bandwidth parameter can be used to isolate the Bragg peaks which contain the first order modulation; an investigation into the optimum values is given in chapter 6. Within this chapter, the bandpass filter widths are 0.5 and 0.25 rads^{-1} for the first and second filtering of the data respectively.

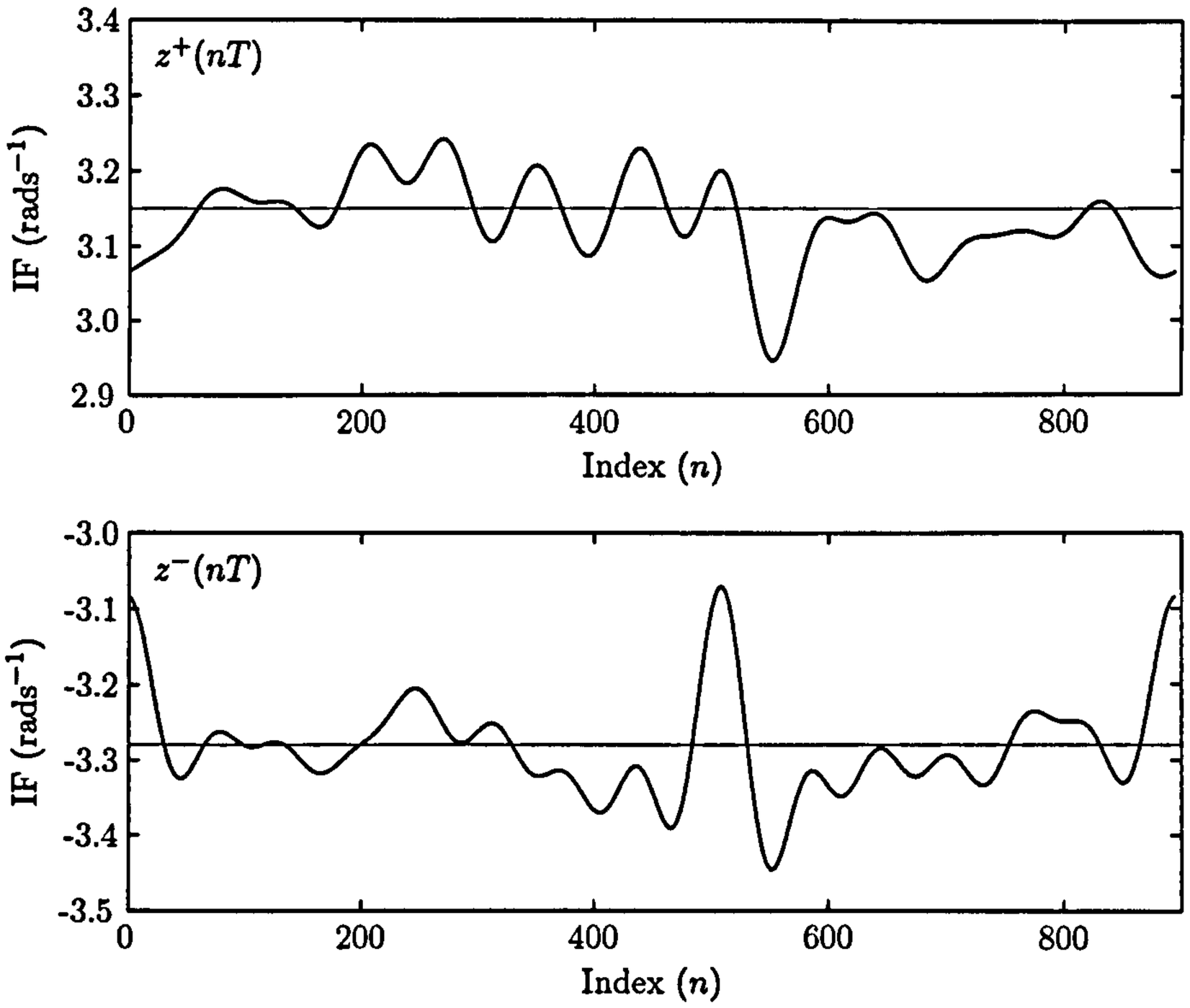

Figure 4.2: IF signals $z^{\pm}(nT)$. The horizontal lines represent the Bragg peak values, $\Lambda^{\pm}$. Data taken from the slave site at 18:05, 06/01/96, cell 36.

Data Filter

First order scattering theory indicates that the positive and negative spectral peaks represent Bragg ocean waves which are propagating radially towards and away from the radar respectively [2]. Differences are expected between $z^+(nT)$ and $z^-(nT)$ due to the non-uniform distribution of Bragg waves on the ocean surface.

The second order structure in backscattered radar signals is a continuous function of frequency. A perturbation solution of the non linear hydrodynamical and electromagnetic boundary conditions at the ocean surface showed that the continuum is dominated by the interaction between pairs of ocean waves which exhibit different wavelengths [33]. The second order sidebands which enclose each Bragg peak are shifted in frequency by the same surface current as the first order components. The objective of the filtering procedure is to remove the measured first order variability from the whole radar signal. The modulation, which causes split Bragg peaks in Doppler spectra, is extracted in two stages: the positive frequencies of the radar signal are filtered using $z^+(n\mathrm{T})$; the negative frequencies of the radar signal are filtered using $z^-(n\mathrm{T})$.

The two halves of the raw backscattered data, $x^{\pm}(nT)$, are isolated using a bandpass filter.

$$x^+(nT) = \frac{1}{N}\sum_{m=0}^{\frac{N}{2}-1} X\left(\frac{2\pi m}{NT}\right)\exp\left\{\frac{2\pi imn}{N}\right\} \qquad (0 \le n < N) \qquad (4.32)$$

$$x^-(nT) = \frac{1}{N}\sum_{m=\frac{N}{2}}^{N-1} X\left(\frac{2\pi m}{NT}\right)\exp\left\{\frac{2\pi imn}{N}\right\} \qquad (0 \le n < N) \qquad (4.33)$$

The IF modulation, $z^{\pm}(nT)$, is extracted from each signal using the frequency shifting property of Fourier transforms.

$$x_{\mathrm{f}}^{\pm}(nT) = x^{\pm}(nT)\,\exp\left\{-iT\sum_{j=0}^{n}(z^{\pm}(jT) \mp \omega_{\mathrm{b}})\right\} \qquad (0 \leq n < N) \tag{4.34}$$

The final filtered signal $x_{\mathrm{f}}(nT)$ is produced by combining the positive and negative frequency components.

$$x_{\mathrm{f}}(nT) = x_{\mathrm{f}}^{+}(nT) + x_{\mathrm{f}}^{-}(nT) \qquad (0 \leq n < N) \tag{4.35}$$

The IF procedure has generated a filtered time signal, $x_{\mathrm{f}}(nT)$, which can be converted into a Doppler spectrum using the periodogram technique described in chapter 3. The influence of the first order modulation has been removed from the signal.

4.1.4 Oceanographic Measurements

The instantaneous frequency estimates of the first order peaks, $\Lambda^{\pm}$, are used to measure radial current components. The Doppler shift due to surface current, Δf, is determined from the positive and negative peak frequencies.

$$\Delta f = \frac{\Lambda^{+} + \Lambda^{-}}{2} \tag{4.36}$$

Wave parameters are extracted from the second order continuum in the Doppler spectra. The Wyatt method uses an iterative inversion procedure to estimate the ocean wave directional spectrum. Limitations of this method, due to variability within the measurement cell, were introduced in chapter 3. Figure 4.3 shows two Doppler3 spectra produced from raw and IF filtered data. The raw spectrum exhibits complex first order structure, resulting in ambiguous Bragg peak locations. The filtered spectrum illustrates the effect of the IF procedure. The first order peaks are sharper and have been shifted to the Bragg frequencies $\pm\omega_b$. A wave inversion can be performed on the filtered spectrum since the nulls separating the first and second order components are distinct

The temporal distribution of the grid cells which failed the spectral quality criteria was illustrated in figure 3.7. This graph exhibits a periodic pattern and a deterioration in the spectral quality was prevalent when the tidal current was turning in direction. During these time periods, when the current magnitude was low, split peaks were frequently caused by the cumulative effect of the dynamic current field during the 45 minute coherent integration time of the Doppler3 measurements. The current velocity gradients associated with the shorter timescales of the periodogram were often too small to distort the first order structure noticeably. An alternative approach to the IF filtering technique would be to remove the measured current shifts from each constituent periodogram before forming a Doppler3 spectrum. Computationally, this is less complex but would only limit the influence of variability in the radar signal.

First order modulation within each periodogram measurement can distort the radar signal during periods of high current magnitude – the simple peak shifting approach would not mitigate the multiple Bragg peak structure in this case. Figure 4.4 shows the Doppler spectra formed from a single five minute time period which represents a point midway through the tidal cycle. The raw spectrum would fail the Holderness quality criteria since the positive Bragg peak exhibits compound structure. The IF signal processing has extracted this modulation from the filtered spectrum. This provides evidence of the advantage of the IF approach. The impact of the periodogram, IF filter and peak shifting approaches are quantified in chapter 8.

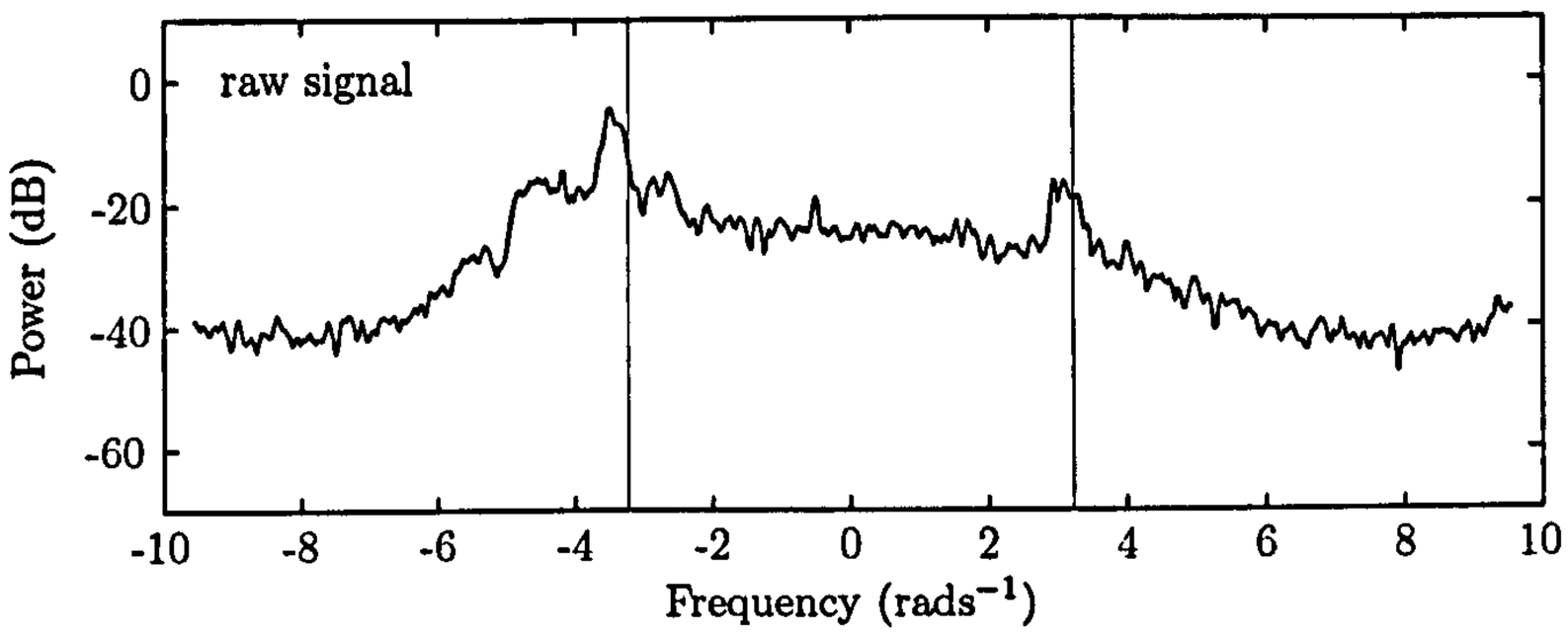

Figure 4.3: Doppler3 spectra generated from raw and IF filtered signals. The vertical lines represent the Bragg frequencies $\pm\omega_b$. Data taken from the slave site at 18:05, 06/01/96, cell 36.

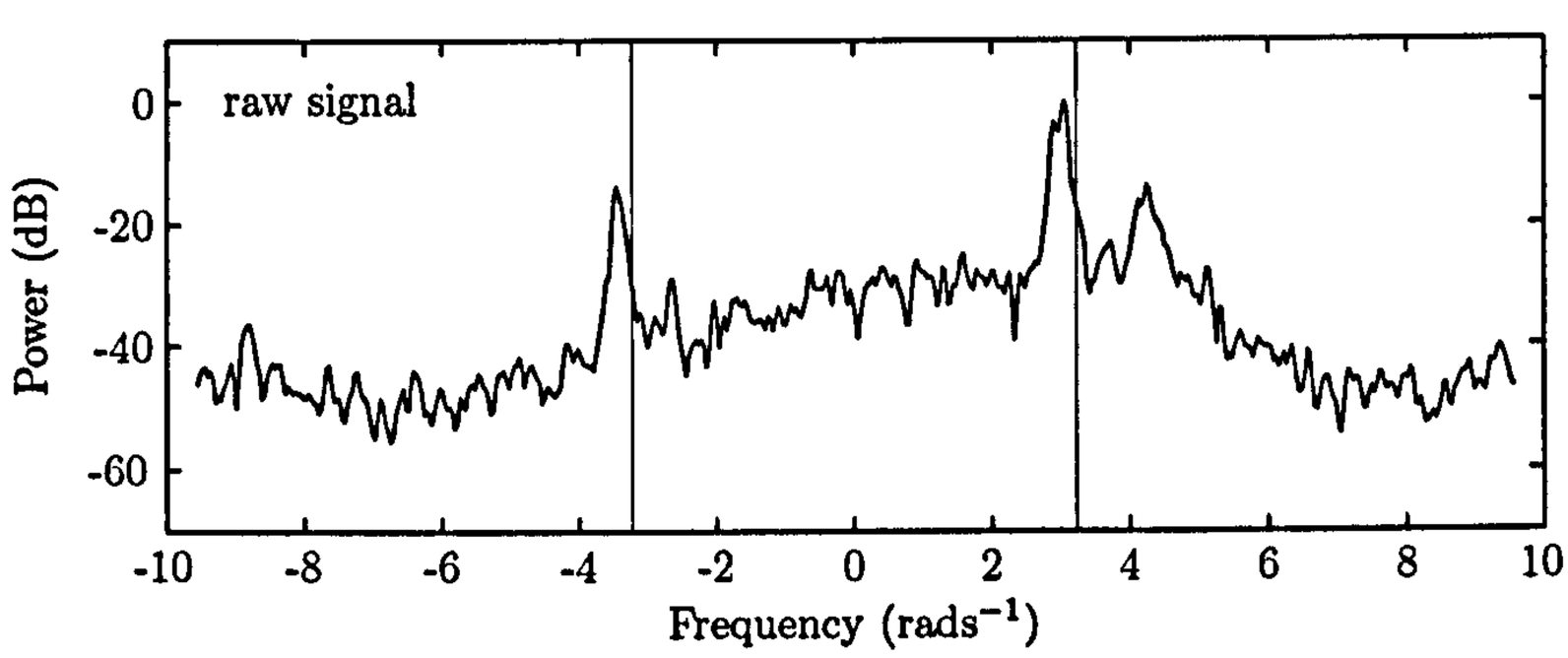

Figure 4.4: Doppler spectra generated from raw and IF filtered signals. The vertical lines represent the Bragg frequencies $\pm\omega_b$. Data taken from the master site at 14:00, 21/12/95, cell 120.

4.2 Autoregressive Method

4.2.1 Historical Review

In 1898, Schuster proposed the periodogram which became the standard technique for spectral analysis. Yule, a British statistician, conjectured an alternative analysis method in 1927. He used a linear regression technique to search for periodicities in modelled time series data [59]. His primary interest was to search for additional features in the analysis of sunspot numbers and, subsequently, he devised the basis of a parametric approach to modern spectral analysis. Yule introduced a least squares autoregression process of the form

$$u(n) = a_1 u(n-1) + a_2 u(n-2) + \epsilon(n), \tag{4.37}$$

for arbitrary a_1 and a_2, where $\epsilon(n)$ represents a small random error at each point [35]. This regression equation has a damped sinusoid solution. The technique was subsequently studied by Walker and the normal equations resulting from this analysis are known as the Yule-Walker equations.

Autoregressive modelling has been studied as an alternative to classical Fourier analysis for ocean remote sensing. Martin and Kearney [36] demonstrated a method for determining radial current components from radar data. Recent work by Vizinho [49] used autoregressive techniques to improve the quality of Doppler spectra for wave measurements.

4.2.2 Autoregressive Modelling

An Autoregressive (AR) model is a time domain model where each data sample is linearly correlated with p previous samples [36]

$$y(n) = -\sum_{k=1}^{p} a(k) y(n-k) + u(n), \tag{4.38}$$

where $y(n)$ are the data samples, $u(n)$ is an uncorrelated driving noise process and p is the model order which determines the frequency resolution. The AR coefficients, $a(k)$, are obtained as solutions to linear equations. The power spectral estimates are uniquely determined from the AR coefficients

$$\mathrm{P}(n) = \frac{T\sigma^2}{\left|1 + \sum_{k=1}^{p} a(k) \exp\{-2\pi i n k T\}\right|^2}, \tag{4.39}$$

where σ^2 is the variance of the driving noise process and T is the data sampling interval. These techniques are appropriate for spectra with sharp peaks representing signals with a narrow band of frequencies; this makes AR modelling a viable tool for HF radar oceanography.

4.2.3 HF Radar Signal Processing

An autoregressive approach for generating frequency spectra from HF radar data is described in this section. The method can be divided into two areas: selecting the best technique for calculating AR coefficients and choosing the optimum model order p.

Autoregressive Coefficients

The autoregressive coefficients can be obtained via a variety of techniques which are described by Marple [35]. Two common approaches are the Burg and modified covariance methods. The Burg method is an efficient algorithm that makes direct AR parameter estimates. The modified covariance technique is a least squares linear prediction estimation approach that performs a combined minimisation with respect to all of the linear prediction coefficients. Marple showed that spectral line splitting can occur with the Burg method which causes problems for current measurements [35]. The modified covariance method is selected because investigations indicate that it is the most efficient and reliable when estimating the first-order spectra [49].

The raw data, $x(nT)$, consist of N discrete data points with a sampling interval of T seconds. The forward linear predictor $\hat{x}^{\mathrm{f}}(nT)$ for each sample $x(nT)$ is given by

$$\hat{x}^{\mathrm{f}}(nT) = -\sum_{k=1}^{p} a_p(k)x((n-k)T), \tag{4.40}$$

where $a_p(k)$ are the forward linear prediction coefficients for an AR model of order p. The forward linear prediction error is defined as

$$e_p^{\mathrm{f}}(n) = x(nT) + \sum_{k=1}^{p} a_p(k)x((n-k)T). \tag{4.41}$$

The backward linear prediction error can be expressed in terms of the forward AR coefficients since the forward and backward AR coefficients for a stationary random process are complex conjugates of each other [35]. The backward linear predictor $\hat{x}^{\mathrm{b}}(nT)$ is

$$\hat{x}^{\mathrm{b}}(kT) = -\sum_{k=1}^{p} a_p^*(k)x((k+p)T), \tag{4.42}$$

which provides the backward linear prediction error

$$e_p^{\mathrm{b}}(n) = x((n-p)T) + \sum_{k=1}^{p} a_p^*(k)x((n-p+k)T). \tag{4.43}$$

The modified covariance method minimises the average of the forward and backward linear prediction squared errors over the data set.

$$\rho_p^{\mathrm{fb}} = \frac{1}{2}\left(\sum_{n=p+1}^{N} |e_p^{\mathrm{f}}(n)|^2 + \sum_{n=p+1}^{N} |e_p^{\mathrm{b}}(n)|^2\right) \tag{4.44}$$

A fast algorithm for the solution of the modified covariance equations is described in detail by Marple [35]. AR parameter estimates are determined by equating the parameters to the optimised linear prediction coefficients.

Model Order

The model order, p, determines the spectral resolution and is crucial to the accuracy of an autoregressive process. A large model order relative to the number of data samples can produce spurious detail in the AR spectra; an insufficient model order reduces the resolution of the AR process and the spectral estimates exhibit a smoothed structure. A value of p which optimises the trade off between increased resolution and decreased

variance must be chosen. Figure 4.5 shows AR spectra generated from Holderness data for model orders in the range $10 \leq p \leq 70$.

Investigations by Vizinho [49] yielded an optimum model order for HF radar data using the modified covariance method. Vizinho used a Monte Carlo study to estimate the variance in the periodogram and AR spectral estimates. The bias and variance of calculated wave parameters were estimated using a synthesised signal. Results indicated that the error parameters were minimised for model orders in the range $20 \leq p \leq 40$ depending on the underlying ocean conditions. Wave parameters were extracted from the spectra and measurements of mean wave period, significant waveheight and wind direction were compared with wavebuoy data. Statistical evaluations yielded an optimum model order of $p = 30$.

4.2.4 Oceanographic Measurements

Radial components of ocean surface currents can be measured directly from the frequency shift of the first order peaks in the AR spectra. Within this thesis, current parameters are generated using an alternative method which is not dependent on the AR model order.

An invariant property of Doppler spectra is the Bragg peak frequency separation, which is independent of the current magnitude. Martin and Kearney [36] demonstrated an AR method for calculating radial current components from HF radar data. The method constrains the peak frequency separation to equal its theoretical value $2\omega_\mathrm{b}$, where

$$\omega_\mathrm{b} = \sqrt{g k_\mathrm{b} \tanh k_\mathrm{b} h} \tag{4.45}$$

represents the Doppler shift due to the radial speed of the Bragg ocean waves. The calculated AR coefficients, $a(k)$, are used to create a normalised z-domain representation of the AR model

$$H_1(z) = \frac{1}{\sum_{k=0}^{p} a(k) z^{-k}}, \tag{4.46}$$

where $z = \exp\{2\pi i n T\}$ and $a(0) = 1$. The AR spectral estimates, $|H_1(z)|^2$, exhibit two dominant components on the unit circle which correspond to the Bragg peak frequencies.

$$z = \exp\{2\pi i(\Delta f \pm \omega_\mathrm{b})T\} \tag{4.47}$$

The $H_1(z)$ representation is used to create an AR process $H_2(z)$

$$H_2(z) = H_1(\zeta_\mathrm{b} z)\, H_1(\zeta_\mathrm{b}^* z), \tag{4.48}$$

where $\zeta_\mathrm{b} = \exp\{2\pi i \omega_\mathrm{b} T\}$. The $H_1(\zeta_\mathrm{b} z)$ term shifts the Bragg peak frequencies to Δf and $\Delta f - 2\omega_b$ while the $H_1(\zeta_\mathrm{b}^* z)$ term shifts the Bragg peak frequencies to Δf and $\Delta f + 2\omega_b$; this produces an extremely large peak at Δf. The Doppler shift due to surface current is calculated from the peak value of $H_2(z)$.

Vizinho [49] applied the Wyatt inversion procedure to autoregressive spectra and demonstrated strong correlation between the wave parameters measured by the periodogram and AR spectral methods. Investigations indicated that the modified covariance method performs better than the periodogram for small data sets. The use of a shorter data collection period limits the current variability inherent in HF radar measurements. This reduces the problem of multiple first order structure due to temporal resolution which was described in chapter 3.

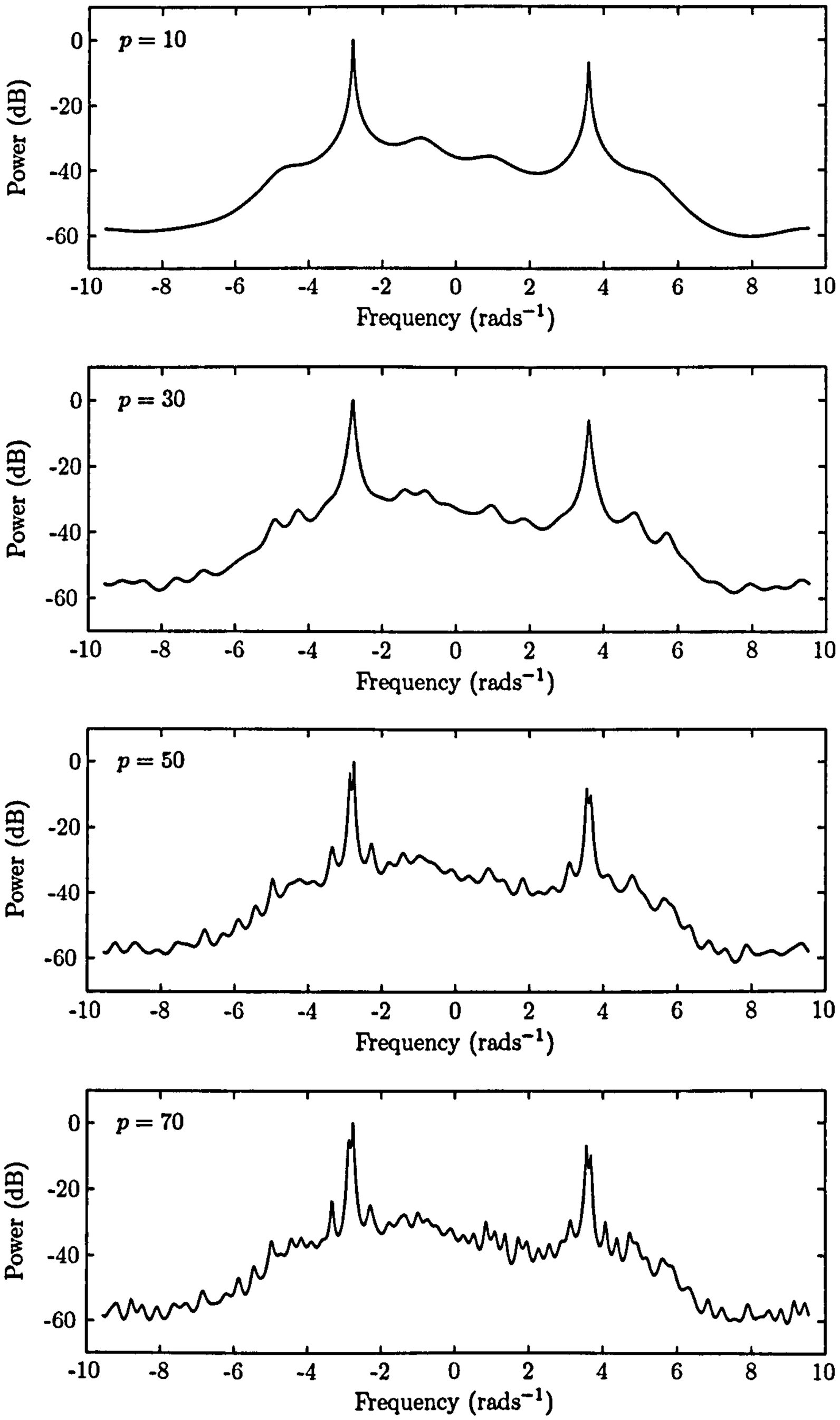

Figure 4.5: Autoregressive spectra for different model orders, $10 \leq p \leq 70$. Data taken from the master site at 20:00, 20/12/95, cell 20.

4.3 MUSIC Method

4.3.1 Historical Review

A modern class of spectral estimation techniques is based on an eigenanalysis of a data matrix. These techniques assume that the data consist of pure sinusoids in white noise and are commonly referred to as frequency estimators since power values are not preserved. These pseudo spectral techniques can be used to determine narrowband frequency components with a higher resolution than autoregressive methods [35].

The MUltiple SIgnal Classification (MUSIC) method belongs to a subset of these techniques which utilise the property that the noise subspace eigenvectors of a data matrix are orthogonal to the signal vectors [28]. The generated function is theoretically infinite at the sinusoidal frequencies. Applications of the technique have been demonstrated in HF radar oceanography: the SeaSonde system utilises the MUSIC algorithm to determine the azimuthal resolution of backscattered electromagnetic signals [3]; the OSMAR2000 radar used a MUSIC approach during a deployment in the eastern China sea [42].

4.3.2 MUSIC Algorithm

The MUSIC method is based on an eigenanalysis of an autocorrelation data matrix A. If there exists a vector $\mathbf{v}$ such that

$$\mathrm{A}\mathbf{v} = \lambda\mathbf{v} \tag{4.49}$$

for some scalar λ, then λ is an eigenvalue of A with corresponding eigenvector $\mathbf{v}$. This linear system of equations can be written as

$$(\mathrm{A} - \lambda\mathrm{I})\mathbf{v} = \mathbf{0}, \tag{4.50}$$

which has solutions given by the characteristic equation

$$\det(\mathrm{A} - \lambda\mathrm{I}) = 0. \tag{4.51}$$

The calculation of the eigenvalues and eigenvectors of a matrix is known as eigendecomposition. The MUSIC method uses an eigendecomposition of an autocorrelation matrix, A, to divide the data into a signal and a noise subspace. An eigendecomposition of A generates eigenvalues λ_i $(1 \leq i \leq p)$ such that

$$\lambda_1 \geq \lambda_2 \geq \ldots \geq \lambda_p, \tag{4.52}$$

where p represents the order of the matrix A. The m dominant eigenvalues, λ_i $(1 \leq i \leq m)$, are known as the principal eigenvalues. The corresponding principal eigenvectors, $\mathbf{v}_i$ $(1 \leq i \leq m)$, span the signal subspace while the remaining eigenvectors, $\mathbf{v}_i$ $(m < i \leq p)$, span the noise subspace [35]. The MUSIC algorithm belongs to a noise subspace class of frequency estimators which utilise the property that the $p - m$ noise subspace eigenvectors $\mathbf{v}_{m+1}, \ldots, \mathbf{v}_p$ of an autocorrelation matrix are orthogonal to the signal vectors [28]. Therefore any linear combination

$$\sum_{k=m+1}^{p} \alpha_k |\mathbf{e}^H(n)\mathbf{v}_k|^2 = \mathbf{e}^H(n) \left(\sum_{k=m+1}^{p} \alpha_k \mathbf{v}_k \mathbf{v}_k^H \right) \mathbf{e}(n), \tag{4.53}$$

with arbitrary parameters α_k, where $\mathbf{e}(n)$ is the sinusoid vector

$$\mathbf{e}(n) = \begin{pmatrix} 1 \\ \exp\{2\pi i n T\} \\ \vdots \\ \exp\{2\pi i n m T\} \end{pmatrix} \tag{4.54}$$

will equal zero whenever $\mathbf{e}(n)$ corresponds to one of the signal vectors. Setting $\alpha_k = 1$ yields the MUSIC frequency estimator which theoretically has infinite value at the signal frequencies.

$$P(n) = \frac{1}{\mathbf{e}^H(n)\left(\sum_{k=m+1}^{p} \mathbf{v}_k \mathbf{v}_k^H\right)\mathbf{e}(n)} \tag{4.55}$$

4.3.3 HF Radar Signal Processing

The MUSIC method utilises an autocorrelation matrix to form frequency estimates. For most physical applications the autocorrelation sequence is unknown but the technique can be extended to alternative data matrices. The covariance and modified covariance matrices have similar eigendecomposition properties to the autocorrelation matrix. The modified covariance matrix has been shown to work best for undamped sinusoids in noise and is subsequently used in this analysis [35]. Using OSCR data, $x(nT)$, a modified covariance matrix, A_p, is formed from two Toeplitz matrices.

$$\mathrm{A}_p = \begin{bmatrix} \mathrm{T}_p \\ \mathrm{T}_p^* J \end{bmatrix}, \tag{4.56}$$

$$\mathrm{T}_p = \begin{bmatrix} x(pT) & \dots & x(0) \\ \vdots & & \vdots \\ x((N-1)T) & \dots & x((N-p-1)T) \end{bmatrix} \tag{4.57}$$

A complex Singular Value Decomposition (SVD) of A_p is used to partition the matrix into a signal and a noise subspace. The m principal eigenvectors span the signal subspace; the singular values of these eigenvectors are larger than the noise subspace values. Figure 4.6 shows the singular values generated from an SVD of a modified covariance matrix in the Holderness deployment. The graph illustrates the two dominant singular values which represent the principal Bragg components in the radar signal. MUSIC frequency estimates are calculated from the $p-2$ noise subspace eigenvectors. Figure 4.7 shows MUSIC spectra generated from Holderness data.

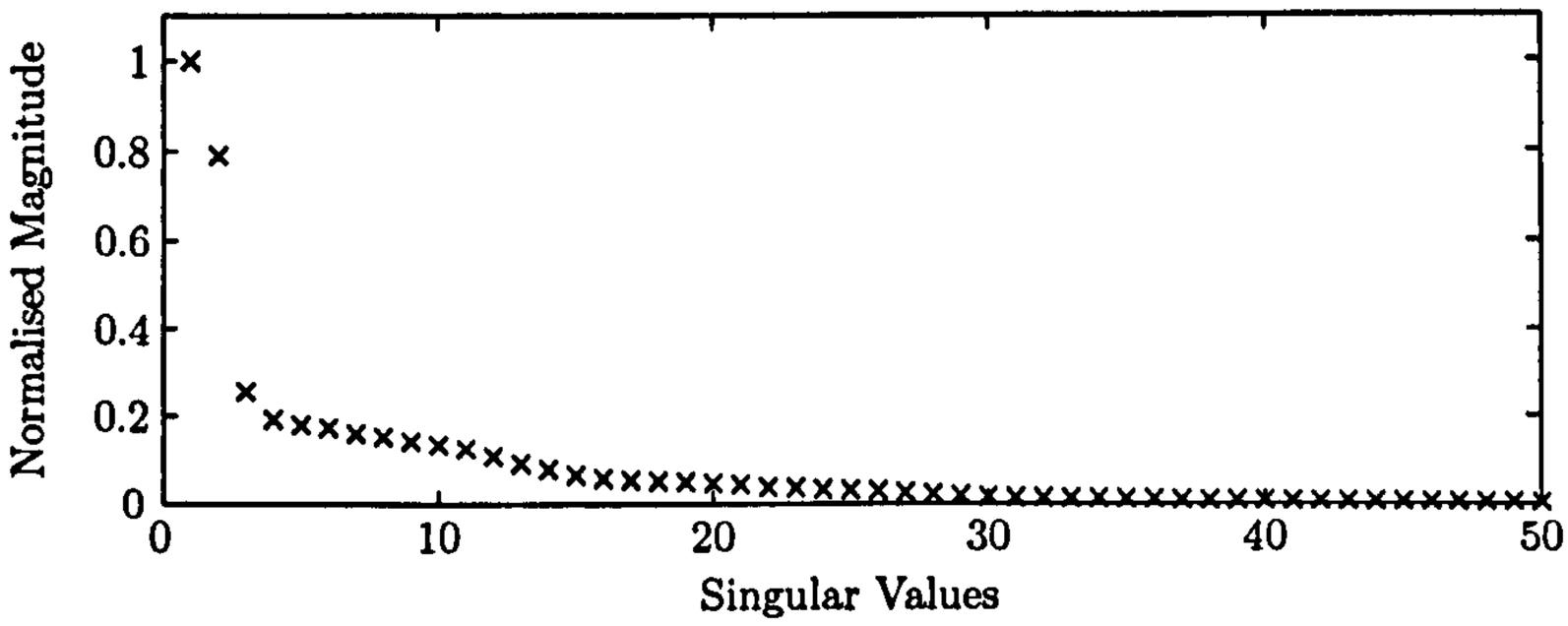

Figure 4.6: Singular values of data matrix, A_p, showing the two dominant Bragg components. Data taken from master site at 20:00, 08/12/95, cell 562.

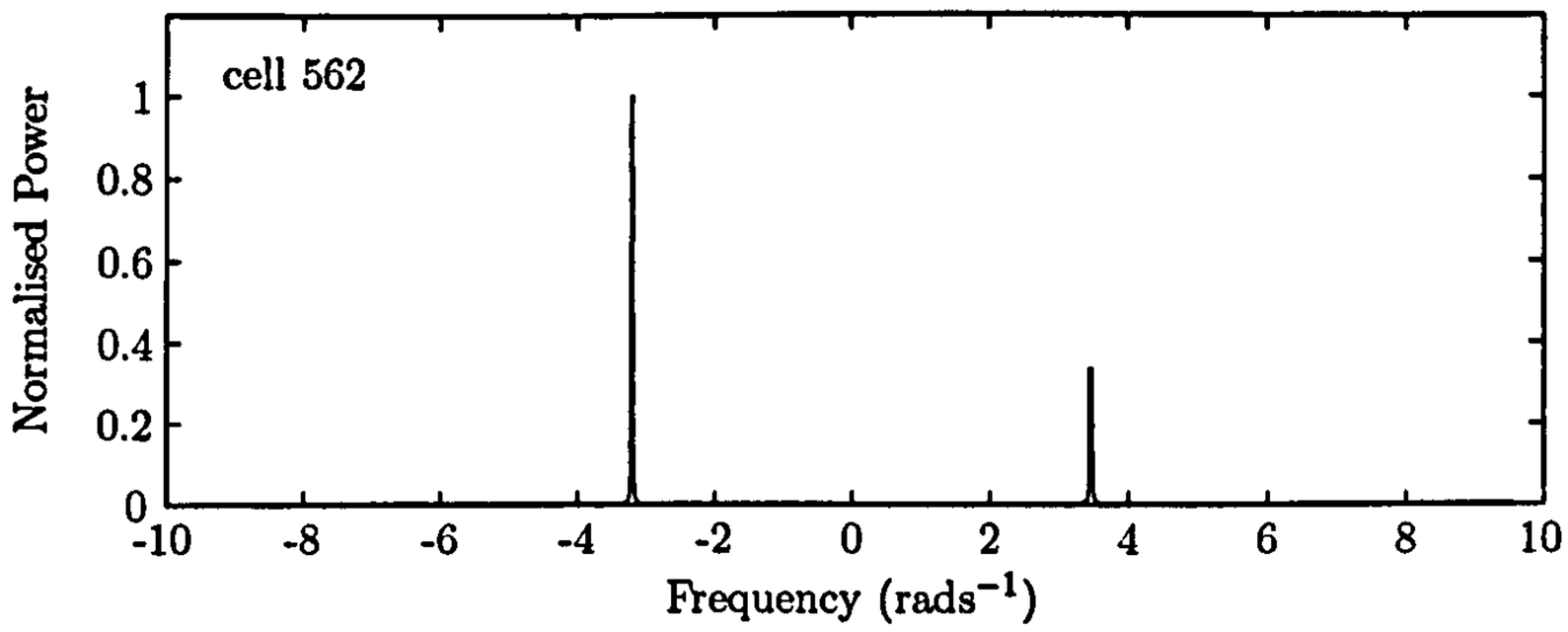

Figure 4.7: MUSIC spectra. Data taken from master site at 20:00, 08/12/95.

4.3.4 Oceanographic Measurements

The spikes in MUSIC spectra represent the Bragg peak frequency locations. If two frequency components, Λ^+ and Λ^-, are resolved from the radar data then the Doppler shift due to surface current is given by

$$\Delta f = \frac{\Lambda^+ + \Lambda^-}{2}. \tag{4.58}$$

However, analysis of Holderness data reveals that the MUSIC technique often fails to resolve both Bragg peaks. In this case, the current component can be estimated from the single resolved peak in the spectrum.

MUSIC is a frequency estimation technique and consequently does not preserve the power characteristics of a signal. Wave measurements utilise the second order portions of a Doppler spectrum so the MUSIC method is only appropriate for measuring surface currents.

4.4 Summary

Three alternative spectral techniques for analysing HF radar signals were introduced in this chapter: an instantaneous frequency filter method which measures the time varying characteristics of each Bragg peak; an autoregressive parametric modelling approach; a MUSIC algorithm which performs an eigendecomposition of radar data. These techniques are evaluated in the following chapter in order to determine the optimum approach for HF radar oceanography.

5 Evaluation of Spectral Techniques

Alternative spectral estimation methods to the standard periodogram were studied in chapter 4. An instantaneous frequency approach has been proposed as a mechanism for removing the first order modulation from backscattered HF radar signals. The aim of this chapter is to evaluate the IF filter technique and determine the optimum spectral analysis method for measuring oceanographic parameters. The chapter is divided into two sections:

- Comparisons of radar measurements with data from a current meter.
- Investigation of an invariant property of Doppler spectra.

5.1 Current Meter Analysis

During the SCAWVEX Holderness experiment, oceanographic parameters were obtained using a variety of in situ instruments including acoustic Doppler current profilers, electromagnetic current meters and pressure wave recorders. Measurements from an InterOcean S4 current meter are analysed in this chapter.

Figure 2.1 shows the geographical location of the S4 current meter which was deployed by the Proudman Oceanographic Laboratory (POL) on a POL monitoring platform approximately 17 metres below the sea's surface. An S4 consists of a 25 cm diameter sphere containing electromagnetic sensors. The device operates by measuring the voltage gradient created by water movement in a magnetic field which is generated by the sensor [8]. Ocean current vectors were sampled at one second intervals for the first 20 minutes of every hour.

5.1.1 Statistical Methodology

Time series data from the S4 current meter and the OSCR radar system are evaluated using statistical methods. Before analysing the relationship between these data, it is important to identify the contrasting measuring principles employed by the instruments. Graber *et al* [16] performed a detailed investigation into the sources of error associated with these differences. The processes are separated into three areas: errors associated with the current meter; errors associated with the HF radar system; and the temporal and spatial sampling differences between the two technologies.

The S4 current meter had a maximum measurement range of ± 3.5 ms^{-1} and an intrinsic resolution of 0.02 cms^{-1} [16]. The instrument error has been shown to be approximately 2% which corresponds to current speed accuracy in the range of ± 0.04 ms^{-1} for the Holderness experiment. The S4 has an azimuthal resolution of ± 2 degrees.

OSCR system errors can be caused by geometric constraints. The accuracy of radar derived vector currents is dependent on the angle between the intersecting radials from the master and slave sites and was discussed in section 2.4. In order to reduce the influence of geometric errors, comparisons between radar and current meter data will be considered in the radar beam directions. This will also eliminate the effect of nonsynchronous data collection from the master and slave sites in the OSCR system.

Measurement differences between the OSCR system and the S4 current meter are also expected due to the contrasting sampling methodologies of the two instruments. The systems measure different characteristics of the temporally and spatially varying ocean current field. HF radar measurements represent a temporal average over a fixed surface area whereas current meters provide point measurements at a fixed depth in the water column. The OSCR radars used in the Holderness experiment measured ocean currents over a surface area of approximately 1 km^2. Spatial inhomogeneity within this region contributes to differences between radar and S4 estimates. HF radar systems measure ocean currents at a depth proportional to the radar wavelength. Stewart and Joy [43] showed that this depth is approximately $\lambda/8\pi$ metres which corresponds to a value of 0.47 metres in the Holderness deployment. The OSCR near-surface data contrast with the S4 current meter measurements due to vertical shear forces [39].

During the OSCR data collection period, a single radial current estimate is generated from each of the master and slave radars; each measurement can be considered as an average of the ocean surface currents with a temporal resolution of five minutes. In order to synchronise the radar and current meter data sets, measurements from the master and slave radars are studied separately. S4 data in the direction of the master radar beam are averaged over the first five minutes of each hour and compared with radial measurements from the master radar; S4 data in the direction of the slave radar beam are averaged over the second five minutes of each hour and compared with radial measurements from the slave radar.

Current components were extracted from OSCR data using the periodogram (PG), instantaneous frequency (IF), autoregressive (AR) and MUSIC spectral techniques. Although the instantaneous frequency filter uses a periodogram to generate Doppler spectra, it will be denoted as the IF method in all subsequent analysis in order to distinguish it from the standard periodogram technique which was described in chapter 3.

Let $(x_1, y_1), \ldots, (x_n, y_n)$, represent n pairs of ocean current observations where x_i and y_i represent the ith measurement from the OSCR and S4 instruments respectively. The mean and variance of the two distributions are given by

$$\overline{x} = \frac{1}{n}\sum_{i=1}^{n} x_i\,, \qquad \sigma_x^2 = \frac{1}{n-1}\sum_{i=1}^{n}(x_i - \overline{x})^2, \tag{5.1}$$

$$\overline{y} = \frac{1}{n}\sum_{i=1}^{n} y_i\,, \qquad \sigma_y^2 = \frac{1}{n-1}\sum_{i=1}^{n}(y_i - \overline{y})^2. \tag{5.2}$$

The product-moment correlation coefficient provides an indication of the strength of the linear relationship between the two variables

$$r_{xy} = \frac{S_{xy}}{\sqrt{S_{xx}S_{yy}}}\,, \tag{5.3}$$

where

$$S_{xx} = \sum_{i=1}^{n} x_i^2 - n\overline{x}^2, \tag{5.4}$$

$$S_{yy} = \sum_{i=1}^{n} y_i^2 - n\overline{y}^2, \tag{5.5}$$

$$S_{xy} = \sum_{i=1}^{n} x_i y_i - n\overline{xy}. \tag{5.6}$$

The coefficient is defined in the range $-1 \leq r_{xy} \leq 1$: a value of $r_{xy} = 1$ represents perfect positive correlation; $r_{xy} = -1$ represents perfect negative correlation; $r_{xy} = 0$ indicates uncorrelated data. The square of the correlation coefficient, r_{xy}^2, is often used in scientific work when comparing data.

Regression analysis is used to determine the linear relationship between the radar and current meter data. In the nineteenth century, French mathematician Adrien Legendre introduced a least squares method for calculating the optimum straight line fit to a data set. The linear equation is of the form

$$y = a + bx, \tag{5.7}$$

where a and b are the y-intercept and gradient of the line respectively.

$$a = \overline{y} - b\overline{x} \tag{5.8}$$

$$b = \frac{S_{xy}}{S_{xx}} \tag{5.9}$$

The root mean square (rms) parameter provides an estimate of the average magnitude differences between the radar and current meter measurements.

$$\varepsilon_{\text{rms}} = \left(\frac{\sum_{i=1}^{n} [(y_i - \overline{y}) - (x_i - \overline{x})]^2}{n} \right)^{\frac{1}{2}} \tag{5.10}$$

5.1.2 Results

Results in this section are taken from a three day period, between the 20th and 23rd December 1995, where continuous data were available in the Holderness area. Figure 5.1 shows OSCR and S4 derived current magnitudes in the master and slave radial directions. Only the IF filter radar currents have been shown since the graphs derived from the PG, IF, AR and MUSIC methods are indistinguishable from each other at this resolution. The data exhibit sinusoidal characteristics, caused by the tidal cycle which dominates the current dynamics in the region. The corresponding power spectra are shown in figure 5.2 which illustrates this tidal component. Figure 5.3 shows the observed correlation between currents derived from the S4 and the four radar spectral techniques. Tables 5.1 and 5.2 show the statistical analysis results derived from the data.

The time series data exhibit strong similarities although the amplitudes of the radar derived currents are consistently larger than the S4 components. Previous studies concerning the Holderness region have attempted to quantify the attenuation of ocean currents with depth. Data from an InterOcean directional wave current meter (S4DW), deployed at a depth of 14 metres, were analysed. Surface currents were estimated from the S4DW by applying a constant factor of 1.4 to the sub surface measurements [39]. This was found to give a close to optimum correction [51]. Data from an experiment at Petten in the Netherlands were also investigated. An S4DW was deployed approximately 10 km offshore at a depth of 20 metres. Analysis revealed a factor of two difference between current parameters from the S4DW and a surface measuring WERA radar system [51].

The S4 in the Holderness deployment was located approximately 17 metres below the ocean surface. Tables 5.1 and 5.2 show the derived least squares parameters which provides gradients in the range ($1.71 < b < 1.75$). An interpolation of the S4DW results provides evidence of a linear relationship between the OSCR and S4 components.

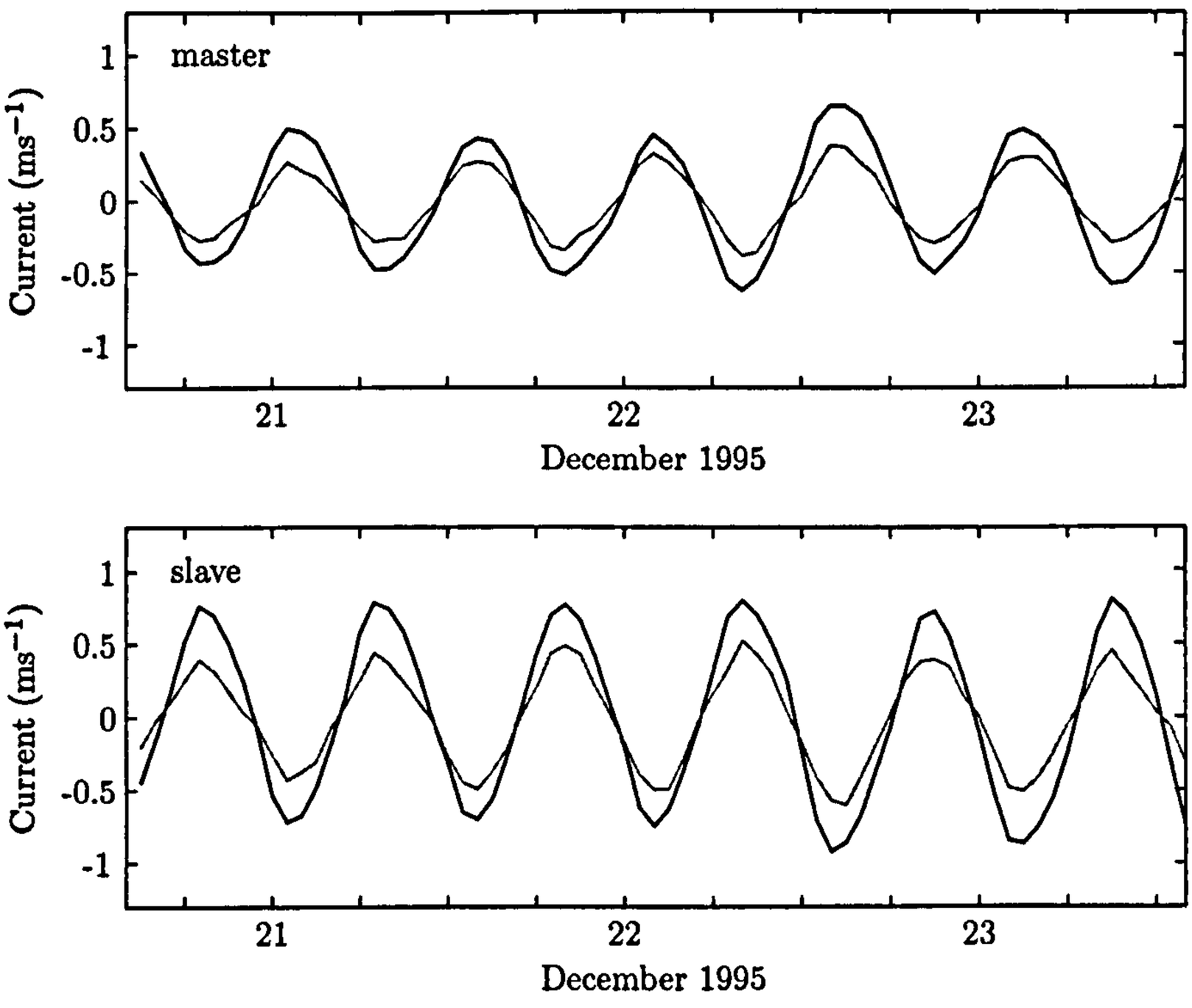

Figure 5.1: Time series of OSCR (dark) and S4 (light) current magnitudes using IF spectral technique. Data taken from a 72 hour time period between 15:00, 20/12/95 and 14:00, 23/12/95.

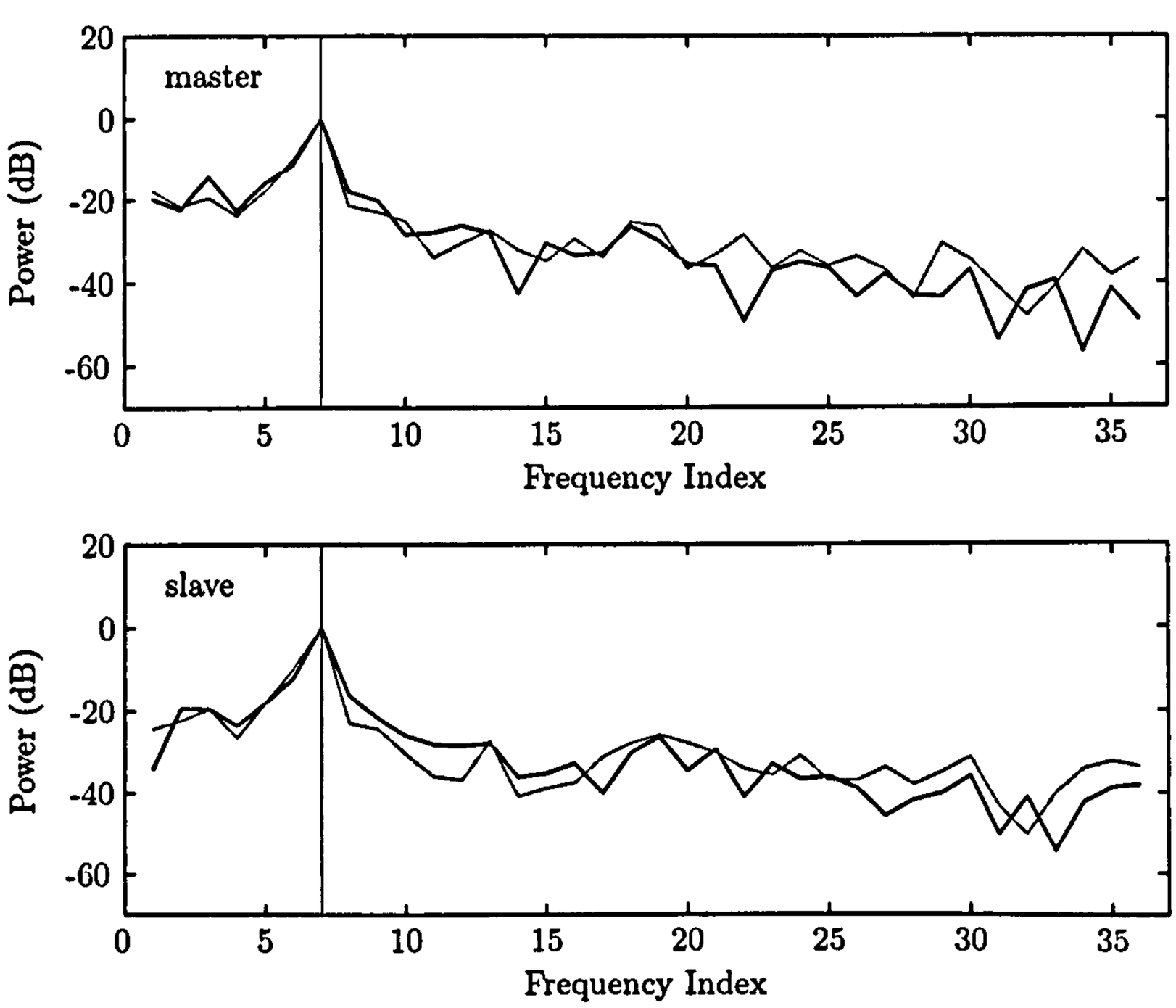

Figure 5.2: Power spectra of OSCR (dark) and S4 (light) time series currents. The vertical lines represent the tidal frequency. Data taken from a 72 hour time period between 15:00, 20/12/95 and 14:00, 23/12/95.

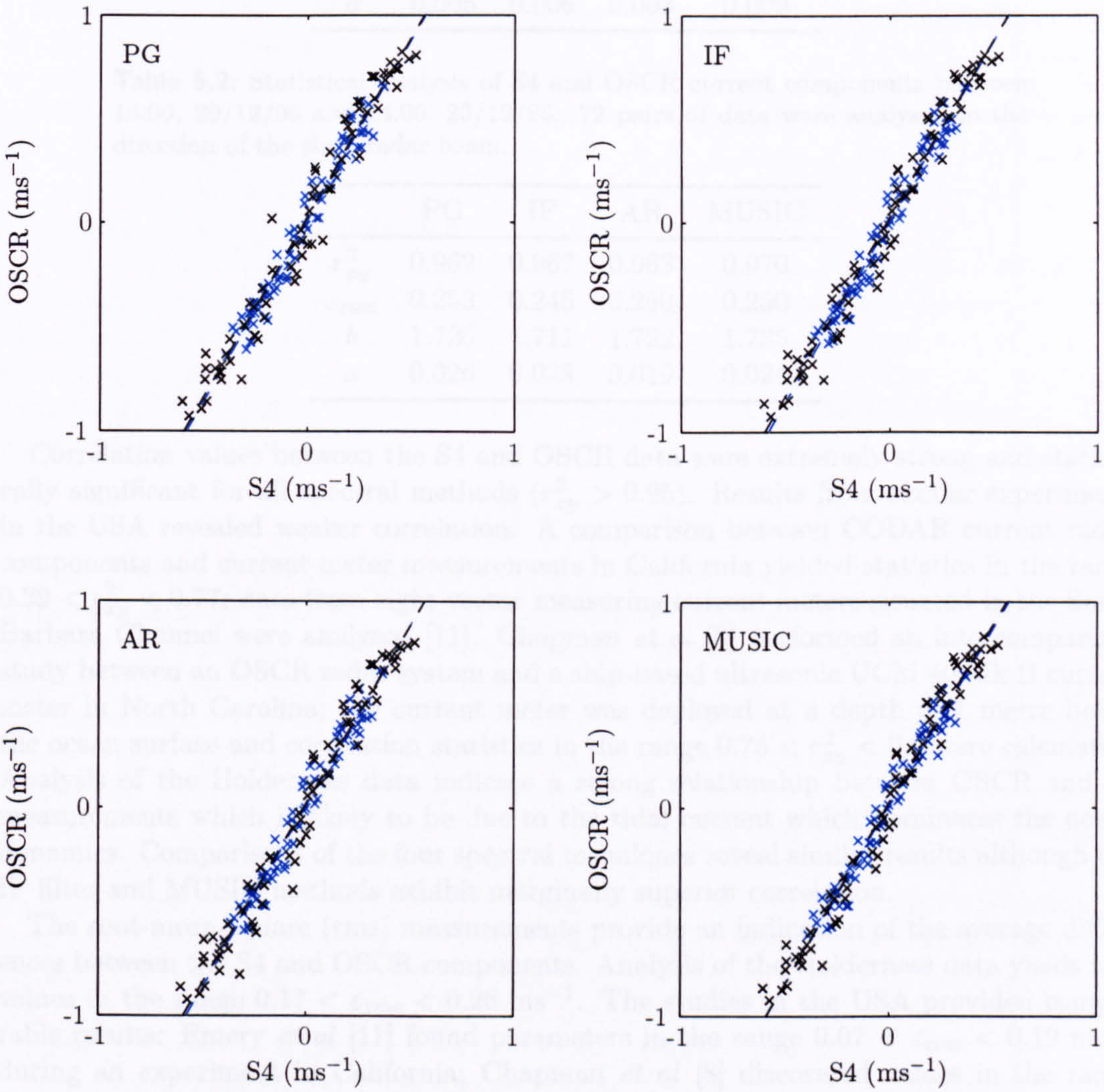

Figure 5.3: Scatter plots of current radial components. S4 vs OSCR. The blue and black crosses represent the master and slave directions respectively. The dashed lines show the regression analysis results. Data taken between 15:00, 20/12/95 and 14:00, 23/12/95.

Table 5.1: Statistical analysis of S4 and OSCR current components between 15:00, 20/12/95 and 14:00, 23/12/95. 72 pairs of data were analysed in the direction of the master radar beam.

	PG	IF	AR	MUSIC
r_{xy}^2	0.960	0.965	0.962	0.962
ε_{rms}	0.172	0.170	0.173	0.167
b	1.734	1.734	1.748	1.719
a	0.005	0.006	0.003	0.009

Table 5.2: Statistical analysis of S4 and OSCR current components between 15:00, 20/12/95 and 14:00, 23/12/95. 72 pairs of data were analysed in the direction of the slave radar beam.

	PG	IF	AR	MUSIC
r_{xy}^2	0.962	0.967	0.963	0.970
ε_{rms}	0.253	0.245	0.250	0.250
b	1.726	1.711	1.722	1.735
a	0.026	0.028	0.019	0.024

Correlation values between the S4 and OSCR data were extremely strong and statistically significant for all spectral methods ($r_{xy}^2 > 0.95$). Results from similar experiments in the USA revealed weaker correlation. A comparison between CODAR current radial components and current meter measurements in California yielded statistics in the range $0.39 < r_{xy}^2 < 0.77$; data from eight vector measuring current meters situated in the Santa Barbara Channel were analysed [11]. Chapman *et al* [8] performed an intercomparison study between an OSCR radar system and a ship-based ultrasonic UCM 40 Mk II current meter in North Carolina; the current meter was deployed at a depth of 1 metre below the ocean surface and correlation statistics in the range $0.75 < r_{xy}^2 < 0.9$ were calculated. Analysis of the Holderness data indicate a strong relationship between OSCR and S4 measurements which is likely to be due to the tidal current which dominates the ocean dynamics. Comparisons of the four spectral techniques reveal similar results although the IF filter and MUSIC methods exhibit marginally superior correlation.

The root-mean-square (rms) measurements provide an indication of the average differences between the S4 and OSCR components. Analysis of the Holderness data yields rms values in the range $0.17 < \varepsilon_{\text{rms}} < 0.26$ ms^{-1}. The studies in the USA provided comparable results: Emery *et al* [11] found parameters in the range $0.07 < \varepsilon_{\text{rms}} < 0.19$ ms^{-1} during an experiment in California; Chapman *et al* [8] discovered values in the range $0.11 < \varepsilon_{\text{rms}} < 0.16$ ms^{-1} in North Carolina. The larger rms values from the Holderness data are likely to be caused by the depth of the current meter in the ocean; the S4 was deployed near the sea floor whereas the instruments used in the USA experiments were located in the top few metres of the ocean. Analysis of the Holderness data indicates that the four spectral techniques generate similar results, although the IF filter and MUSIC methods provide the lowest rms values.

5.2 Spectral Properties

The accuracy of the generated oceanic parameters is dependent on the quality of the Doppler spectra. This section studies the characteristics of spectra produced from backscattered data from the sea's surface. Figure 5.4 shows Doppler spectra produced from the Holderness data using the periodogram, IF filter, AR and MUSIC spectral techniques. The structure of the Doppler spectra is dependent on the underlying ocean conditions. This unknown parameter provides complexity in evaluating the four spectral techniques.

An invariant property of Doppler spectra is the separation of the positive and negative Bragg peaks. The frequencies of these dominant peaks are determined by the phase velocity of the corresponding Bragg ocean waves. If the radial component of surface current is zero, then the peaks are situated at $\pm\omega_b$. An underlying surface current shifts both Bragg peaks by an amount proportional to the current velocity. The frequency separation of the two peaks remains constant and can be used to provide an indication of the quality of the spectral techniques.

Data from the Holderness deployment were used to generate time series of Bragg peak separation values. The data were converted into Doppler spectra using the spectral analysis techniques described in previous chapters. The Bragg peak frequency locations, $\Lambda^{\pm}$, were approximated using a centroid calculation in the region surrounding the maxima in each Doppler spectrum. The bias, χ, was determined by calculating the deviation of the measured peak separation from the theoretical value.

$$\chi = \Lambda^{+} - \Lambda^{-} - 2\omega_b \tag{5.11}$$

The structure of the Doppler spectra is influenced by factors pertaining to the OSCR radar such as SNR levels, system noise, antenna sidelobes and radio interference. In order to study the spectral techniques under a variety of conditions, data were analysed from three grid cells at different ranges from the radar sites. Figure 5.5 shows the locations of the measurement cells in the Holderness region. The SNR in the backscattered data is related to the range of the target cell since signal strength attenuates with range.

Table 5.3 shows the statistical analysis results derived from χ during a 48 hour period between the 20th and 22nd December 1995. the means, $\overline{\chi}$, and variances, σ_{χ}^2, of the spectral data are related to the range of the target cell due to the SNR in the received signal. Analysis of the spectral techniques reveals that the IF mean biases are significantly smaller than the periodogram and AR methods. This indicates that the IF method accurately resolves the Bragg peak frequencies which is important for current measurements. The AR method provides the smallest standard deviations although the IF filter also exhibits significantly reduced variance compared to the periodogram technique.

Problems were encountered during the analysis since the MUSIC technique often failed to resolve both Bragg peaks. Ocean current components can be estimated from the frequency shift of a single resolved peak but a calculation of the Bragg peak separation is not possible. This phenomenon was evident during a large proportion of the above measurement period and, as a result, the MUSIC method was analysed over a shorter time period of 18 hours during which both Bragg peaks were resolved. The MUSIC technique yielded a mean value of -0.0034 which was larger in magnitude than the alternative spectral methods; the periodogram, IF filter and AR techniques provided mean bias values of -0.0029, 0.0014 and -0.0028 respectively.

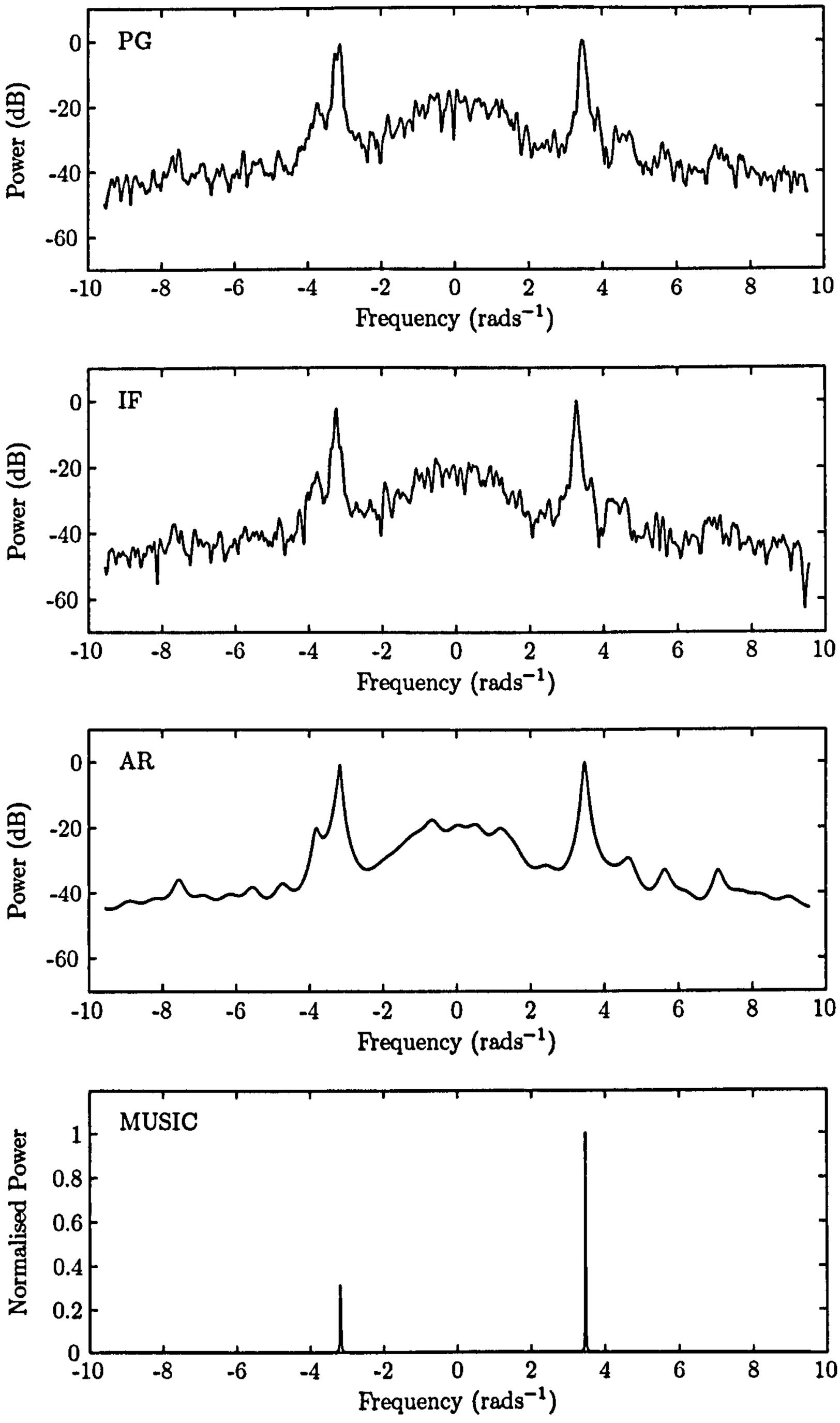

Figure 5.4: Doppler spectra produced by PG, IF, AR and MUSIC spectral techniques. Data taken from the master site at 20:00, 8/12/95, cell 77.

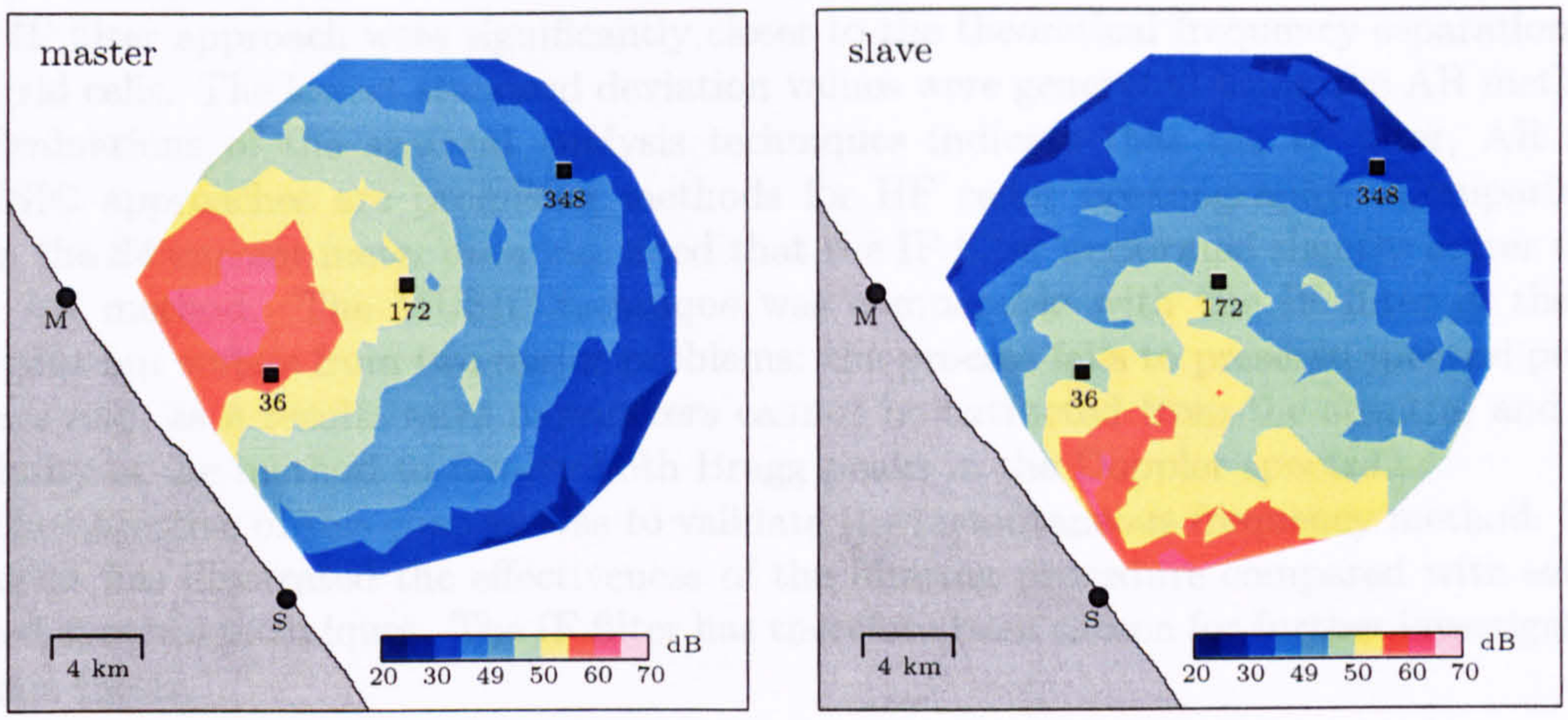

Figure 5.5: The measurement cells for the peak separation analysis showing the SNR from the master and slave radar sites. Data taken at 18:00, 21/12/95.

Table 5.3: Mean, $\overline{\chi}$, and standard deviation, σ_χ, of peak separation biases using PG, IF and AR spectral techniques. 144 pairs of data were analysed between 16:00, 20/12/95 and 15:40, 22/12/95.

		master		slave	
	cell	$\overline{\chi}$	σ_χ	$\overline{\chi}$	σ_χ
PG	36	-0.0043	0.0089	-0.0050	0.0137
	172	-0.0048	0.0093	-0.0046	0.0073
	348	-0.0039	0.0102	-0.0037	0.0095
IF	36	0.0008	0.0080	-0.0000	0.0074
	172	0.0007	0.0073	0.0001	0.0075
	348	-0.0003	0.0078	0.0002	0.0069
AR	36	-0.0045	0.0056	-0.0059	0.0129
	172	-0.0044	0.0059	-0.0038	0.0041
	348	-0.0049	0.0053	-0.0035	0.0053

5.3 Summary

Within this chapter, four different spectral techniques have been evaluated using data from the Holderness deployment. Statistical comparisons were conducted between ocean current measurements from an OSCR radar system and an S4 current meter. Correlation values between the radar techniques and the S4 provided strong evidence of a linear relationship between the data sets. The correlation coefficient parameters ($r^2_{xy} > 0.95$) were statistically significant and compared favourably with two similar experiments conducted in the USA. Analysis of the four spectral techniques revealed similar results although the IF filter and MUSIC methods performed marginally better.

An invariant property of Doppler spectra was studied. Time series of the Bragg peak separation biases were calculated over a 48 hour period. The IF filter and AR techniques both exhibited increased accuracy compared with the large fluctuations present in the periodogram data. Statistical analysis indicated that mean bias values generated using

the IF filter approach were significantly closer to the theoretical frequency separation for all grid cells. The lowest standard deviation values were generated using the AR method.

Evaluations of the spectral analysis techniques indicate that the IF filter, AR and MUSIC approaches are promising methods for HF radar oceanography. Comparisons with the S4 current meter data indicated that the IF filter performed slightly better than the AR method. The MUSIC technique was comparable with the IF filter in the S4 analysis but suffers from two major problems: the process fails to preserve spectral power values and, as a result, wave parameters cannot be extracted from the spectra; and the inability of the method to resolve both Bragg peaks in the Doppler spectra.

The objective of this chapter was to validate the instantaneous frequency method. The analysis has illustrated the effectiveness of the filtering procedure compared with established spectral techniques. The IF filter has therefore been chosen for further investigation in this thesis.

6 Instantaneous Frequency Filter

Alternative spectral analysis techniques to the periodogram were introduced in chapter 4. These were evaluated using statistical methods in chapter 5. The potential of the instantaneous frequency filter was identified and is examined in more detail within this chapter:

- Noise contributions to the accuracy of the method are studied.
- Simulated data are used to determine various properties of the filter.
- Oceanographic conditions are modelled.
- The optimum filter bandwidth parameters are determined.

6.1 HF Radar Data

This section examines the effect of noise on the radar data. The signal-to-noise ratio (SNR) measures the strength of a signal relative to the background noise and is expressed in logarithmic decibel (dB) scale. The ratio is determined from the power contained in the signal and noise components of the data, represented by P_s and P_n respectively.

$$\mathrm{SNR} = 10 \log_{10} \left(\frac{P_s}{P_n} \right) \tag{6.1}$$

SNR is dependent on the range of the measurement cell from the radar site. The attenuation of signal amplitude with range is determined by the propagation loss of the radar signal and the scattering strength of the sea surface [18].

Holderness data from two grid cells, located at different ranges from the master radar, were analysed and a strong correlation between SNR and IF variance was identified. Figure 6.1 shows IF and amplitude signals generated from the positive Bragg components in the backscattered data. Cell 8 illustrates a region close to the radar where the signal's amplitude is strong during the majority of the measurement period. The corresponding IF signal exhibits a relatively smooth structure. Cell 75 is situated at a greater range from the radar site and represents an area with lower SNR. The amplitude signal is weaker and consequently the IF signal contains higher variance.

Parent and Bourdillon examined the behaviour of IF signals from a skywave radar system in France [37]. They observed discontinuities in the data when the amplitudes of the positive and negative peak signals were low. Analysis of Holderness data reveals similar results. Figure 6.1 shows that the sharp variations in the IF functions coincide with the minimum values in the amplitude signal; the IF estimates, $z^{\pm}(nT)$, become corrupted when the amplitudes in $y^{\pm}(nT)$ are low, due to the influence of background noise.

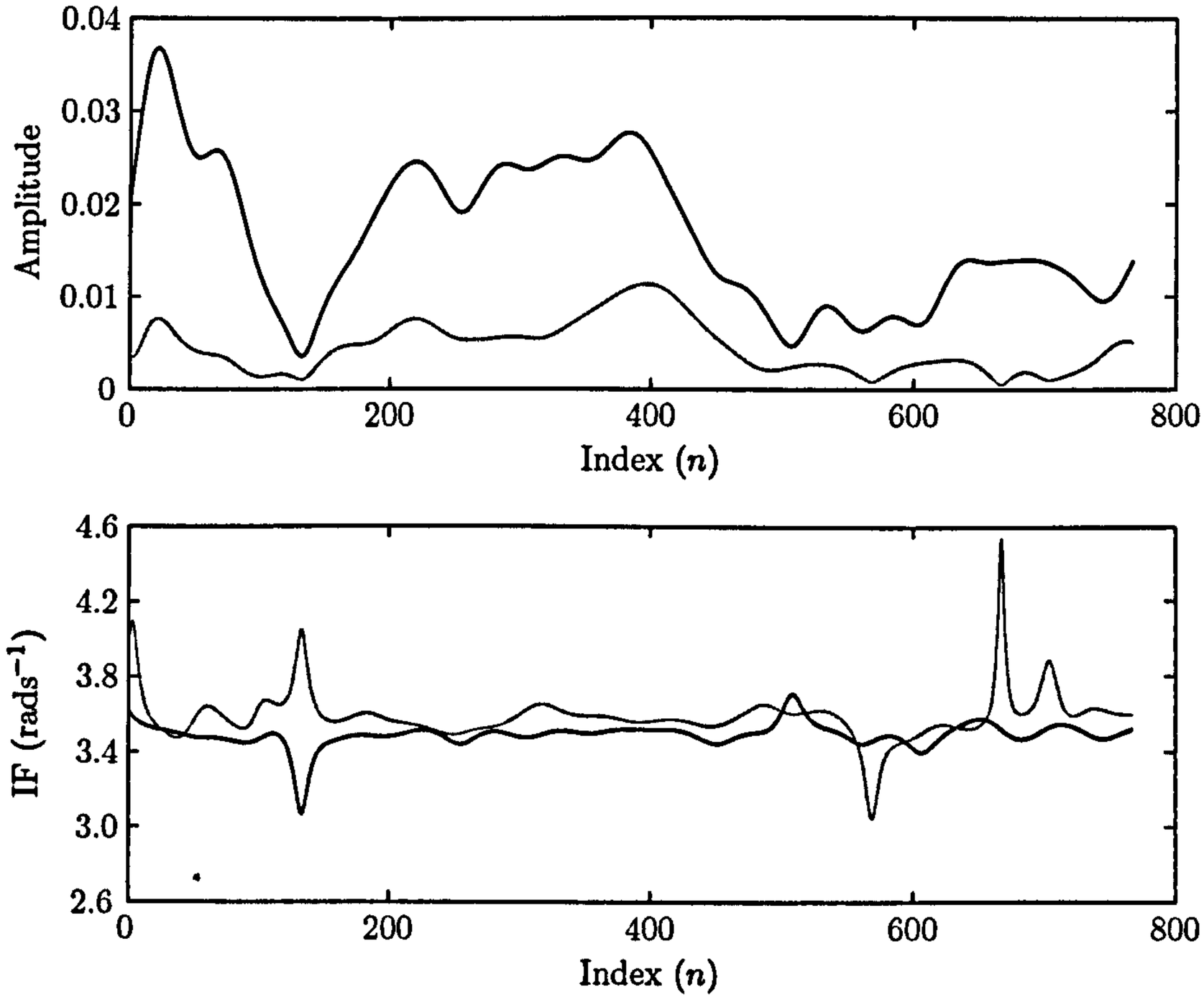

Figure 6.1: Amplitude and IF signals derived from positive Bragg components. Data taken from master site at 20:00, 08/12/95 for cells 8 (dark) and 75 (light).

These examples suggest that a significant proportion of the variance contained in IF signals can be attributed to noise. The Bragg peak frequencies, $\Lambda^{\pm}$, are determined from the weighted mean of the IF signals. The peak time signal amplitudes are used as a weighting function which minimises the effect of noise in current measurements.

$$\Lambda^{\pm} = \frac{\sum_{n=0}^{N-1} |y^{\pm}(nT)|^2 \, z^{\pm}(nT)}{\sum_{n=0}^{N-1} |y^{\pm}(nT)|^2} \tag{6.2}$$

Lowpass filtering can be used to reduce the noise influence in IF signals. The accuracy of the filtered radar signals will be increased which, consequently, should improve the quality of the derived wave parameters. It is important that only the noise contributions are extracted from the signal, since the IF structure may provide additional insight into underlying oceanographic processes.

Figure 6.2 illustrates the implications of lowpass filtering IF signals with bandwidth 2ρ rads^{-1}. The aim of the procedure is to remove any discontinuities in the data which are due to noise. The noise contribution to the signal decreases with ρ and the IF signals exhibit a smoother structure. Lowpass filter widths in the upper range of values of ρ reduce the magnitude of only the large discontinuities in the data; values of ρ in the lower range cause the IF signal to approach a constant value as the data extracted by the lowpass filter tends towards a delta function.

Holderness data were analysed in order to determine the optimum value for ρ. Some difficulty was encountered in distinguishing between the cases when the IF structure was caused by noise and when it may be due to current variability. Numerous data from different temporal and spatial regions were examined: $\rho = 0.3$ rads^{-1} was selected since this value restricts the large discontinuities in the data caused by noise, whilst retaining a significant proportion of the first order structure.

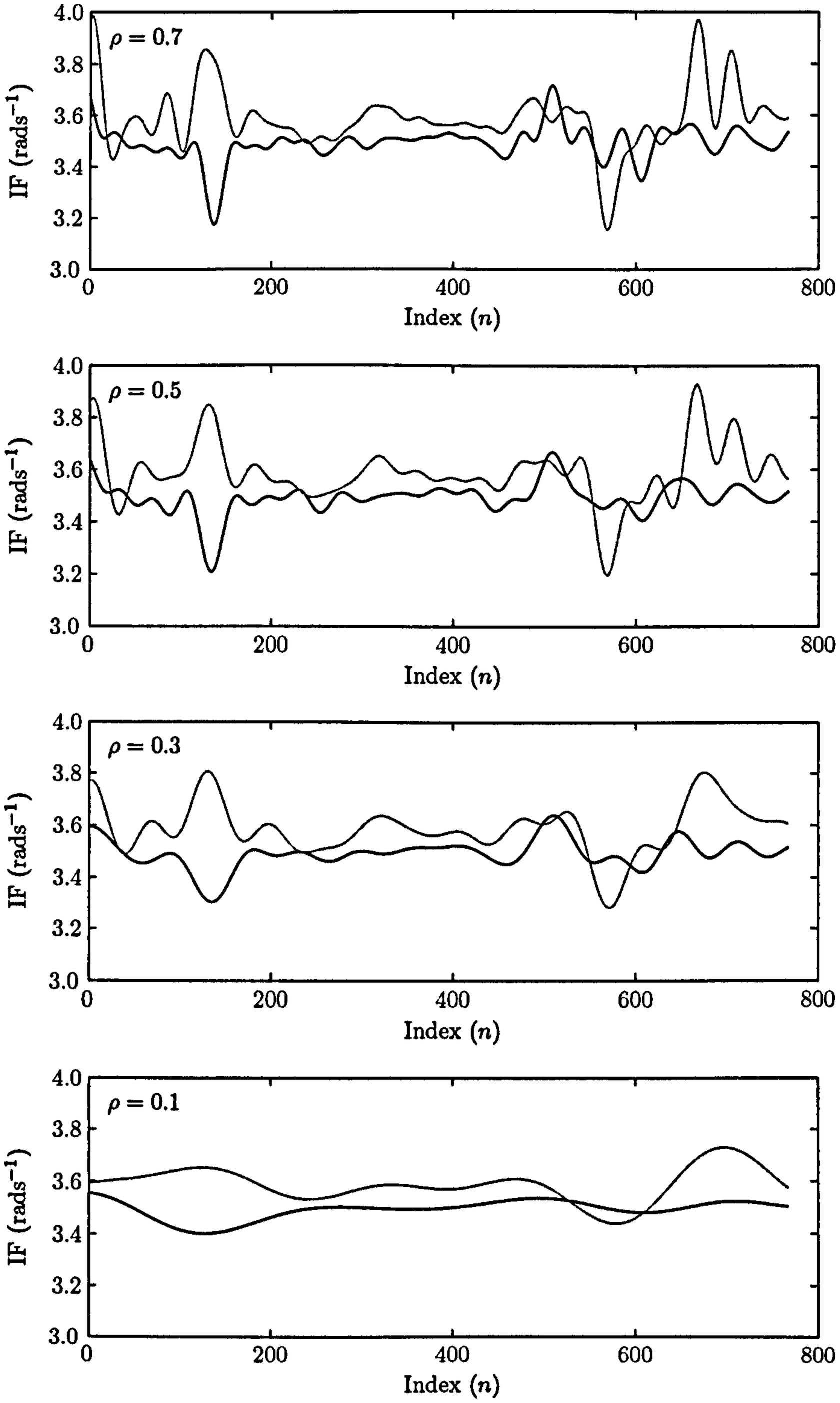

Figure 6.2: Lowpass filtered IF signals derived from positive Bragg components for cell 8 (dark) and cell 75 (light). Data taken from the master site at 20:00, 08/12/95 for $0.1 \leq \rho \leq 0.7$.

6.2 Simulated Data

Simulated data are used to study the impact of the IF filter signal processing. A simple analytic function is introduced which is used as the basis signal for the following modelling. The influence of additive noise is also investigated.

6.2.1 Basis Signal

The signal $x(nT)$ represents an oceanographic situation where the measurement region comprises incoming and outgoing Bragg wave trains travelling parallel to the radar beam.

$$x(nT) = 2\alpha \cos(\omega_b nT) \qquad (0 \leq n < N) \tag{6.3}$$

Bragg ocean waves travel with a phase velocity, c_b, which is described by the gravity wave dispersion relation (equation 3.11). $x(nT)$ represents the first order Bragg signal where ω_b is the Bragg frequency, α is the constant signal amplitude and T is the data sampling rate of the radar. By writing the Bragg frequency as a multiple of the sampling frequency

$$\omega_b = \frac{2\pi r}{NT}, \tag{6.4}$$

the discrete Fourier transform of $x(nT)$ can be computed $(0 \leq m < N)$.

$$X\left(\frac{2\pi m}{NT}\right) = \sum_{n=0}^{N-1} 2\alpha \cos\left(\frac{2\pi r n}{N}\right) \exp\left\{\frac{-2\pi i m n}{N}\right\} \tag{6.5}$$

$$= \alpha \sum_{n=0}^{N-1} \exp\left\{\frac{-2\pi i n(r+m)}{N}\right\} + \alpha \sum_{n=0}^{N-1} \exp\left\{\frac{2\pi i n(r-m)}{N}\right\} \tag{6.6}$$

The summation of these geometric series' provides

$$X\left(\frac{2\pi m}{NT}\right) = X^-\left(\frac{2\pi m}{NT}\right) + X^+\left(\frac{2\pi m}{NT}\right), \tag{6.7}$$

where X^- and X^+ represent the negative and positive Bragg components of the frequency domain signal respectively.

$$X^-\left(\frac{2\pi m}{NT}\right) = \frac{\alpha \exp\left\{\frac{-\pi i(N-1)(r+m)}{N}\right\} \sin(\pi(r+m))}{\sin\left(\frac{\pi(r-m)}{N}\right)} \tag{6.8}$$

$$X^+\left(\frac{2\pi m}{NT}\right) = \frac{\alpha \exp\left\{\frac{\pi i(N-1)(r-m)}{N}\right\} \sin(\pi(r-m))}{\sin\left(\frac{\pi(r-m)}{N}\right)} \tag{6.9}$$

The continuous Fourier transform of a complex exponential signal is a delta function. Since ω_b is not an integer multiple of the sampling frequency, the power in the discrete case leaks into neighbouring frequency bins.

Figure 6.3 shows Doppler spectra generated from raw and IF filtered simulated data which are characterised by two distinct peaks positioned at the Bragg frequency locations $\pm\omega_b$. The peaks have been corrupted by the periodogram signal processing. The first order structure, situated approximately 100 dB below the maximum values in the spectrum, has been caused by the window function which was applied to the data in order to control the effect of sidelobes in spectral estimation [20].

The IF filter method estimates the time varying frequencies of each Bragg peak. The first order time signals, $y^{\pm}(nT)$, were derived in chapter 4 ($1 \leq n < N$)

$$y^{\pm}(nT) = \frac{\sin\left(\frac{\pi n(2\theta+1)}{N}\right)}{N\sin\left(\frac{\pi n}{N}\right)} \exp\left\{\frac{2\pi i n\beta^{\pm}}{N}\right\} * x(nT), \tag{6.10}$$

where $*$ is the discrete convolution function. The simulated signal can be expressed as

$$y^{\pm}(nT) = \frac{2\alpha\sin\left(\frac{\pi n(2\theta+1)}{N}\right)}{N\sin\left(\frac{\pi n}{N}\right)} \exp\left\{\frac{2\pi i n\beta^{\pm}}{N}\right\} * \cos\left(\frac{2\pi r n}{N}\right), \tag{6.11}$$

which can be expanded to provide an equation for the time signals of the positive and negative Bragg peaks.

$$y^{\pm}(nT) = \frac{2\alpha}{N}\sum_{k=0}^{N-1} \frac{\exp\left\{\frac{2\pi i k\beta^{\pm}}{N}\right\}\sin\left(\frac{\pi k(2\theta+1)}{N}\right)\cos\left(\frac{2\pi r(n-k)}{N}\right)}{\sin\left(\frac{\pi k}{N}\right)} \tag{6.12}$$

The IF values which are generated from the time derivatives of $y^{\pm}(nT)$, are used to form a filtered signal, $x_f(nT)$. Theoretically the IF filter signal processing, which is designed to remove any first order modulation, should not alter the original signal since $x(nT)$ consists of constant frequency components. It is important that the extra signal processing, inherent in the IF filter technique, does not adversely affect high quality data. The Doppler spectrum generated from the filtered signal is shown in figure 6.3. A qualitative comparison indicates congruity between the raw and filtered Bragg peak components. The spectrum formed from $x_f(nT)$ exhibits elevated sidelobes, approximately 90 dB below the peak power level, caused by the additional signal processing. Radar signals backscattered from the ocean surface are characterised by noise at much higher levels so this phenomenon is insignificant.

6.2.2 Data Periodicity

A Fourier Transform (FT) is a mathematical technique which decomposes a signal into periodic trigonometric functions: sines and cosines. Radar signals backscattered from the ocean's surface are non-periodic data spanning a finite temporal range. The periodogram method uses overlapping windowed segments to reduce the effect of non-periodicity at the data endpoints. A Blackman-Harris window is applied to each segment in order to reduce the data smoothly to zero at the boundary of the periodic extension.

The instantaneous frequency technique uses a bandpass filter to extract the Bragg peaks from a power spectrum. The time signal of each peak is obtained using an inverse FT; an IF calculation yields an estimate of the frequency modulation. Figure 6.4 shows IF signals of the positive and negative Bragg peaks generated from $x(nT)$: the truncation causes discontinuities at the signal endpoints. The inverse FT corrupts the extremities of the data, forcing the signal to become periodic. To combat this problem, the endpoints of $z^{\pm}(nT)$ are disregarded.

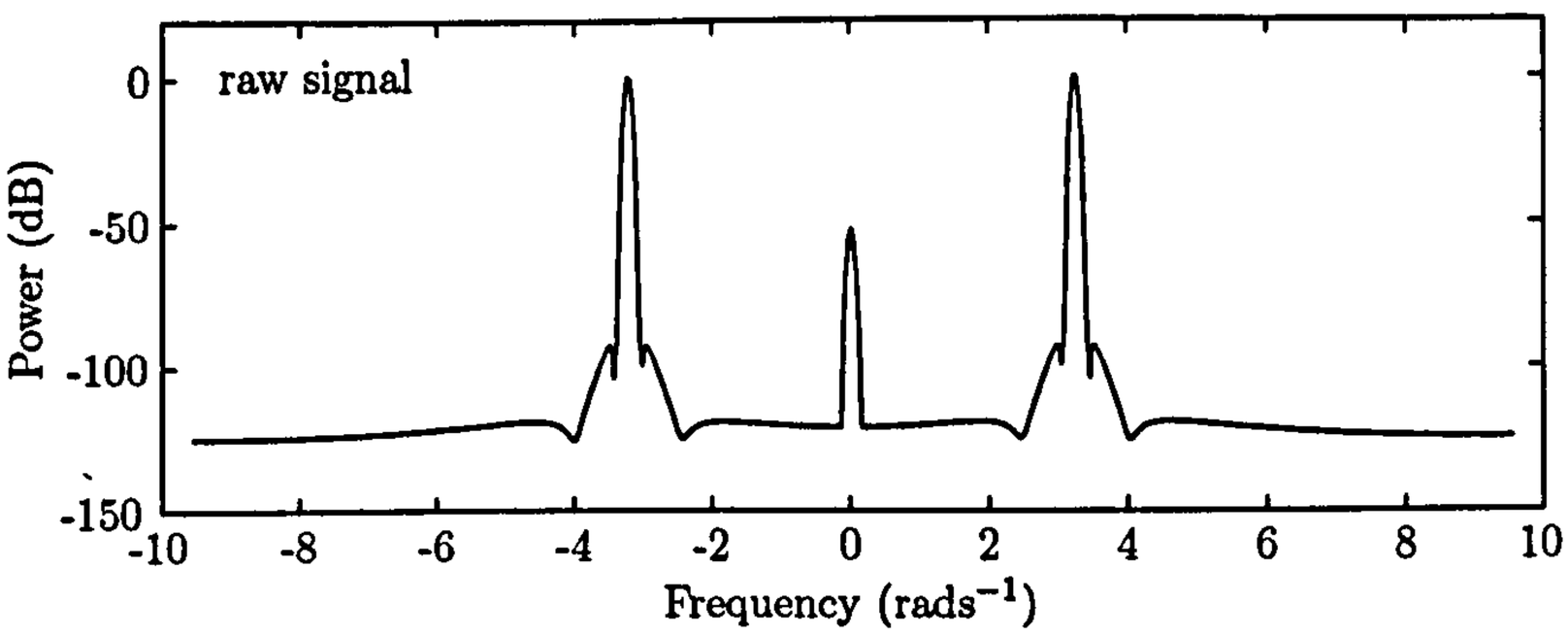

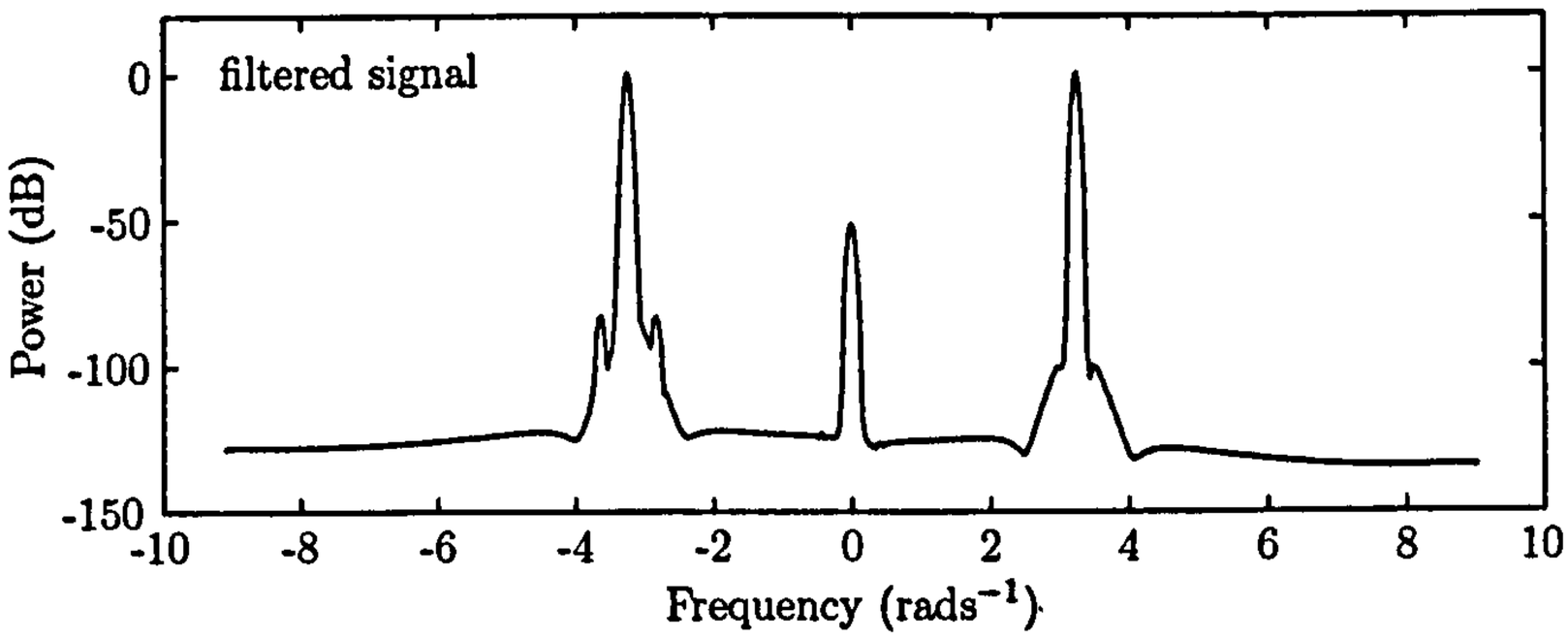

Figure 6.3: Doppler spectra generated from raw and IF filtered simulated data. Basis signal.

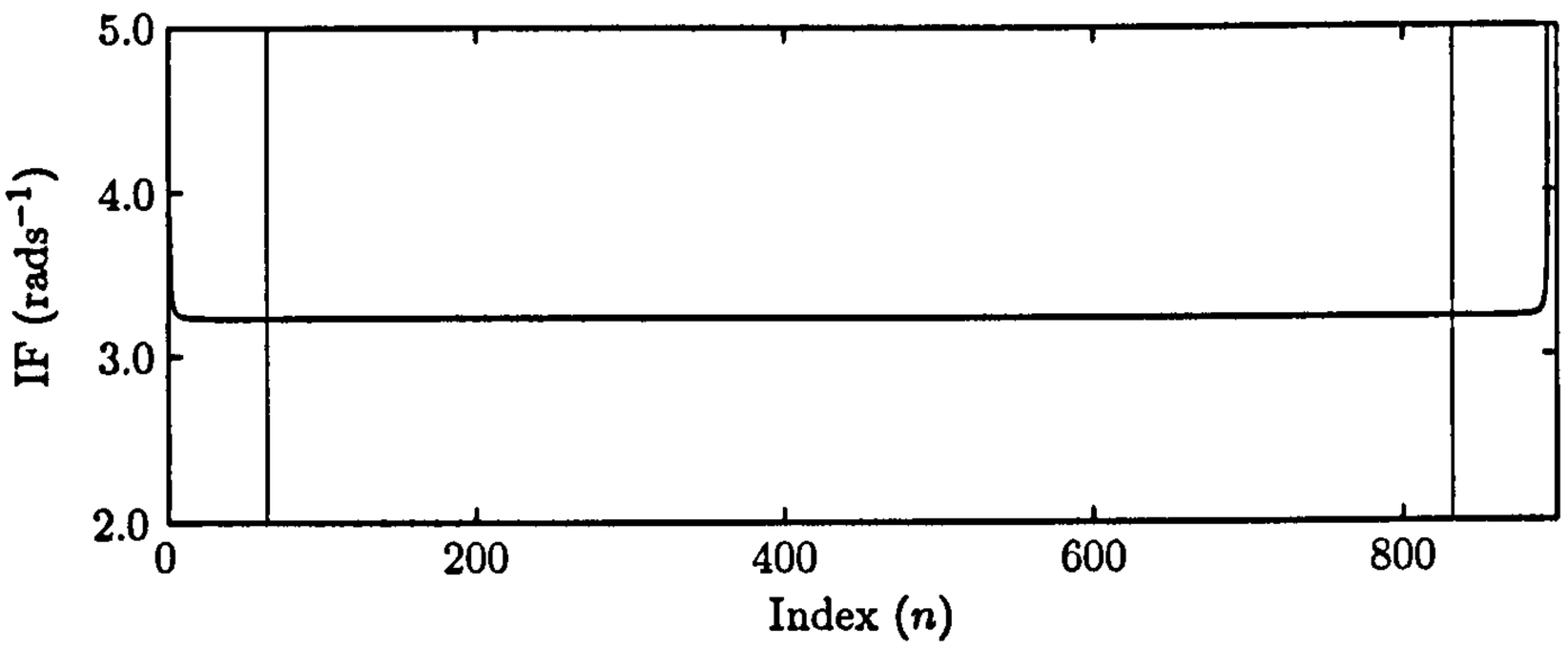

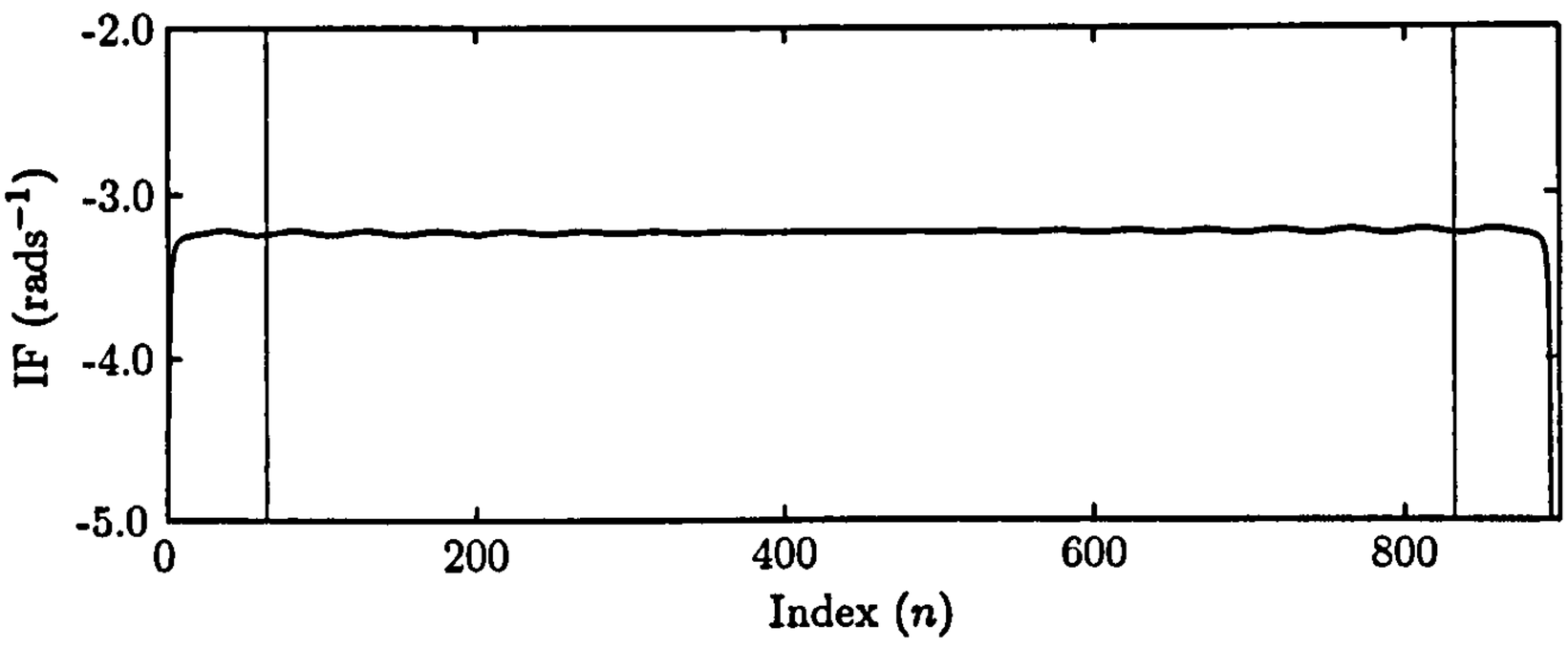

Figure 6.4: IF signals generated from simulated data. Basis signal. The vertical lines represent the extent of the endpoint truncation with $\Omega = 64$.

The time signals of the positive and negative Bragg peaks, $y^{\pm}(nT)$, comprise N data samples. The first and last Ω endpoints are extracted from each signal, leaving $N - 2\Omega$ remaining data points. In the Holderness signal processing, a choice of $\Omega = 64$ was made for two reasons:

- A qualitative examination of radar data indicates that the distortion is generally contained within this region.
- The resulting filtered radar signals, $x_f(nT)$, can be processed easily into Doppler spectra using the periodogram signal processing described in chapter 3. The data are split into 3 overlapping sets, each containing 512 samples, with a 75% overlap between consecutive segments.

For the remainder of this thesis, the endpoints will be removed during the IF filter processing in order to reduce the errors associated with non-periodic data. Figure 6.4 illustrates the extent of the truncation with $\Omega = 64$.

6.2.3 Noise

An additional term can be added to $x(nT)$ to simulate noise contributions to the radar signal. A complex noise term, $\eta(nT)$, can be modelled using gaussian white noise with zero mean; the variance, σ_η^2, represents the power in the process [49].

$$x(nT) = 2\alpha \cos(\omega_b nT) + \eta(nT) \qquad (0 \leq n < N) \tag{6.13}$$

Figure 6.5 shows Doppler spectra generated from raw and IF filtered data with an SNR level of 40 dB. The spectra exhibit strong similarities and the Bragg peaks are clear and distinct. The peak frequency locations can be accurately identified since there is no first order modulation contained in the signal. The extra signal processing involved in the IF filtering does not appear to cause any additional distortion in the spectrum.

Figure 6.6 shows the calculated IF signals, $z^{\pm}(nT)$, for varying SNR levels. The signal, $x(nT)$, consists of two complex exponential functions with constant Bragg frequency components: the Doppler shift due to surface current is identically zero at all time points. The IF signals with SNR = 60 dB exhibit strong correlation with this constant Doppler shift. As the noise level escalates, the variance increases in the IF signals.

Table 6.1 shows the bias, $\beta^{\pm}$, and standard deviation, $\sigma_z^{\pm}$, values derived from the IF peak signals. The bias parameter is defined as the difference in magnitude between the actual and measured IF frequency shifts

$$\beta^{\pm} = \left| \Lambda^{\pm} \mp \omega_b \right|, \tag{6.14}$$

where $\Lambda^{\pm}$ is the mean of $z^{\pm}(nT)$, weighted by the signal amplitude (equation 6.2). For high SNR, the measured current shifts are close to the theoretical zero constant value. As the SNR level decreases, the current shift values become increasingly inaccurate. When SNR = 10 dB, the measured errors correspond to a current speed of approximately 0.04ms^{-1} and the IF estimates become unsatisfactory; the spectral quality criteria for ocean measurements require SNR levels in excess of 10 dB. The variance of $z^{\pm}(nT)$ is dependent on the width of the bandpass filters which are used to isolate the Bragg peaks. Determining the optimum values for these parameters is critical to the accuracy of the IF filtering approach and is discussed in section 6.4.

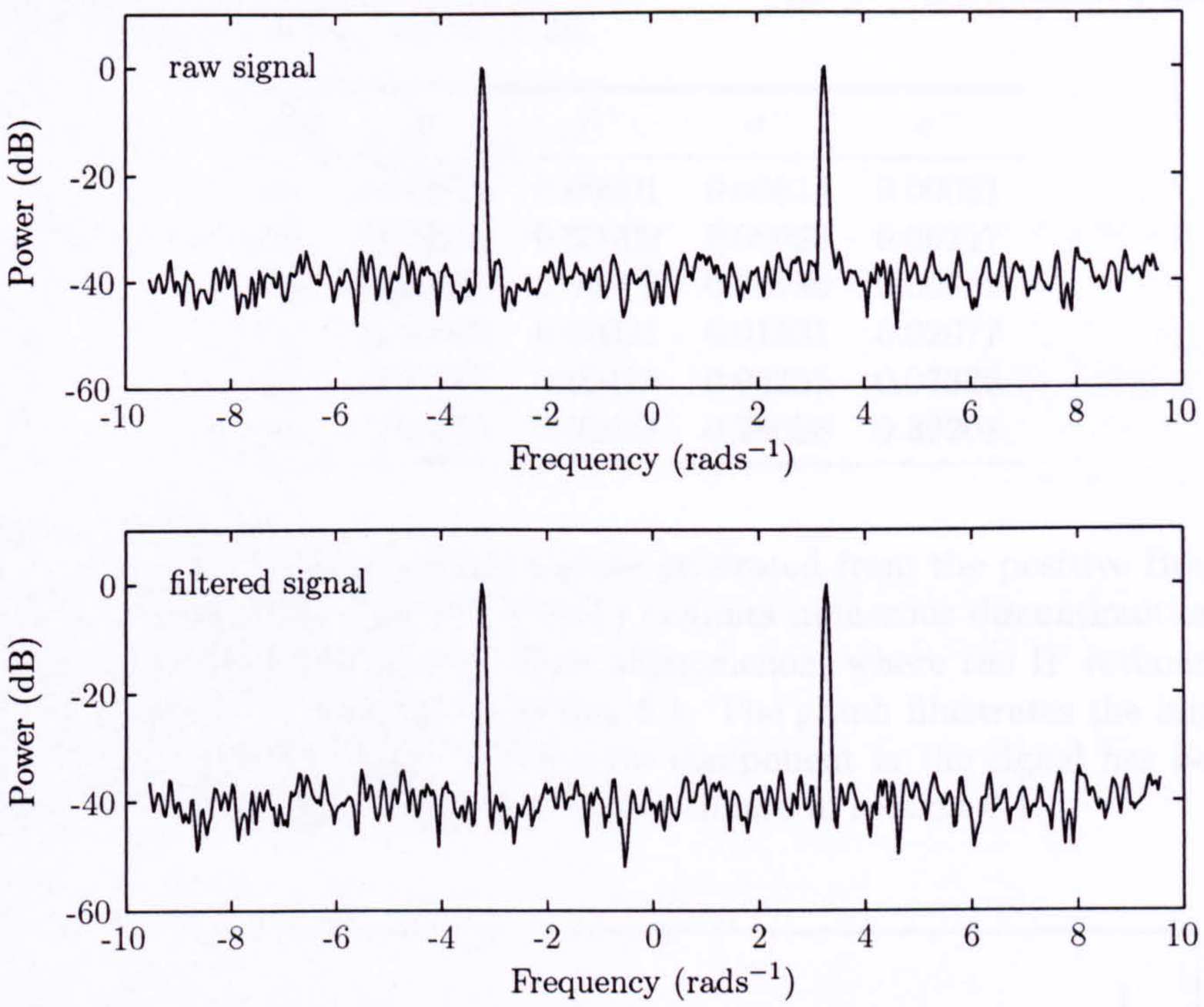

Figure 6.5: Doppler spectra generated from raw and filtered simulated data with additive noise. SNR = 40 dB.

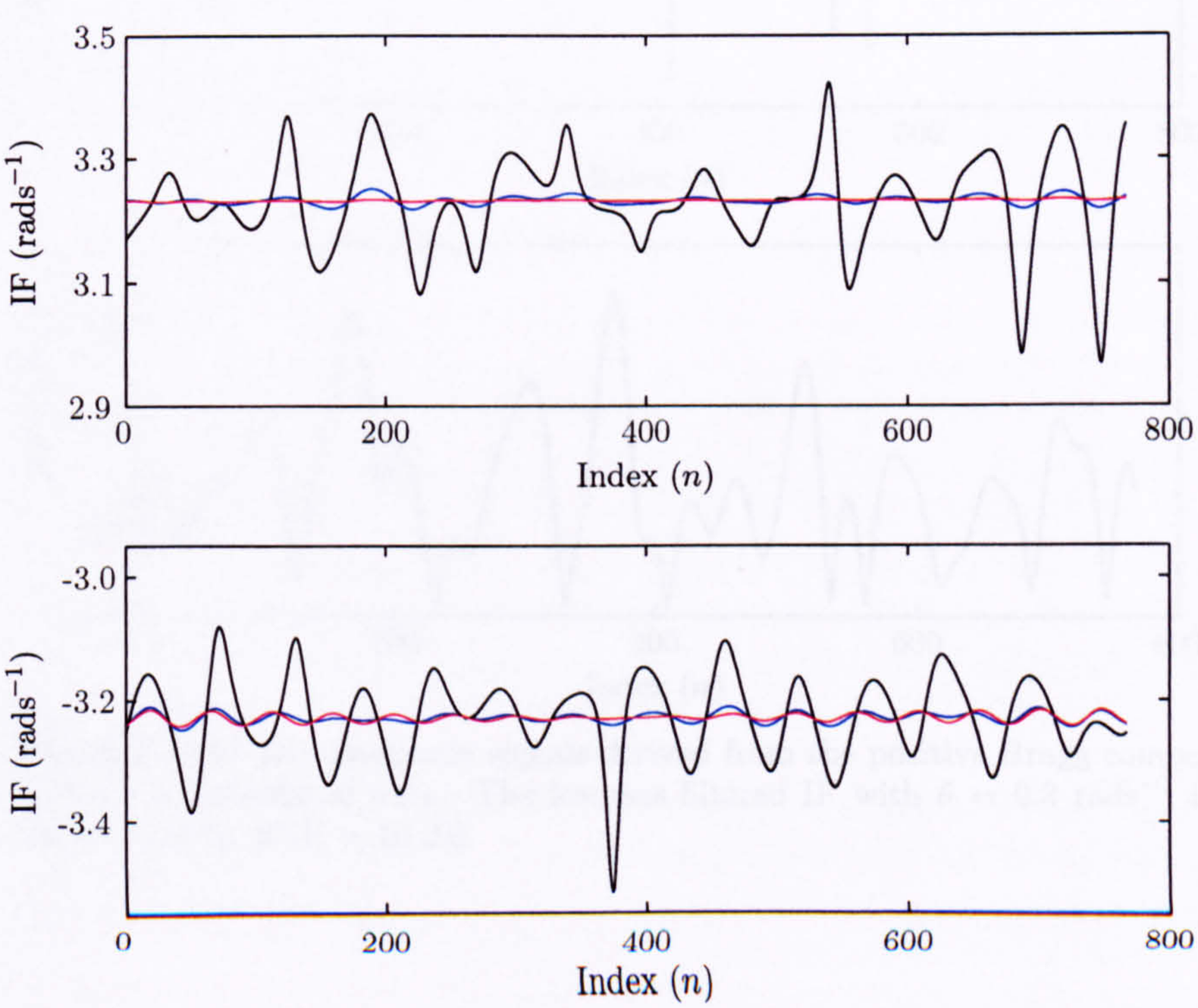

Figure 6.6: IF signals generated from simulated data with additive noise. SNR = 20 dB (black), 40 dB (blue), 60 dB (red).

Table 6.1: Bias and standard deviation of IF signals using simulated data. SNR levels in the range 60 to 10 dB.

SNR	β^-	β^+	σ^-	σ^+
60	0.00014	0.00001	0.00614	0.00081
50	0.00015	0.00002	0.00623	0.00217
40	0.00021	0.00004	0.00789	0.00662
30	0.00092	0.00031	0.01881	0.02077
20	0.00797	0.00493	0.06755	0.07326
10	0.04274	0.02631	0.28098	0.39201

Figure 6.7 shows IF and amplitude signals generated from the positive Bragg components of $x(nT)$ with SNR = 10 dB. $z^+(nT)$ exhibits numerous discontinuities when the amplitude of the peak signal is low. This phenomenon, where the IF estimates become corrupted by noise, was identified in section 6.1. The graph illustrates the impact of the lowpass filter with $\rho = 0.3$ rads^{-1}. The noise component in the signal has been limited which confirms the validity of the radar data estimate in section 6.1.

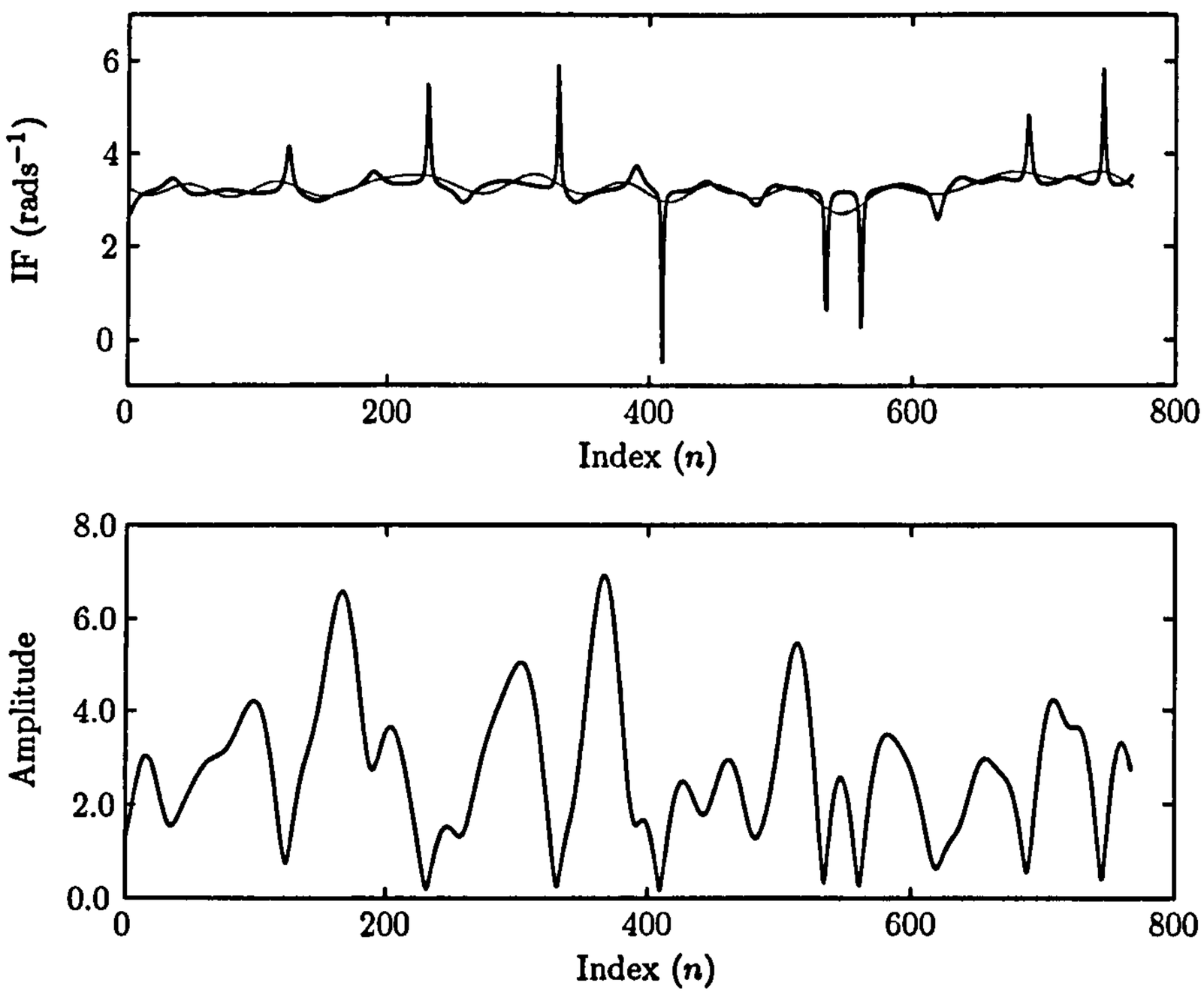

Figure 6.7: IF and amplitude signals derived from the positive Bragg component of the simulated data. The lowpass filtered IF with $\theta = 0.3$ rads^{-1} is shown in gray. SNR = 10 dB.

6.3 Oceanographic Modelling

The influence of oceanographic processes on radar signals is investigated in this section. A range of oceanic conditions are modelled using simulated data. In each case, the Doppler spectra and IF signal of the positive Bragg peak, $z^+(n\mathrm{T})$, are shown in order to illustrate the impact of the filtering procedure. The IF signals have been generated using a single filter with a bandpass half-width of $\theta = 0.4$ rads^{-1} and lowpass filtered with a frequency bound of $\rho = 0.3$ rads^{-1}. This work attempts to identify any limitations in the signal processing technique and to evaluate the performance of the filter under a variety of conditions.

6.3.1 Ocean Currents

The aim of the IF filtering procedure is to measure the complex first order structure that can occur in radar signals. This may be caused by current variability so it is important to identify whether the IF signal processing can successfully detect this modulation.

An underlying ocean surface current causes the power in the backscattered radar signal to be shifted in frequency. A current with radial component $u(nT)$ ms^{-1} towards the radar creates an additional Doppler shift of $k_\mathrm{b}u(nT)$ rads^{-1} at time nT, where k_b represents the Bragg wavenumber (equation 3.12). The corresponding radar signal, $x(nT)$, can be expressed as

$$x(nT) = \alpha \exp\{-i(\omega_\mathrm{b} nT - \phi_u)\} + \alpha \exp\{i(\omega_\mathrm{b} nT + \phi_u)\} \qquad (0 \le n < N), \tag{6.15}$$

where

$$\phi_u = \sum_{j=0}^{n} k_\mathrm{b} u(jT)T. \tag{6.16}$$

A complex noise term, $\eta(nT)$, has been added to each signal to simulate an SNR level approximately 40 dB below the dominant peak. The IF signal of the positive Bragg peak is given by

$$z^+(nT) = \omega_\mathrm{b} + k_\mathrm{b} u(nT) \qquad (0 \le n < N). \tag{6.17}$$

Constant Current

A constant current within the radar measurement region can be modelled by

$$u(nT) = u_0 \qquad (0 \le n < N). \tag{6.18}$$

Figure 6.8 shows the generated spectra for a current magnitude of $u_0 = 0.5$ ms^{-1}. The IF filter signal processing has correctly identified the constant current component in the data. The current shift has been extracted from the filtered signal which subsequently translates the first order peaks to the Bragg frequencies $\pm\omega_\mathrm{b}$. IF signals are shown for radial components in the range $0.25 \le u_0 \le 0.75$.

This is an idealistic example which requires temporal and spatial homogeneity throughout the radar measurement period. The following cases examine the effects of current variability in the radar signal.

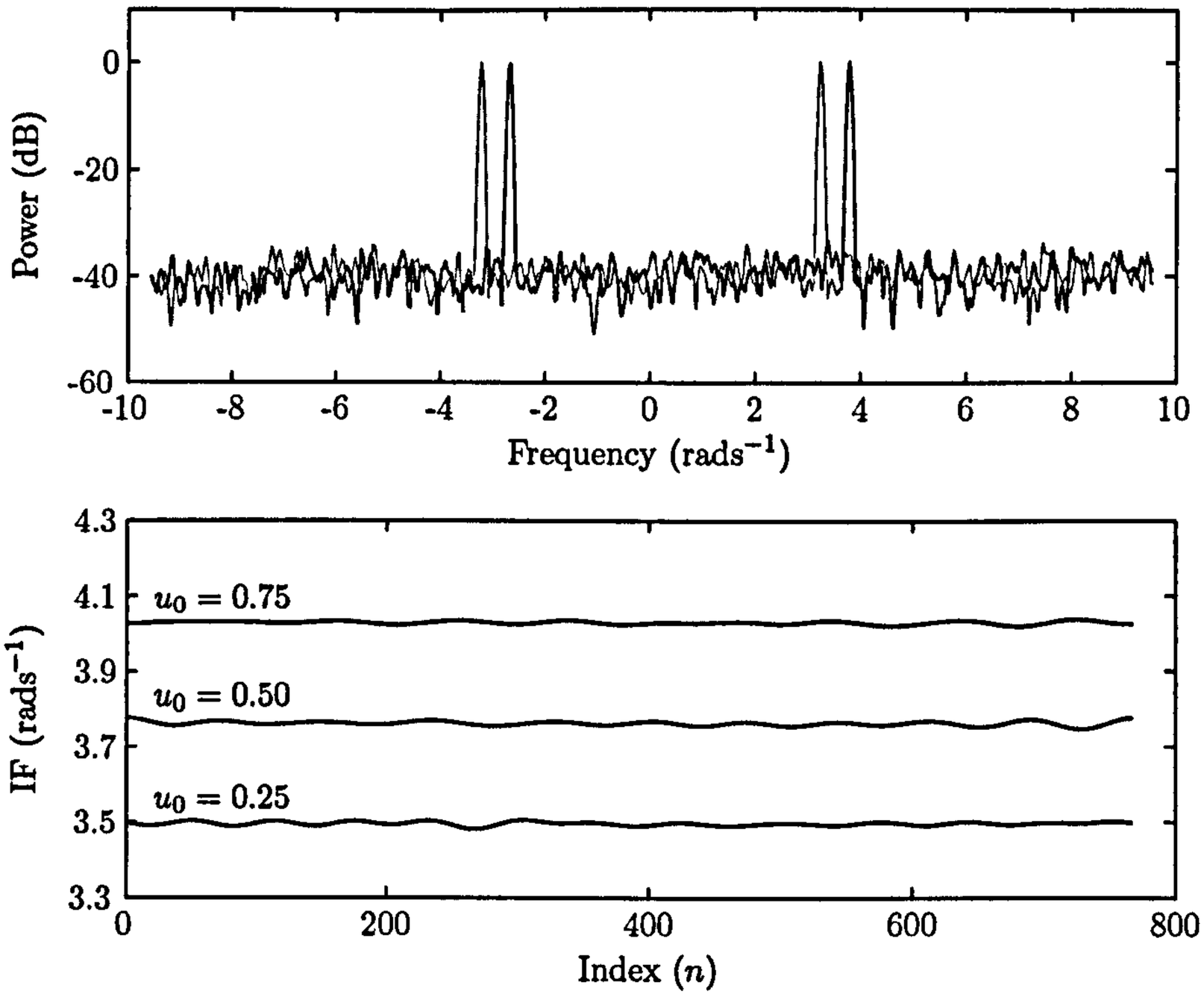

Figure 6.8: Constant current. Doppler spectra (top) generated from raw (dark) and filtered (light) data with $u_0 = 0.5$ ms^{-1}. IF signals (bottom) for $0.25 \leq u_0 \leq 0.75$ ms^{-1}.

Tidal Current

The ocean dynamics within the Holderness region are dominated by a strong tidal cycle which can be modelled by

$$u(nT) = a \sin\left(\frac{2\pi nT}{P} + \frac{2\pi\phi}{P}\right) \qquad (0 \leq n < N), \tag{6.19}$$

where a is the maximum current magnitude and P is the duration of the tidal period in seconds. The parameter ϕ represents the time into the tidal cycle that the radar measurement period commences. The maximum tidal current occurs 3 hours into the cycle whilst the largest current gradient occurs after 6 hours, at the turn of the tide.

Figure 6.9 shows the Doppler spectra and IF values during the maximum tidal current. A value of $a = 1.0$ ms^{-1} was chosen to simulate the highest recorded current magnitudes during the Holderness deployment. The current variation during the data collection period has negligible effect on the first order structure. The Bragg peaks have been shifted to the Bragg frequencies $\pm\omega_b$.

Figure 6.10 shows the calculated signals midway through the tidal cycle when the current gradient is at a maximum. A successful current measuring technique would be expected to provide an estimate which represents a temporal average over the data collection period; the IF filter method accurately identifies the mean current during this time. Current shift measurements are examined in greater detail in section 6.4.

The Bragg peaks in each spectrum are clear and distinct. A comparison of the raw and filtered spectra indicates that the tidal modulation occurring within the radar measurement period is insignificant.

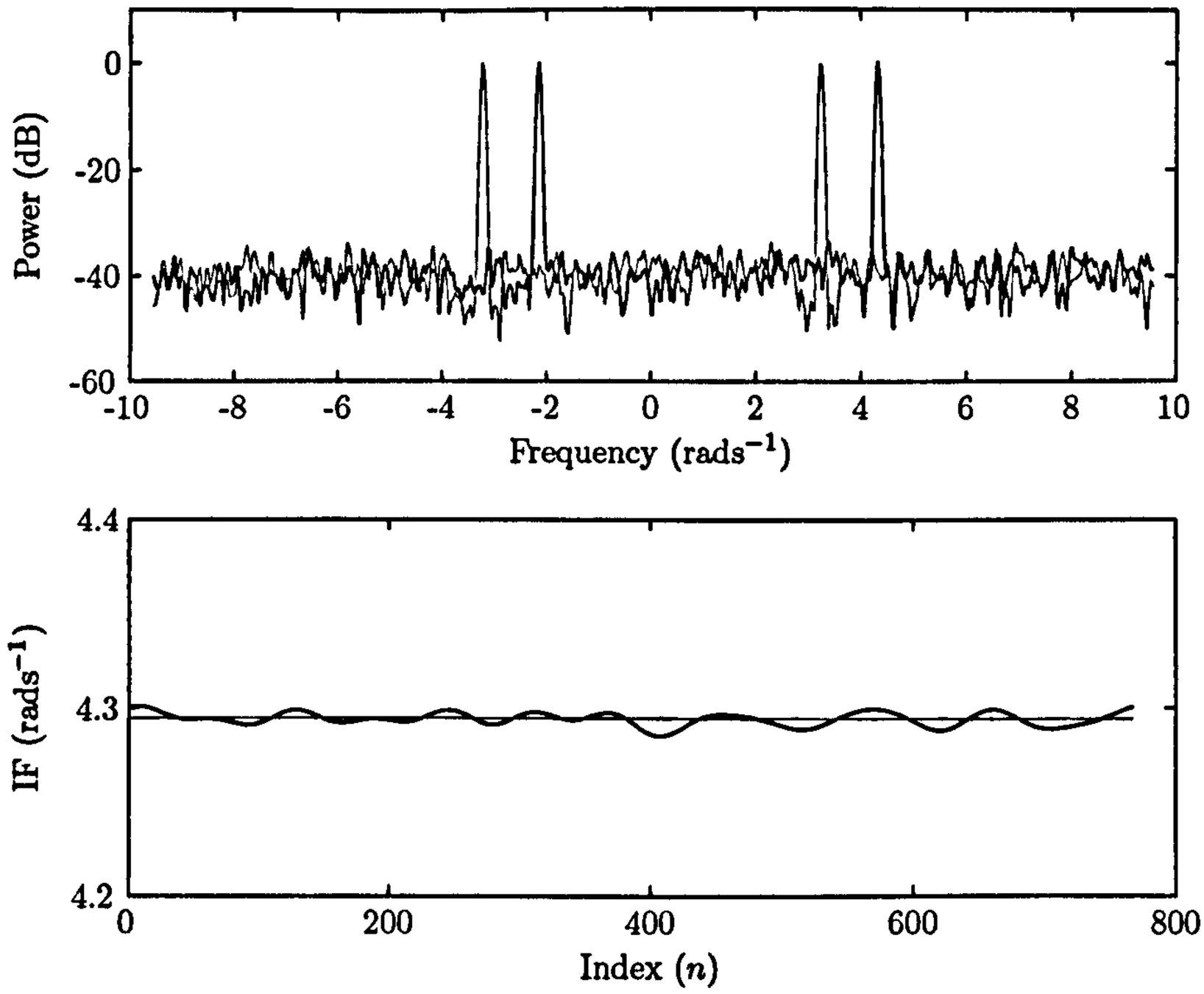

Figure 6.9: Tidal cycle at maximum current magnitude. $a = 1.0$ ms^{-1}. Doppler spectra (top) generated from raw (dark) and filtered (light) data. IF signals (bottom) of calculated (dark) and theoretical (light) values.

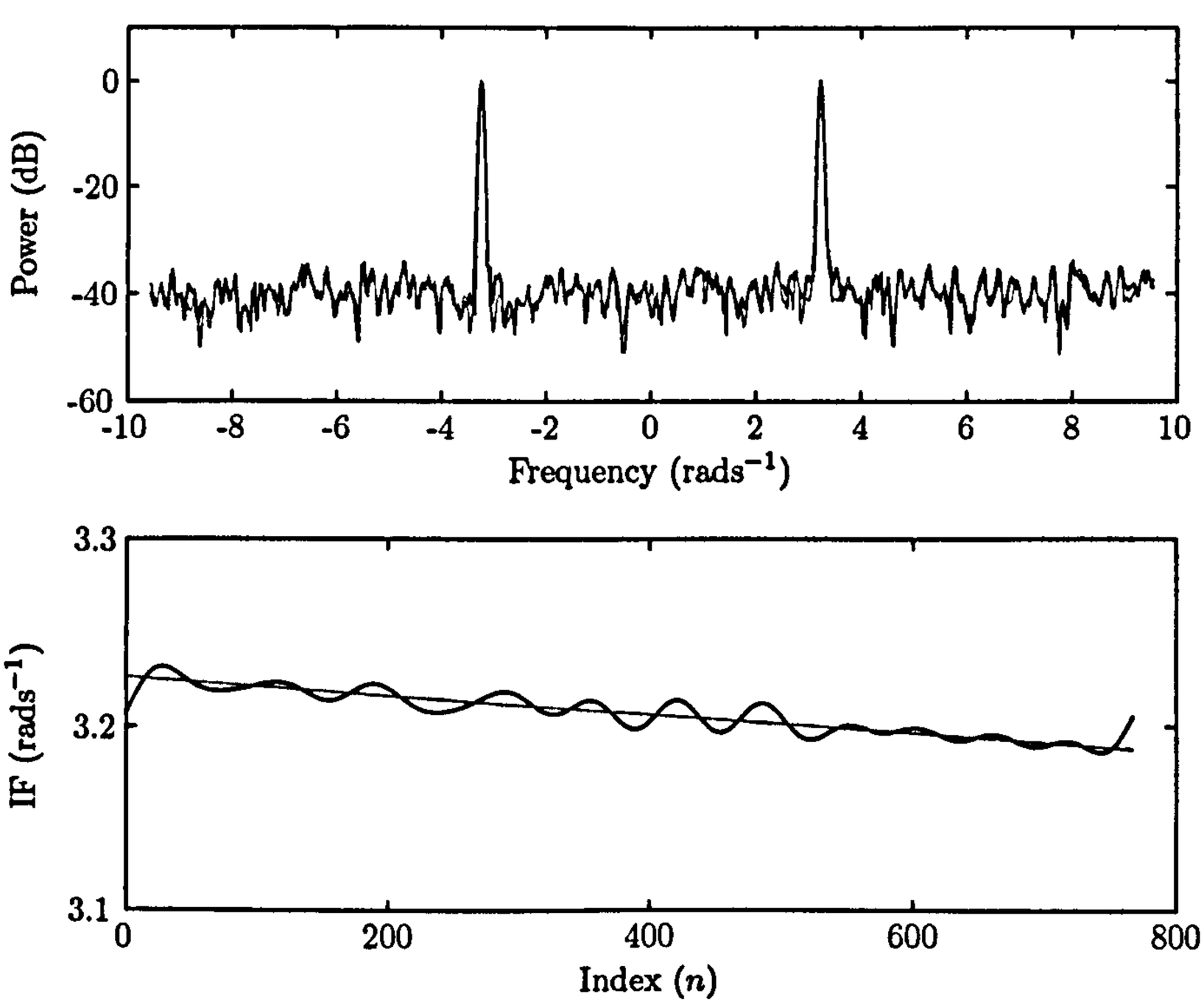

Figure 6.10: Tidal cycle at maximum current gradient. $a = 1.0$ ms^{-1}. Doppler spectra (top) generated from raw (dark) and filtered (light) data. IF signals (bottom) of calculated (dark) and theoretical (light) values.

Linear Current

An ocean surface current which changes linearly with time can be modelled by

$$u(nT) = u_0 + \frac{\mu n}{N-1} \qquad (0 \leq n < N), \tag{6.20}$$

where u_0 is the initial current state at time $n = 0$ and $u_0 + \mu$ represents the final magnitude at time $n = N - 1$. Figure 6.11 shows the Doppler spectra generated from the raw and filtered signals. The raw spectrum exhibits compound first order structure: the Bragg peaks have broadened due to the frequency modulation created by the linear current. The problems caused by this Bragg peak structure and the impact on the derived oceanographic parameters were discussed in chapter 3. The motivation behind developing the IF filter technique was to identify and remove any modulation in the first order peaks in order to increase the reliability of oceanic measurements.

The IF signals, $z^+(nT)$, generated from this simulation illustrate how the filter has identified the current variability in the peak signal. The IF values provide a current estimate which represents a temporal average over the radar measurement period. The influence of current variability has been extracted from the filtered spectrum and the first order components have been shifted to the Bragg frequencies.

Discrete Current Bands

An underlying ocean current which changes in discrete steps can be modelled by

$$u(nT) = u_0 + \mu b \qquad \left(\frac{bN}{B} \leq n < \frac{(b+1)N}{B}\right), \tag{6.21}$$

for B evenly distributed discrete components $(0 \leq b < B)$ where u_0 and $u_0 + (B-1)\mu$ are the initial and final current magnitudes respectively. The parameter μ represents the step in current between consecutive bands.

Figure 6.12 shows the IF signals $z^+(n\mathrm{T})$ generated from this simulated situation for three decreasing current bands between 0.7 and 0.2 ms^{-1}. This corresponds to a frequency shift between each step of approximately 0.266 rads^{-1} which represents an extreme example. The current modulation is greater than any values recorded in the Holderness deployment and is used to test for any limitations in the IF filtering procedure.

The Bragg peaks in the raw spectrum have been corrupted by the current modulation contained in the signal. This modulation has been identified and removed from the filtered signal. The current value derived from the IF signal provides an average of the individual current bands.

This structure is analogous to the ocean current kinematics that distort a large proportion of Doppler3 spectra. An analysis of Doppler3 spectra in chapter 3 revealed that the split peaks were often caused by the disjoint data collection period: the OSCR system constrains the separation of each constituent periodogram to 20 minutes. The Bragg peaks in each individual spectrum were frequently clear and distinct.

A computationally simpler approach was suggested in section 4.1 that mitigated the first order structure in Doppler3 spectra by removing the current shift from each individual spectrum before averaging. The discrete current bands modelled in the above example illustrate a case where the simpler averaging approach would not work. The current modulation is contained within the shorter timescales associated with the periodogram measurements. This encapsulates the advantage of the IF filtering technique over conventional methods.

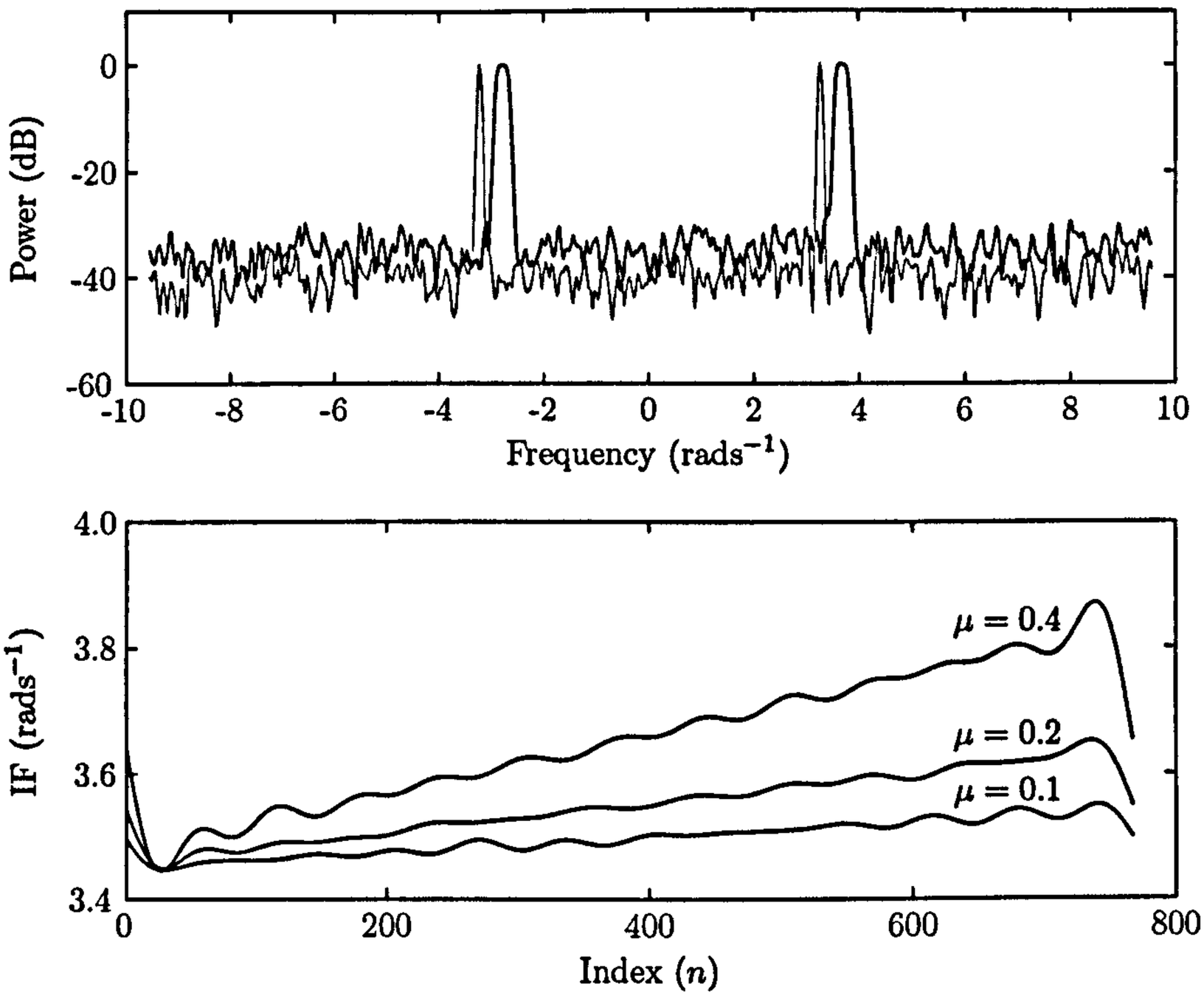

Figure 6.11: Linear current. $u_0 = 0.2$ ms^{-1}. Doppler spectra (top) generated from raw (dark) and filtered (light) data with $\mu = 0.4$ ms^{-1}. IF signals (bottom) for $0.1 \leq \mu \leq 0.4$ ms^{-1}

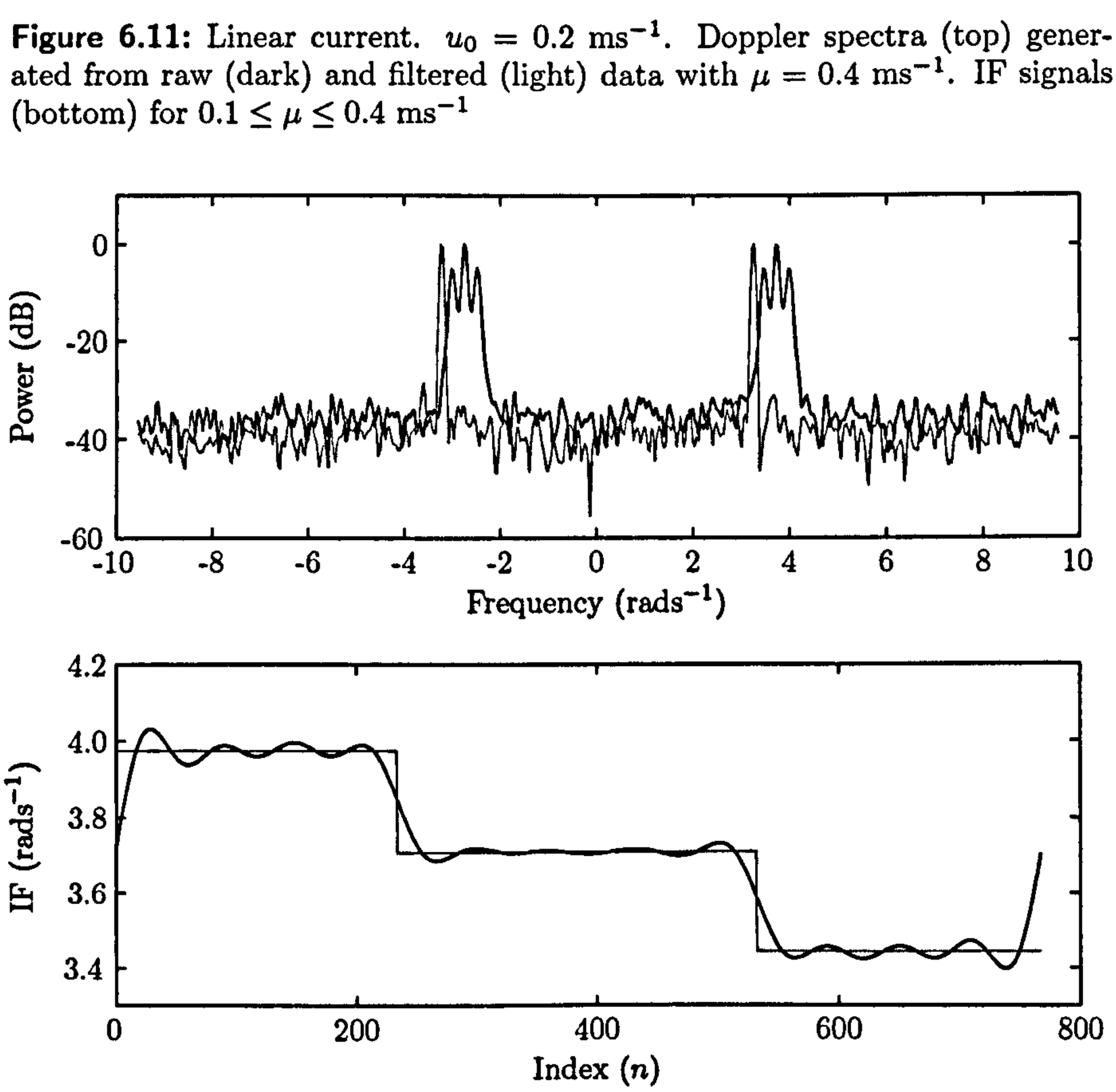

Figure 6.12: Discrete current bands. $u_0 = 0.7$ ms^{-1}, $\mu = -0.25$ ms^{-1}. Doppler spectra (top) generated from raw (dark) and filtered (light) data. IF signals (bottom) of calculated (dark) and theoretical (light) values.

Sinusoidal Current Modulation

A sinusoidal modulation in the underlying ocean current can be expressed as

$$u(nT) = a \sin\left(\frac{2\pi r n}{N}\right) \qquad (0 \leq n < N), \tag{6.22}$$

where a represents the maximum amplitude. The sine wave performs r oscillations within the radar measurement period. Figure 6.13 shows the Doppler spectra and IF signals generated from this signal with $a = 0.2$ ms^{-1} and $r = 1$. The first order peaks exhibit compound structure caused by the current modulation. The IF filter method identifies the current shift throughout the time period and removes the variability from the signal. The Bragg peaks in the filtered spectrum are clear and distinct.

Figure 6.14 shows the influence of the instantaneous frequency procedure for a sine wave which performs five oscillations during the data collection period. The IF signals illustrate the effectiveness of the filtering technique at measuring and extracting the time varying characteristics of radar signals.

Current Turbulence

Turbulence is a widespread oceanic phenomenon and it is important that the IF filter can identify this process which may be a driving mechanism of the spectral distortion. Data from the S4 current meter, deployed in the Holderness region, were used to simulate turbulence in the radar signal. The configuration of the S4 was described in chapter 5. The instrument was located at a depth of approximately 17 metres below the ocean's surface so differences would be anticipated between the S4 and radar processes due to shear forces. However, statistical analysis revealed strong correlation between the OSCR and S4 derived current structure so the temporal variability of the current meter measurements may provide an acceptable approximation of the surface processes.

The S4 sampled current vectors at one second intervals over a 20 minute time period. The data corresponding to the five minute master and slave collection periods were extracted. The resultant signals, $u(nT)$, were interpolated to provide data at the sampling rate of the OSCR system in the direction of the master and slave radar beams.

The current turbulence data were added to the basis radar signal. Figure 6.15 illustrates an example of the IF signals derived from the data for SNR levels of 30 dB and 40 dB. The modelled turbulence was generated from the temporal variation of the S4 data at 22:00, 20/12/95. The major structural components of the turbulence have been identified by the signal processing. Analysis of S4 data from numerous time points confirm the ability of the filtering procedure to measure the turbulent processes.

The variability in the IF signals is related to the SNR level of the radar data. Figure 6.15 reveals that the larger discrepancies between the simulated and radar derived turbulence occur at the minima in the corresponding amplitude signals. This phenomenon was identified in section 6.1 and attributed to the influence of background noise. Accurate identification and extraction of the first order Bragg peaks will limit this variability – the optimum filter bandwidth parameters are determined in section 6.4.

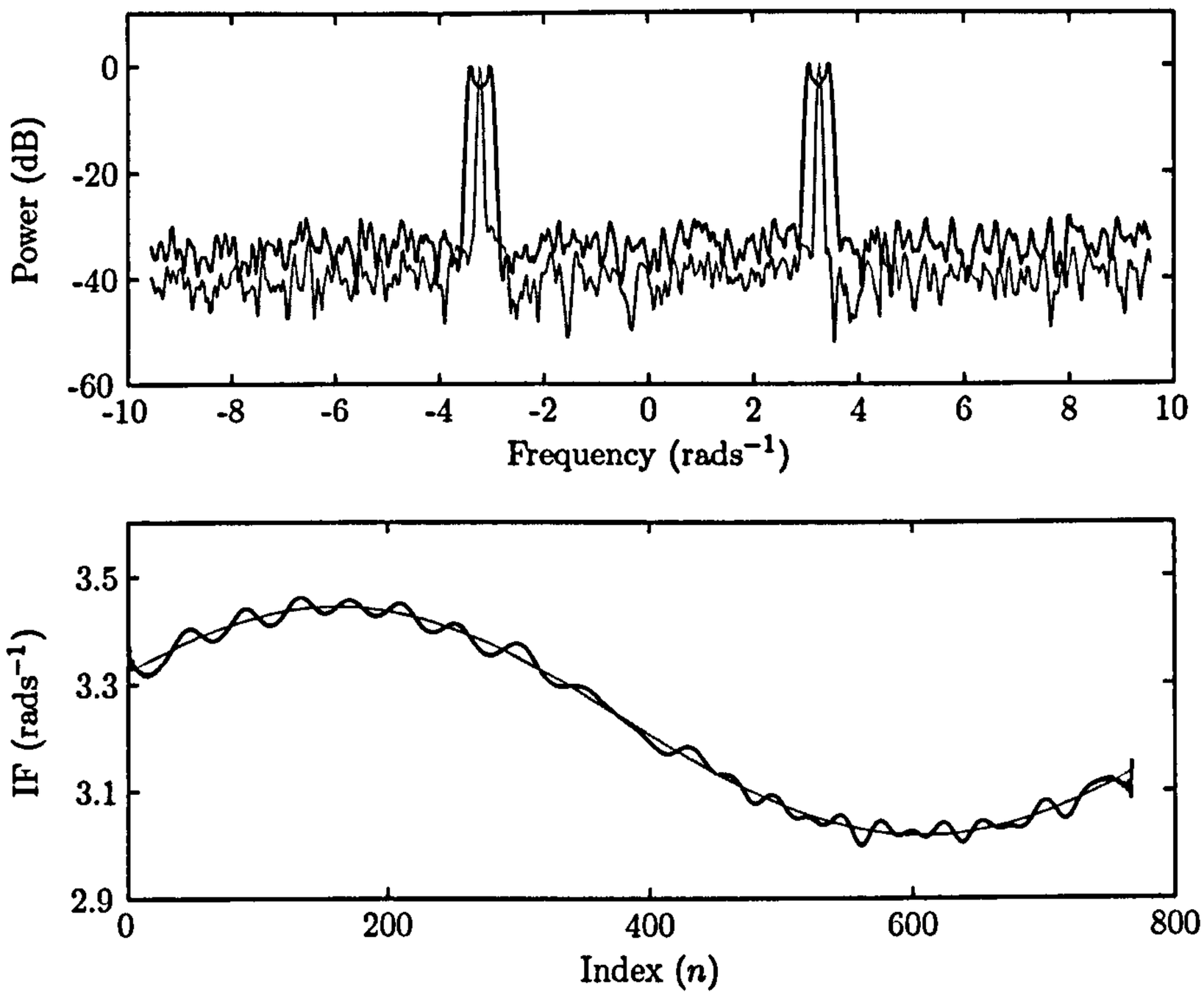

Figure 6.13: Sinusoidal current modulation. $r = 1$, $a = 0.2$ ms^{-1}. Doppler spectra (top) generated from raw (dark) and filtered (light) data. IF signals (bottom) of calculated (dark) and theoretical (light) values.

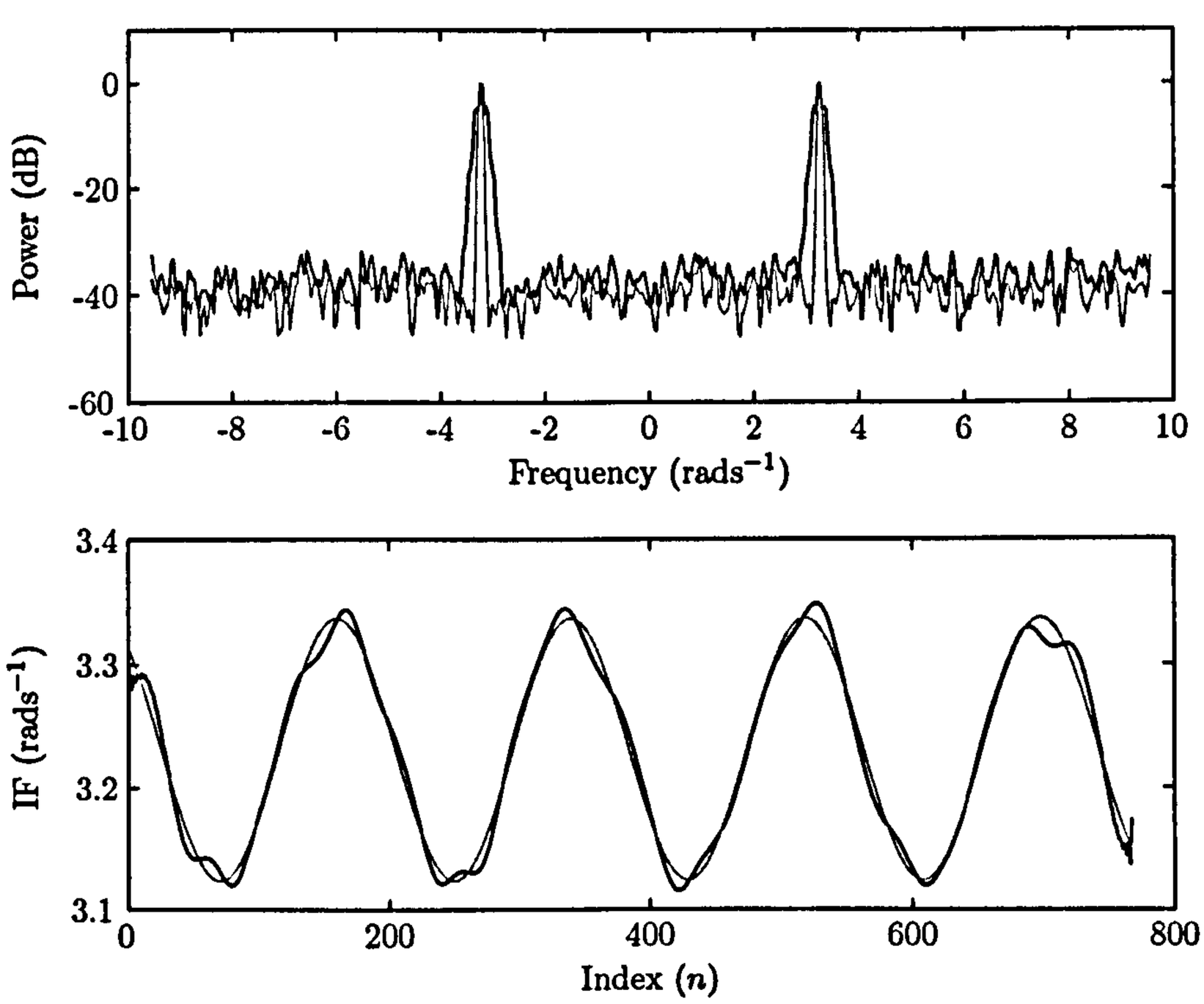

Figure 6.14: Sinusoidal current modulation. $r = 5$, $a = 0.1$ ms^{-1}. Doppler spectra (top) generated from raw (dark) and filtered (light) data. IF signals (bottom) of calculated (dark) and theoretical (light) values.

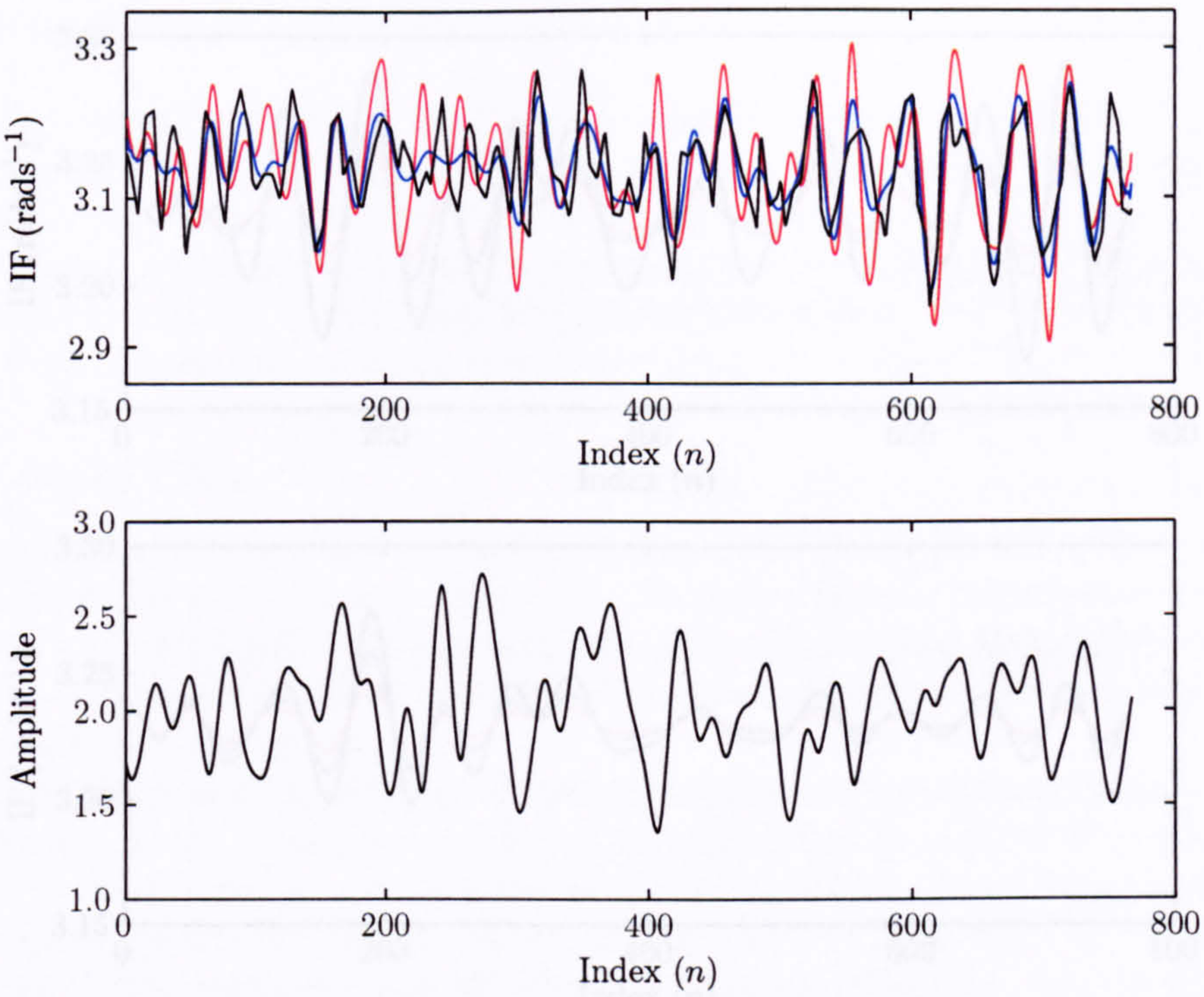

Figure 6.15: Current turbulence. IF signals (top) for SNR = 30 dB (red) and 40 dB (blue). The black line represents the S4 turbulence that was added to the radar signal. Amplitude signal (bottom) of Bragg peak. Data taken from the S4 current meter in the direction of the master radar beam at 22:00, 20/12/95.

6.3.2 Signal Amplitude

The amplitude of the backscattered radar signal is dependent on a number of factors such as the range of the target cell from the radar and the amount of constructive interference between the transmitted radio waves and the ocean's surface. The influence of the signal amplitude on the IF estimates is examined in this section.

The magnitude of the backscattered signal is related to the number of Bragg ocean waves, travelling directly towards and away from the radar, within the measurement cell [33]. The distribution of incoming and outgoing Bragg wave trains may be uneven and can be modelled by

$$x(nT) = \alpha \exp\{-i\omega_b nT\} + \mu\alpha \exp\{i\omega_b nT\} + \eta(nT) \qquad (0 \leq n < N). \tag{6.23}$$

Figure 6.16 shows IF signals generated from this simulated signal for constant amplitude factors in the range $0.25 \leq \mu \leq 0.75$. For larger values of μ, the IF signals show stronger correlation with the theoretical current shift which is identically zero; as μ decreases, the noise contribution to the signals increases which, subsequently, causes additional variance in the IF estimates. This phenomenon is frequently evident in radar data when the smaller first order peaks become hidden within the second order spectral components.

The raw and filtered Doppler spectra generated from these signals are indistinguishable and exhibit distinct first order peaks – the positive Bragg peaks are located $10\log_{10}\mu^2$ dB below the maximum power levels. The change in signal amplitude causes no additional distortion in the IF filter processing.

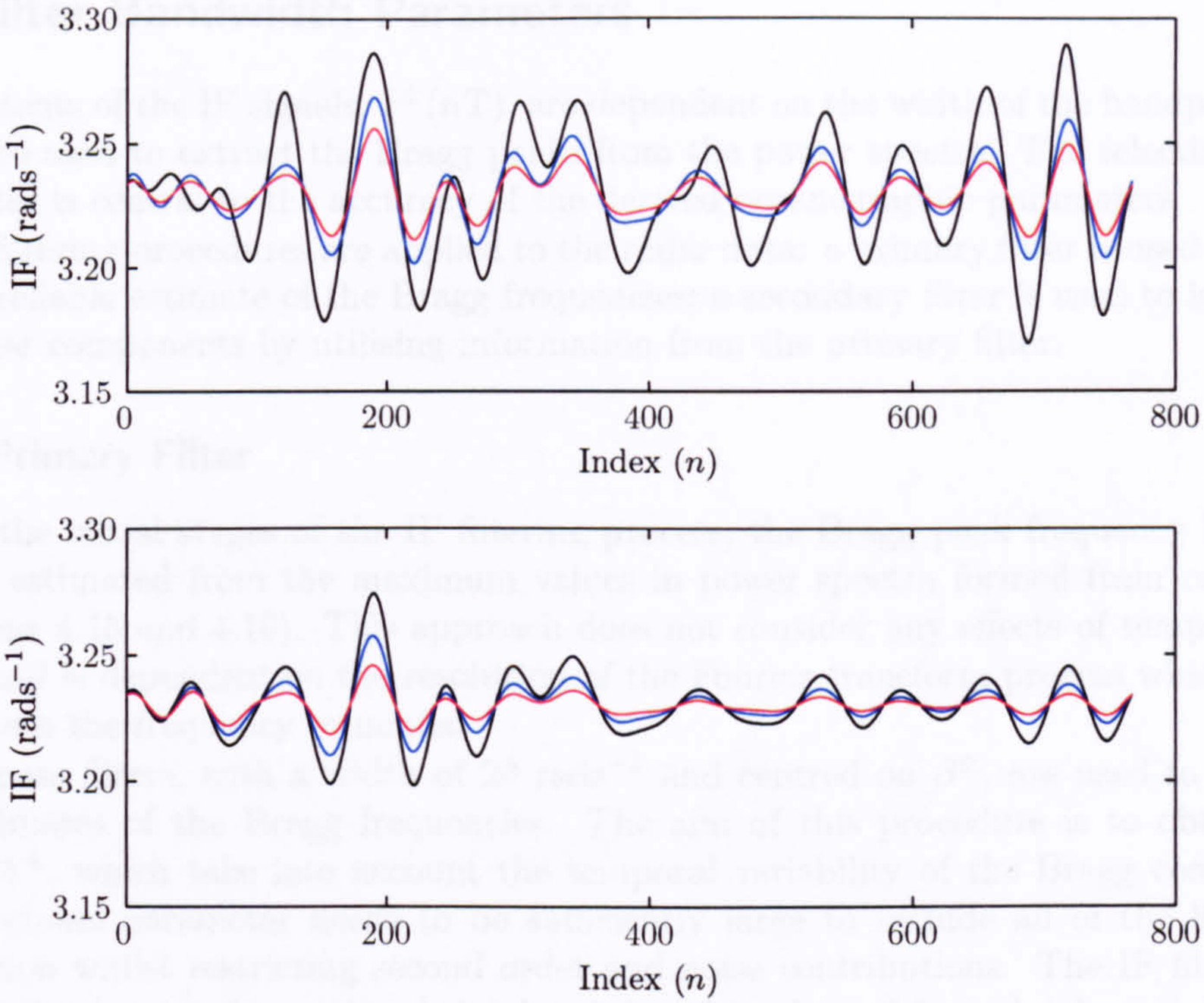

Figure 6.16: IF signals of positive Bragg peak. Constant signal amplitude (top) for $\mu = 0.25$ (black), 0.5 (blue), 0.75 (red). Variable signal amplitude (bottom) for $\gamma = 5$ (black), 10 (blue), 20 (red).

Oceanographic processes can evolve over smaller time scales than the radar measurement period. Temporal inhomogeneity within this period can result in amplitude variations in the backscattered radar signal. This situation can be modelled by

$$x(nT) = \alpha(nT)\exp\{-i\omega_b nT\} + \alpha(nT)\exp\{i\omega_b nT\} + \eta(nT) \qquad (0 \leq n < N), \quad (6.24)$$

where $\alpha(nT)$ represents the variation of amplitude as a function of time. A temporal increase in the number of Bragg waves contained within the measurement cell would cause an increase in the signal amplitude. A linear increase by a factor of γ from an initial state of $\alpha(0) = \alpha_0$ can be expressed as

$$\alpha(nT) = \alpha_0 + \frac{\gamma\alpha_0 n}{N-1} \qquad (0 \leq n < N). \quad (6.25)$$

Figure 6.16 shows the IF signals generated from the positive Bragg peak for $5 \leq \gamma \leq 20$. As the signal amplitudes increase throughout the time period, the signal-to-noise ratio increases which reduces the variance in the IF values. The modulation in the signal amplitude does not alter the spectral structure in the corresponding filtered Doppler spectra.

6.4 Filter Bandwidth Parameters

The contents of the IF signals, $z^{\pm}(n\mathrm{T})$, are dependent on the width of the bandpass filters which are used to extract the Bragg peaks from the power spectra. The selection of this parameter is central to the accuracy of the derived oceanographic parameters.

Two filtering procedures are applied to the radar data: a primary filter is used to obtain a more reliable estimate of the Bragg frequencies; a secondary filter is used to isolate the first order components by utilising information from the primary filter.

6.4.1 Primary Filter

During the initial stages of the IF filtering process, the Bragg peak frequency locations, $\beta^{\pm}$, are estimated from the maximum values in power spectra formed from radar data (equations 4.15 and 4.16). This approach does not consider any effects of temporal variability and is dependent on the resolution of the Fourier transform process which is used to generate the frequency estimates.

Bandpass filters, with a width of 2θ rads^{-1} and centred on $\beta^{\pm}$, are used to calculate new estimates of the Bragg frequencies. The aim of this procedure is to obtain peak values, $\Lambda^{\pm}$, which take into account the temporal variability of the Bragg components. The bandpass parameter needs to be sufficiently large to include all of the first order modulation whilst restricting second order and noise contributions. The IF filter signal processing was applied to real and simulated data for values of θ ranging between 0.02 and 1.0 rads^{-1}. The bias in each IF signal was defined as the magnitude difference between the theoretical and measured peak frequencies.

Simulated signals were analysed using the oceanographic modelling described in section 6.3. Figure 6.17 shows the positive Bragg peak biases at SNR levels of 20, 40 and 60 dB. The linear current rises from 0.2 to 0.6 ms^{-1} during the time period. The current bands increase in three discrete steps between 0.2 and 0.4 ms^{-1}. Following the IF endpoint removal, the frequency modulations associated with these modelled data are approximately 0.36 and 0.22 rads^{-1} for the linear and discrete currents respectively.

The graphs show that for larger SNR, the errors in the estimated Bragg frequencies are smaller since the noise contribution to the IF calculation is reduced. The minima for the linear and discrete currents occur at approximately 0.35 and 0.23 rads^{-1} respectively. Analysis of the simulated data for a variety of different modelled cases indicates that the frequency locations of these minima are dependent on the magnitude of the current modulation. The biases increase substantially for θ below these values since the IF signals generated within this region are distorted: the extracted peak signals do not include all the frequency modulation contained in the radar signal. For values of θ above the minima, the biases either remain stable or increase very gradually; these errors are negligible compared with the errors caused by insufficient values of θ.

HF radar data from the Holderness deployment were also analysed in order to determine the optimum range of bandwidth parameters. Figure 6.18 shows the positive Bragg peak biases and standard deviations for three contrasting grid cells. For radar signals backscattered from the ocean surface, the theoretical Bragg peak frequencies are unknown. An estimate is made from a centroid calculation in the vicinity of the maximum values in each Doppler spectrum. This approach introduces the measurement errors which originally provided the motivation behind developing the IF filter technique. In order to combat this problem, only good quality spectra were used in this analysis. Since the Bragg peaks in the selected Doppler spectra are clean and undistorted, the corresponding frequency estimates can be considered reliable.

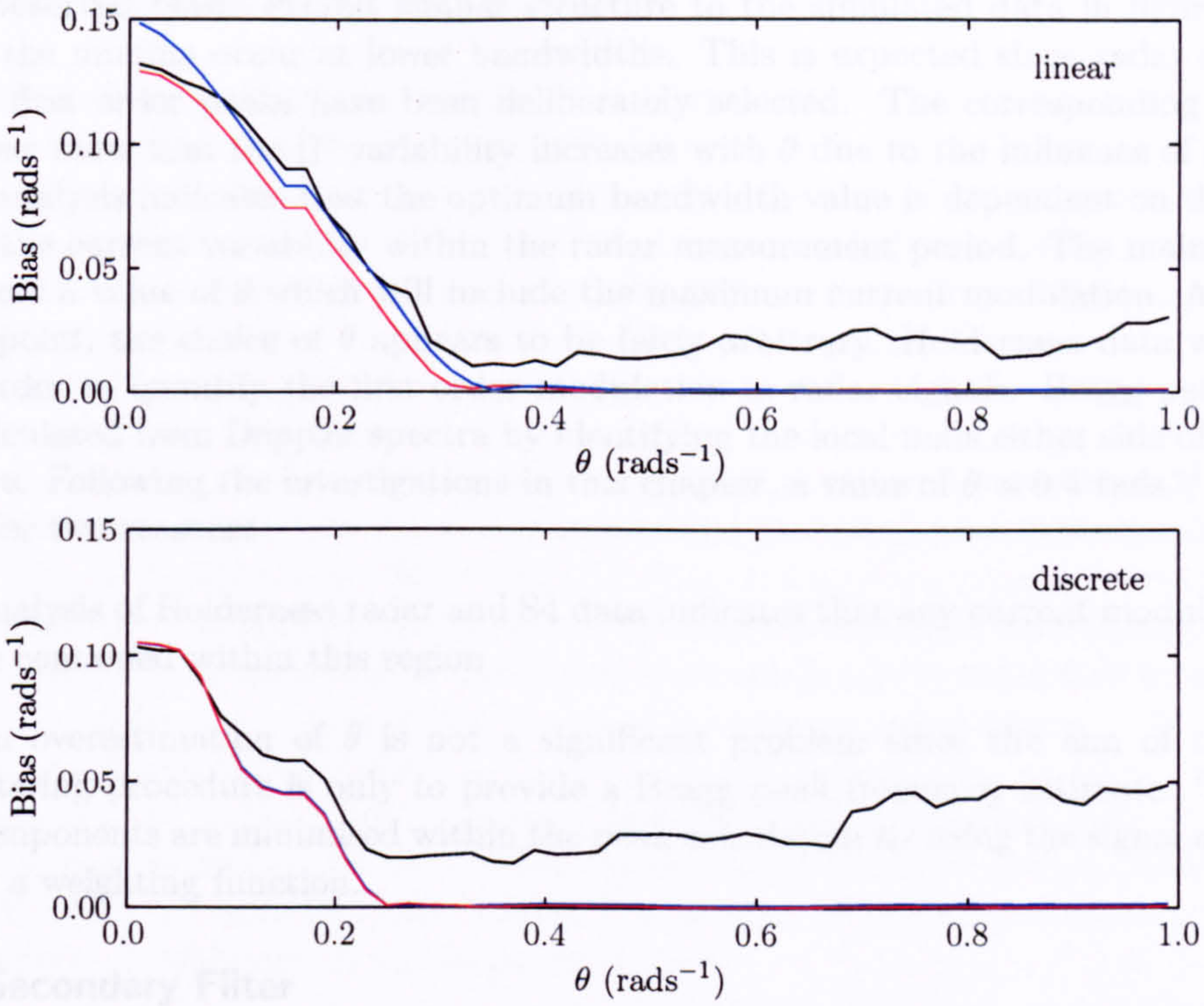

Figure 6.17: Biases in Bragg frequency estimates using simulated data. Linear current (top) and discrete current bands (bottom) for SNR = 20 dB (black), 40 dB (blue), 60 dB (red).

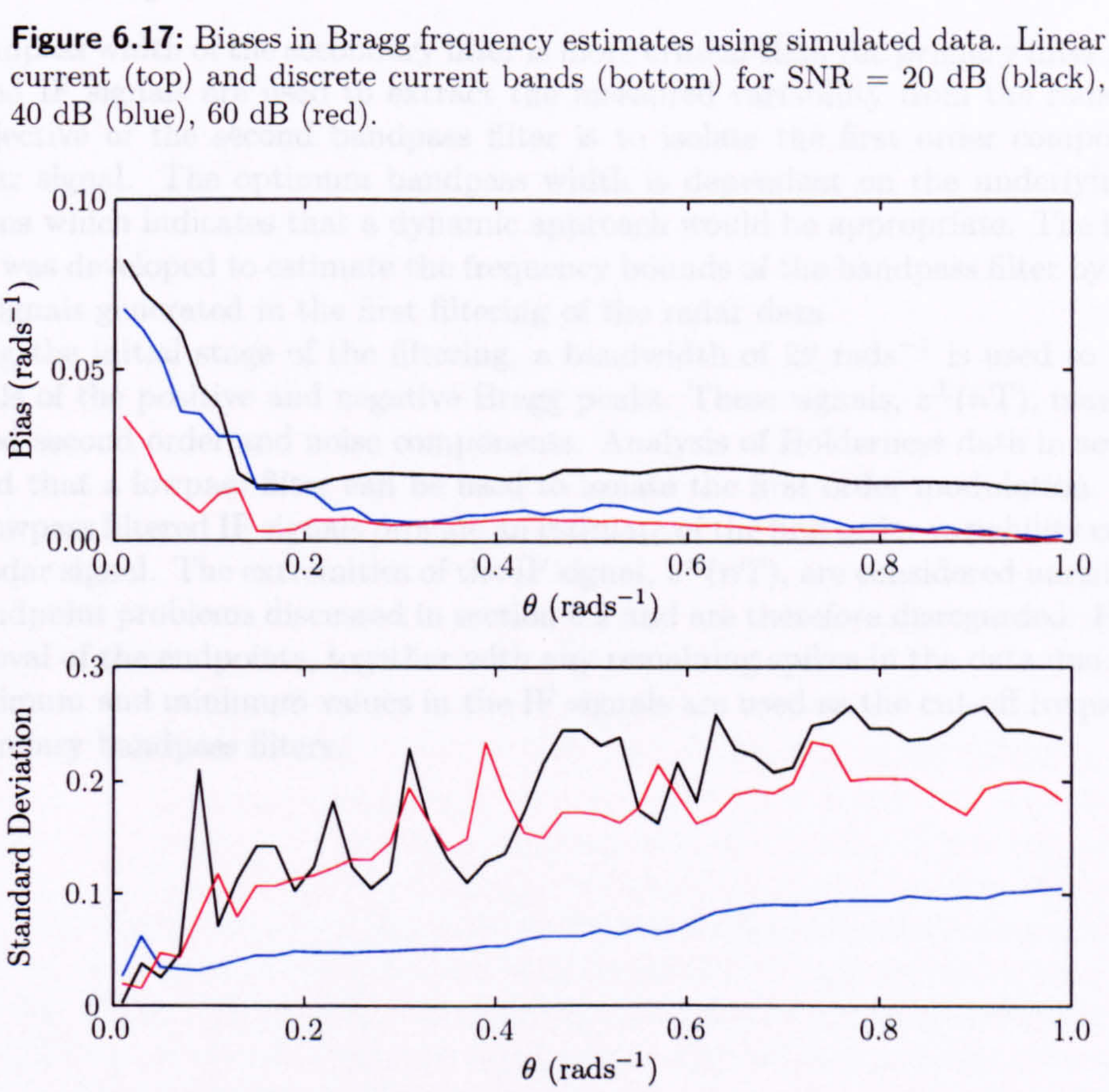

Figure 6.18: Bias (top) and standard deviation (bottom) parameters generated from Bragg frequency estimates of positive peak. Data taken from master site at 14:00, 21/12/95 for cells 60 (black), 80 (blue), 120 (red).

The observed biases exhibit similar structure to the simulated data in figure 6.17 although the minima occur at lower bandwidths. This is expected since radar data with distinct first order peaks have been deliberately selected. The corresponding standard deviations show that the IF variability increases with θ due to the influence of noise.

This analysis indicates that the optimum bandwidth value is dependent on the magnitude of the current variability within the radar measurement period. The main criterion is to select a value of θ which will include the maximum current modulation. Above this critical point, the choice of θ appears to be fairly arbitrary. Holderness data were studied in order to quantify the first order modulation in radar signals. Bragg peak widths were calculated from Doppler spectra by identifying the local nulls either side of the peak structure. Following the investigations in this chapter, a value of $\theta = 0.4$ rads^{-1} has been chosen for two reasons:

- Analysis of Holderness radar and S4 data indicates that any current modulation will be contained within this region
- An overestimation of θ is not a significant problem since the aim of the initial filtering procedure is only to provide a Bragg peak frequency estimate. The noise components are minimised within the peak calculation by using the signal amplitude as a weighting function.

6.4.2 Secondary Filter

The bandpass width of the secondary filter is more critical than the primary filter since the generated IF signals are used to extract the measured variability from the radar signal. The objective of the second bandpass filter is to isolate the first order components in the radar signal. The optimum bandpass width is dependent on the underlying ocean conditions which indicates that a dynamic approach would be appropriate. The following method was developed to estimate the frequency bounds of the bandpass filter by utilising the IF signals generated in the first filtering of the radar data.

During the initial stage of the filtering, a bandwidth of 2θ rads^{-1} is used to generate IF signals of the positive and negative Bragg peaks. These signals, $z^{\pm}(n\mathrm{T})$, may contain unwanted second order and noise components. Analysis of Holderness data in section 6.1 indicated that a lowpass filter can be used to isolate the first order modulation.

The lowpass filtered IF signals provide an estimate of the first order variability contained in the radar signal. The extremities of the IF signal, $z^{\pm}(n\mathrm{T})$, are considered unreliable due to the endpoint problems discussed in section 6.2 and are therefore disregarded. Following the removal of the endpoints, together with any remaining spikes in the data due to noise, the maximum and minimum values in the IF signals are used as the cut-off frequencies in the secondary bandpass filters.

6.5 Summary

The IF filter spectral technique has been examined in detail within this chapter. Simulated and radar data were used to determine properties of the method.

Discontinuities in the instantaneous frequency signals were attributed to the SNR level in the backscattered data. The IF estimates are corrupted by noise at low signal amplitudes. Lowpass filtering was proposed as a method to reduce this erroneous structure and a half-width of $\rho = 0.3$ rads^{-1} was selected.

Simulated data were examined to ascertain the impact of the IF signal processing. Endpoint problems, caused by the truncation of the non-periodic data, were discussed. The influence of noise on the variance of the generated IF signals was analysed and related to the width of the bandpass filter. Oceanographic processes were modelled in order to identify any limitations in the approach.

The accuracy of the filtering method is dependent on the bandwidth parameters. The optimum values were calculated by analysing the peak frequency biases: a primary filter width of $\theta = 0.4$ rads^{-1} was selected; a dynamic approach was introduced to determine the extent of the secondary filter.

The potential of the IF filter to measure the time varying characteristics of HF radar signals has been demonstrated. Simulated current modulation has been successfully identified and extracted from the radar signal. The impact of this procedure on ocean wave measurements is evaluated in the following chapter.

7 Ocean Wave Measurements

Oceanographic data from the OSCR system and an S4 current meter were evaluated in chapter 5. Statistical analysis revealed strong correlation between the radar and S4 current components. A study of the IF filter in chapter 6 illustrated the potential of the technique to measure the time varying characteristics of ocean currents. The impact of the filter on ocean wave measurements is investigated in this chapter:

- The temporal variability of wave parameters in the Holderness region is evaluated using data from a directional waverider buoy.

- The spatial structure of the ocean wave fields is analysed.

7.1 The Ocean Wave Directional Spectrum

The sea surface is a complex and chaotic phenomenon caused by the interaction of ocean waves, with different wavelengths and amplitudes, which are propagating in a variety of directions. The first recognised mathematical treatment of ocean waves was developed by Longuet-Higgins in 1957 [22]. He introduced a conceptual model of the sea surface by considering the superposition of regular trigonometric waves with random amplitudes, directions and phases. In recent years, the ocean wave directional spectrum, $S(f,\theta)$, has become the established quantity which is used to describe this stochastic field. Significant advances have been made in measuring $S(f,\theta)$ and numerous in situ and remote sensing instruments have been developed. The full directional spectrum describes the distribution of wave energy in terms of frequency, f, and direction, θ, and is often expressed as

$$S(f,\theta) = S(f)\ G(f,\theta), \tag{7.1}$$

where the spectral density function, $S(f)$, is formed by integrating $S(f,\theta)$ with respect to θ,

$$S(f) = \int_0^{2\pi} S(f,\theta)\ \mathrm{d}\theta, \tag{7.2}$$

and $G(f,\theta)$ is a normalised term which describes the directional distribution [48].

$$\int_0^{\infty}\int_0^{2\pi} G(f,\theta)\ \mathrm{d}\theta\,\mathrm{d}f = 1 \tag{7.3}$$

Various sea state parameters can be derived from the spectrum. Data from the OSCR radar system and a directional waverider buoy are studied in this chapter. These instruments provide estimates of $S(f,\theta)$ which are analysed in order to generate measurements of waveheight, direction and period. The significant waveheight parameter, H_s, provides a measure of the total energy in the wave spectrum.

$$H_s = 4\left[\int_{-\infty}^{\infty} S(f)\ \mathrm{d}f\right]^{\frac{1}{2}} \tag{7.4}$$

The mean period, T_1, is determined from the first moment of $S(f)$

$$T_1 = \frac{\int_{f_1}^{f_2} S(f)\,\mathrm{d}f}{\int_{f_1}^{f_2} fS(f)\,\mathrm{d}f}, \tag{7.5}$$

where the integration is evaluated between the finite frequency limits f_1 and f_2. The mean direction, θ_m, is derived from the Fourier coefficients of the full directional spectrum.

$$\tan\theta_\mathrm{m} = \frac{\int_{f_1}^{f_2} S(f)\sin\theta(f)\,\mathrm{d}f}{\int_{f_1}^{f_2} S(f)\cos\theta(f)\,\mathrm{d}f} \tag{7.6}$$

The integration limits, f_1 and f_2, are constrained to different frequency bands during the following analysis in order to isolate specific ocean wave conditions such as swell and wind-sea parameters.

7.2 Temporal Analysis

The temporal structure of ocean wave parameters generated from the OSCR system and a directional waverider are evaluated in this section. Data from both instruments were available over a period of approximately one month between December 1995 and January 1996. Estimates of directional spectra and various wave parameters were obtained and comparisons were made using the statistical methods described in section 5.1.1.

7.2.1 Directional Waverider Data

Numerous techniques for measuring ocean waves have been developed over the years although the most established instruments are wave buoys: these are regarded as giving the closest approximation to the underlying ocean wave field. The industry standard for offshore wave recording is the directional waverider (DWR) [48].

During the Holderness experiment, a Datawell DWR was deployed within the HF radar measurement region by the Proudman Oceanographic Laboratory (POL). Figure 2.1 shows the geographical location of the instrument. Estimates of the directional spectra were calculated onboard the buoy and the output signals were transmitted via an HF radio link to an onshore receiver for analysis.

A DWR consists of a spherical, 90 cm diameter, moored buoy containing a vertical accelerometer which follows the motion of the water it displaces. The sensor is mounted on an inertia stabilised platform and measures the true vertical acceleration [22]. A three component fluxgate compass and a two axis horizontal accelerometer are attached to the hull of the buoy and used to measure the pitch and roll parameters. A transformation matrix, which contains information about the relationship between the buoy vector coordinates and the fixed coordinates, is used to determine north-south and east-west components of acceleration. A DWR does not measure the directional spectrum directly but instead provides estimates of a limited number of Fourier coefficients; directional spectra can be constructed from these Fourier values using a modelling approach.

7.2.2 Results

In order to synchronise the wave measurements, each set of radar data (which provides an average over a one hour time period) were paired with DWR data taken at half past each hour. Quantitative and qualitative results are established although there are inherent

limitations in these approaches due to the contrasting measurement principles utilised by the instruments.

Figure 7.1 shows time series data, between the 17th December 1995 and the 8th January 1996, of significant waveheight, mean direction, mean period and peak period. The wave parameters are integrated over the maximum frequency range of the radar software (0.01 to 0.4 Hz) with the exception of the peak period, T_p, which is evaluated within ± 20 mHz of the dominant peak in the frequency spectrum. The solid line represents the wavebuoy data which were almost continuous during the 552 hour time period. The red and blue crosses represent the data generated from the radar using the standard periodogram and IF filter techniques respectively. An initial overview indicates congruence between the OSCR and DWR derived wave parameters although measurements are only available from the radar within discrete temporal bands. The discontinuous structure of the radar data can be attributed to a number of factors such as hardware failure, and logistical limitations.

The aim of the IF filtering technique that has been developed in this thesis is to extract the first order modulation from the radar signal which, consequently, will enable an increased number of cells to be inverted. In order to apply the Wyatt inversion procedure, the Doppler spectra from the master and slave radar sites must pass the quality criteria described in section 3.4.1. The application of the IF filter to data from the Holderness deployment caused a significant increase in the number of invertible cells. An investigation into the temporal and spatial structure of these cells is provided in chapter 8.

Table 7.1 shows the statistical analysis results derived from the DWR and OSCR data. The correlation between the generated wave parameters is illustrated in figure 7.2 where the lines in each graph represent the least squares fit to the data. The plots show evidence of biases between the mean period and direction parameters derived from the OSCR and DWR instruments.

Figure 7.1 shows that during periods of high sea states, the radar tends to overestimate the significant waveheight. The mean period parameter, T_1, is dependent on the distribution of energy over all frequencies and, consequently, the inaccuracies in $S(f)$ cause a lower T_1 value which accounts for the bias in figure 7.2. This limitation has been identified in HF radar data due to a departure from the second order spectral theory and is the subject of investigation at the University of Sheffield [56]. The OSCR radar system utilised old beamforming technology and the algorithm used to determine beam directions has an azimuthal resolution of approximately 15 degrees. During the Holderness deployment, problems were identified in the slave beam directions caused by sidelobe contamination and siting errors [31]. These may contribute to the biases in mean direction between the DWR and OSCR instruments.

An analysis of the radar spectral techniques suggests that overall, the IF filter performs better than the periodogram in comparisons with the waverider. The significant waveheight values generated from the raw and filtered spectra are similar – the data exhibit strong correlation ($r^2_{xy} > 0.83$) and comparable rms error values. The IF filter method provides significantly stronger coherence with the DWR for the direction, mean period and peak period parameters.

Following previous investigations at the University of Sheffield [31], two time periods of interest have been identified which are studied in more detail below. These have been selected since they correspond with times when radar and DWR data were both available and the meteorological conditions were recorded. Measurements of the directional and frequency wave spectra have been generated from the two instruments for analysis. The aim of this work is to evaluate the accuracy of the radar techniques at measuring the wave spectrum under a variety of different ocean conditions.

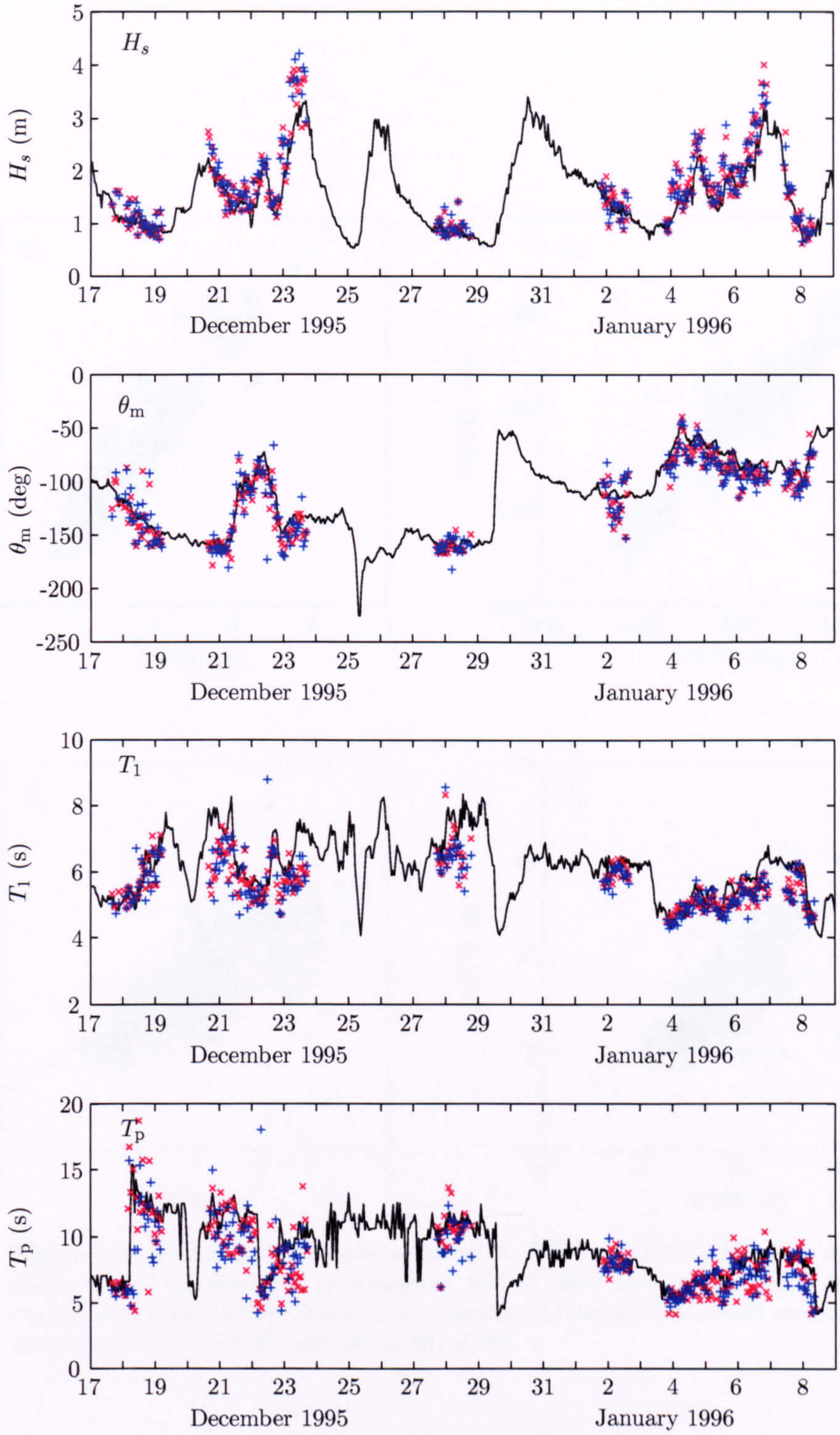

Figure 7.1: Time series of OSCR and DWR wave parameters. The black line represents the continuous DWR measurements. The blue and red crosses represent the radar data generated using the periodogram and IF filter techniques respectively. Data taken between 00:00, 17/12/95 and 23:00, 08/01/96.

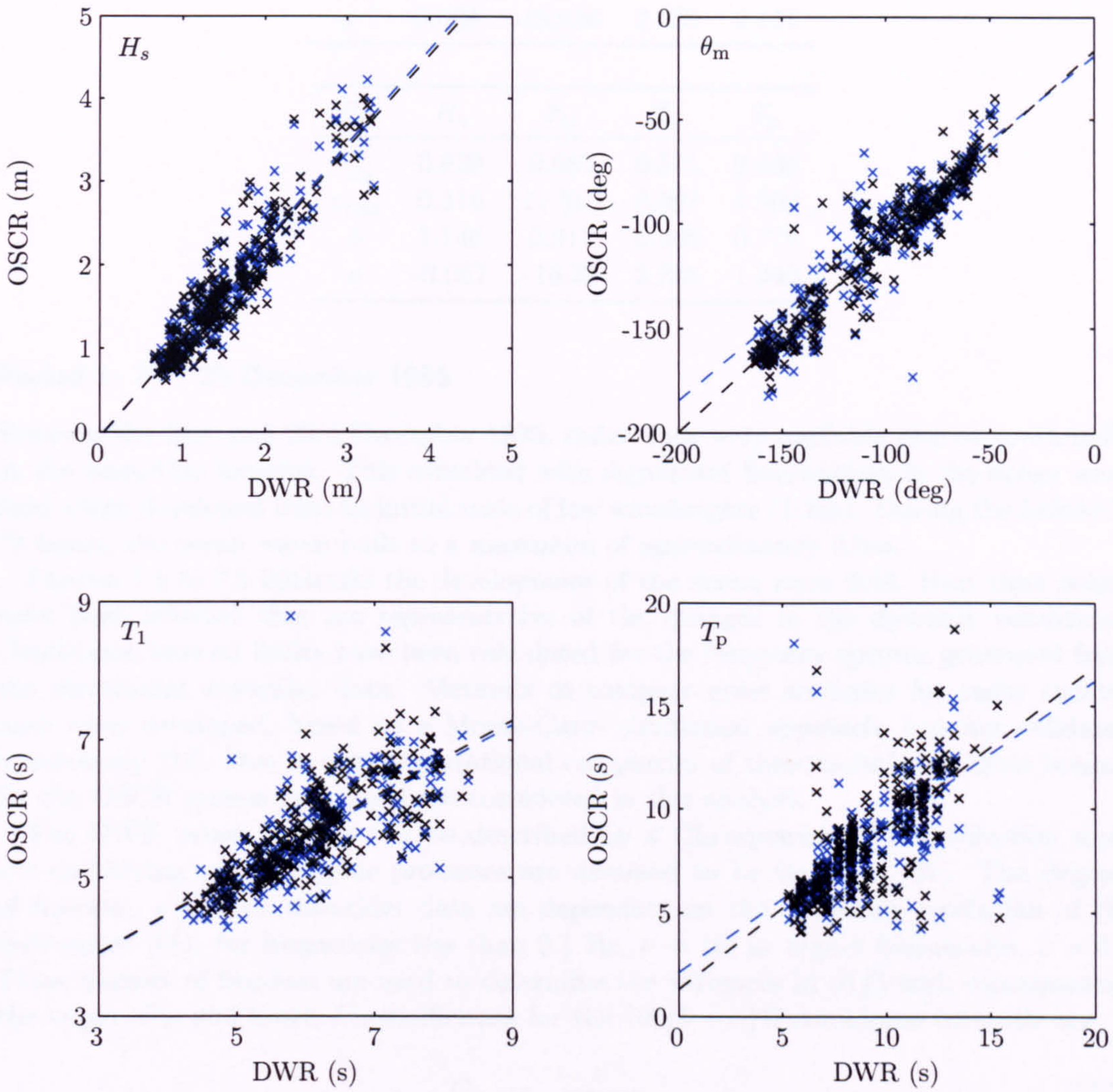

Figure 7.2: Scatter plots of wave parameters. DWR vs OSCR. The blue and black crosses represent the periodogram and IF filter data respectively. The dashed lines show the linear regression results. 243 pairs of data were analysed between 00:00, 17/12/95 and 23:00, 08/01/96.

Table 7.1: Statistical analysis of DWR and OSCR wave parameters using the periodogram and IF filter techniques. 243 pairs of data were analysed between 00:00, 17/12/95 and 23:00, 08/01/96.

PG	H_s	θ_{m}	T_1	T_{p}
r^2_{xy}	0.847	0.821	0.486	0.249
$\varepsilon_{\mathrm{rms}}$	0.297	14.260	0.661	2.861
b	1.166	0.829	0.550	0.702
a	-0.068	-18.828	2.269	2.151

IF	H_s	θ_{m}	T_1	T_{p}
r^2_{xy}	0.839	0.887	0.571	0.468
$\varepsilon_{\mathrm{rms}}$	0.316	11.510	0.597	1.960
b	1.146	0.917	0.560	0.778
a	-0.057	-16.35	2.245	1.340

Period 1: 21 - 23 December 1995

Between the 21st and 23rd December 1995, radar data were available almost continually at the waverider location. This coincided with significant fluctuations in the ocean wave field which developed from an initial state of low waveheights (1-2m). During the following 72 hours, the ocean waves built to a maximum of approximately 3.5m.

Figures 7.3 to 7.5 illustrate the development of the ocean wave field. Four time points have been selected that are representative of the changes in the dynamic conditions. Confidence interval limits have been calculated for the frequency spectra generated from the directional waverider data. Methods to compute error statistics for radar spectra have been developed, based on a Monte-Carlo simulation approach, but not validated conclusively [31]. Due to the computational complexity of these techniques, error bounds for the OSCR system have not been considered in this analysis.

The DWR power spectra can be described by a Chi-squared (χ^2) distribution since the underlying oceanographic processes are assumed to be Gaussian [31]. The degrees of freedom, ν, in the waverider data are dependent on the frequency resolution of the instrument [55]: for frequencies less than 0.1 Hz, $\nu = 16$; at higher frequencies, $\nu = 32$. These degrees of freedom are used to determine the variances in $S(f)$ and, consequently, the upper, C_{u}, and lower, C_{l}, coefficients for the $100(1-\alpha)\%$ confidence intervals are

$$C_{\mathrm{u}} = \frac{\nu}{\chi^2_{\nu,\alpha/2}}, \tag{7.7}$$

$$C_{\mathrm{l}} = \frac{\nu}{\chi^2_{\nu,1-\alpha/2}}. \tag{7.8}$$

Figure 7.3 shows the 90% confidence limits which were calculated from the DWR data. Differences are expected between the radar and buoy spectra since the DWR provides point measurements whereas HF radar data represent a temporal average over a larger spatial region. During the 72 hour time period, the OSCR derived wave spectra showed good agreement with the DWR measurements; both radar techniques tracked the underlying oceanic conditions over a range of different wave fields. A qualitative analysis of the data indicated that the major features that characterised the DWR spectra were more discernible in the IF filter data. A significant proportion of the spectra generated from

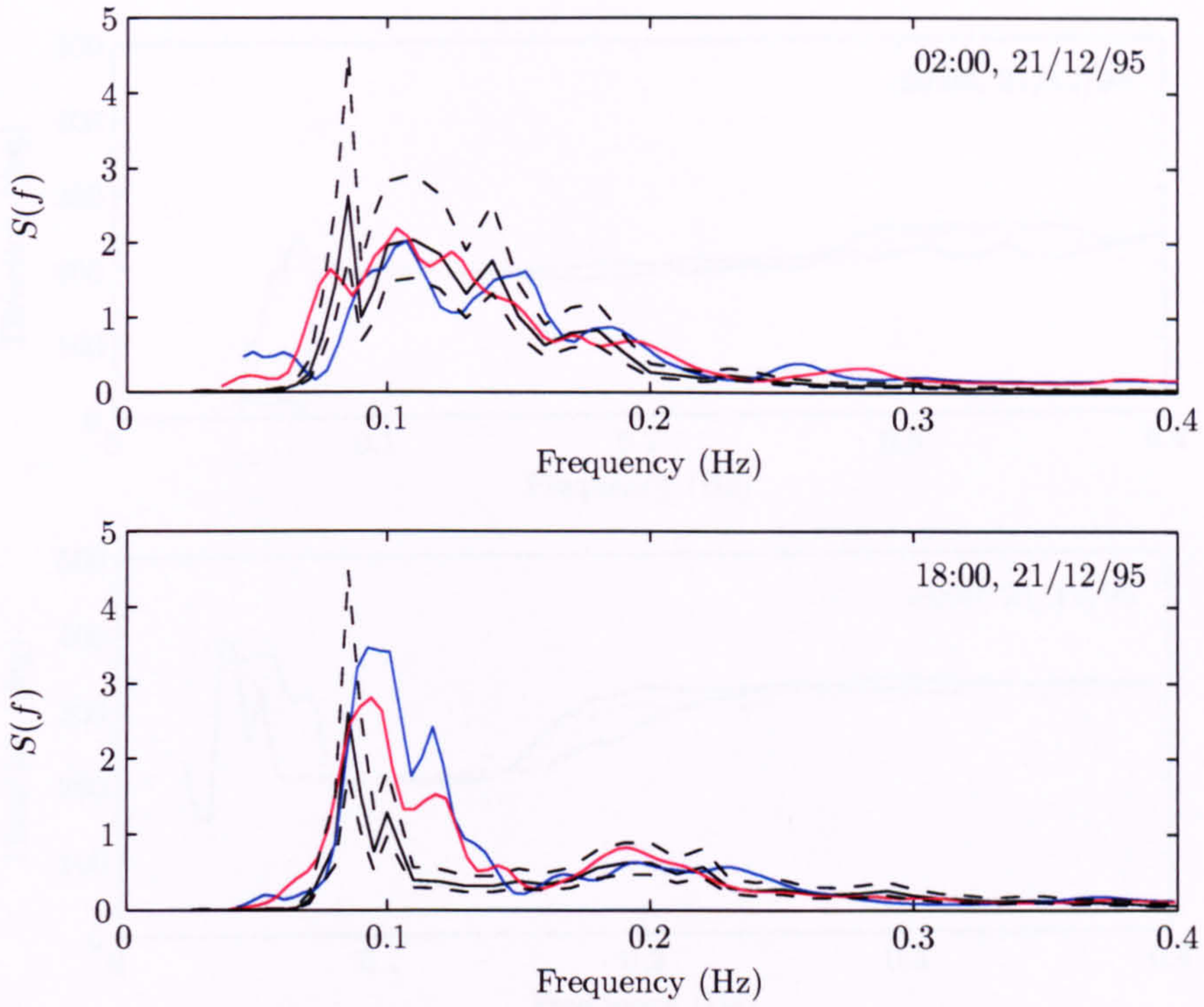

Figure 7.3: Wave frequency spectra measured using DWR (black), periodogram (blue) and IF filter (red) techniques. The broken lines represent the 90% confidence interval limits for the DWR. Data taken from period 1 between 02:00, 21/12/95 and 00:00, 23/12/95.

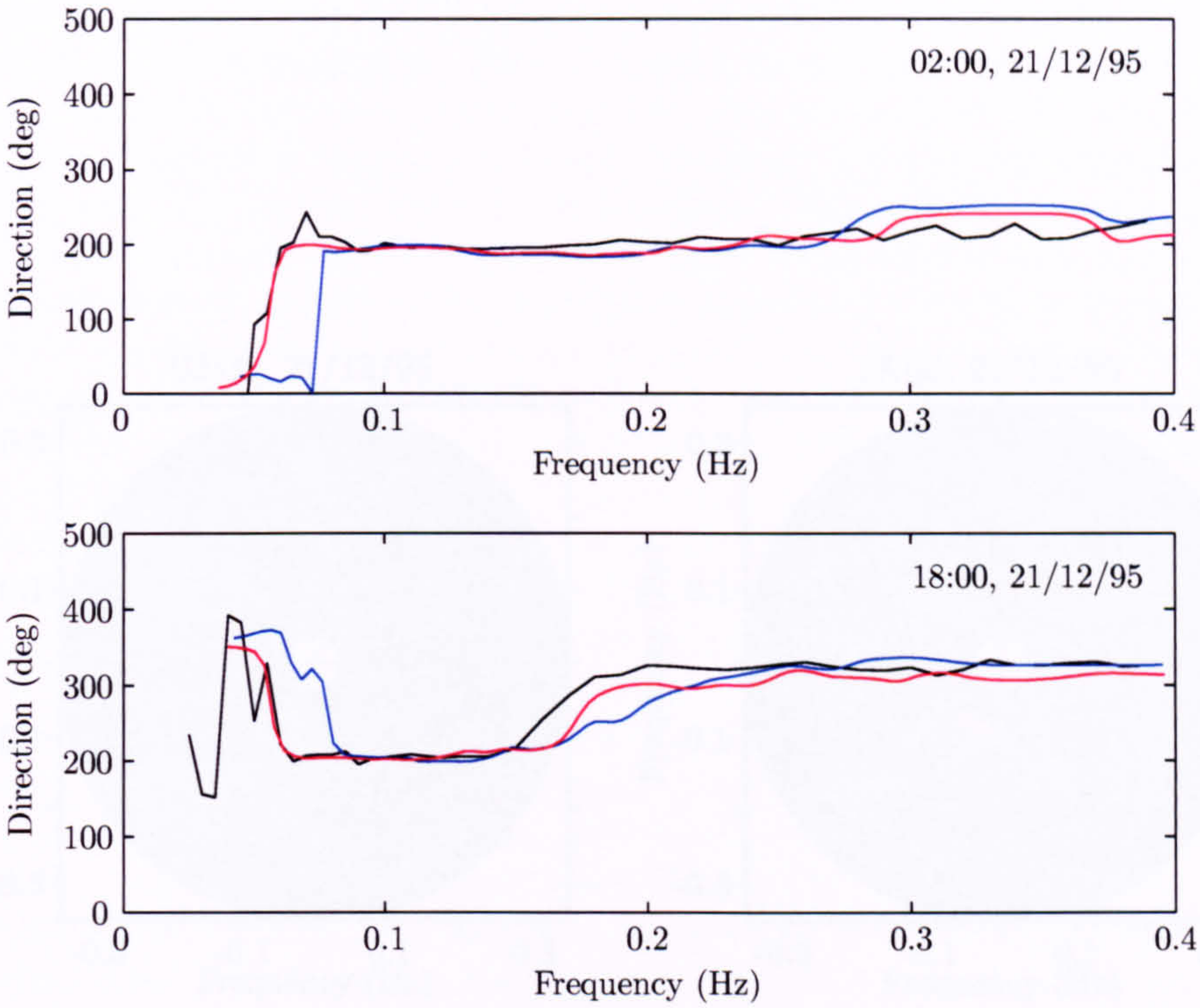

Figure 7.4: Wave mean direction spectra measured using DWR (black), periodogram (blue) and IF filter (red) techniques. Data taken from period 1 between 02:00, 21/12/95 and 00:00, 23/12/95.

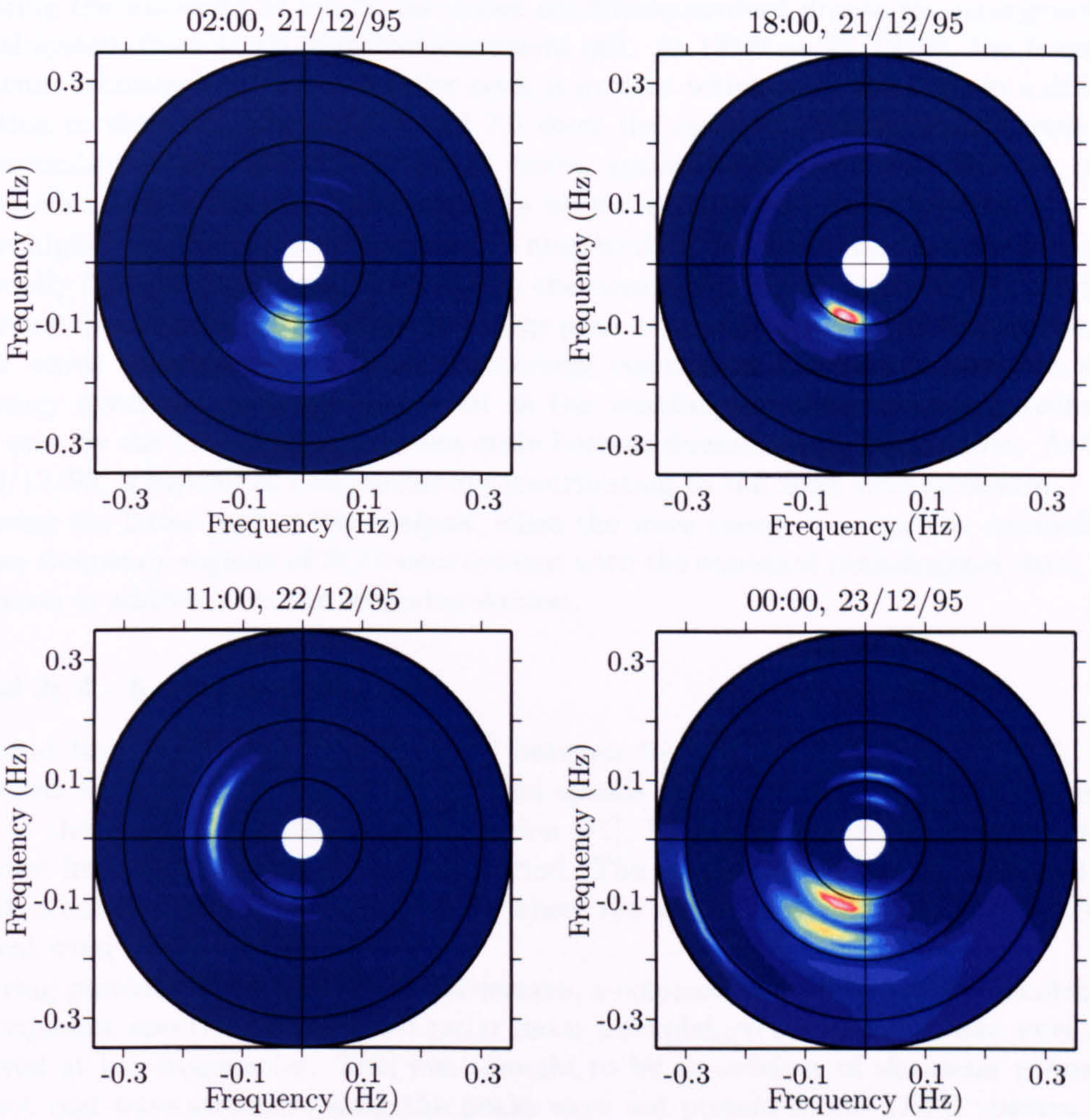

Figure 7.5: Wave directional spectra measured using IF filter technique. Data taken from period 1 between 02:00, 21/12/95 and 00:00, 23/12/95.

the IF filtered data is contained within the error bounds, particularly during periods of high sea states where the periodogram tends to over estimate the wave energy.

At 02:00 on 21/12/95, the frequency spectrum (figure 7.3) is characterised by a single peak located at approximately 0.1 Hz. This peak corresponds to the swell which was dominating the ocean conditions at this time [31]. Figure 7.4 shows the mean direction of the waves as a function of frequency. The low frequency waves are travelling at an angle of approximately 200 degrees towards the coastline. Figure 7.5 shows the directional spectrum which confirms these oceanic conditions. Meteorological charts indicate that this swell was probably caused by a low pressure region over Norway to the north.

During the following 24 hours, the ocean conditions evolved due to the emergence of a frontal system from south of the measurement cell. At 18:00 on 21/12/95, the frequency spectrum becomes bimodal. A smaller peak is evident which is propagating in a different direction to the swell. Figures 7.4 and 7.5 show the range of directions associated with this secondary peak. The shorter ocean waves, generated by the frontal system, create this smaller peak which can be identified in both the DWR and radar spectra.

The higher frequency waves increased in amplitude throughout the next few hours and eventually became the dominant feature in the ocean system. At 11:00 on 22/12/95, the frequency spectrum is characterised by a large peak at approximately 0.15 Hz, representing ocean waves travelling towards the Holderness coastline. The energy over the entire frequency spectrum gradually increased as the waveheights built up to approximately 3.5m and, by the following day, the sea state became dominated by wind waves. At 00:00 on 23/12/95, a myriad of frequencies are contributing to the wave field structure.

During the latter part of the analysis, when the wave energy was highest, anomalies in the low frequency regions of $S(f)$ were evident with the standard periodogram data. This limitation is addressed in the following section.

Period 2: 4 - 6 January 1996

A second time period has been analysed between the 4th and 6th January 1996. High sea states were observed due to strong wind speeds that were produced by a depression lying to the north of the measurement region [31]. Figure 7.6 shows the development of the wave frequency spectra during this period. The spectra are generally unimodal with a peak occurring between 0.1 and 0.2 Hz where the wave conditions are being generated by local wind in the region.

During previous investigations at Holderness, a common characteristic was identified in the frequency spectra derived from radar data; unexplained secondary peaks were often observed at low frequencies. This was thought to be an artefact of the radar processing and not real wave structure since the peaks were not present in the DWR spectra. The structure has been attributed to various phenomena such as interference in the radar signal, noise, current variability, antenna sidelobes and wave inversion limitations [31].

Figure 7.6 illustrates this problem where the later frequency spectra generated from the standard periodogram data exhibit a secondary peak. These peaks, located at approximately 0.05 Hz, are not present in the IF filter or DWR data. Figure 7.7 shows the corresponding Doppler3 spectra generated from the slave radar site. It is evident that the Bragg peaks in the spectra at the affected time points are distorted. This presents problems in the wave inversion technique since the minima which separate the first and second order components of the Doppler3 spectra are ambiguous. The radar wave signal processing can incorrectly identify these multiple first order peaks as second order structure which will subsequently generate large low frequency components in the wave parameters. Over 20% of the wave data may be affected by this phenomenon.

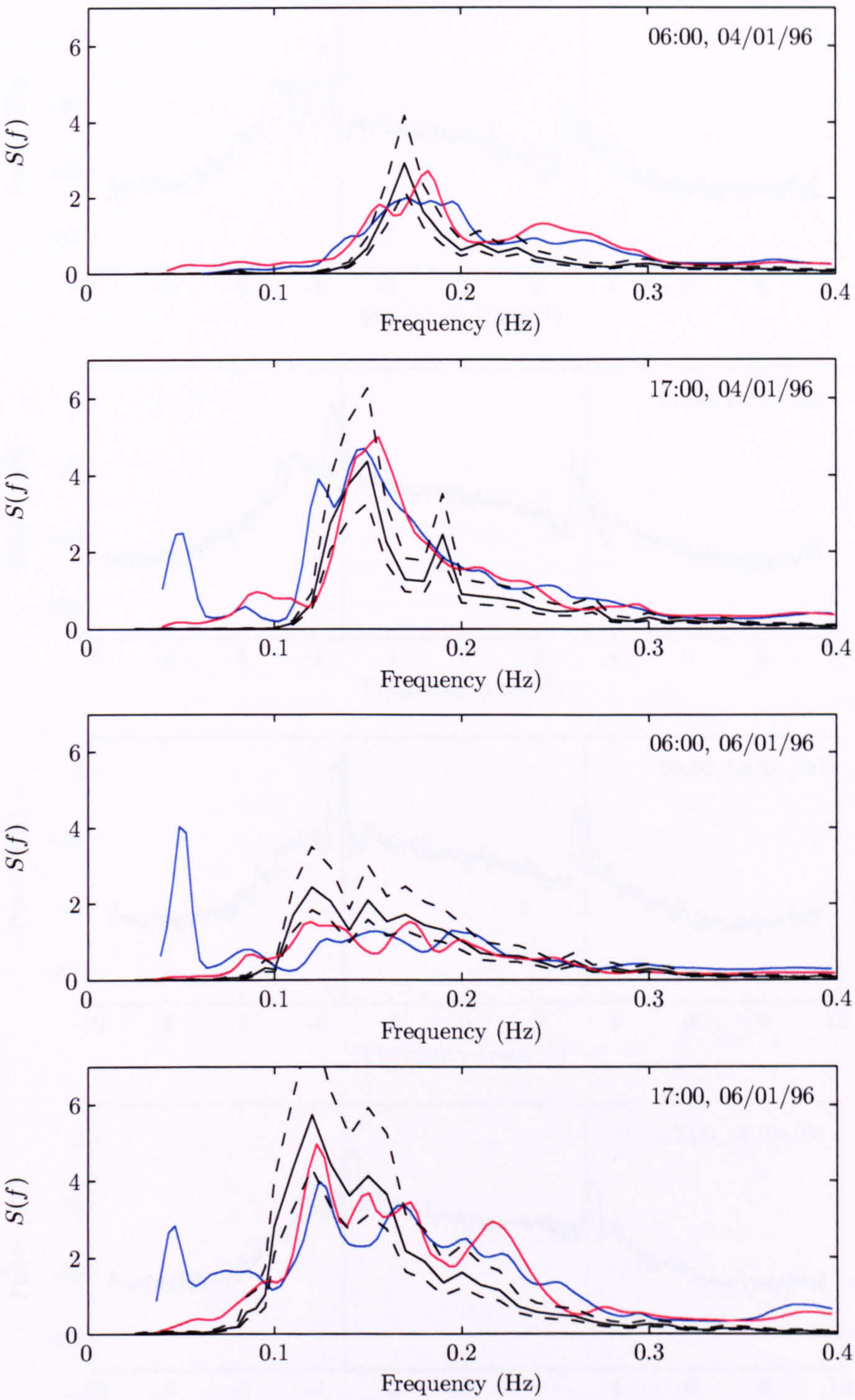

Figure 7.6: Wave frequency spectra measured using DWR (black), periodogram (blue) and IF filter (red) techniques. The broken lines represent the 90% confidence interval limits for the DWR. Data taken from period 2 between 06:00, 04/01/96 and 17:00, 06/01/96.

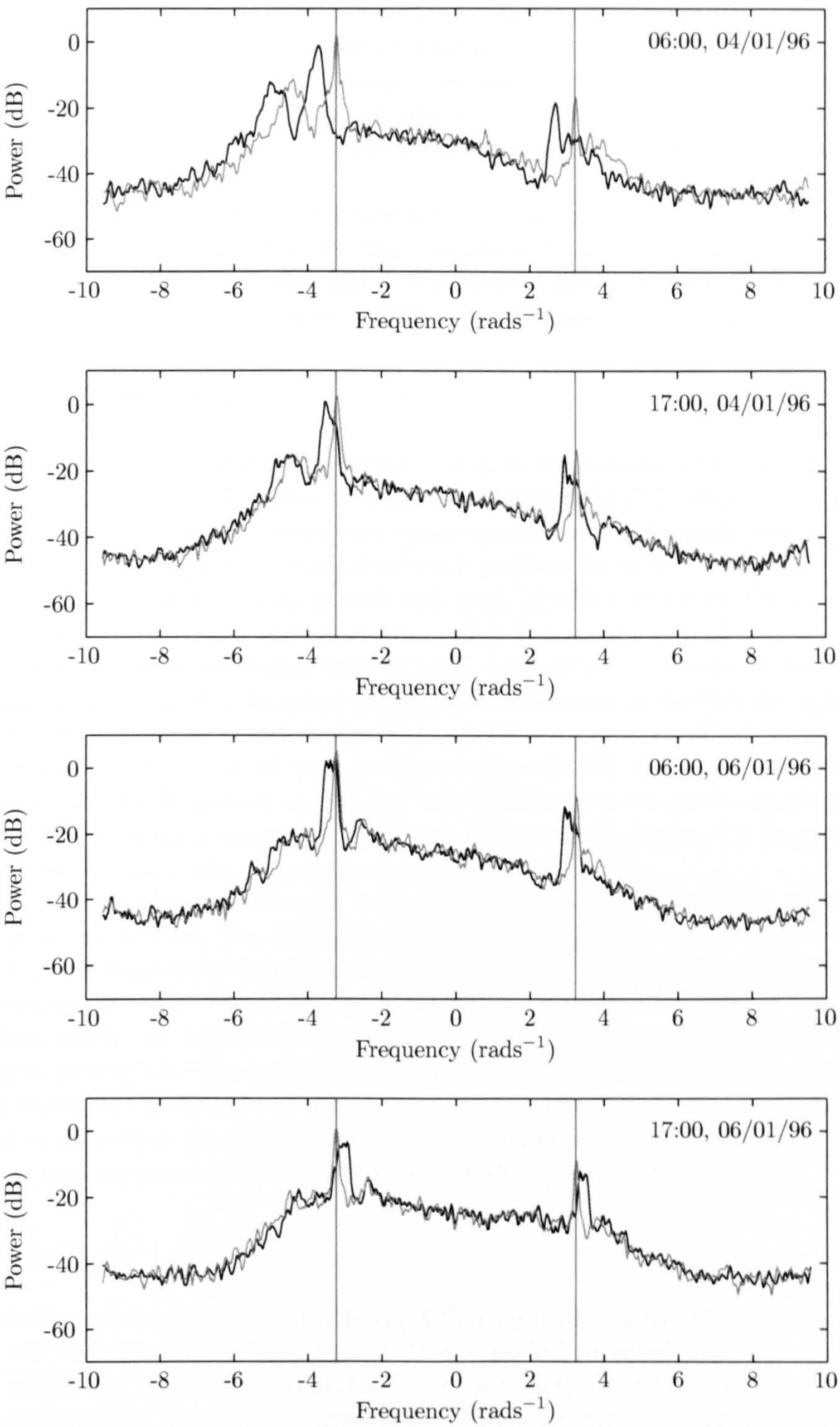

Figure 7.7: Doppler3 spectra generated from raw (dark) and IF filtered (light) signals during period 2. The vertical lines represent the Bragg frequencies $\pm\omega_b$. Data taken from slave site between 06:00, 04/01/96 and 17:00, 06/01/96.

The IF filter spectral technique has been designed to identify and remove this modulation from radar data. Figure 7.7 shows the influence of the filter on the first order spectral structure. The Bragg peaks are sharper and, consequently, the low frequency structure in the corresponding wave spectra has been removed. An analysis of numerous wave spectra during this time period reveals that a large proportion of the erroneous structure has been extracted using the IF filter. Figure 7.6 shows that the spectra generated from the IF filtered data are more likely to be contained within the 90% confidence intervals derived from the DWR data.

Time series of waveheights in the low frequency band ($0.01 \leq f \leq 0.1$) were studied in order to quantify the impact of the IF filter. Statistical analysis yielded correlation coefficients of 0.625 and 0.658 for the raw and filtered data respectively. The filter also exhibited an improved root mean square value (0.222) compared with the raw data (0.231).

7.3 Spatial Analysis

Wave parameters were evaluated in section 7.2 at a single fixed point in the Holderness region. The advantage of HF radar, compared to conventional in situ instruments, is its unique capability to generate concurrent oceanographic measurements over an expansive area. This enables the spatial structure of wave parameters to be investigated.

Figure 7.8 shows maps of peak period and peak direction between the 21st and 23rd December 1995. The maps were generated using the standard periodogram technique and are characterised by scattered areas of high variability. The cause of these disjointed regions has been identified as large low frequency components in the Doppler spectra of the corresponding radar cells. Validation of the spatial structure is difficult since data from alternative instruments, such as wave buoys, are unavailable. However, due to the spatial resolution of the OSCR system, correlation would be expected between neighbouring grid cells. The discontinuities symptomatic of the wave fields in figure 7.8 suggest that the observed structure may not be an oceanographic phenomenon.

Figure 7.9 shows the maps created from the filtered data. The impact of the IF filter processing is conspicuous. The first order components, which caused distortion in the raw Doppler spectra, have been extracted and this results in a more homogeneous formation. Smooth transitions exist within the wave field although regions of higher variability are also evident which can be attributed to the meteorological and oceanographic conditions described in section 7.2. The emergence of a frontal system from south of the measurement region at 18:00 on 21/12/95 is clearly evident in the filtered map. This was confirmed by independent data from the UK Met Office and provides evidence of the advantage of the IF filtering technique over the conventional periodogram method.

7.4 Summary

Ocean wave measurements from OSCR and DWR instruments have been evaluated in this chapter. An examination of data from a 23 day period revealed that HF radar technology can accurately track wave parameters over a variety of ocean conditions. Statistical analysis showed that the IF filter approach provided stronger correlation with the DWR than the standard periodogram method. The number of spectra which could be inverted using the IF filter approach was superior to the periodogram.

Investigations of specific time periods revealed that multiple first order structure within radar data can limit the accuracy of the generated directional wave spectra estimates. Filtering of the radar signal has been shown to be effective in removing this modulation.

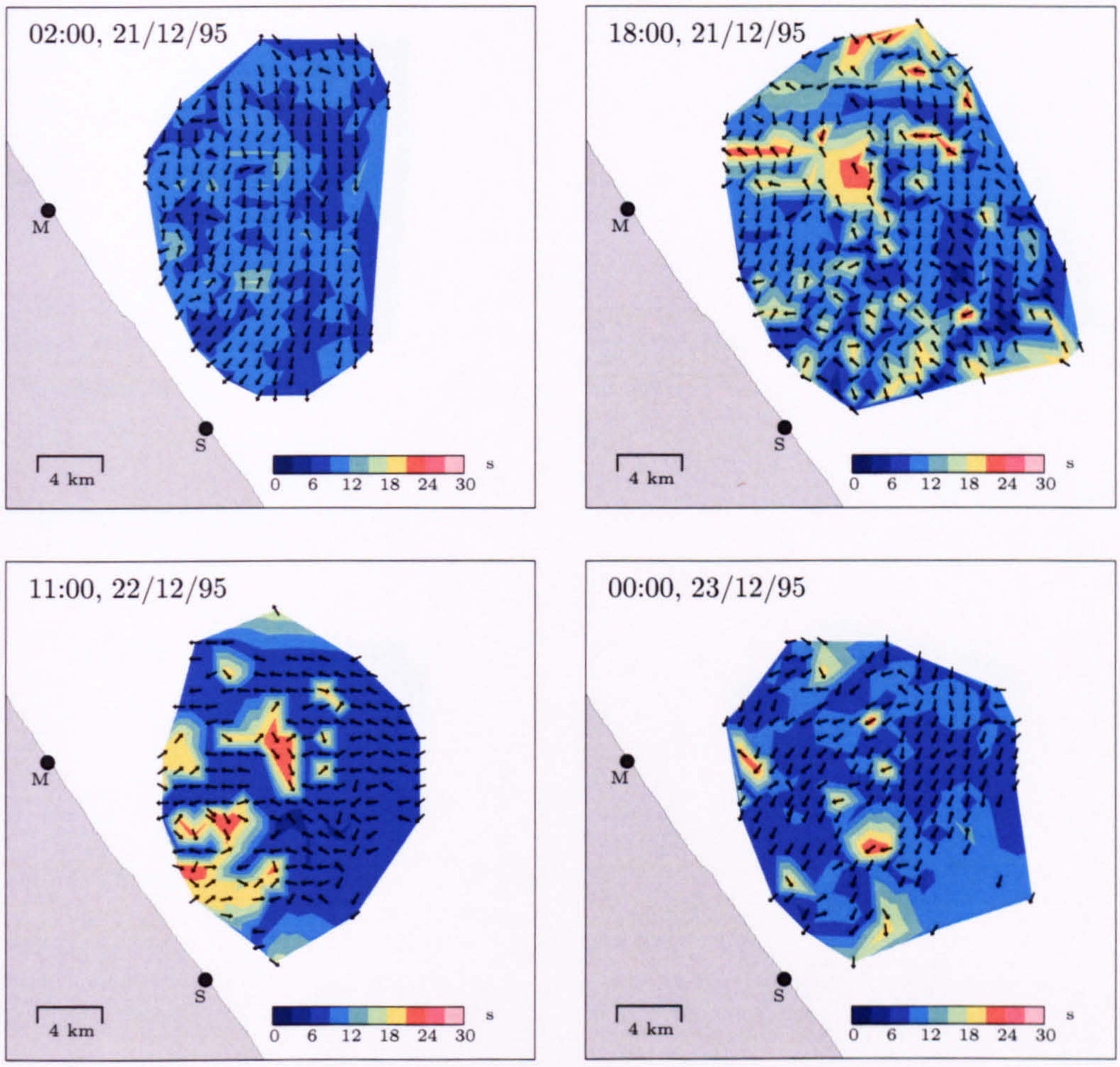

Figure 7.8: Peak period and peak direction measured using periodogram technique. Data taken from period 1 between 02:00, 21/12/95 and 00:00, 23/12/95.

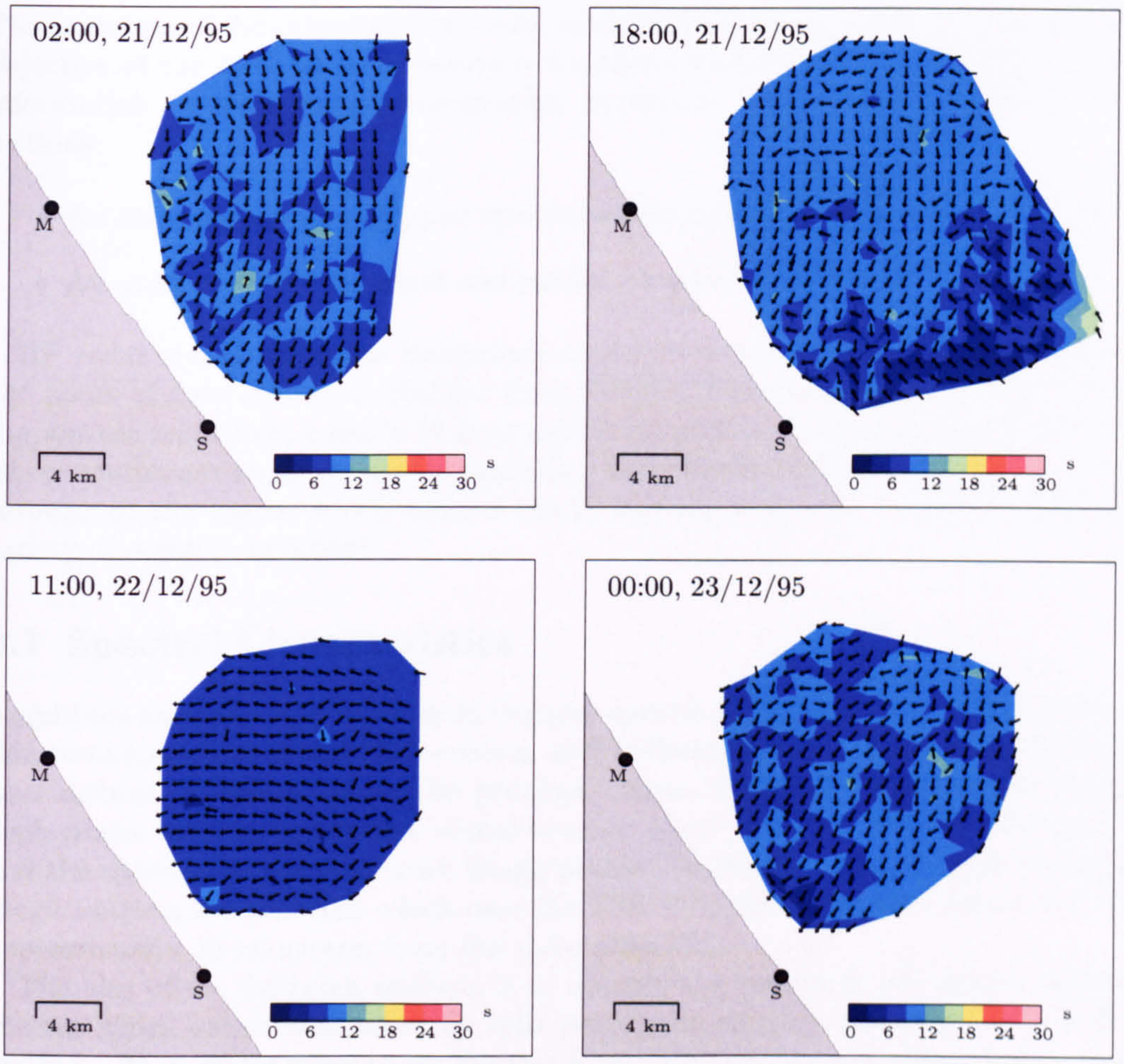

Figure 7.9: Peak period and peak direction measured using IF filter technique. Data taken from period 1 between 02:00, 21/12/95 and 00:00, 23/12/95.

8 First Order Modulation

Ocean wave measurements were studied in chapter 7 using the standard periodogram and IF filter techniques. Statistical analysis indicated that wave parameters derived from filtered radar signals exhibit the strongest correlation with directional waverider data. The structure of the extracted first order modulation is investigated in this chapter. The objective of the analysis is to ascertain whether this data can provide any constructive information on underlying oceanographic processes. The chapter is divided into two sections:

- An investigation into Doppler spectra which fail the SCAWVEX quality criteria.
- An analysis of the temporal and spatial structure of IF signals.

HF radar signals from the Holderness deployment were studied, providing a total of 144 hours of data over three disjoint time periods. The examples illustrated within this chapter are taken from a single 72 hour period between the 20th and 23rd December 1995 where continuous radar data were available. Variable sea state parameters were recorded throughout this period which enabled the IF filtering technique to be examined under a variety of oceanic conditions.

8.1 Spectral Characteristics

Amplitude and frequency stability in Doppler spectra are prerequisites of the Wyatt inversion technique. The SCAWVEX criteria used to determine the quality of Doppler spectra were defined in section 3.4.1. The principal causes of spectral failure in the Holderness deployment were an insufficient signal-to-noise ratio (SNR) in the backscattered signal and the splitting of the first order Bragg peaks. The attenuation of signal strength with range restricts the grid cells which pass the SNR criterion to within a maximum range of approximately 30 kilometres from the radar sites [31].

The aim of the following analysis is to identify the temporal and spatial structure of spectra which are contaminated by split peaks and evaluate the impact of the IF filter method. Wave measurements are derived from Doppler3 spectra which have a temporal resolution of 45 minutes – variability within this time period can limit the number and quality of the generated oceanographic parameters.

8.1.1 Temporal Structure

An instantaneous frequency technique has been developed in this thesis in order to combat the problem of compound Bragg peak structure. The filter isolates and extracts the first order modulation which enables an increased number of spectra to be inverted using the Wyatt method. An alternative, less complex, approach was proposed in chapter 4 which involved shifting the peaks of each constituent periodogram to the Bragg frequencies, $\pm\omega_b$, before forming a Doppler3 spectrum.

Figure 8.1 shows the number of grid cells which failed the spectral quality criteria during a continuous 72 hour period using the periodogram, IF filter and peak shifting techniques. The periodogram data exhibit a tidal pattern and a deterioration in spectral quality occurs at six hourly intervals. The temporal development of the average current field within the Holderness region is shown in figure 8.2. The ocean surface currents are dominated by a tidal cycle; the current travels at an angle parallel to the coastline, alternating in direction every six hours. The pattern of split peaks is related to this current structure. The maxima occur at tidal frequencies when the current is turning in direction and the amplitude is low. The number of cells which failed the signal-to-noise ratio criteria was dependent on the operational constraints of the OSCR system and remained relatively constant.

An overall increase in the number of spectra exhibiting split peaks over the time period shown is likely to be related to an increase in significant waveheight. A link between the first order modulation in HF radar signals and the underlying sea state was observed during the Holderness deployment and is investigated in section 8.2.

The impact of the alternative spectral techniques is quantified in table 8.1. On average, only 103 of the 565 Holderness grid cells (18%) contain spectra of invertible quality using the standard periodogram. Split peaks account for approximately one third of the spectral failures. Over twice as many cells (38%) can be inverted by applying the IF filtering procedure to the raw radar data. The filter has largely eradicated the phenomenon of multiple first order structure in HF radar signals. The cells which fail the quality criteria are almost exclusively caused by a low SNR level – which the filter is not designed to improve. The more straightforward peak shifting approach also reduces the number of failed cells which are attributable to split peaks. However, the filter exhibits a significant advantage over this method – first order modulation within each constituent periodogram, which can cause distortion, is extracted from the Doppler3 spectra.

Table 8.1: The mean number of cells which fail the spectral quality criteria and the subset which fail due to split Bragg peaks. Data taken from a 72 hour time period between 15:00, 20/12/95 and 14:00, 23/12/95.

Technique	All	Split Peaks
Periodogram	462	149
Peak Shifting	375	80
IF Filter	351	22

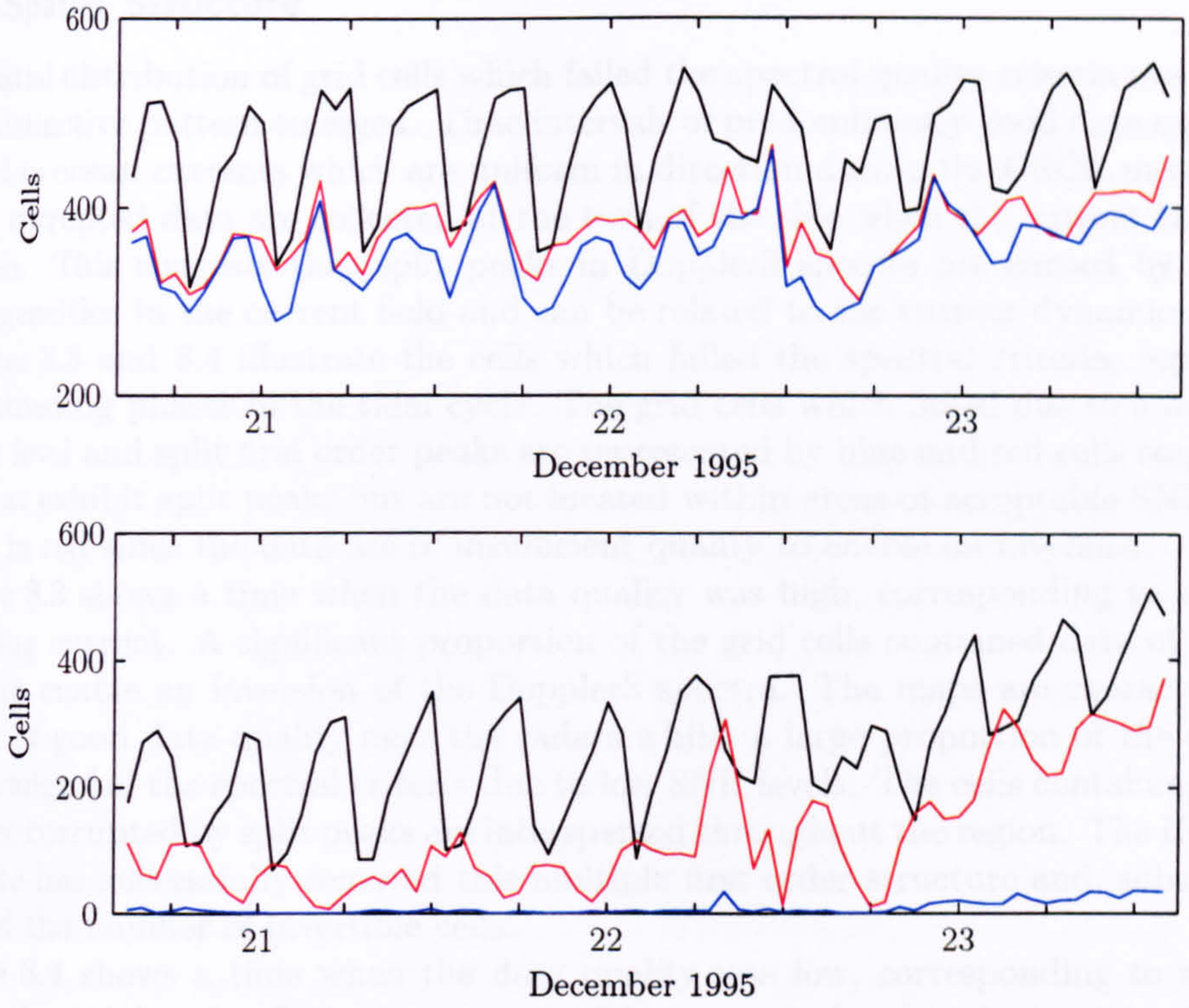

Figure 8.1: Number of cells which failed the spectral quality criteria (top) and the split peak criterion (bottom) for raw (black), filtered (blue) and peak shifted (red) data.

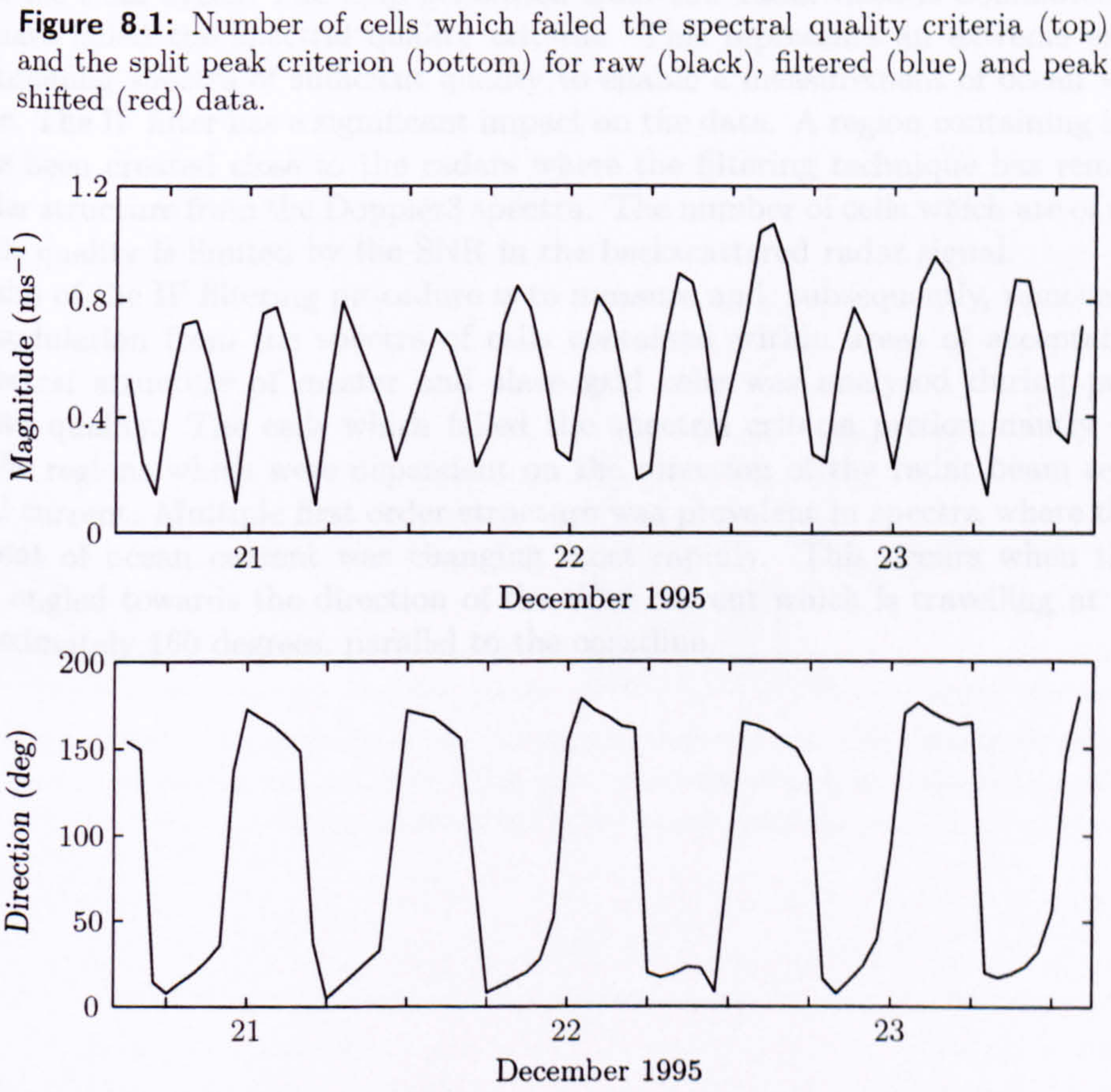

Figure 8.2: Time series showing the magnitude (top) and direction (bottom) of the average ocean current field in the Holderness region.

8.1.2 Spatial Structure

The spatial distribution of grid cells which failed the spectral quality criteria was analysed and a distinctive pattern emerged. Time intervals of predominantly good data quality correspond to ocean currents which are uniform in direction during the OSCR measurement period; corrupted data are collected at the turn of the tide when the current is changing direction. This suggests that split peaks in Doppler3 spectra are caused by temporal inhomogeneities in the current field and can be related to the current dynamics.

Figures 8.3 and 8.4 illustrate the cells which failed the spectral criteria, representing two contrasting phases in the tidal cycle. The grid cells which failed due to a low signal-to-noise level and split first order peaks are represented by blue and red cells respectively. Cells that exhibit split peaks but are not located within areas of acceptable SNR are not marked in red since the data are of insufficient quality to enable an inversion.

Figure 8.3 shows a time when the data quality was high, corresponding to a uniform underlying current. A significant proportion of the grid cells contained data of sufficient quality to enable an inversion of the Doppler3 spectra. The maps are characterised by a region of good data quality near the radars whilst a large proportion of the cells at a greater range fail the spectral criteria due to low SNR levels. The cells containing spectra which are corrupted by split peaks are interspersed throughout the region. The IF filtering procedure has successfully removed this multiple first order structure and, subsequently, increased the number of invertible cells.

Figure 8.4 shows a time when the data quality was low, corresponding to a turning point in the tidal cycle. The map generated from raw radar data is dominated by cells which have failed the spectral quality criteria. This represents an extreme example – cells containing spectra of sufficient quality to enable a measurement of ocean waves are sporadic. The IF filter has a significant impact on the data. A region containing invertible cells has been created close to the radars where the filtering technique has removed the first order structure from the Doppler3 spectra. The number of cells which are of sufficient invertible quality is limited by the SNR in the backscattered radar signal.

The aim of the IF filtering procedure is to measure and, subsequently, remove the first order modulation from the spectra of cells contained within areas of acceptable SNR. The spectral structure of master and slave grid cells was analysed during periods of poor data quality. The cells which failed the spectral criteria predominantly occurred in specific regions which were dependent on the direction of the radar beam relative to the tidal current. Multiple first order structure was prevalent in spectra where the radial component of ocean current was changing most rapidly. This occurs when the radar beam is angled towards the direction of the tidal current which is travelling at an angle of approximately 160 degrees, parallel to the coastline.

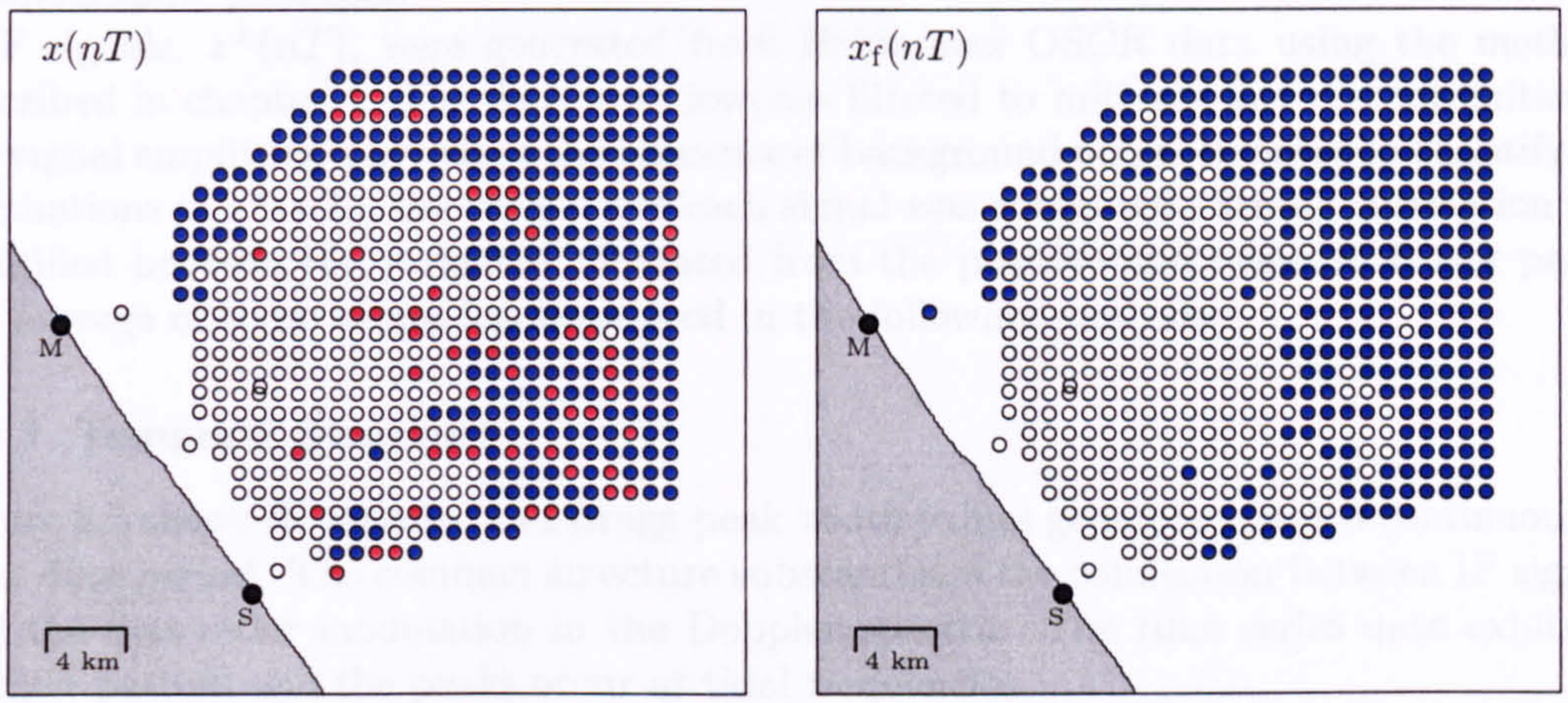

Figure 8.3: Spatial structure of cells which failed the spectral quality criteria using raw and IF filtered data. The cells which failed due to a low SNR and split first order peaks are represented by blue and red cells respectively. Data taken at 01:00, 21/12/95.

Figure 8.4: Spatial structure of cells which failed the spectral quality criteria using raw and IF filtered data. The cells which failed due to a low SNR and split first order peaks are represented by blue and red cells respectively. Data taken at 13:00, 23/12/95.

8.2 Instantaneous Frequency

IF signals provide a measure of the first order modulation contained in radar backscatter from the ocean's surface. The mechanisms which affect these data will differ from those which cause the split Bragg peaks investigated in section 8.1 as Doppler3 spectra are averaged over longer timescales than IF measurements. The aim of the following analysis is to identify whether the IF signals exhibit any properties which can be related to oceanographic processes.

IF signals, $z^{\pm}(nT)$, were generated from Holderness OSCR data using the methods described in chapter 4. The data were lowpass filtered to mitigate any discontinuities at low signal amplitude and reduce the influence of background noise. In order to quantify the fluctuations in $z^{\pm}(nT)$, the variance of each signal was computed. Strong correlation was identified between the variances generated from the positive and negative Bragg peaks; the average of these values has been used in the following analysis.

8.2.1 Temporal Structure

Figure 8.5 shows IF variance and Bragg peak width values generated from a continuous 72 hour data period. The common structure substantiates the connection between IF signals and the first order modulation in the Doppler spectra. The time series data exhibit a distinct pattern and the peaks occur at tidal frequencies.

The corresponding ocean current parameters are shown in figure 8.6. The IF variance maxima correlate with peak values in the current amplitude. The minima occur at the turn of the tide when the current direction is changing and the amplitude is low. The tidal current gradients which cause split peaks in Doppler3 spectra are not associated with the fluctuations in the IF signals.

The observed relationship between IF variance and the tidal current in the Holderness region is illustrated in figure 8.7. The maps represent extreme states of the tidal cycle, separated by three hour intervals, where the current amplitude alternates between minimum and maximum values. Regions of low IF variance correlate with periods of low current amplitude at the turn of the tide. Elevated variances are prevalent when the magnitude of the underlying current is high during the data collection period.

These results suggest that the mechanisms driving the IF structure could well be related to current turbulence. Turbulence is an ubiquitous process in ocean dynamics which may explain the observed distribution of IF variance since turbulent velocity in the surface layer of the ocean is related to the current magnitude [38]. Heron [23] investigated this phenomenon during an experiment in Australia and concluded that turbulent flow was a contributing factor to the broadening of the first order peaks.

Timeseries analysis also provides evidence of a link between IF variances and the underlying ocean state. The variable conditions observed during the Holderness deployment were described in chapter 7. Results from the two identified time periods are illustrated.

The 48 hour period between the 4th and 6th January 1996 was characterised by high sea states which were generated by strong winds from a depression lying to the north of the measurement region [31]. Figure 8.8 shows the IF variances and ocean waveheights recorded at the location of the Datawell directional waverider during this time period. Areas of high waveheight appear to correlate with increased IF variance.

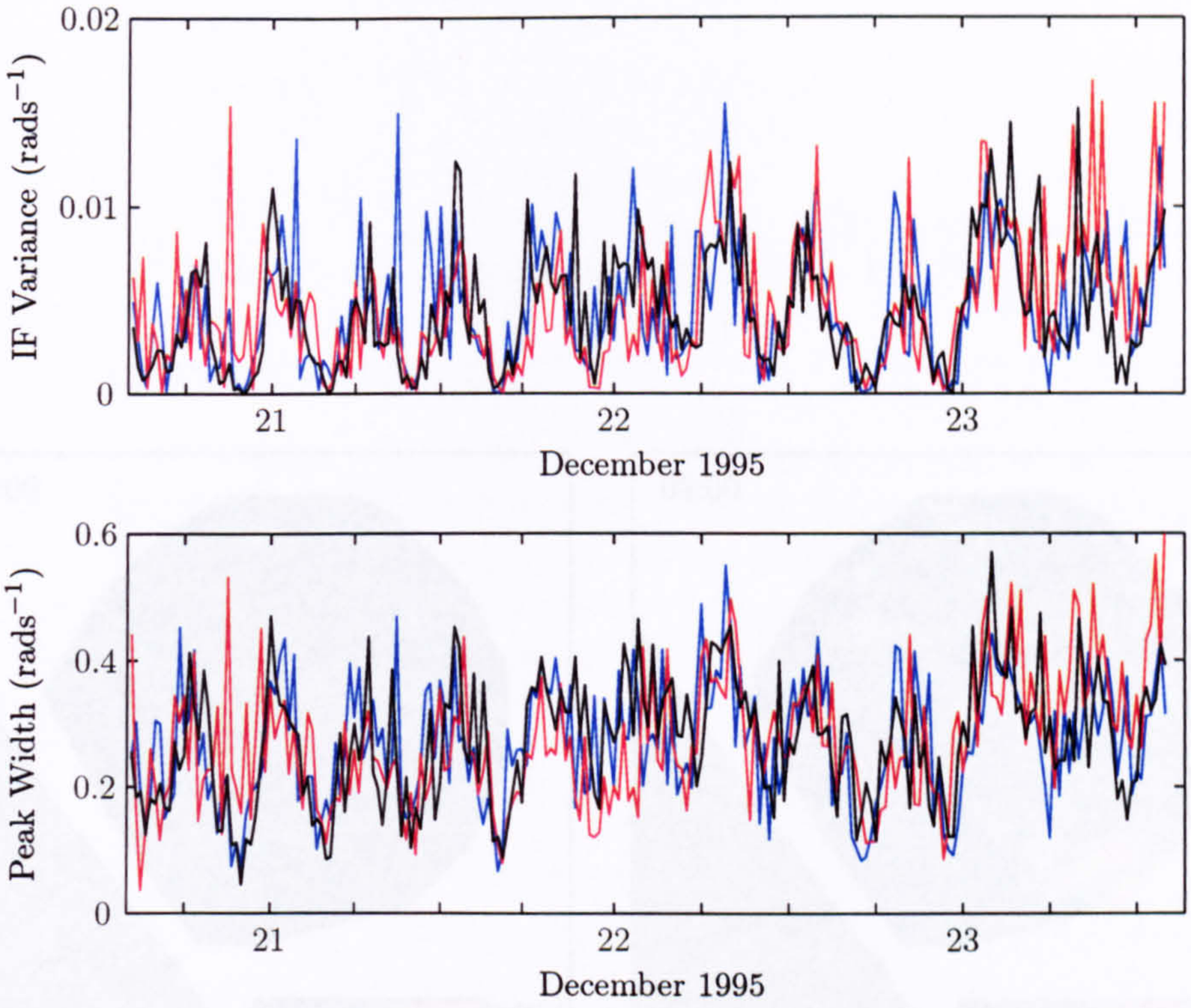

Figure 8.5: Time series of IF variances (top) and Bragg peak widths (bottom) from master radar site for cells 20 (black), 36 (blue) and 58 (red).

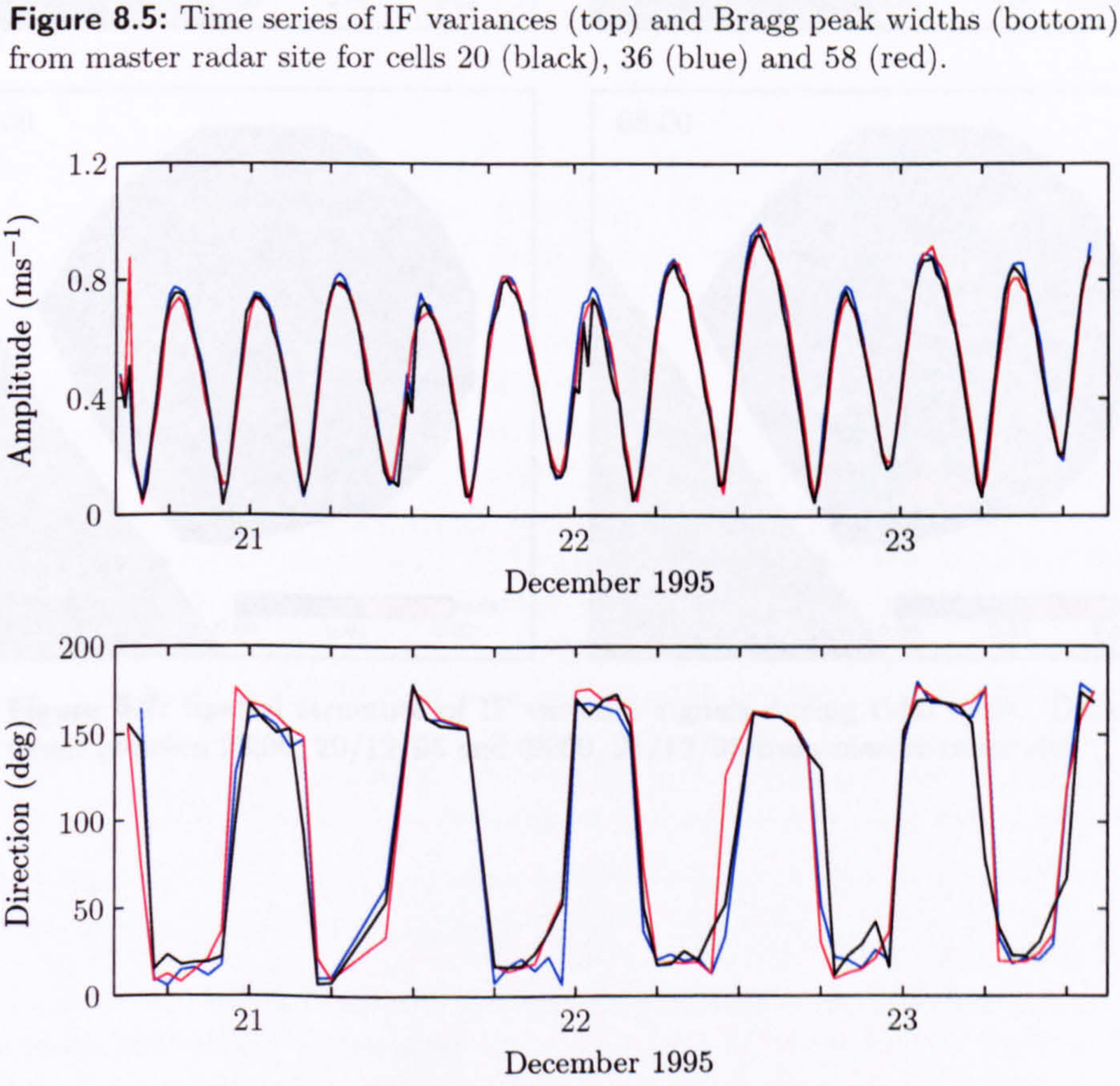

Figure 8.6: Time series of ocean current amplitude (top) and direction (bottom) for cells 20 (blue), 36 (black) and 58 (red).

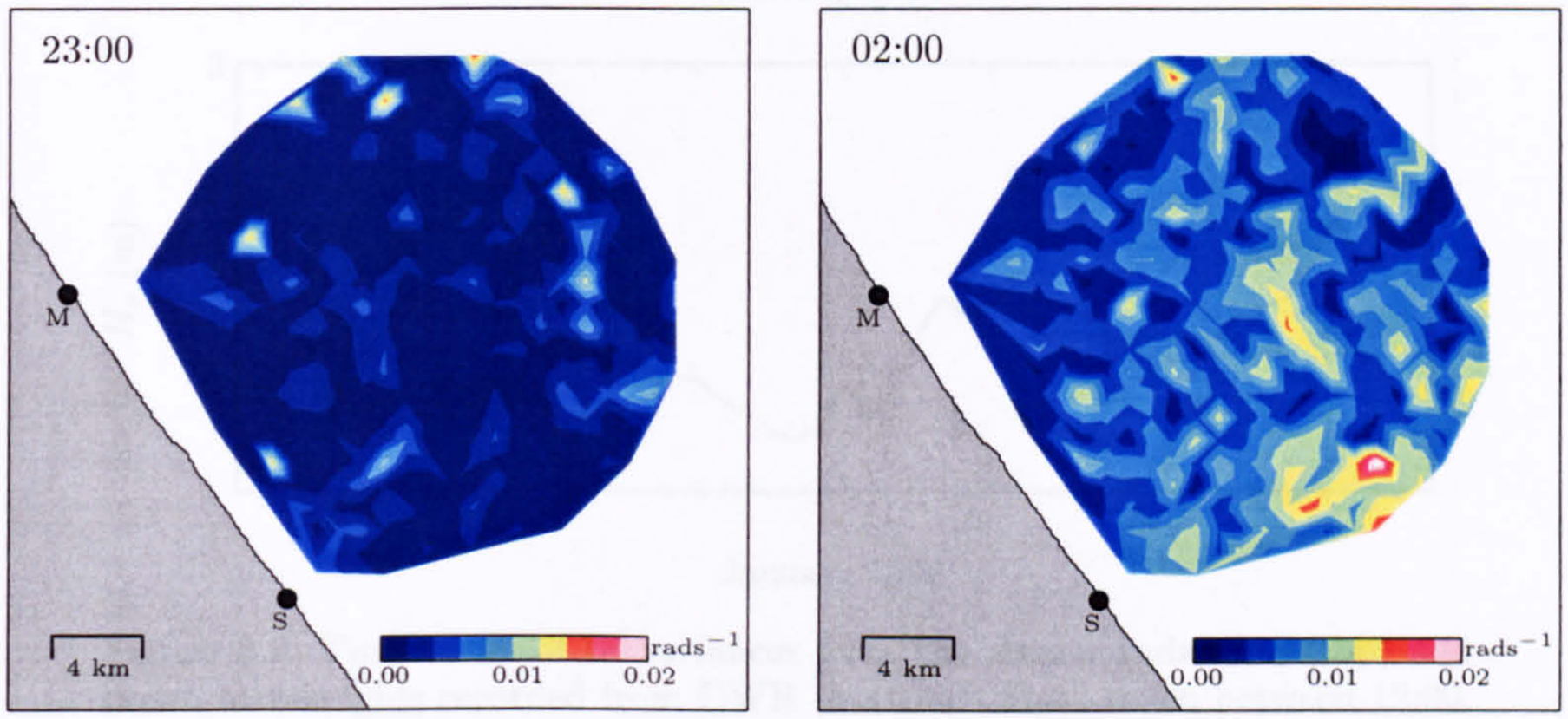

Figure 8.7: Spatial structure of IF variance signals during tidal cycle. Data taken between 23:00, 20/12/95 and 08:00, 21/12/95 from master radar site.

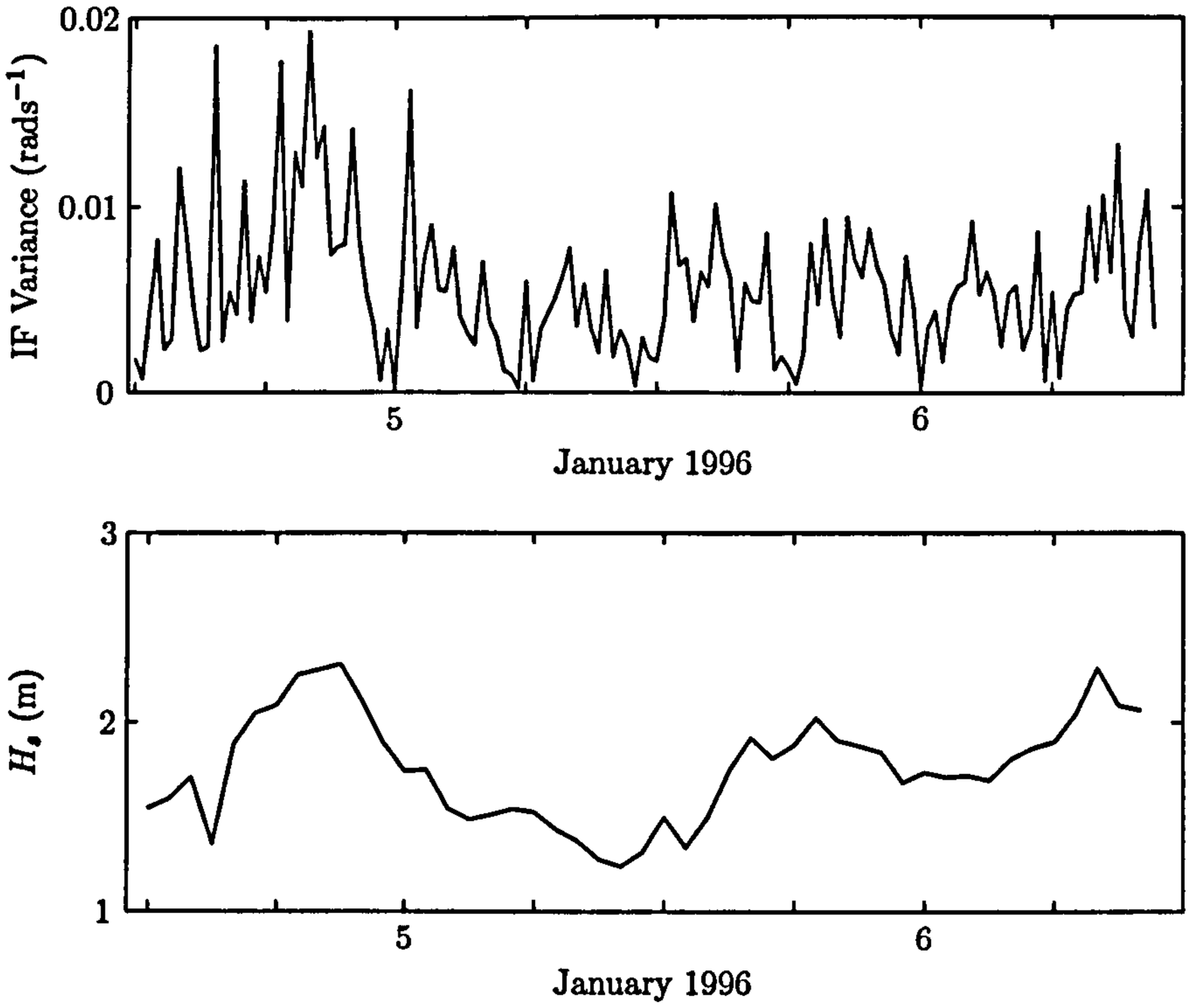

Figure 8.8: Time series of IF variances from the master radar site (top) and ocean waveheights recorded from DWR (bottom). Data taken between 12:00, 04/01/96 and 10:00, 06/01/96.

Figures 8.9 and 8.10 illustrate this phenomenon during an 18 hour period of increasing sea states between the 22nd and 23rd December 1995. The corresponding IF variance time series can be seen in figure 8.5. Each map is separated by a six hour interval in order to isolate the data at a common phase in the tidal cycle. Figure 8.9 shows the development of the ocean wave field as the waves built from an initial height of one metre to a maximum of approximately five metres. Figure 8.10 shows the corresponding IF variance structure. A distinct increase in variance can be observed throughout the region during the measurement period. The observed escalation in wave energy, which causes wave breaking, could be a contributing factor to turbulent processes.

Investigations into the composition of IF signals have proved inconclusive. Turbulence has been conjectured as a potential driving mechanism of the IF structure but further analysis is required to provide evidence to substantiate this hypothesis. However, a study of turbulent processes in the Holderness region is difficult for a number of reasons:

- Errors were identified in radar backscatter due to antenna sidelobes in the OSCR system [31]. This hinders the isolation of the oceanographic data structure.
- The Holderness region is dominated by a tidal regime and consequently an investigation into properties of non-tidally driven currents would have limitations.
- Data from in situ instruments are required in order to understand the turbulent processes in the Holderness area.

The influence of turbulence on radar signals may provide the stimulus for investigation in future work using data from more recent and diverse HF radar deployments.

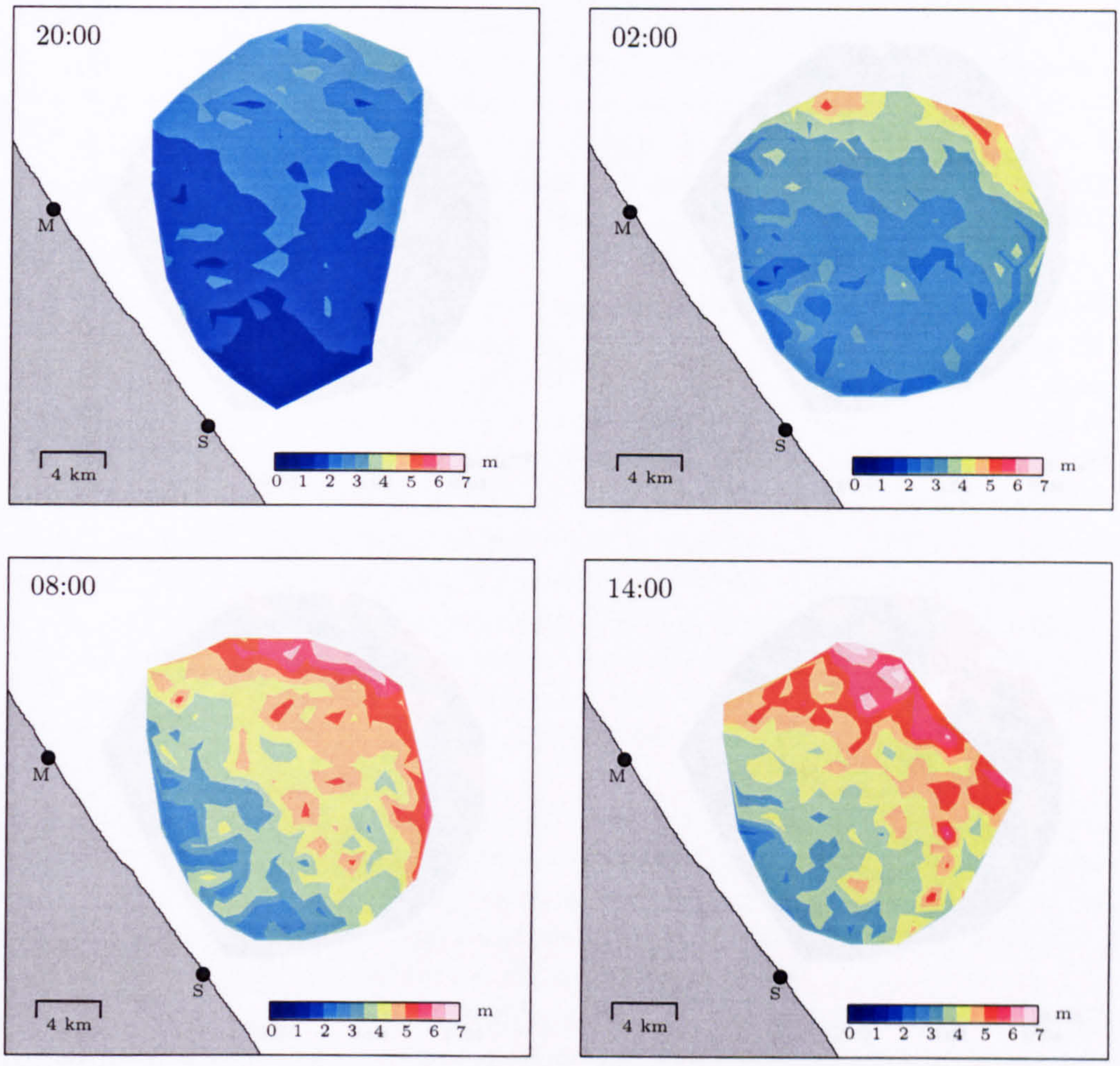

Figure 8.9: Significant waveheight maps. Data taken between 20:00, 22/12/95 and 14:00, 23/12/95.

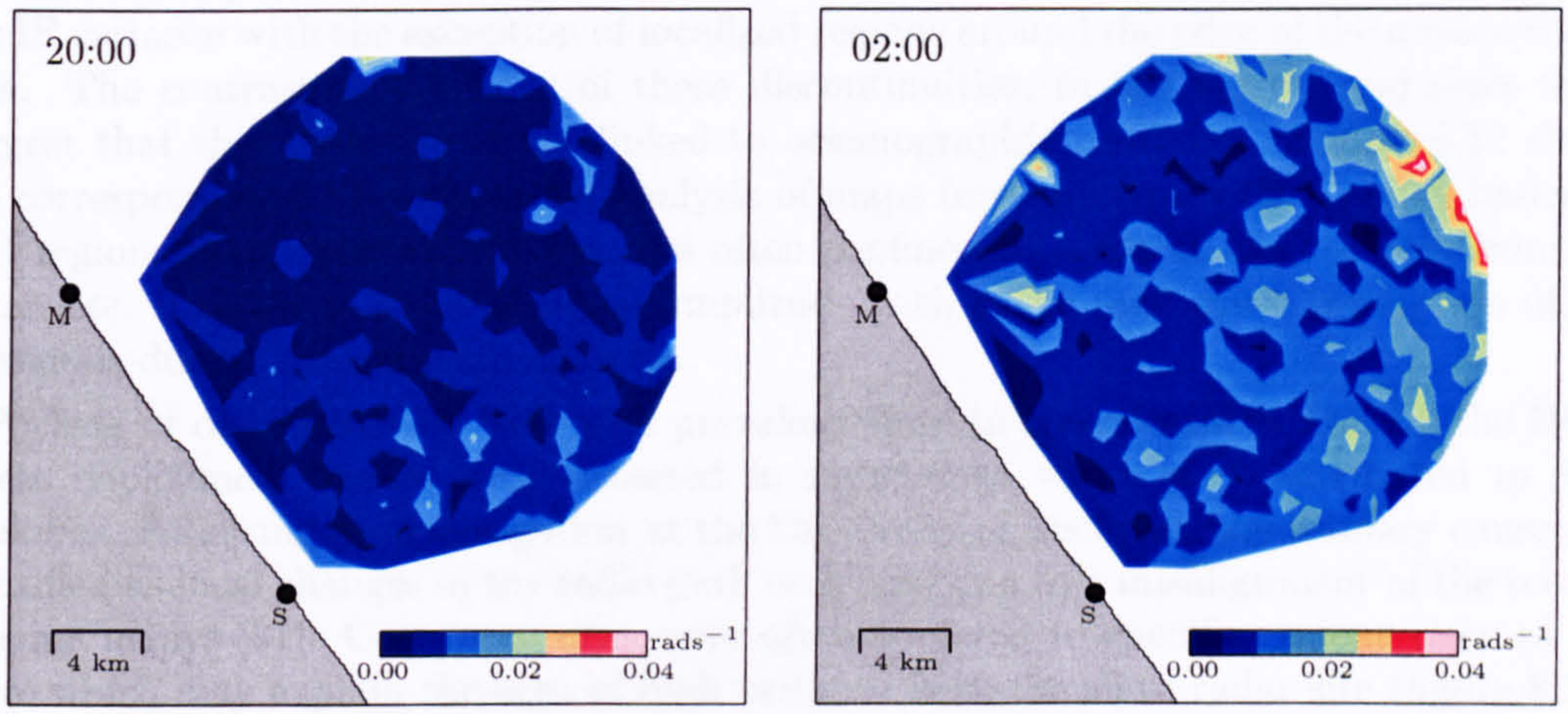

Figure 8.10: Spatial structure of IF variances. Data taken from master site between 20:00, 22/12/95 and 14:00, 23/12/95.

8.2.2 Spatial Structure

This section attempts to identify whether the small scale structures observed in maps of IF variance are influenced by oceanographic processes; results from chapter 6 suggest that this spatial distribution may be caused by noise. The interaction of various oceanic parameters has been investigated in order to explore any emerging patterns. An overview of processes which may affect the backscattered radar signal is described. Examples from two time points are illustrated to encapsulate some common traits.

Figure 8.11 shows IF variances at 18:00 on 21/12/95 which corresponds to a period of low current amplitude when the tide was changing direction. The maps are dominated by low IF variance with the exception of localized regions around the edge of the measurement area. The contrasting positions of these discontinuities, in the master and slave data, suggest that this structure is not linked to oceanographic processes. Figure 8.12 shows the corresponding SNR values. An analysis of maps from numerous time points indicates that regions of extreme IF variance are often confined to areas at large ranges from the radar site. The attenuation of signal amplitude with range may cause corruption of the IF signals due to the influence of noise.

Pockets of discontinuities were also prevalent close to the coastline. During the Holderness deployment, errors were detected in radar data which were attributed to high sidelobes. Following an investigation at the University of Sheffield, the primary cause was identified as local changes in the radio path over land due to a misalignment of the receive antenna arrays [31]. Corrupted data were often confined to specific regions close to the shore which may explain the area of high variance from the slave radar site (figure 8.11).

Figure 8.13 shows the generated IF variances at 02:00 on 22/12/95 which represent a time midway through the tidal cycle. The underlying ocean current field was moving uniformly in a direction parallel to the coastline. The map generated from master radar data exhibits a frequently identified characteristic from the Holderness deployment; regions of high IF variance are widespread towards the south-east boundary of the measurement area. This is probably caused by an increased noise contribution in the IF signal due to the decrease of SNR with range.

The dynamics of various oceanic processes were studied in order to identify whether they can be related to the observed micro structure in IF signals. The interactions between the directional distributions of ocean waves, currents and winds were examined to identify any relevant structure. Figure 8.14 illustrates the intersecting angles between the wave and current/wind fields at 02:00 on 22/12/95.

The spatial structure of the master and slave IF variance maps exhibits no discernible correlation; the OSCR system generates non-synchronous data from the two radar sites so differences are anticipated between the signals. However, oceanic processes normally develop over longer timescales than the temporal resolution of the radar data collection period. Similarities in the master and slave maps would be expected if the processes driving the IF structure were purely an oceanographic effect. Alternatively, the observed distribution of IF variances could be a directional effect which is dependent on the intersection angles between the radar beams and oceanic parameters. An analysis of the interactions between the OSCR radials and the current/wave/wind data failed to reveal any patterns and occurred at a much larger scale than the IF structure.

A comprehensive study of oceanic parameters provided no evidence of a link with the spatial distribution of IF signals. A total of 144 hours of data from the Holderness region was investigated. The generated IF signals exhibited no distinguishable structure which could be attributed to oceanographic processes and are likely be caused by noise.

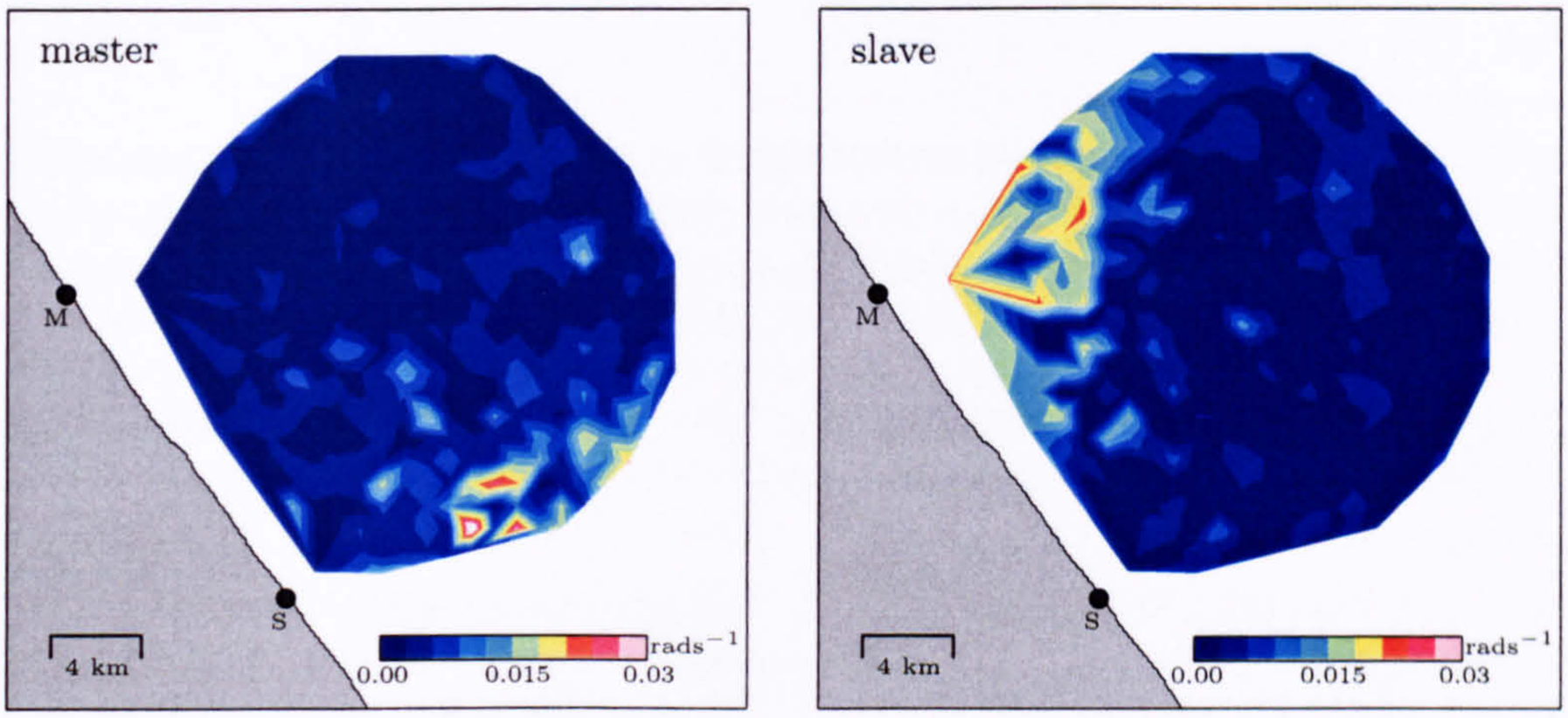

Figure 8.11: Spatial structure of IF variances from the master and slave radar sites. Data taken at 18:00, 21/12/95.

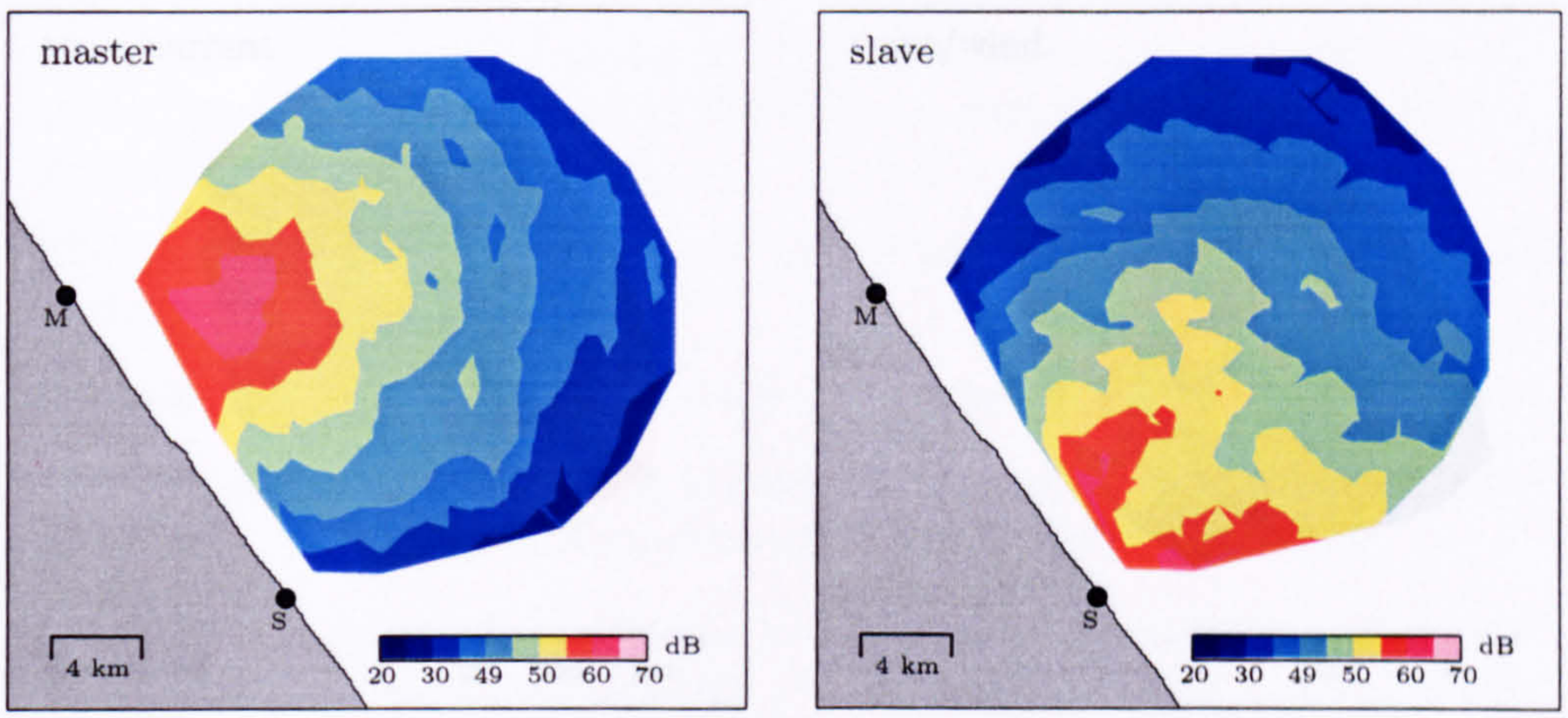

Figure 8.12: Spatial structure of SNR from the master and slave radar sites. Data taken at 18:00, 21/12/95.

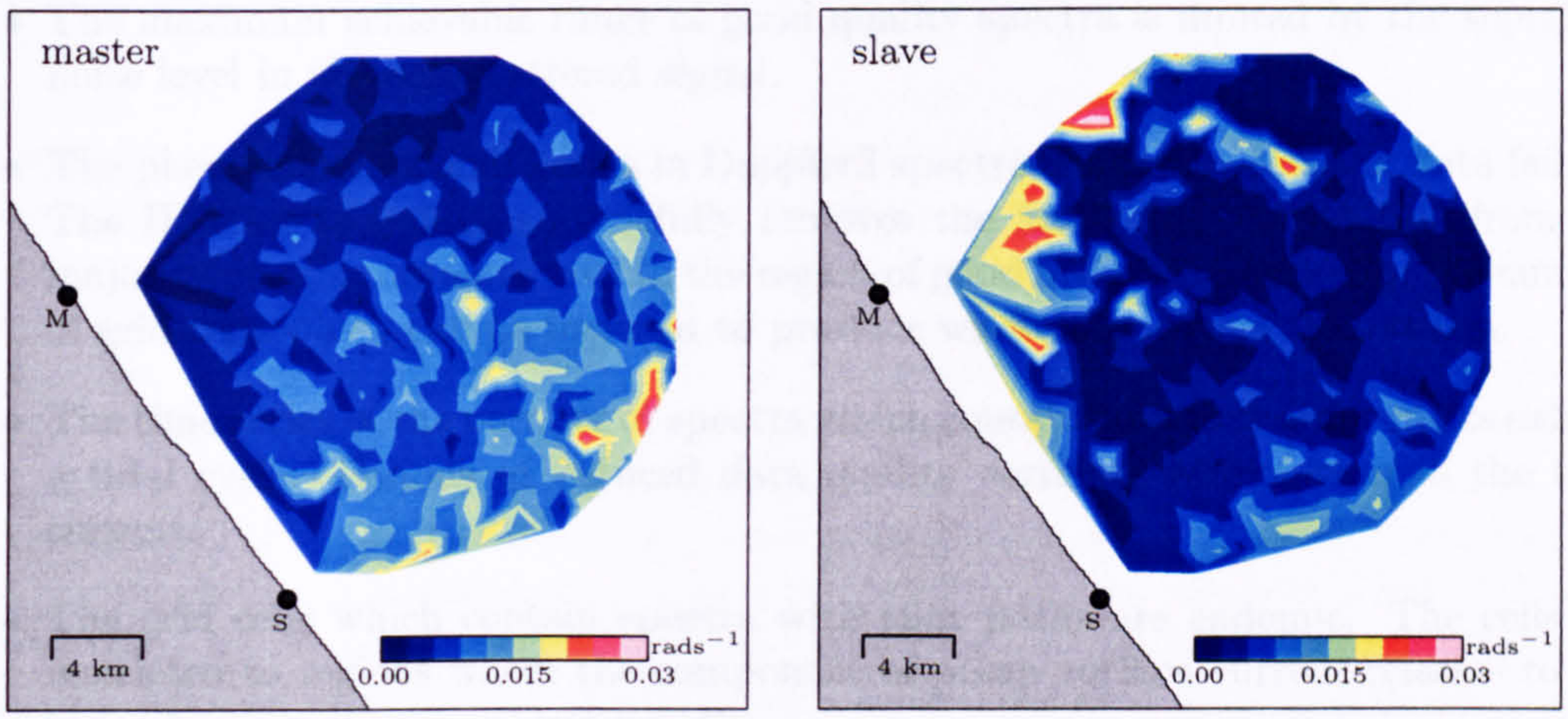

Figure 8.13: Spatial structure of IF variances from the master and slave radar sites. Data taken at 02:00, 22/12/95.

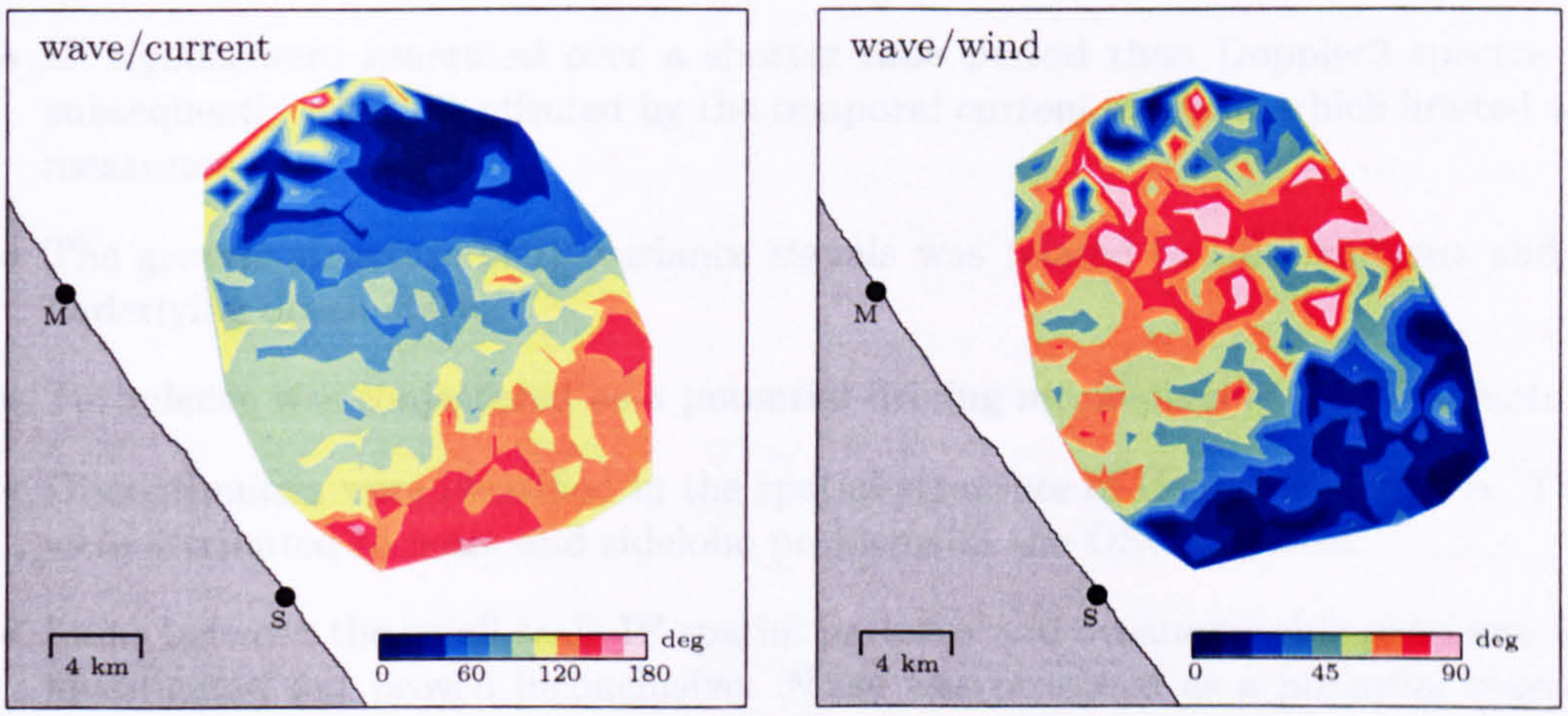

Figure 8.14: Spatial structure of interaction between the wave field and current/wind directions. Data taken at 02:00, 22/12/95.

8.3 Summary

The first order modulation measured using the IF filter technique has been studied in this chapter. The temporal and spatial structure of Doppler3 spectra and IF signals have been investigated and the results illustrated using HF radar data from the Holderness deployment.

Doppler3 spectra which failed the SCAWVEX quality criteria were examined and various properties were identified:

- The maximum achievable range of good quality spectra is limited by the signal-to-noise level in the backscattered signal.

- The phenomenon of split peaks in Doppler3 spectra is a major cause of data failure. The IF filter technique successfully removes the first order modulation from the majority of cells contained within the region of good SNR. Consequently, the number of grid cells which can be inverted to produce wave measurements increases.

- The time series of the number of spectra which contain split first order peaks exhibit a tidal cycle. Periods of reduced data quality correlate with a turn in the tidal current.

- The grid cells which contain spectra with split peaks are endemic. The cells are restricted to regions where the component of ocean surface current relative to the radar beam is changing most rapidly.

The structure of instantaneous frequency signals was studied and provided the following results:

- IF signals were generated over a shorter time period than Doppler3 spectra and subsequently were less affected by the temporal current gradient which limited wave measurements.

- The generic structure of IF variance signals was related to tidal currents and the underlying ocean state.

- Turbulence was conjectured as a potential driving mechanism of the IF structure.

- Discontinuities were identified in the spatial structure of IF variance signals. These were attributed to noise and sidelobe problems in the OSCR system.

- Links between the small scale IF spatial patterns and oceanographic processes were investigated but proved inconclusive. Noise was proposed as a potential source of the observed IF structure.

9 Conclusions

The work in this thesis has been motivated by limitations in the conventional signal processing techniques for HF radar oceanography. An instantaneous frequency filtering approach has been developed in order to mitigate the effect of first order modulation which can corrupt the Doppler spectra. A significant enhancement in the quality and quantity of ocean wave measurements has been established.

Generic properties of HF radar and the configuration of the Holderness experiment were discussed in chapter 2. The Holderness deployment was analysed in this thesis as extensive time periods of raw data were available from the OSCR radar system.

The periodogram is the standard spectral analysis technique used in ocean remote sensing. Chapter 3 provided an overview of the periodogram signal processing and described methods for extracting oceanographic parameters from the Doppler spectra: the frequency shift of the first order Bragg peaks is proportional to the radial component of surface current; a non-linear Fredholm integral equation relates the second order continuous sidebands to the ocean wave directional spectrum. The requirement of amplitude and frequency stability for wave measurements necessitated the averaging of three consecutive spectra. This reduced the temporal resolution of each spectral estimate to approximately 45 minutes which created problems in the wave inversion procedure. The periodogram technique assumes stationarity within the temporal and spatial scales of the radar system. Inhomogeneity in the underlying current field was identified as a cause of split Bragg peaks which limited the spectral quality. In the Holderness deployment, up to 80% of the grid cells were unusable for wave measurements due to this phenomenon.

The objective of the thesis was to ascertain whether more sophisticated signal processing could limit the spectral distortion. An instantaneous frequency technique was conjectured as a mechanism for measuring the temporal variability of the Bragg components. This concept was investigated and the potential of a filtering approach to extract the first order modulation and reduce the extent of the spectral corruption became evident.

Two alternative techniques were also examined in chapter 4 in order to validate the IF method. An autoregressive parametric modelling approach was described which provided radial current estimates by constraining the frequency separation of the Bragg components to their theoretical value. A modified covariance method was selected to determine the AR coefficients from the radar data. A MUSIC pseudo spectral method was presented, based on an eigenanalysis of an autocorrelation matrix. A complex singular value decomposition was used to partition the data matrix into a signal and noise subspace. The orthogonality property of the corresponding eigenvectors was utilised to generate current components.

The periodogram, instantaneous frequency, autoregressive and MUSIC techniques were evaluated in chapter 5 using statistical methods. Data from an S4 current meter in the Holderness region were analysed over a continuous 72 hour period. Congruity was observed in the structure of the OSCR and S4 derived components although the amplitudes of the radar data were consistently larger; this was attributed to the attenuation of ocean currents with depth. The vertical shear factor that differentiated the radar surface data from the subsurface S4 data was consistent with results from other deployments. Correlation statistics provided strong evidence of a linear relationship between the data sets and indicated that the IF filter and MUSIC techniques performed marginally better than

the periodogram and autoregressive methods. The frequency separation of the generated Doppler spectra – an invariant property of backscattered radar signals – was investigated. The IF and AR approaches exhibited elevated accuracy compared with the large fluctuations which characterised the periodogram data.

The objective of chapter 6 was to develop the IF filter and address any limitations in the procedure. Discontinuities were observed in the IF estimates during periods of low signal amplitude due to background noise. A lowpass filtering algorithm was implemented to reduce the noise corruption in the IF data. Simulated data were used to identify various properties of the filter. The effect of truncating non-periodic data was investigated and the IF signal endpoints were subsequently disregarded during the filter processing. Oceanographic conditions were modelled in order to illustrate the impact of the filtering procedure. The optimum bandwidth parameters were determined: the width of the primary filter is dependent on the maximum current modulation in the measurement region and a value of $\theta = 0.4$ rads^{-1} was selected in the Holderness deployment; a dynamic approach was formulated to determine the boundary of the secondary filter.

Ocean wave measurements were discussed in chapter 7. The temporal variability of wave parameters was evaluated using data from a directional waverider. Statistical analysis revealed that HF radar technology can track the underlying ocean conditions with a high degree of accuracy. The IF filter approach provided stronger correlation with the waverider data than the periodogram. The development of directional and frequency wave spectra was examined during periods of rapidly evolving sea states. Erroneous peaks were often identified in the low frequency components of the wave spectra derived from raw radar data. These anomalies were attributed to compound first order structure in the backscattered signals and were successfully removed by the IF filtering procedure.

The distorted Doppler spectra and the composition of the instantaneous frequency signals were investigated in chapter 8. Split Bragg peaks were identified as a major cause of data failure in the Holderness deployment. The cells which failed the wave inversion criteria exhibited a strong tidal cycle and periods of reduced data quality correlated with a turn in the current direction. The generic structure of the extracted IF signals was related to this tidal current and the underlying sea state. Time series analysis over a 72 hour period revealed that the average percentage of invertible cells for the periodogram, peak shifting and IF filter approaches was 18%, 34% and 38% respectively. The complex first order structure has been reduced significantly by the IF filter and the failed grid cells are almost exclusively caused by a low SNR level in the backscattered signal.

HF radar is rapidly becoming established as a powerful oceanographic tool with a unique ability to measure the temporally and spatially varying ocean field over an expansive region. The instantaneous frequency filter presented in this thesis has provided an interesting development and its impact on the quantity and quality of Holderness measurements has been extensive. However, the filter requires testing in more diverse oceanic environments in order to validate the method conclusively. Turbulence was conjectured as a possible driving mechanism of the IF structure but investigations in the Holderness deployment were limited by the strong tidal regime which dominated the ocean conditions. An application of the filter in a non tidally driven region would provide the stimulus for a renewed analysis of the IF signals which may elucidate the underlying ocean dynamics.

Bibliography

[1] Barrick, D.E., 1972, First-order theory and analysis of MF/HF/VHF scatter from the sea, *IEEE Transactions on Antennas and Propagation, AP-20*, pp 2-10

[2] Barrick, D.E., 1977, Extraction of wave parameters from measured HF radar sea-echo Doppler spectra, *Radio Science, 3*, pp 415-424

[3] Barrick, D.E., Lipa, B.J., 1997, Evolution of bearing determination in HF current mapping radars, *Oceanography, 10*, pp 72-75

[4] Barrick, D.E., Evans, M.W., Weber, B.L., 1977, Ocean currents mapped by radar, *Science, 198*, pp 138-144

[5] Bernoulli, D., 1738, *Hydrodynamica*, Switzerland

[6] Boashash, B., Jones, G., O'Shea, P., 1989, Instantaneous frequency of signals: concepts, estimation techniques and applications, *Advanced algorithms and architectures for signal processing IV, 1152*, pp 382-399

[7] Carson, J., Fry, T., 1937, Variable frequency electric circuit theory with application to the theory of frequency modulation, *Bell System Tech. J., 16*, pp 513-540

[8] Chapman, R.D., Shay, L.K., Graber, H.C., Edson, J.B., Karachintsev, A., Trump, C.L., Ross, D.B., 1997, On the accuracy of HF radar surface current measurements: intercomparisons with ship-based sensors, *J. Geophyscal Research, 102*, pp 18,737-18,748

[9] Chapman, R.D., Graber, H.C., 1997, Validation of HF radar measurements, *Occanography, 10*, pp 76-79

[10] Crombie, D.D., 1955, Doppler spectrum of sea echo at 13.56 Mc/s, *Nature, 175*, pp 681-682

[11] Emery, B.M., Washburn, L., Harlan, J.A., 2003, Evaluating radial current measurements from CODAR high frequency radars with moored current meters, *J. Atmospheric and Oceanic Technology, 21*, pp 1259-1271

[12] Essen, H., Gurgel, K.W., 2000, On the accuracy of current measurements by means of HF radar, *J. Oceanic Engineering, 25*, pp 472-480

[13] Fernandez, D.M., Graber, H.C., Paduan, J.D., Barrick, D.E., 1997, Mapping wind direction with HF radar, *Oceanography, 10*, pp 93-95

[14] Fourier, J.B.J., 1822, *Analytical theory of heat*, France

[15] Graber, H.C., Heron, M.L., 1997, Waveheight measurements from HF radar, *Oceanography, 10*, pp 90-92

[16] Graber, H.C., Haus, B.K., 1997, HF radar comparisons with moored estimates of current speed and direction: expected differences and implications, *J. Geophysical Research, 102*, pp 18749-18766

[17] Green, J.J., Wyatt, L.R., 2005, Row-action inversion of the Barrick-Weber equations, to appear in *J. Atmospheric and Oceanic Technology*

[18] Gurgel, K.-W., 1999, High-frequency radars: physical limitations and recent developments, *Coastal Engineering, 37*, pp 200-218

[19] Gurgel, K.-W., Antonischki, G., Essen, H.-H., Schlick, T., 1999, Wellen Radar (WERA): a new ground-wave HF radar for ocean remote sensing, *Coastal Engineering, 37*, pp 219-234

[20] Harris, F.J., 1978, On the use of windows for harmonic analysis with the discrete Fourier transform, *Proceedings of the IEEE, 66*, pp 51-83

[21] Hashimoto, N., Tokuda, M., 1999, A bayesian approach for estimation of directional wave spectra with HF radar, *Coastal Engineering Journal, 41*, pp 137-149

[22] Hauser, D., Kahma, K.K., Krogstad, H.E., Lehner, S., Monbaliu, J., Wyatt, L.R., 2003, *Measuring and analysing the directional spectra of ocean waves, COST Action 714*, Luxembourg

[23] Heron, M.L., 1985, Line broadening on HF ocean surface radar backscatter spectra, *J. Oceanic Engineering, 10*, pp 397-401

[24] Hickey, K., Khan, R.H., Walsh, J., 1995, Parametric estimation of ocean surface currents with HF radar, *J. Oceanic Engineering, 20*, pp 139-144

[25] Hisaki, Y., 1996, Nonlinear inversion of the integral equation to estimate ocean wave spectra from HF radar, *Radio Science, 31*, pp 25-39

[26] Howell, R., Walsh, J., 1993, Measurement of ocean wave spectra using narrow beam HF radar, *J. Oceanic Engineering, 18*, pp 296-305

[27] Jeans, P.K., Donnelly, R., 1986, Four-element CODAR beam forming, *J. Oceanic Engineering, 11*, 296-303

[28] Kay, S.M., 1988, *Modern spectral estimation: theory and application*, Prentice Hall

[29] Khan, R.H., 1991, Ocean-clutter model for high-frequency radar, *J. Oceanic Engineering, 16*, pp 181-188

[30] Kingsley, S.P., Quegan, S., 1992, *Understanding radar systems*, McGraw-Hill

[31] Ledgard, L.J., Wyatt, L.R., 1998, Measurement of ocean waves using the OSCR HF radar system, *SCEOS report, vol. 1, Sheffield University*

[32] Lipa, B.J., 1978, Inversion of second-order radar echos from the sea, *J. Geophysical Research, 83*, pp 959-962

[33] Lipa, B.J., Barrick, D.E., 1986, Extraction of sea state from HF radar sea echo: mathematical theory and modeling, *Radio Science, 21*, pp. 81-100

[34] Mandel, L., 1974, Interpretation of instantaneous frequencies, *American Journal of Physics, 42*, pp 840-846

[35] Marple, S.L., 1987, *Digital spectral analysis with applications*, Prentice Hall

[36] Martin, R.J., Kearney, M.J., 1997, Remote sea current sensing using HF radar: an Autoregressive Approach, *J. Oceanic Engineering, 22*, pp 151-155

[37] Parent, J., Bourdillon, A., 1988, A method to correct HF skywave backscattered signals for ionospheric frequency modulation, *IEEE Transactions on Antennas and Propagation, 36*, pp 127-135

[38] Phillips, O.M., 1966, *The dynamics of the upper ocean*, Cambridge

[39] Prandle, D., 1982, The vertical structure of tidal currents, *Geophysical and Astrophysical Fluid Dynamics, 22*, pp 29-49

[40] Press, W.H., 1986, *Numerical recipies, the art of scientific computing*, Cambridge

[41] Schuster, A., 1898, On the investigation of hidden periodicities with application to a supposed twenty-six day period of meteorological phenomena, *Terr. Mag, 3*, pp 13-41

[42] Shaolin, Y., Hengyu, K., Jiechang, H., Shicai, W., Zijie, Y., Biyang, W., Xiongbin, W., 2001, Super-resolution ocean surface current algorithm based on MUSIC for OSMAR2000, *Oceans 2001, 2*, pp 930-941

[43] Stewart, R.H., Joy, J.W., 1974, HF radar measurement of surface currents, *Deep-Sea Res., 21*, pp 1039-1049

[44] Sun, M., Sclabassi, R.J., 1993, Discrete-time instantaneous frequency and its computation, *IEEE Transactions on Signal Processing, 41*, pp 1867-1880

[45] Teague, C.C., 1997, HF radar instruments, past to present, *Oceanography, 10*, pp 40-44

[46] Traylen, S.M., Wyatt, L.W., 1999, A filter design for the removal of current interaction effects, *IEE Electronic Engineering in Oceanography, 439*, pp 178-182

[47] Tretter, S.A., 1985, Estimating the frequency of a noisy sinusoid by linear regression, *IEEE Transactions on Information Theory, 31*, pp 832-835

[48] Tucker, M.J., 1991, *Waves in ocean engineering: measurement, analysis, interpretation*, Ellis Horwood

[49] Vizinho, A., 1998, Modern spectral analysis in HF radar remote sensing, *PhD thesis, University of Sheffield, Department of Applied Mathematics*

[50] Vizinho, S., 2001, Evaluation of the use of the modified-covariance method in HF radar ocean measurement, *J. Oceanic Engineering, 26*, pp 832-840

[51] Wolf, J., 2003, Intercomparison of S4DW and DWR, *Measuring and analysing the directional spectra of ocean waves, COST Action 714*, Luxembourg

[52] Wyatt, L.R., 1990, A relaxation method for integral inversion applied to HF radar measurement of the ocean wave directional spectrum, *Int. J. Remote Sensing, 11*, 1481-1494

[53] Wyatt, L.R., 1994, Coastal surface current and wave measurement with high frequency radar: limitations and prospects, *Mixing and Transport in the Environment*, Beven, K., Chatwin, P.C., Millbank, J.H., published by Wiley, pp 295-306

[54] Wyatt, L.R., 1997, The ocean wave directional spectrum, *Oceanography, 10*, pp 85-89

[55] Wyatt, L.R., Thompson, S.P., Burton, R.R., 1999, Evaluation of high frequency radar wave measurement, *Coastal Engineering, 37*, pp 259-282

[56] Wyatt, l.R., 2000, Limits to the inversion of HF radar backscatter for ocean wave measurement, *J. Atmospheric and Oceanic Technology, 17*, pp 1651-1666

[57] Wyatt, L.R., Green, J.J., Middleditch, A., Moorhead, M.D., Howarth, J., Holt, M., Keogh, S., 2004, Operational wave, current and wind measurements with the Pisces HF radar, submitted to *J. Oceanic Engineering*

[58] Wyatt, L.R., Liakhovetski, G., Graber, H., Haus, B., 2005, Factors affecting the accuracy of HF radar wave measurements, to appear in *J. Atmospheric and Oceanic Technology*

[59] Yule, G.U., 1927, On a method of investigating periodicites in disturbed series, with special reference to Wolfer's sunspot numbers, *Philos. Trans. R. Soc. London, 226*, pp 267-298